




Chair of Chemistry of Polymeric Materials

Doctoral Thesis



Orthogonal Photoreactions for the
Realization of Multifunctional
Photopolymers

Stefanie Monika Müller

May 2024



EIDESSTÄTTLICHE ERKLÄRUNG

Ich erkläre an Eides statt, dass ich diese Arbeit selbstständig verfasst, andere als die angegebenen Quellen und Hilfsmittel nicht benutzt, den Einsatz von generativen Methoden und Modellen der künstlichen Intelligenz vollständig und wahrheitsgetreu ausgewiesen habe, und mich auch sonst keiner unerlaubten Hilfsmittel bedient habe.

Ich erkläre, dass ich den Satzungsteil „Gute wissenschaftliche Praxis“ der Montanuniversität Leoben gelesen, verstanden und befolgt habe.

Weiters erkläre ich, dass die elektronische und gedruckte Version der eingereichten wissenschaftlichen Abschlussarbeit formal und inhaltlich identisch sind.

Datum 11.05.2024

Unterschrift Verfasser/in
Stefanie Monika Müller

Acknowledgments

I want to thank, first and foremost, my principle supervisor, Prof. Dr. Thomas Grießer for the opportunity to do research under his guidance, his continuous support, encouraging words and the scientific freedom I was given within my project. Special thanks go to Priv.-Doz. Dr. Sandra Schlögl, my co-supervisor, for all the scientific input, positive feedback and her continuous optimism.

I want to thank my colleagues at MUL as well as the PCCL for the good collaboration in the lab - especially David, Walter, Flo and Eli for countless hours of conversation while running experiments, for encouragements, scientific advice and celebrating the small victories.

I want to thank my group, Janine, Romana, Kathi, Paul, Gemma, Carina, Pauline, Alex, Rita, Johannes and Julian, for always having my back and being there through the ups and downs, for the good times we had in the park, in the office and in the lab. Especially Rita and Alex, who accompanied me through the best and worst times during that last year of my PhD. Thank you for the after-work games, the hugs, the GaLiGrüs and for sharing tears and laughter throughout our common time in the office.

I want to thank Claudia Wieser for being the best, fastest and most supportive person we could wish for in administrative matters.

I want to thank Christopher Bowman for welcoming me in his lab at the University of Colorado, Boulder for three months, and Thomas for letting me go to take this opportunity. Special thanks to the Bowman group for treating me as one of them for the short time I could stay. Thanks to Marianela for her time showing me how to prepare samples, to John and Alex for scientific discussions, to Meagan for taking me on a hiking trip, to Sean for chatting about literally anything, to Bruce and Ben for fun times doing cool lithography stuff and to Andrew spending hours with me trying to write decent holograms. It was only a short period of time I spent in Boulder, but it made me genuinely happy.

I want to thank my friends outside the university for taking my mind off work and for the countless hours spent outdoors doing the things I love most with the best people. Particularly, Lisa, Martin, Christl, Eli, Nico - thanks for being there for me throughout the past four years (and beyond)! Special thanks to Lisa for trying to understand "my" chemistry, to Lisa for after-work climbing adventures, to Barbara for sharing songs and talking about anything, to Julian for always making me smile and to "the Munchkins" - Gundula, Krissi and Carina - for their friendship and emotional support beyond our shared master thesis. I wouldn't be who I am without all of you!

Last but not least, I want to thank my parents, Dieter and Sabine, for their unconditional love and support. For letting me go off to study quite far from home, letting me leave for the US for several months, yet always welcoming me back home with open arms and open hearts. Thanks for sparking my scientific interest when I was only a little child and for showing me that science is all about puzzles to be solved - and puzzles are fun!

Funding: The Montanuniversitaet is gratefully acknowledged for the main financial support. Additionally, parts of the research work was performed within the COMET-Module project "Chemitecture" (project-no.: 21647048) at Montanuniversitaet Leoben (Department for Polymer Engineering and Science) within the framework of the COMET-program of the Federal Ministry for Climate Action, Environment, Energy, Mobility, Innovation and Technology and the Federal Ministry for Digital Economic Affairs with contributions by the Polymer Competence Center Leoben GmbH (PCCL, Austria). The PCCL is funded by the Austrian Government and the State Governments of Styria, Upper and Lower Austria.

Statement on the use of generative AI tools: Generative AI tools were tested in the initial states of this thesis for acquisition of literature (ChatGPT-4), however they were found to give incomplete and oftentimes incorrect answers. Therefore it was refrained from using ChatGPT for any (further) academic inquiry and literature research was done on the common, non-AI-assisted platforms scholar.google.com and scifinder-n.cas.org. In terms of language enhancing AI, no more than some single sentences or short paragraphs were translated or improved upon their wording with ChatGPT-4 or DeepL. However, the online dictionary Linguee (linguee.de) was frequently used to find synonyms and for the translation of single words and phrases. The combined assistance of AI can be summarized to be less than 1% of the overall work-load.

Abstract

Additive manufacturing and the quest for novel, smart and renewable materials for 3D printing and light-based applications has become a major focus in polymer science. The aim of this thesis was the further development of 3D printing resins with regard to these characteristics, as well as the development of a novel multifunctional resin system by implementation of orthogonal photoreactions into the 3D printing process.

In a first approach the introduction of network disparity through the use of two orthogonal photoinitiators was investigated. In a thiol-acrylate resin with excess acrylate the polymerization was controlled by the use of two disparate light sources. Thereby thiol-Michael addition (anionic) or radical polymerization (thiol-ene or acrylate homopolymerization) could be separately initiated. While a stepwise curing with a relatively large difference in thermo-mechanical properties could be demonstrated, the hypothesis of the molecular structure having a significant effect on the material properties could not be confirmed.

In a second, more comprehensive study, a dual-cure, single-vat resin was developed, based on radical polymerization of a thiol-methacrylate monomer system containing covalently bound chalcone units as dimerizable crosslinkers. Thermo-mechanical properties can be spatially and temporally controlled via the λ -orthogonal [2+2] cycloaddition reaction of the chalconyl groups during printing or post-processing. Using defined doses of light (405 nm) after polymerization (450 nm), the T_g and elastic modulus can be altered in a continuous way, generating not only two but numerous distinct material properties. Shape memory experiments as well as multi-wavelength 3D printing was shown on macro- and micro-scale to present the vast opportunities for this novel 3D-printable material. Further functional groups were investigated upon their reactivity upon irradiation with the most common wavelengths creating a library of photo-crosslinkable moieties. Notably, the reactivity did not always align with the recorded ultraviolet-visible absorption spectrum, confirming a reactivity analysis crucial for all light-induced processes especially if orthogonality is desired.

In all studies photo-DSC and FTIR kinetics were used as a tool to investigate and characterize curing behavior. These methods were used to contribute to detailed investigations on a number of novel photoinitiators and biobased molecules for advanced applications in future additive manufacturing were additionally evaluated. Thereby, two bio-based methacrylates, eugenyl methacrylate (EM) and vanillyl alcohol methacrylate (VAM) were investigated upon their curing behavior along a range of temperatures to optimize processing conditions in paper coating. Finding VAM to be the more reactive of the two bio-based alternatives, exhibiting a water contact angle (106°) comparable to existing coatings if PDMS-ECEMS is used as an additive (10 wt%). This makes vanillyl alcohol methacrylate a suitable sustainable alternative for hydrophobic paper coatings. Additionally, Novel type I radical photoinitiators, based on tin or germanium, were investigated upon their curing behavior. They can be used in future applications as an alternative to state-of-the-art phosphorous PIs with reduced toxicity¹ and pronounced reactivity in the energy-efficient, innocuous visible light region. Lastly, bio-based monomers with methacrylate, vinyl and alkyne functionalities were evaluated for their applicability in novel resins for 3D-printable biological scaffolds or coatings.

Finally, a literature review is given as a comprehensive overview on single-molecule (type I) radical photoinitiators. The focus is put on visible light activation, comprising not only phosphorous but also silicon, germanium and tin compounds, as a way to more benign and energy-conscious curing.

The three main topics of this thesis are (i) photoinitiators and their characterization, (ii) bio-based monomers for radical photo-polymerization and (iii) molecules for the implementation into dual-cure 3D printing resins for smart materials. They all contribute to a better understanding of all constituents used, their reaction mechanism, curing behavior and influence on the final material properties, crucial for sophisticated material development towards advanced 3D printing of smart materials.

Keywords:

photochemistry • thiol-ene systems • orthogonality • shape memory • reaction kinetics

Kurzfassung

Additive Fertigung und die Suche nach neuartigen, intelligenten und erneuerbaren Materialien für den 3D-Druck und andere lichtbasierte Anwendungen sind in den letzten Jahren zu einem Schwerpunkt in der Polymerforschung geworden. Das Hauptziel dieser Arbeit war die Weiterentwicklung von 3D-Druckharzen im Bezug auf ebendiese Merkmale, sowie die Entwicklung eines neuartigen Harzsystems für den Multimaterialdruck durch die Implementierung orthogonaler Photoreaktionen in den 3D-Druckprozess.

Zum einen wurde die Einführung von Netzwerkdisparität durch die Verwendung von zwei orthogonalen Photoinitiatoren untersucht. In einem Thiol-Acrylatharz mit Acrylatüberschuss wurde die Polymerisation über Thiol-Michael Addition (anionisch) und Thiol-ene bzw. Acrylathomopolymerisation (radikalisch) durch Einsatz zweier verschiedener Lichtquellen gesteuert. Während eine stufenweise Aushärtung mit relativ großem Unterschied in den thermomechanischen Eigenschaften demonstriert werden konnte, wurde die These Widerlegt, dass sich der molekulare Aufbau im Polymer maßgeblich auf die Materialeigenschaften auswirkt.

In einer zweiten, umfassenden Studie wurde ein “dual-cure single-vat” Harz entwickelt, welches eine Vielzahl an thermodynamischen Eigenschaften je nach Art und Länge der Belichtung hervorbringen kann. Es basiert auf der radikalischen Polymerisation eines Thiol-Methacrylat-Monomersystems, welches kovalent gebundene Chalkoneinheiten als dimerisierbare Vernetzer enthält. Die thermomechanischen Eigenschaften können über die λ -orthogonale [2+2]-Cycloadditionsreaktion der Chalconylgruppen während des Drucks oder in der Post-Produktion orts aufgelöst und zeitlich gesteuert werden. Durch den Einsatz definierter Lichtdosen (405 nm) nach der Polymerisation (450 nm) können der T_g und der Elastizitätsmodulus kontinuierlich verändert werden, wodurch nicht nur zwei, sondern eine Vielzahl an unterschiedlichen Materialeigenschaften aus einem Harz gewonnen werden können. Experimente zum Formgedächtnis (shape-memory) sowie zum 3D-Druck mit mehreren Wellenlängen im Makro- und Mikromaßstab zeigen das enorme Potential dieses neuartigen 3D-druckbaren Materials.

Chalconyl und weitere funktionelle Gruppen wurden zuvor auf ihre Reaktivität bei Belichtung mit den gebräuchlichsten Wellenlängen untersucht, wodurch eine Bibliothek an photovernetzbaaren Gruppen erstellt werden konnte. Dies ist nötig, da die tatsächliche Reaktivität unter einer gewissen Lichtquelle oft deutlich von der, durch das Absorptionsspektrum erwarteten, Reaktivität abweicht.

Alle hier durchgeführten Studien zur Untersuchung des Aushärteverhaltens wurden mittels Photo-DSC und FTIR-Kinetik durchgeführt. So konnte auch zur Charakterisierung einer Vielzahl neuartiger Photoinitiatoren und biobasierter Moleküle für die zukünftige Anwendung im 3D-Druck sowie photo-härtenden Beschichtungen beigetragen werden. Insbesondere wurden zwei biobasierte Methacrylate, Eugenylmethacrylat (EM) und Vanillylalkoholmethacrylat (VAM), im Hinblick auf ihr Aushärteverhalten bei verschiedenen Temperaturen untersucht, um die Prozessbedingungen für die Herstellung von beschichtetem Papier zu optimieren. Dabei zeigte sich VAM als das reaktivere der beiden biobasierten Monomere und ist mit einem Wasserkontaktwinkel von 106° , bei Zugabe von 10 Gew.% PDMS-ECEMS,

vergleichbar mit kommerziellen Beschichtungen. Dies macht Vanillylalkoholmethacrylat zu einer geeigneten nachhaltigen Alternative für hydrophobe Papierbeschichtungen. Weiters konnten zinn- und germaniumbasierte, radikalische Typ-I Photoinitiatoren untersucht werden, welche durch ihre verbesserte Absorption im sichtbaren Bereich, sowie ihre reduzierte Toxizität¹ echte energieeffiziente, unschädliche Alternativen zu herkömmlichen Phosphorinitiatoren bilden könnten. Schließlich wurden aminosäurebasierte Monomere mit Methacrylat-, Vinyl- und Alkinfunktionalität für neuartige Harze zur Herstellung von 3D-druckbaren biokompatiblen und bioabbaubaren Gerüststrukturen oder Beschichtungen für den medizinischen Bereich entwickelt.

Abschließend bietet ein umfassender Review Einblick in die aktuellsten Entwicklungen auf dem Gebiet der radikalischen Typ-I Photoinitiatoren. Der Schwerpunkt liegt dabei auf der Aktivierung ebendieser Initiatoren unter sichtbarem Licht und umfasst neben herkömmlichen Phosphorverbindungen auch silizium-, germanium- und zinnbasierte Verbindungen, welche eine umweltfreundlichere und energiebewusstere Aushärtung ermöglichen sollen. Die drei Hauptthemen dieser Arbeit sind somit (i) Photoinitiatoren und ihre Charakterisierung, (ii) biobasierte Monomere für die radikalische Photopolymerisation und (iii) λ -orthogonale Harze für die Verwendung im Multimaterialdruck für intelligente Materialien. Sie alle tragen zu einem besseren Verständnis der verwendeten Harzbestandteile, ihrer Reaktivität, ihres Aushärtungsverhaltens und ihres Einflusses auf die finalen Materialeigenschaften bei, was für die Entwicklung raffinierter Materialien für den 3D-Druck intelligenter Materialien entscheidend ist.

Stichwörter:

Photochemie • Thiol-en Systeme • Orthogonalität • Shape Memory Effekt • Kinetik

Index

— Introduction —	1
— Methodology —	3
Chapter 1	
— Theoretical Background —	4
1.1 Photopolymers	5
1.1.1 Photoinitiators	5
1.1.2 Photoinduced Cycloadditions	14
1.1.3 Correlation Absorption and Reactivity	16
1.2 Thiol-based Chemistry for Polymer Networks	18
1.2.1 Thiol-Michael Reaction	18
1.2.2 Thiol-ene Reaction	18
1.2.3 Differences in Thiol-ene Polymers	19
1.2.4 Thiol-ene Chemistry in Applications	21
1.3 Material Processing with Light	21
1.3.1 Methods for Patterning and Additive Manufacturing	22
1.3.2 Applications	27
Chapter 2	
— Dual Cure Systems —	32
2.1 Network Homogeneity	33
2.2 Absorption Behavior and Reactivity	34
2.3 Library of Photo-Reactive Groups for Dual-cure 3D Printing	35
2.3.1 Abietate	35
2.3.2 Anthracene	36
2.3.3 Chalcone	37

2.3.4	Cinnamoyl	38
2.3.5	Iminostilbene	39
2.3.6	Styrylpyrene	40
2.3.7	Uracil and Its Derivatives	41
2.3.8	Conclusion	43
2.3.9	Materials and Methods	44
2.4	Chalcones as Sequentially Orthogonal Crosslinkers in Multi-material 3D printing of Macro- and Microscopic Soft Active Devices	46
2.4.1	Resin Design	47
2.4.2	Local Control of Network Density to Enable Stimuli-responsive 3D Macrostructures	49
2.4.3	Local Control of Network Density to Enable Stimuli-responsive 3D Microstructures	50
2.4.4	Conclusion	52
2.4.5	Materials and Methods	52
2.5	Utilizing Disparate Polymerization Mechanisms for a Dual-Cure Resin	56
2.5.1	Materials and Methods	57
2.6	Supporting Information Chapter 2	59
2.6.1	Supporting Information Chapter 2.3	59
2.6.2	Supporting Information Chapter 2.4	60
2.6.3	Supporting Information Chapter 2.5	65

Chapter 3

— Photocuring Behavior of Novel Molecules and Resins —		66
3.1	Low Molecular Weight Biomass-derived Methacrylate Monomers for Paper Coatings	67
3.1.1	Photocuring behavior	67
3.1.2	Photopolymerized EM and VAM coatings on paper	69
3.1.3	Conclusion	70

3.1.4	Materials and Methods	71
3.2	Investigation of Reaction Kinetics by Photo-DSC and FTIR Spectroscopy . . .	72
3.2.1	Differential Scanning Photo Calorimetry	72
3.2.2	Fourier-transform Infrared Spectroscopy	75
3.3	Supporting Information Chapter 3.1	78
 Chapter 4		
— Type I Photoinitiators —		80
4.1	Phosphinoxides and Phosphinates	81
4.2	Heavier Group 14 Elements	86
4.2.1	Silicon	86
4.2.2	Germanium	88
4.2.3	Tin	90
4.3	Other Types of Photoinitiators	92
4.4	Summary and Outlook	96
 — Conclusion and Outlook —		98
 Bibliography		101
 List of Abbreviations		119
 List of Figures		123
 List of Tables		128
 Complete List of Publications		129
 Curriculum Vitae.		132

Introduction

Additive manufacturing of polymers has gained increasing interest over the last decades, as its high resolution, fast production speed and ability to generate complex and customized structures pose only some advantages over traditional manufacturing.² Especially lithography-based methods, such as digital light processing or two-photon polymerization, allow precise spatial control over chemical reactions in a solvent-free polymerization.³ Inducing curing only in the illuminated regions comes with high precision on printed parts and provides a possibility for additional chemical selectivity via the choice of wavelength.

Consequently, light-based polymer processing has transitioned from conventional applications, such as coatings, adhesives, inks, microelectronics and dental fillings, to more advanced fields, such as biomaterials for bones and tissue engineering, holography for imaging and data storage and 3D printing of nano-scale parts.⁴ Moreover, photochemistry facilitates the development of smart materials that respond to different stimuli, leading to applications in actuators, sensors, and self-healing materials.⁴⁻¹² These advancements and novel processing opportunities demand a thorough investigation of resin constituents and their optimization towards curing behavior, material properties and bio-compatibility.

The exploration of new molecules and materials as well as the expansion of existing libraries toward new horizons is an exciting path. In the field of type I radical photoinitiators (PIs) there is an increasing interest for initiation under visible light and the tuning of the PI's absorption wavelength. Thereby perfect spectral overlap with the light source is intended for the best initiation performance at low energy input¹³ and λ -orthogonal initiation systems are desired.^{14,15} Looking at phosphinioxides as the work-horse of modern-day photoinitiation, their weaknesses lie first and foremost in their limit of reactivity at low energy wavelengths. Liska et al. rediscovered the class of acylgermanes for photoinitiation purposes^{16,17} which led others to further investigate heavier group 14 elements as phosphorous substituent.¹⁸⁻³⁰ By substitution of the phosphine oxide by a germanium or tin analog the absorption wavelength of the PI could be tuned and the quantum yield increased. Additionally, these PIs possess reduced toxicity¹ and show high potential for the use in biological applications, making curing in the innocuous visible light region possible. In this thesis, a number of additional germanium and tin-based compounds were evaluated upon their suitability as novel photoinitiators.

Thinking of biological and bio-compatible materials, novel monomers are being investigated for the use as scaffolds in implants, but also invitro testing.³¹ While many inks and resins have been found for life-science applications³²⁻³⁴, the current challenge lies in achieving biodegradability while maintaining certain mechanical properties and bio-compatibility.³⁵ Herein, bio-based monomers with methacrylate, vinyl and alkyne functionalities were evaluated for their applicability in novel resins for 3D-printable biological scaffolds or coatings. Bio-based and bio-degradable mono- and polymers should be of great interest considering future tendencies in industry for increased demand on recyclability and the use of renewable feedstocks.

Additionally, the evolution in 3D printing devices has opened up the possibility of implementing more than one light source into the printer-setup. This calls for novel photopolymers, tailored to these new opportunities. Utilizing the difference in energy-input by the set of lamps, specific chemical reactions can be triggered within the resin. Incorporating so-called orthogonal chemistries in the monomer system facilitates the control of mate-

rial properties solely through light. Only a minuscule amount of research was published on two-wavelength printing^{36–39} despite the number of investigated photo-reactive and λ -orthogonal systems^{14,40–44}.

Two concepts of incorporating λ -orthogonality into thiol-(meth)acrylate resins will be discussed in this work. One, where two separate PIs are triggered to build the polymer network in a step-wise manner utilizing the disparate polymerization mechanisms. The second, where additional crosslinks can be formed after the initial polymerization. These crosslinkers are moieties, directly implemented into the polymer network, which can undergo cycloaddition upon irradiation. A vast amount of such moieties is known to undergo photochemical reactions, which could be utilized for photo-crosslinking and the generation of alterations in material properties during and after printing⁴⁰. To select suitable candidates depending on the illumination wavelength, a library of photo-crosslinkable monomers for 3D printing was established.

Photochemistry and its application in 3D and 4D printing is an extremely interesting field with a high impact on an advancing field in industry. The research opportunities are vast and it was impossible to explore all ideas, that came to mind, working with these exciting systems, molecules and devices. Overall, a number of novel molecules were explored for improved curing behavior, reduced toxicity, bio-based polymers and advanced applications in smart materials.

Methodology

This thesis comprises some theoretical as well as experimental parts.

The theoretical literature research was conducted on the platforms *scifinder.com* and *scholar.google.com* with selected keywords according to the research topic. Specifically **Chapter 1** and **Chapter 4** are fully based on published literature with all sources given at the end of this document. The experimental work encompasses organic synthesis, purification methods (liquid-liquid extraction, filtration, column chromatography), photo-induced sample preparation and chemical and mechanical characterization.

Chemical characterization was mainly used for structural confirmation after synthesis (nuclear magnetic resonance spectroscopy) and for tracking of chemical reactions (ultraviolet-visible and Fourier transform infrared spectroscopy). Differential scanning photo calorimetry and photo-rheological experiments were used to track the curing behavior of resins. Testing of the mechanical properties of the resulting polymers was done mainly by dynamic mechanical analysis for macroscopic samples, and atomic force microscopy as well as nano-indentation for extremely small surface modifications.

Sample preparation and additive manufacturing was done by molding, nano-imprint lithography, digital light processing three-dimensional printing and in two-photon mode on a laser scanning confocal microscope.

All chemicals were purchased from TCI, Sigma Aldrich or Fisher Scientific and used without further purification unless stated otherwise.

1

Theoretical Background

photochemistry The branch of chemistry concerned with photochemical reactions.⁴⁵

photochemical reaction A chemical reaction caused by light or ultraviolet radiation. The incident photons are absorbed by reactant molecules to give excited molecules or free radicals, which undergo further reaction.⁴⁵

Photochemistry is not only an important concept in chemistry, but plays a role in a broad range of fields, such as physics, astrophysics, biology, medicine and material science.⁴⁶ A well known photochemical reaction in biology is photosynthesis, converting carbon dioxide and water to organic building blocks with the help of chlorophyll as a pigment to absorb light. Another photo-induced process commonly known, is sunburn, where DNA is damaged by prolonged exposure to UV light. In medicine, light is used to trigger reactions, e.g. in photochemotherapy, to achieve a more local application of certain treatments. In photography, the photochemical reduction of silver salts to metallic silver was used since the 19th century to create a latent image depending on the amount of light received and eventually a photograph.^{47,48}

Spatial, as well as temporal control, paired with the opportunity to select specific reactivity by choosing a certain intensity and wavelength makes photo-induced processes especially appealing for material science. Photochemical techniques, such as 3D printing and microfabrication, are employed to create novel materials with tailored functionalities, including photopolymers, photoresists, and nanocomposites, which are essential for applications ranging from electronics and photonics to biomedicine and energy storage. Within the last 40 years photopolymerization has been used in a number of conventional applications, such as coating, adhesives, inks, microelectronics, dental fillings and additive manufacturing. Many studies have been conducted on further evolving photo-based techniques and materials for more advanced applications, such as biomaterials for bones and tissue engineering, holography for imaging and data storage as well as a variety of 3D printing techniques for stimuli responsive materials and nano-scale parts. Through controlled exposure to light, materials can be patterned with high resolution, enabling the fabrication of complex structures and devices. Furthermore, photochemistry facilitates the development of smart materials that respond to light stimuli, leading to applications in light-driven actuators, sensors, and self-healing materials.⁴⁻¹²

The integration of photochemical processes in material science not only expands the toolkit for material fabrication and design but also opens new possibilities for sustainable and energy-efficient manufacturing practices, underscoring the transformative potential of photochemistry in advancing material technologies.

This thesis will be focused on photo-induced reactions for 3D printing of materials mainly containing (meth)acrylates, -enes and thiols using radical and anionic initiators.

1.1 Photopolymers

The concept of photochemistry in material science is mostly focused on polymers. While thermoplastic polymers consist of linear or branched chains, which allows them to be remelted and reformed over and over again, thermosets are three-dimensionally crosslinked polymers, which do not melt upon reheating. On the aspect of sustainability, this is a drawback and recent studies are looking into ways of recycling and renewable sources for novel monomers.^{49,50} However, thermosets are known for their high thermal stability, chemical resistance, and mechanical strength, making them suitable for high performance applications requiring durable materials.⁵¹ Combining these properties in products with recyclability and alternative feedstocks are two of the main challenges in current materials research.

Generally, using light as a trigger for polymerization comes with a set of advantages over other methods used in polymer chemistry. Photons come with a vast amount of energy, specifically a mole of photons at 365 nm is 130 times higher in energy than the thermal energy (kT) available at 25 °C. Which means, while chemical reaction processes like isomerization or bond breaking do not readily occur at ambient temperature due to a lack of energy available, they are readily initiated upon irradiation and the absorption of photons helping to overcome the activation barrier. Providing this kind of energy at ambient conditions without extensive heating or large amount of solvents makes photopolymerization of growing interest for the enhancement of "greener" processes. Photoinitiators for a variety of wavelengths, with growing interest in visible light sources have been developed, with light emitting diodes (LEDs) as energy efficient counterparts (see **Chapter 4**). Finally, while thermal activation comprises an expanded area (a surface coating or a whole part), illumination can be focused on specific areas, exhibiting not only temporal, but also spatial control over the polymerization process. In a two-dimensional setup, this can be achieved with the help of a photomask, an array of LEDs or a focused beam of light, controlled via a mirror-array, e.g. in micro-chip production, while a consecutive illumination of a set of layers enables 3D printing (**Chapter 1.3**). Additionally, direct 3D printing can be achieved by focusing a laser to specific regions within a resin volume. By using a long wavelength and exploiting the principle of two-photon absorption, structures of high resolution and small feature sizes can be created.⁵²⁻⁵⁵

Using photoinitiators (instead of thermal initiators) at ambient conditions can be of use for monomers with low ceiling temperature, biochemical applications, such as the immobilization of enzymes, for large area applications or for applications where heating is unacceptable, such as dental fillings.⁴

1.1.1 Photoinitiators

Photoinitiators, being special chemical compounds with the ability to form reactive species upon illumination, can start the same kind of reactions as thermal initiators or other catalysts/initiators, however they are non-reactive in their ground state. Only upon illumination with a certain wavelength of light can they produce a reactive species. There must be an overlap in the spectra of the spectral emission of the light source and the absorption spectrum of the reactive molecule (See **Chapter 1.1.3**).

All photoinduced reactions are initiated by the absorption of light energy, i.e. a photon ⁱ, and the subsequent transition from the ground state to its excited state (S_1).

According to the Stark-Einstein law, the absorption of a photon can only occur by a single molecule, also described as a single-quantum process.⁴⁵ Energetic states can be depicted in a Jablonski diagram (**Figure 1.1**), illustrating electronic states within a molecule and indicating transitions as a number of possible processes: 1) photophysical processes, which end up with the original molecule in its ground state, exhibiting radiation (luminescence), heat or transferring energy to another molecule after collision. 2) photochemical processes, such as photodissociation, rearrangement (isomerization), primary bond formation (**Chapter 1.1.2**) or the formation of reactive species by photo-ionization or homolytic cleavage.^{53,56}

If the interaction of a molecule with light results in no net chemical change and can be described as $R + h\nu \rightarrow R^* \rightarrow R$, where R is the ground state molecule and R^* its excited state, it is called a photophysical process. Whereas an overall photochemical reaction pathway can be described as $R + h\nu \rightarrow R^* \rightarrow I \rightarrow P$, with I as a reactive intermediate and P the reaction product.⁵⁷

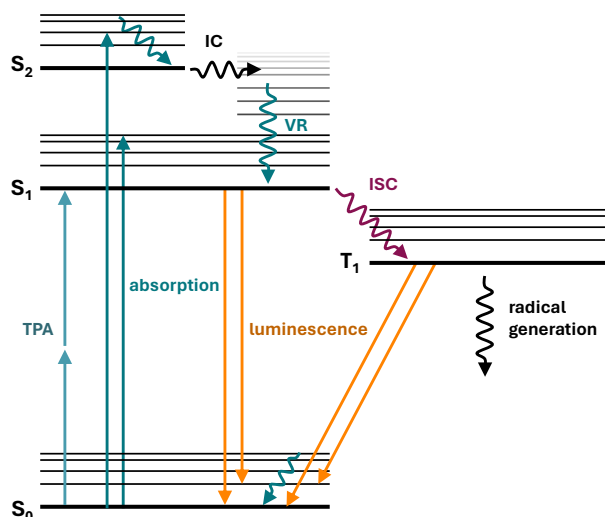


Figure 1.1 – Jablonski diagram. The excited singlet state (S_1) undergoes intersystem crossing (ISC) to a triplet state (T_1), which can lead to various photochemical reactions (e.g., radical generation as presented here). Other processes, that can take place are two photon absorption (TPA) with a virtual intermediate state, internal conversion (IC) to a lower excited singlet state, vibrational relaxation (VR) within the energy levels of one excited state with heat dissipation and the relaxation by luminescence (fluorescence from S_1 or phosphorescence from T_1).

When a photon is absorbed by a molecule in ground state (S_0), an electron is promoted to its excited state (S_1 or S_2) exhibiting the same electron spin. An electron can leave this excited state by fluorescence ($S_1 \rightarrow S_0$) or through internal conversion by heat dissipation, leading to a lower excited state with the same spin and eventually back to its original state S_0 . Additionally, intersystem crossing (ISC) to a triplet state (T_1) is possible, where an electron transitions between two energetic states with different spin multiplicity in a

i **photon**: A particle with zero rest mass consisting of a quantum of electromagnetic radiation. The photon may also be regarded as a unit of energy equal to hf , where h is the Planck constant and f is the frequency of the radiation in hertz. Photons travel at the speed of light. They are required to explain the photoelectric effect and other phenomena that require light to have particle character. The name photon was proposed by Gilbert Newton Lewis in 1926.⁴⁵

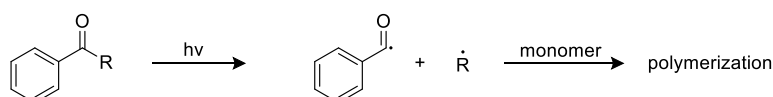
spinprohibited, radiation-free way. Due to their parallel spin and the relatively slow process of ISC, triplet states are typically more stable than singlet states, once formed, making them more easily available for further processes. Relaxation from a triplet state can occur by emission of light (phosphorescence) or by a primary photochemical process, such as the generation of a radical species.^{47,53,58,59}

Polymerization reactions are classified according to the conditions they are conducted in (solvent-based, bulk, thermally initiated, photo initiated etc.) as well as the chemical reaction mechanism involved, which correlates to *I* in the photochemical initiation reaction. Therefore three main types of photopolymerization can be distinguished (1) radical, (2) cationic and (3) anionic, as well as mixed-mode radical and ionic.

Radical Photopolymerization

Radical photoinitiators can be classified into type I and type II, cleavage and H-abstraction, respectively (**Figure 1.2**). type I PIs are likely to be α -hydroxyalkyl ketones, acylphosphine oxides or benzoin derivatives, undergoing α -cleavage upon illumination. However other molecules like trichloromethyl triazine derivatives undergoing β -scission can also produce reactive radicals. The important characteristic is the uni-molecular nature of the initiation process. Whereas in the bimolecular type II PIs, H-abstraction or electron transfer leads to the radical species, which requires the presence of a co-initiator molecule as a hydrogen-donor. While most type II PIs already produce a radical in the first reaction step, these radicals might be too stable to react towards the monomer species due to steric hindrance and delocalization of unpaired electrons, such as ketyl radicals. Upon H-abstraction from a suitable donor, a more reactive radical is produced, which is then able to initiate the polymerization reaction. One of the most prominent type II photoinitiators, especially for visible light applications, is camphorquinone (CQ), used with a variety of (tertiary) amines and thiols as co-initiators.^{4,60–63}

Norrish Type I



Norrish Type II

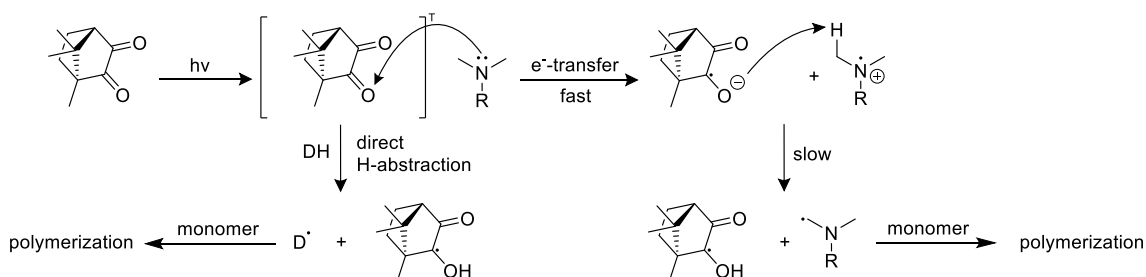


Figure 1.2 – Radical formation upon irradiation. Type I photoinitiators show direct homolytic cleavage. Camphorquinone as a type II photoinitiator, requires a co-initiator to provide an easily available hydrogen for more reactive radical species.^{4,56,64,65}

Posing a bi-molecular process, type II initiator systems face relatively low quantum yields

due to non reactive quenching and the H-abstraction as a rate limiting step. Even though CQ was established as one of the first commercial PIs for visible light applications, research is more and more focusing on type I photoinitiators in this field. Recent developments in the field of type I photoinitiators for visible light applications are explored in chapter **Chapter 4**.

Generally speaking, if a radical is produced via a photo-chemical reaction, a chain reaction is started and polymerization occurs in a monomer mixture (**Figure 1.3**). The polymerization is **initiated**, when the PI radical reacts with the first monomer. Where the rate of the initiation reaction is dependent on the reactivity of the radical towards the monomer. As mentioned earlier, in type II PI systems, a more reactive radical is generated using a co-initiator, as the initial radical itself is too stable for reasonable polymerization rates. **Propagation** of the polymerization reaction happens through the collision of radical species of different chain-lengths with another monomer, thereby extending the chain by one unit. This reaction generates a new radical at the end of the newly added monomer unit, which can then react with another monomer to continue the chain growth. Additionally **chain-transfer reactions** can occur, where the growth of the current polymer chain is terminated, while simultaneously initiating a new chain. The active site (radical) is thereby transferred to another species (monomer, solvent, polymer or chain transfer agent). Chain transfer is a critical mechanism in controlling the molecular weight and molecular weight distribution of the resulting polymer, where chain transfer agents like thiols, disulfides and halocarbons (CCl_4 , CBr_4) are frequently used.⁶⁶ While propagation and chain-transfer reaction keep the number of free radicals constant, the net number of active sites is reduced in a **termination reaction**. Termination occurs on two different pathways, combination and disproportionation, respectively. Combination reactions can be described as a simple head-to-head coupling of two radicals, while disproportionation involves the transfer of a beta-hydrogen from one radical to another. Both termination reactions take place in radical polymerization, however, the predominant mechanism is strongly dependent on the molecular structure of the monomer species.^{47,57,67}

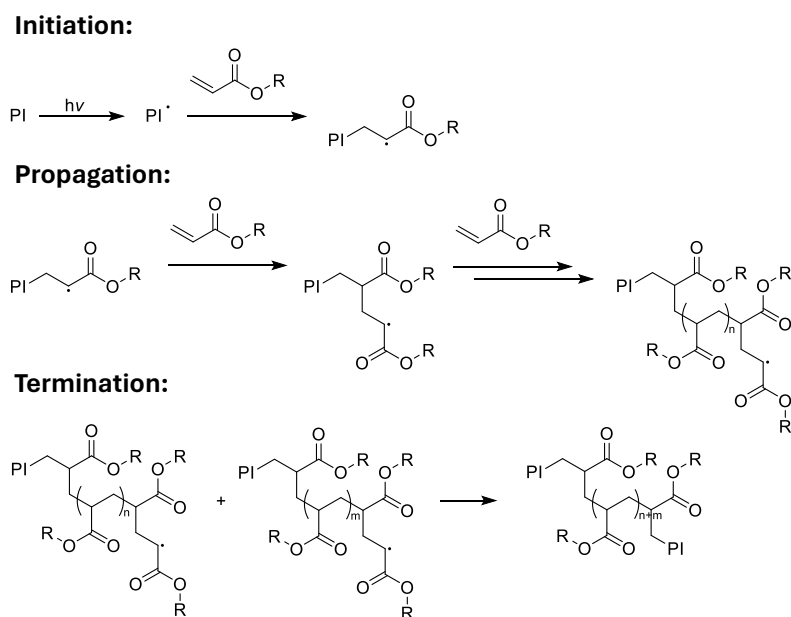


Figure 1.3 – Processes in radical polymerization. Initiation by reaction of a photoinitiator (PI) with an acrylate monomer (as an example). Propagation by repeated addition of a monomer. Termination by recombination of two radical species.

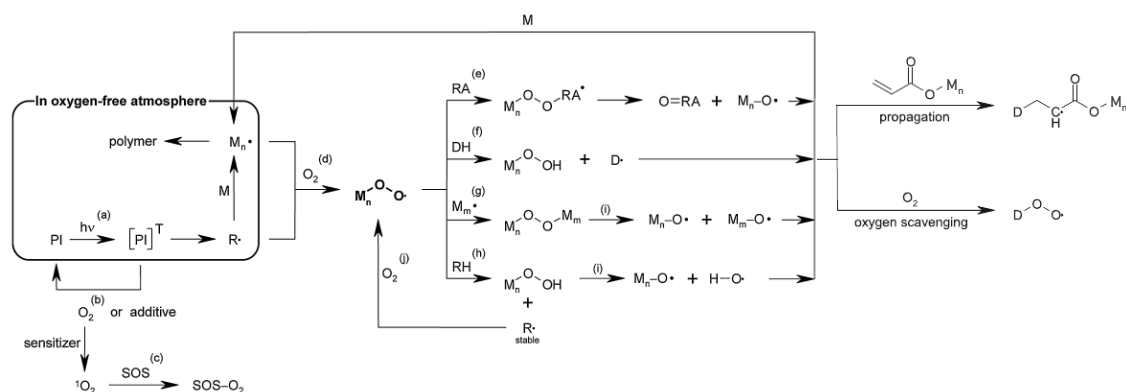


Figure 1.4 – Processes in radical polymerization to prevent oxygen inhibition. (a) initiation stage strategies, (b) quenching of excited PI state, (c) singlet oxygen scavengers (SOS), (d) formation of unreactive peroxy radicals from initiating or propagating radical, (e) reducing agents, (f) hydrogen donors, (g) termination by radical-radical recombination, (h) hydrogen abstraction, (i) peroxide decomposition, (j) scavenging of a molecule of oxygen, and (k) reinitiation of polymerization. Reproduced with permission.⁷⁰

Another way of termination in radical polymerization reactions, especially for (meth)acrylates, is **oxygen inhibition**. When an initiating or propagating radical reacts with oxygen, a peroxy radical is formed. While still a radical species, it has low reactivity towards most monomers, which leads to an incomplete conversion, mostly affecting the surface of a cured part or coating, resulting in tacky products with poor mechanical properties and durability. To overcome oxygen inhibition a number of strategies has been applied (**Figure 1.4**):

1. initiation stage strategies, such as lamination or the use of an inert atmosphere.
2. singlet oxygen scavengers, such as diphenyl furan or dibutyl anthracene, capturing oxygen molecules via [4+2] cycloaddition.
3. reducing agents, such as PPh₃ or other phosphines and phosphites.
4. hydrogen donors, such as amines, thiols and ethers.

Hydrogen donors provide a hydrogen atom, which caps the previously formed peroxy radical, and produces a new radical species, which can re-initiate the polymerization. While reducing the chain length, similar to a chain-transfer reaction, this process will keep the propagation going. Similarly, a reducing agent can be oxidized by the peroxy radical to form a new propagating radical species.^{68–70}

Cationic Photopolymerization

Cationic photoinitiators are also called photo acid generators (PAG), as a protonic Brønsted acid or a Lewis acid is produced upon irradiation followed by a series of decomposition reactions (see **Figure 1.5**). Some examples for PAGs include diazonium salt, diaryliodonium salt, sulfonium salts, iron arene salt, sulfonyloxyketone, and triarylsiloxysiloxane. Polymerization can be initiated directly by the generated acid or upon proton formation by reaction with H₂O or other compounds. Propagation happens similar to a radical reaction, by repeated addition of a monomer onto an active (cationic) site. However, termination reactions are rare. They only occur upon chain transfer to impurities or other species, such as alcohols,

producing a less reactive cation. Once the cationic species is generated, it remains active even when the irradiation is stopped (dark reaction) or the monomer is depleted. The polymerization can be resumed if new monomers are added, therefore, it is also called a "living" polymerization. Due to its slow kinetics compared to radical polymerization, dark reaction is crucial for the final conversion and properties. As depicted in **Figure 1.5**, the cationic species is generated via a radical pathway and most PAGs produce a free radical species as well, therefore also acting as initiators for free-radical polymerization. Typical monomers for cationic polymerization are epoxides, lactones and cyclic ethers as well as nucleophilic vinyl monomers. Some advantages of cationic photopolymerization are oxygen tolerance, low shrinkage due to ring-opening epoxide reactions and the potential use of low viscosity monomers.^{53,71-74}

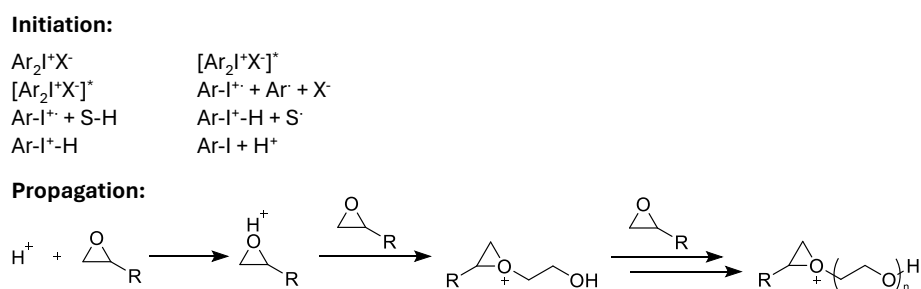


Figure 1.5 – The process of initial acid formation in diaryliodonium salts upon irradiation.⁷⁴ And of propagation in an epoxy resin. Modified and reprinted with permission from⁷⁴. Copyright 1977 American Chemical Society.

Anionic Photopolymerization

While radical photopolymerization is commonly used in industry, cationic polymerization only attributes for 10% of the market share and anionic photopolymerization is rare.⁷⁵ However, some resist materials and desired polymers are not accessible through radical or cationic mechanisms, making anionic polymerization interesting for the control it provides over composition and polymer structure.^{76,77} As anionic photoinitiators, inorganic and organometallic complexes are known as well as ammonium salts, cinnamic acid derivatives, metallocenes and triarylmethyl derivatives. Upon illumination they form a reactive anion, which directly adds to a monomer carbon-carbon bond, setting off the polymerization reaction.⁷⁷ Additionally, photo base generators (PBGs) have been developed by coupling amines and other stronger basic species like guanidine to a photosensitive functional group. Indolines, amineimides, tetraphenylborates, 2-(2-Nitrophenyl)propyloxycarbonyl (NPPOC) and their derivatives have been utilized as such photocleavable protecting groups.⁵¹ The cleavage of a photobase is depicted in Figure 1.6 with NPPOC-TMG as an example. A thereby generated base can initiate the anionic polymerization reaction, similar to the cationic process or act as a catalyst in a polyaddition reaction. However, the strength of the generated base is a critical aspect of whether or not the polymerization can be started. Some typical monomers for anionic polymerization are alcohols and isocyanates, epoxy systems as well as thiol-ene systems for Michael addition.⁵³ Just as their acid counterparts, PBGs ensure the process to be inert against oxygen and to have a living character with a pronounced dark reaction.⁵³

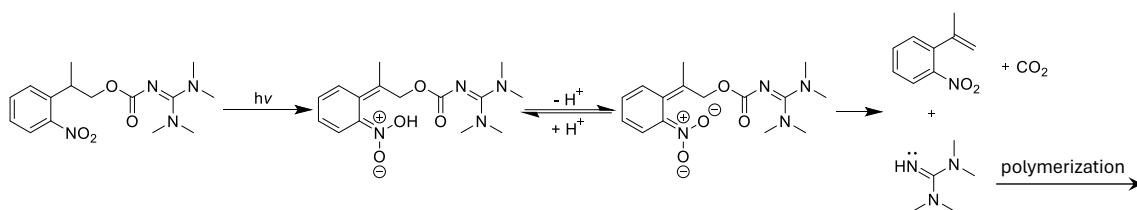


Figure 1.6 – Photo-induced formation of a base for anionic polymerization from NPOC-TMG. Modified and reprinted with permission from⁷⁸.

How to Chose a Photoinitiator

When selecting a photoinitiator, the first thing to consider is which **initiating species** needs to be produced depending on the monomer or monomer mixture used. As discussed earlier, there are free-radical, anionic and cationic photoinitiators available. Table **Table 1.1** gives a short overview of monomers and possible polymerization pathways. However, some of those PIs do not only generate a single species but are designed to initiate both radical and ionic polymerization, such as some carbazole-based compounds developed by Al Mousawi et al.⁷⁹ or they produce an ion via a radical intermediate or sideproduct.^{80,81} The direct reaction of the radical within the resin cannot be excluded and would need the assistance of other additives⁸² to be eliminated. Therefore, if species or reactive groups susceptible to the other mechanism are present, the PI has to be chosen with even more care. Zhang et al. investigated several strong base generating PIs with and without sensitizer and found, that the non-sensitized systems showed pure base-catalyzed thiol-Michael activity.⁵¹

Further, the reactivity of the photoinitiator has to **match the light source**. As described earlier, to even initiate any kind of reaction within a photoinitiator, a photon has to be absorbed and an electron has to be promoted to an excited state. In order for this to happen, the energy of the absorbed photon has to match the disparity in energy between the ground state (S_0) and one of the excited states (S_n). To give a clue about light-matter interactions of the PI, an absorption spectrum can be recorded. The PI is thereby dissolved in a suitable solvent, with a low cut-off wavelength (e.g. acetonitril, chloroform) at a concentration of about 0.01-0.1 mM. A laser subsequently irradiates the sample, scanning through a range of wavelengths, and the depletion of light intensity by wavelength is detected on the other side of the sample. Hence it directly detects the interaction of molecule with light of a certain energy, depicted as more or less separated absorption bands and a full absorption spectrum. On a molecular level, each of these absorption bands correlates to an orbital transition of an electron. While $\sigma \rightarrow \sigma^*$ and $n \rightarrow \sigma^*$ transitions need a lot of energy, absorbing strongly in the region 100-250 nm, $\pi \rightarrow \pi^*$ and $n \rightarrow \pi^*$ electron transitions can absorb up to to IR region (**Figure 1.7, Table 1.1**). The height (extinction coefficient) of an absorption band correlates to transition moment. Its appearance as a band rather than single lines is due to the vibronic and rotational sub-levels involved.

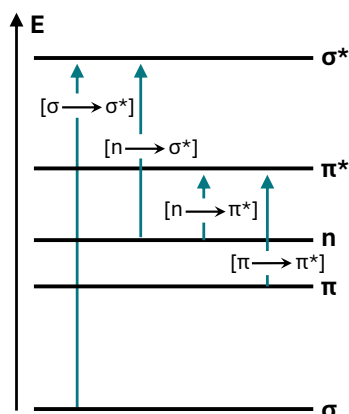


Figure 1.7 – Scheme of possible orbital transitions upon photon absorption. Reproduced and adapted with permission from⁵⁶.

Table 1.1 – Correlation between orbital electron transition and absorption region. Reproduced and adapted with permission from⁵⁶.

Electron transition	Absorption region [nm]
$\sigma \rightarrow \sigma^*$	100-200
$n \rightarrow \sigma^*$	150-250
$\pi \rightarrow \pi^*$	
isolated π -bonds	180-250
conjugated π^* -bonds	220-IR
$\sigma \rightarrow \sigma^*$	
isolated groups	220-320
conjugated segments	250-IR

As depicted in **Table 1.1**, the molecular structure plays a vital role on the energy needed for certain transitions. While an isolated π -bond shows between 180 and 250 nm, conjugated systems can red-shift the absorption tremendously.⁵⁶

In some photocurable systems, as the ones investigated in this thesis, it is necessary to utilize two distinct photochemical processes initiated independently from each other. This perfect state of independence is called **orthogonality**. The two rules for orthogonality postulate, that (1) there must be a wavelength or wavelength region only absorbed by compound A and a second wavelength region solely absorbed by compound B (**Figure 1.8 A**). The order of irradiation does not matter and a certain reaction is solely triggered by its corresponding wavelength illumination. (2) While two reactions are (separately triggered) ongoing within the system, no cross-over reactions between chromophors are possible. Neither the excited states nor the reaction products or intermediates interfere with the second parallel reaction and no crossover reaction between compound A and B occurs.^{40,83}

Until now, truly orthogonal systems are scarce, as lower wavelength regions always show more broad absorption due to higher energies available to the system for excitation and subsequent reactivity. Even if the absorption spectrum of a compound has a minimum and the reactivity is extremely low, orthogonality often has to be supported by kinetic factors. If there is a huge difference in quantum yield between two processes and illumination is short, there will be hardly any change in one reaction whereas full conversion can be observed on another.^{40,83} Bialas et al. have created a system where o-methyl benzaldehyde dimerization can be triggered independently from [2+2] cycloaddition of styryl pyrene at 330 nm.⁸⁴ At 330 nm only the cis-trans isomerization of styrylpyrene, as well as the cyclobutane cleavage (cycloreversion) of the photodimer are active, leading to the formation of a photostationary state and suppressing notable conversion of the dimer. Additionally, no cross-reaction between the two molecules was found. Other truly orthogonal systems comprise photoswitches⁸⁵, ligation reactions⁸⁶ and inhibition reactions⁸⁷. Most other studies have found relative differences in reactivity⁸⁸, but lack precision. Scott et al. explored a system for precise, high resolution laser writing.⁸⁷ In a sophisticated optical

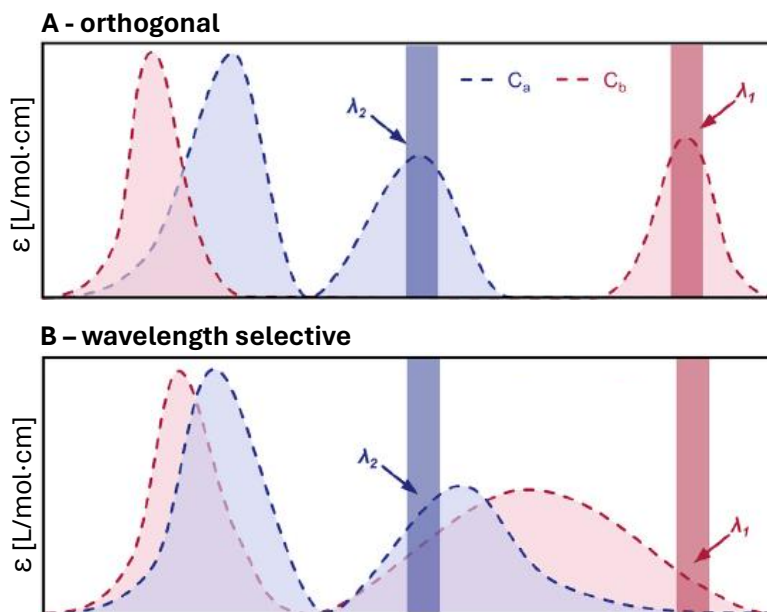


Figure 1.8 – Absorption in a mixture of two chromophores C_A and C_B . (A) fully orthogonal system with two separate wavelengths for activation. (B) wavelength selective system with sequential activation of C_B before C_A . Reused with permission from⁴⁰.

setup, they utilized the inhibiting effect of thiuram disulfide (TED) activated at 364 nm to suppress polymerization by camphorquinone (CQ) at 473 nm. The UV-cleavable TED produces dithiocarbamyl radicals, that recombine with propagating polymer chains, thereby end-capping it and ending the polymerization.

There are more and more studies on sequentially orthogonal systems, utilizing the lower energy wavelength first, to evade problems of overlapping absorption spectra. This behavior is sometimes also described as wavelength-selectivity (**Figure 1.8 B**). While one reaction can be triggered independently, another wavelength starts both reactions simultaneously. The applications range from photoresists^{89,90}, post-functionalization⁹¹ and 3D-printing³⁹ over photoswitches^{92,93} to medical applications^{94,95}. A more detailed discussion on wavelength selective reactions, especially for 3D printing applications, will be given in **Chapter 2**.

Besides these three major points for initiator selection, especially important in novel initiating systems and research, some other factors play a mayor role for their application in industry. The efficiency of the polymerization, for instance, is directly influenced by the **cure speed** of the PI, making rapid cure essential for high-throughput environments like inkjet printing and 3D printing. Yet, beyond mere speed, considerations such as the PIs **photobleaching behavior** and its tendency to cause **yellowing** become critical for the depth of cure and the final product's optical clarity and color stability, respectively, such as in coatings and dental composites. Both of these effects originate from photochemical cleavage reactions. While photobleaching occurs as the chromophore (absorbing in the visible spectrum) is broken down, yellowing can happen due to the build up of side products of said reaction with higher wavelength absorptivity.^{96,97}

Moreover, the economic aspect of commercial **availability and cost** determine the overall viability of the process, particularly in large-scale operations. Storage stability ensures the retention of effectiveness over time, thereby guaranteeing reliability. The basic, but crucial property of **solubility** of the PI in a certain monomer system ensures not only the

feasibility of the process but also the uniformity and consistency of the cure. Therefore several derivatizations of known PIs have been made to obtain a liquid, instead of a solid PI.^{98,99} In contexts where product safety and integrity are paramount, such as in food packaging or medical devices, the PIs **toxicity**, **odor** and potential for **migration** poses significant concerns, necessitating choices that minimize such risks.

In essence, the selection of a photoinitiator is a delicate balance of these diverse factors, requiring a holistic approach to match the specific nuances of each application. This often involves iterative testing and refinement to achieve an optimal blend of performance, safety, and cost-effectiveness, ensuring that the chosen PI not only meets but exceeds the application's requirements.⁴

1.1.2 Photoinduced Cycloadditions

Cycloaddition reactions are bimolecular reactions involving two reaction partners, that form a ring structure with two new σ -bonds upon re-organization of π -electrons.¹⁰⁰ To classify such reactions, the number of π -electrons of both reaction partners is stated as in [2+2], [2+4] or [4+4] (**Figure 1.9**) with some well-known examples being the Paterno-Büchi or Diels-Alder reaction. The discovery of this special [2+4] cycloaddition as a versatile tool in carbon-carbon bond formation even led to Otto Diels and Kurt Alder receiving the Nobel Prize in Chemistry in 1950.¹⁰¹

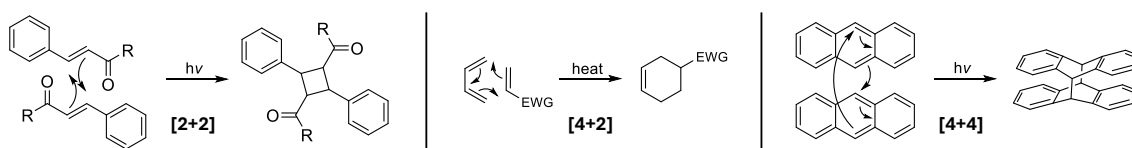


Figure 1.9 – Different types of cycloaddition reactions according to the number of electrons involved.¹⁰⁰

Another Nobel Prize in Chemistry, in 1981, was awarded in this field, as Woodward and Hoffmann stated that orbital symmetry needs to be conserved during pericyclic reactions, which is now commonly known as the Woodward-Hoffmann rules (**Figure 1.10**).

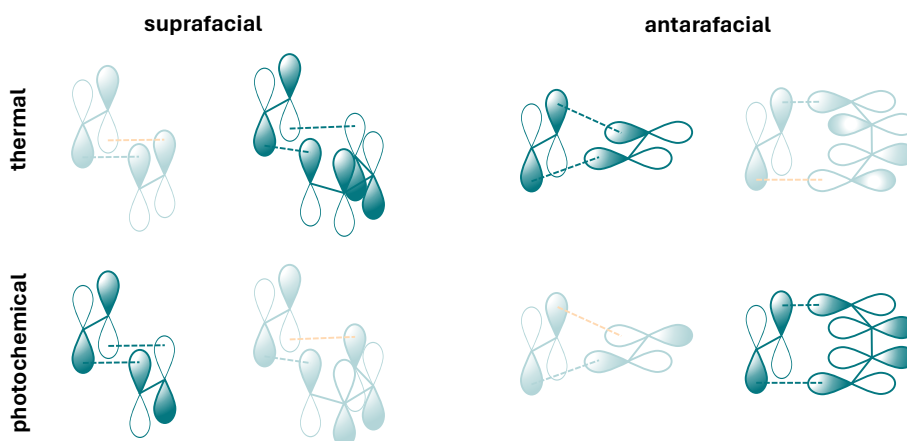
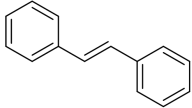
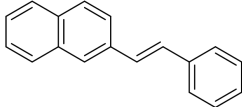
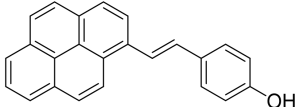


Figure 1.10 – Orbital illustration of the Woodward-Hoffmann rules for cycloadditions with the LUMO on the left and the HOMO on the right of each pair. While bonding is possible if both orbitals show bonding overlap (blue dotted lines), bond formation is not possible if one orbital overlap is antibonding (orange dotted line). Forbidden reactions are greyed out. Adapted from^{100,102}.

Table 1.2 – Upon extension of the conjugated system, the absorption of a molecule can be shifted to higher wavelengths as the energy gap for photon absorption is reduced.

Molecule structure	Name	Absorption maximum [nm]
	stilbene ^{107,108}	294
	naphthylstilbene ¹⁰⁹	316
	styrylpyrene ³	375

When looking at the orbital structure, the highest occupied molecular orbital (HOMO) of one reaction partner and the lowest unoccupied molecular orbital (LUMO) of the other can be described as the frontier molecular orbitals (FMO) involved in the reaction. For a new bond to be formed, the orbital overlap needs to be bonding. In a face-to-face arrangement (suprafacial), which is the energetically more likely state for small π -systems opposed to antarafacial, this bonding overlap happens for systems with $4n + 2\pi$ -electrons in the ground state. As an example, a diene (4 π -electrons) and a dienophile (2 π -electrons) can undergo cycloaddition in a thermal reaction (Diels-Alder reaction), as their FMO overlap in a bonding way, forming two new σ -bonds. On the contrary, a [2+2] cycloaddition is forbidden by the Woodward-Hoffmann rules, as the LUMO and the HOMO of the two 2 π -electron-reactants only form one bonding, but one anti-bonding orbital overlap. However, as a photon is absorbed and an electron is excited to a higher energy state, the anti-bonding LUMO is suddenly occupied, making it the new HOMO. With an anti-bonding HOMO, the symmetry of the FMOs changes drastically, basically reversing the before-mentioned rules. Hence, $4n$ π -electron systems (e.g. [2+2] or [4+4]) in a suprafacial arrangement readily react in cycloaddition reactions upon photon absorption.¹⁰³

For a cycloaddition to happen between two molecules with the same amount of π -electrons involved, first the absorption of a photon must take place. Hence, the absorption spectrum of (at least) one of the compounds has to match the irradiation wavelength and result in a reactive, excited state. Besides cycloaddition, the cis-trans isomerization is a competing reaction from this excited state. Next, there needs to be spatial proximity between an excited bonding site and one in its ground state, which can make the reaction slow or even unlikely at low concentrations of active sites.⁵⁶ A number of C=C bond containing compounds can undergo light-induced cycloaddition, including (cyclic) α -diketones, carbonyl groups, maleimides, alkynes and alkenes, especially in conjugated systems.^{104–106} The conjugated system is thereby crucial to decrease the energetic gap towards an excited state and red-shift the activation wavelength (**Table 1.2**).

Many photo-cycloaddition reactions have been discovered in the mid 20th century, such as the reactivity of coumarin¹¹⁰, acenaphthylene^{111,112}, indene, furan or maleic acid anhydride¹¹¹ and even some photosensitive polymers have already been developed. Minsk, Robertson et al. discovered that cinnamic acid esters of poly(vinyl alcohol) and of cellulose become insoluble by UV irradiation and investigated the wavelength sensitivity and the

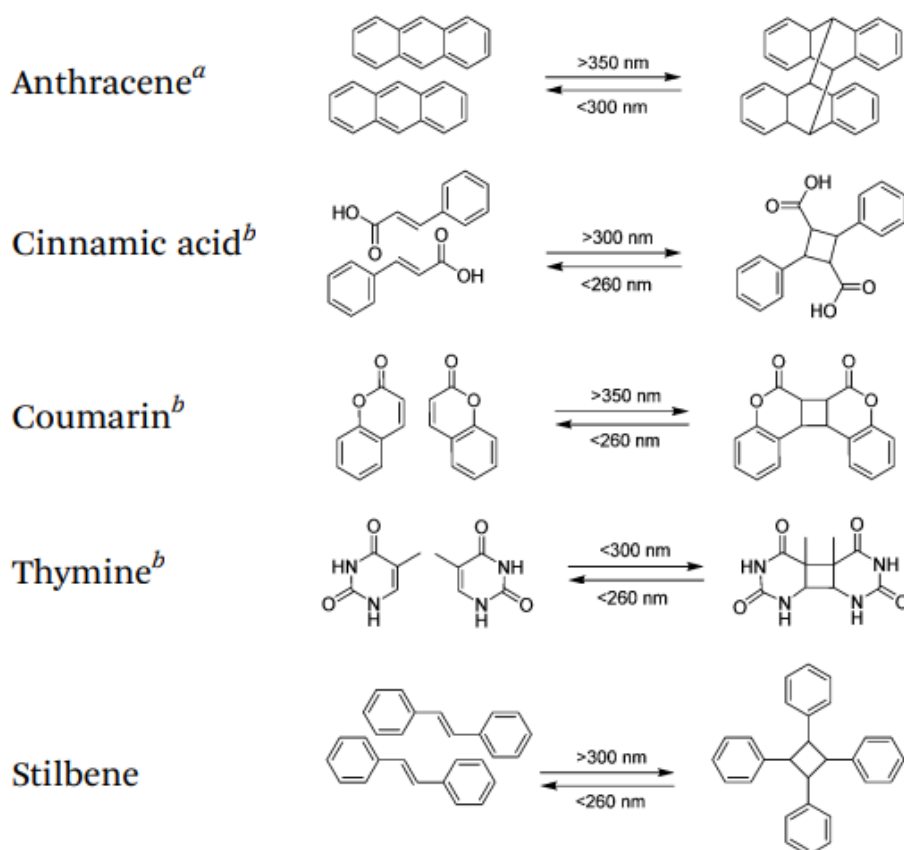


Figure 1.11 – Some moieties capable of undergoing dimerization via photo-induced cycloaddition as well as cleavage upon cycloreversion.¹⁰⁷ ^a Undergoes $[4\pi + 4\pi]$ -cycloaddition. ^b Undergoes $[2\pi + 2\pi]$ -cycloaddition.

influence of several additives and solvents.^{113,114} Tanaka not only showed that poly(vinyl cinnamylideneacetate) is crosslinkable above 300 nm, but also showed the reversible nature of the $[2+2]$ cycloaddition in cinnamoyl moieties upon 254 nm irradiation.¹¹⁵ Tsuda, prepared Poly(vinyl 2-furylacrylate) showing an absorption peak at about 297 nm and photodimerization of the side groups upon UV-irradiation.¹¹⁶

Over time more and more photocrosslinkable groups have been introduced into polymeric systems (**Figure 1.11**), mainly to target the tailored transition from soluble to insoluble. By increasing the size of the conjugated π -electron system efforts were made to increase the light sensitivity and shift the absorption wavelengths to progressively higher regions (red-shift). A PVA, bearing low molar amounts of stilbazolium groups, showed long-wavelength absorption at 364 nm¹¹⁷, dibenzazepine was successfully crosslinked at 365 nm^{118,119} and styrylpyrene at wavelengths 405 nm and longer³, with the search for even higher absorptivities not yet completed.

1.1.3 Correlation Absorption and Reactivity

The nature of an absorption spectrum as a graphical representation of the photon absorption behavior of a molecule implies it to be a direct translation towards the reactivity of said molecule. However, in recent years more and more photoreactions have been found to pro-

ceed at higher wavelengths than they should according to their absorption spectrum.^{84,120} Barner-Kowollik and his group have therefore started to investigate this behavior in more depth and created a methodology for the recording of so-called "action plots". Action plots should depict not only the absorption behavior of a molecule, but also its reactivity towards a certain, photo-induced reaction. A stock solution of the photoreactive compound or mixture is produced and separate samples are independently subjected to monochromatic light from a tunable laser or an LED with narrow emission spectrum. An identical, stable number of photons is delivered to the sample at each wavelength. After illumination the sample is analyzed in terms of conversion via UV-Vis absorption spectroscopy or nuclear magnetic resonance (NMR) frequency changes. The initial absorption spectrum as well as the conversion at each wavelength are plotted (**Figure 1.12**).

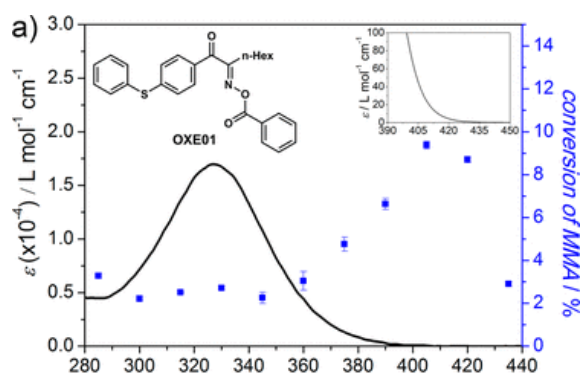


Figure 1.12 – Action plot for the polymerization reaction of MMA with a novel photoinitiator (OXE01). Showing the absorption spectrum of OXE01 as well as the wavelength-dependent conversion of MMA. Reproduced with permission from¹²¹. Copyright 2017 American Chemical Society.

In most action plots a red-shift in reactivity versus absorption spectrum is visible, sometimes subtle, other times monumental with shifts of up to 100 nm.¹²² While a complete understanding of the mismatch remains elusive, there have been a number of theories explored to explain this effect.

Fermi's Golden Rule is a principle stating that "the stronger the overlap in the wavefunctions of the respective electronic states, the higher the probability of transition and hence the transition rate".¹²³ This correlates to the magnitude of absorption peaks as the relative likelihood of a transition occurring at each wavelength, and the width as the range of vibrational and rotational energies per excited state. Emanating from absorption, a number of paths for photochemical processes is possible and simple absorption spectroscopy does not help gaining quantitative information on relaxation pathways and lifetimes. However, the lifetime of certain excited states is essential for subsequent reactivity. While singlet states are usually short-lived triplet states have a longer lifetime and are particularly important for many chemical reactions. Also, relaxation pathways have different quantum yields, so that the ISC pathway from T_1 to S_1 could be more efficient than from another excited singlet state (S_n). Therefore, a lower energy excitation (to a lower excited singlet state) could give rise to a faster and more efficient reaction. The "hot-spectra" hypothesis is yet another potential factor as absorption spectra of certain molecules obtained in the gas phase have shown to be red-shifted.¹²⁴ While irradiation happens at ambient temperatures, internal conversion and vibrational relaxation processes ($S_1 \rightarrow S_0$) can lead to a rise of temperature on a molecular level. All of these processes contribute to the ongoing process of trying to understand the discrepancy of absorptivity and reactivity of photoactive molecules, not solving the question completely, but giving valuable insights in processes beyond simply

photon absorption.¹²²

1.2 Thiol-based Chemistry for Polymer Networks

The thiol-ene reaction is regarded as a prominent instance of click chemistry. It involves the reaction between a thiol and an alkene (ene), yielding an alkyl sulfide (thioether). The hydrothiolation of the vinyl group, as its fundamental process, was initially documented in 1905¹²⁵. This reaction pathway can be broadly categorized into two mechanisms: (1) base/nucleophile-initiated, also known as thiol-Michael reaction, and (2) radical-mediated thiol-ene reactions.

1.2.1 Thiol-Michael Reaction

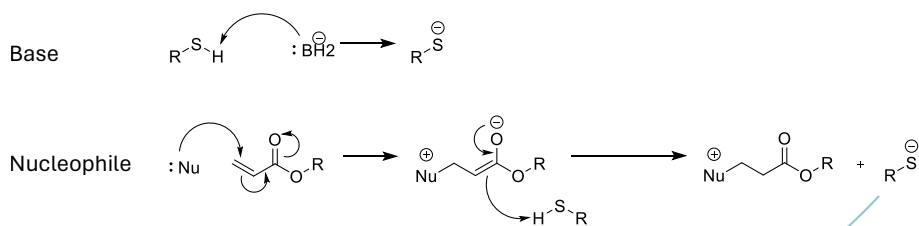
The thiol-Michael reaction, is the base- or nucleophile-initiated reaction between a thiol (-SH) and a C=C double bond. It is part of a group of addition reactions discovered by Arthur Michael in 1887¹²⁶ where a negatively charged enolate intermediate is formed upon strong nucleophilic attack on the β -carbon of an α, β -unsaturated carbonyl followed by a deprotonation (re-gaining the catalyst) to yield the Michael adduct. Via this synthetic route the formation of C-C, C-N, C-S, C-O and other C-X bonds is possible.¹²⁷ The thiol-Michael addition, specifically, has first been reported by Allen et al. in the 1960s.¹²⁸ Thiol-Michael addition can be initiated by a number of catalysts, such as strong bases, weak organo-bases (e.g. Et₃N), nucleophiles such as phosphines, Lewis acids, molecular iodine, metals and organometallics.^{127,129,130} The use of a photocleavable protecting group on a base (photo base generator, PBG), makes it additionally susceptible to irradiation and possible to being used in photo-based, spatially controlled processes. In a first step, the negatively charged thiolate anion is formed by interaction with either a base or a nucleophile, which can further react (as a Michael donor) with an activated, electron deficient C=C (Michael acceptor). The generated enolate anion then abstracts a proton from another thiol, regenerating the thiolate anion to continue the propagation reaction (**Figure 1.13**).

The prerequisite of electron deficiency in the double bond makes the thiol-Michael addition slightly less versatile than the radical-mediated thiol-ene reaction. However, the abundance of such reactants is high and includes (meth)acrylates, fumarate esters and maleimide derivatives. The overall reactivity depends on the strength and concentration of base catalyst, the pK_a of the thiol, steric accessibility of the thiol, solvent polarity and the extent of electronegativity of the C=C bond.¹³¹ Thiol-Michael addition can happen in the dark if traces of base are present. This drastically reduces shelf life of some thiol-ene formulations and increases the need for stabilizers. In a polymerization via thiol-Michael addition, the polymer grows following a step-growth mechanism.

1.2.2 Thiol-ene Reaction

The radical-mediated thiol-ene reaction can operate through a photochemical pathway applying a PI.¹³² Initiation begins with the formation of a thiyl radical by hydrogen transfer onto the initiating fragment. Some photoinitiators have been developed, directly forming a thiyl radical upon cleavage of the photosensitive thio-formate group, skipping this initial

Initiation:



Polymerization:

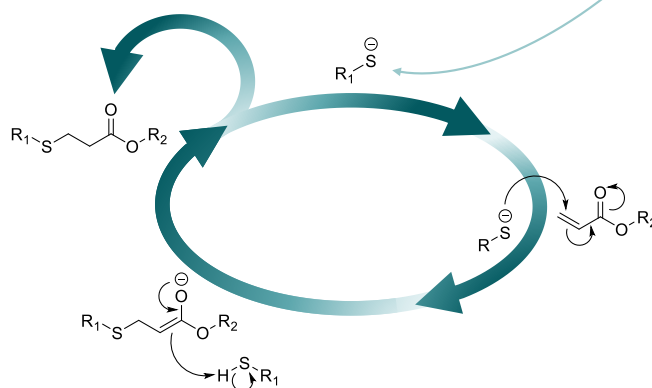


Figure 1.13 – Schematic representation of the reaction mechanism in initiation and during thiol-Michael addition polymerization reaction.

step.¹³³ The thiyl radical consequently attacks the unsaturated double bond, yielding an intermediate carbon-centered radical. Chain transfer by hydrogen abstraction from another thiol results in the final formation of the addition product, with anti-Markovnikov orientation.^{57,131} Just like the thiol-Michael addition reaction, the radical thiol-ene process follows a step-growth mechanism. In most thiol-ene systems the final product does not differ between those two reaction mechanisms, however, the kinetics and the nature of the reaction itself are profoundly different. Additionally, it is worth mentioning, that some enes, such as acrylates and methacrylates, can readily undergo homopolymerization in the presence of radicals. Thereby a newly created, carbon-centered radical adds to another double bond in a radical chain-growth reaction, instead of undergoing thiol-hydrogen abstraction, resulting in a mixed-mode polymerization (**Figure 1.14**).¹³⁴

The general reactivity of an ene towards a thiol-ene reaction increases with electron density of the double bond. Hoyle et al. put a number of reactants in the following order: norbornene > vinyl ether > propenyl > alkene = vinyl ester > N-vinylamide > allyl ether = allyl triazine = allyl isocyanurate > acrylate > N-substituted maleimide > acrylonitrile = methacrylate > styrene > conjugated diene.¹³⁵ Reactivity is effected by steric effects, electron density, ring strain (in norbornenes) and high stability of intermediate carbon centered radicals, which interrupt the propagation by hydrogen abstraction. Another study on thiol-ene reactivity calculated the order as shown in **Figure 1.15**.

1.2.3 Differences in Thiol-ene Polymers

As mentioned earlier, both, the thiol-ene and the thiol-Michael mechanism, are considered "click" reactions. Kolb, Finn and Sharpless introduced the term "click chemistry" in 2001, defining it as a number of "nearly perfect" reactions. They described a set of criteria for

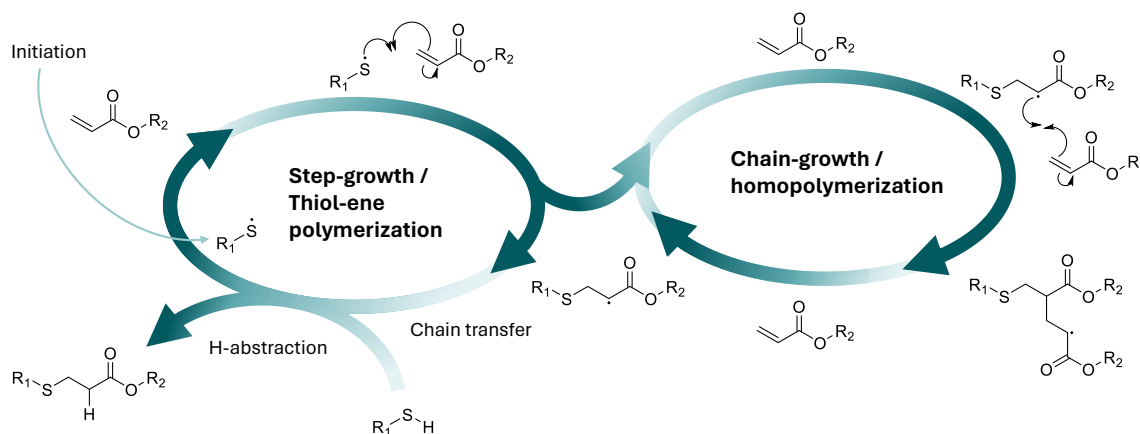


Figure 1.14 – Radical initiators do not only start thiol-ene addition polymerization, but also simultaneous (meth)acrylate homopolymerization. This regime is called "mixed-mode" polymerization.

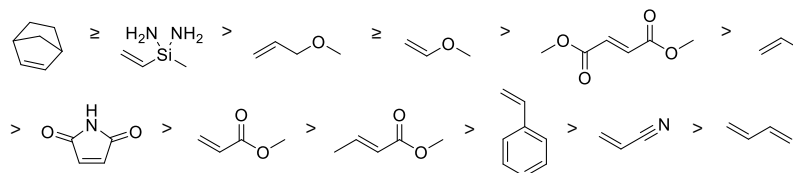


Figure 1.15 – Predicted order of reactivity of different thiols toward thiol-ene addition reaction. Reproduced with permission from¹³⁶. Copyright 2012 American Chemical Society.

reactions of small molecules to belong in this category. *"The reaction must be modular, wide in scope, give very high yields, generate only inoffensive byproducts that can be removed by non-chromatographic methods, and be stereospecific (but not necessarily enantioselective). The required process characteristics include simple reaction conditions (ideally, the process should be insensitive to oxygen and water), readily available starting materials and reagents, the use of no solvent or a solvent that is benign (such as water) or easily removed, and simple product isolation. Purification—if required—must be by non-chromatographic methods, such as crystallization or distillation, and the product must be stable under physiological conditions."*¹³⁷

The thiol-ene and the thiol-Michael reaction carry many of those attributes, such as high yield, only small amounts of initiator that are necessary, reactivity in bulk (solventless), no need for purification, reactivity at ambient conditions (room temperature, at air and moisture), yielding a single regioselective product and a wide range of thiols and enes, that are commercially available.¹³⁴

But not only their convenient reaction conditions and kinetics, but also the resulting material properties are intriguing. While classical radical-mediated polymers from (meth)acrylates have been readily used in coating, contact lenses and photolithographic processes, especially oxygen inhibition and shrinkage stress have been major problems in some applications.¹³⁴ Adding multifunctional thiols to multifunctional (meth)acrylate systems, yielded cross-linked polymers with high conversion and reduced shrinkage stress experienced during the polymerization process. This can be explained, as a late gelling point as the step-growth mechanism increases the mobility, reduces diffusion limitations and offers increased freedom for molecular movement up to high conversions. A highly homogeneous network is formed due to the stoichiometric reaction between functional groups and a narrow chain length distribution. Looking at the glass transition range (T_g), a

polymer from pure (meth)acrylate could have a T_g range from around 200°C, while the addition of thiols narrows the transition range to 30-50°C.¹³⁴ A narrow T_g is especially important for areas of energy absorption and smart materials, where the direct addressing of a specific region through temperature is key in shape memory materials. Additionally, with only a small percentage of thiol added, the oxygen inhibition is overcome as peroxy radicals readily react further with thiols, re-producing reactive thiyl radicals.

1.2.4 Thiol-ene Chemistry in Applications

Since the discovery of thiol-ene click reactions, the applications in small molecule synthesis and polymeric applications are manifold and reach from the field of bio-chemistry and medicine to micro-fluidics and optics. In small molecule synthesis, Kuroki et al. used the relatively weak thioether bond, formed during thiol-ene reaction, as a thiol protecting group in synthesis. While the protection was specific due to the nature of the click reaction, the protecting group was readily cleaved upon treatment with a strong base (tert-potassium butoxide).^{127,138} Using thiol-Michael addition to produce a linear polymer, stable up to 200°C, Vandenberg et al. also took advantage of the weak thioesters formed, for the degradability of their material in NaOH and more physiological conditions (phosphate buffer).^{127,139} Using the same principle, Hubbell et al. pioneered in using thiol-Michael addition in hydrogels to achieve hydrolytically or enzymatically degradable materials for drug release over several days.¹⁴⁰ Again in the field of hydrogels, Anseth et al. investigated mixed-mode thiol-acrylate hydrogels for their potential as tissue-engineering matrices and the implementation of certain peptides into the system for targeted cell behavior.^{127,141}

Many post-polymerization modifications have been done on surfaces, especially in lithographic patterning processes utilizing the accessibility of this click reaction by light to alter surface wettability, adhesion induced protein attachment and change sensory responses.^{134,142} Jonkheijm et al., for examples, showed the spatially controlled immobilization of biomolecules (biotin), after masked illumination of a thiol-functionalized surface.¹⁴³ Boyer et al. drastically changed the surface properties of TiO₂ nanoparticles by incorporation of oligo(ethyleneglycol) methacrylate onto the before thiol-functionalized surface. By introducing those polymeric chains onto the nanoparticles, it did not only increase their water solubility, but also reduced the cytotoxicity towards specific cells, confirming its importance in nanomedicine applications.¹⁴⁴

It can be said, that the thiol-ene/thiol-Michael chemistry, with its "click" character, is already in use in a countless number of research areas and applications. The simplicity of the reaction, combined with the capability of photoinitiation, poses enormous advantages, explains the rapid growth of interest and is expected to fuel further advances into novel and emerging applications.^{127,131,134}

1.3 Material Processing with Light

Using light for material processing opens up unique possibilities especially in terms of precision and design freedom. Photolithography is a fundamental technique in semiconductor manufacturing, utilizing light to transfer patterns onto substrates with high precision for microelectronics. Nanoimprinting and 3D printing extend this concept to very small and

three-dimensional structures, offering unprecedented versatility in manufacturing complex geometries with enhanced efficiency and resolution. These processes outline the potential of light-based methodologies across multiple industries, from electronics to biomedical engineering.

1.3.1 Methods for Patterning and Additive Manufacturing

Photolithography

Photolithography is the process to transfer a pattern onto a substrate using light. A photo-sensitive material, also called photoresist, is selectively exposed to light, either by using an optical mask to shade certain areas or by direct, selective irradiation by laser or electron beam. Irradiation triggers some reaction in the photoresist, which can help either its crosslinking (negative resist) or its degradation (positive resist). Subsequent to irradiation, the non-crosslinked material can be removed to expose the desired pattern on the surface and potential further steps, such as etching or material deposition, can only be performed on the exposed areas. Photolithographic patterns are either used as templates for subsequent surface patterning, as described above and as traditionally done in semiconductor production, or used as stand-alone patterns. Therefore, they have found applications in the production of LEDs, photonic crystals, liquid-crystal displays, microarrays of cells, sensors, activators and devices for data storage.¹⁴⁵

Historically, the evolution of photolithography involves a continuous effort of decreasing the exposure wavelength to maximize resolution. In integrated circuit designs, this allows for smaller features, less power consumption and lower cost.^{146,147} Since the 1960s light sources for lithography shifted from mercury vapour lamps (g-line at 435 nm and i-line at 365 nm), to excimer lasers at 248 nm and argon fluoride lasers at 193 nm to the most recent application of a laser-pulsed tin droplet plasma to emit extreme UV light at 13.5 nm. This new technology enables patterning in the extremely low nm region (3-5 nm).¹⁴⁸⁻¹⁵⁰ Additionally, optical and chemical systems have been designed to reduce the developing region and reduce energy demand and cost.^{151,152} Leggett has shown how scanning near field optical microscopy (SNOM) can be used for lithography, pushing the spatial resolution significantly beyond the limits of conventional wavelength-limited photochemical methods.¹⁵³ McLeod et al. have developed a two-color irradiation scheme, utilizing optics in combination with orthogonal photochemistry to achieve sub-100 nm resolution while employing inexpensive continuous wave diode lasers (single photon absorption) and very high write velocities.⁸⁷

Nanoimprinting

Nanoimprinting or nanoimprint lithography is a method to transfer micro- to nano-scale patterns onto a polymer surface. A negative mould is pressed against a softened thermoplastic or a liquid polymer precursor, where applied pressure, adhesion or capillarity ensure a good mold imprint. After thermosetting of the material, the mould is removed and clear surface features remain on the polymer. Nanoimprint lithography is a fast technique for simple patterning used in semiconductors, electronics, nonlinear optical and microfluidic devices, and substrates for cell and bacterial growth.¹⁴⁵

3D Printing

Additive manufacturing, also known as 3D printing, is a versatile technology to manufacture complex functional 3D structures. Materials range from thermoplastics and thermosets to hydrogels, but also metals and ceramics can be 3D printed.^{154–156} Additive manufacturing (AM) was first introduced in the 1980s for special needs in model making and rapid prototyping. Since, it has emerged as a versatile method for fast and customized production of parts without the need of molds or machining. Today, 3D printers of various types are commercially available and some models are even affordable for home-use. Over 50 types of 3D printing technologies based on different principles have been developed thus far, comprising powder bed fusion, vat photopolymerization, material jetting, material extrusion, binder jetting, sheet lamination, and energy deposition as the seven main categories. Their common ground is a layer-by-layer build up from scratch, using computer-controlled translation stages according to 3D computer models. A computer aided design (CAD) model is created and digitally sliced into layers of desired thickness to create a layer-by-layer pattern or point-by-point path applied by the 3D printer.¹⁵⁴ AM has opened a whole new world in terms of freedom of design, as complex structures can easily be produced in a single production step (**Figure 1.16**). For example, chains and interlinked hinges can be produced without the need of post-process connections (soldering joints, splices), and complex solutions for improved heat dissipation (cooling channels) or reduced material usage in ultralight building by sophisticated static solutions can be realized.^{154,157,158}

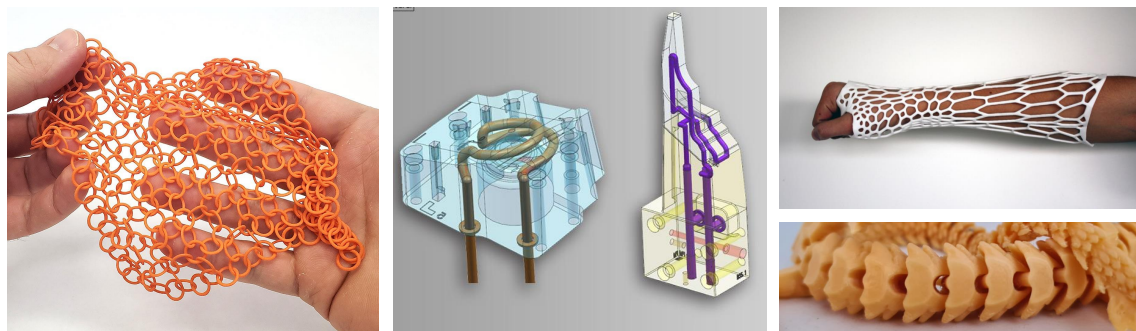


Figure 1.16 – Some examples for sophisticated, 3D printed objects.^{159–161}

In polymer 3D printing, extrusion-based technologies are commonly known, using thermoplastic materials by melting and subsequent deposition of the softened filament. While posing the advantage of easy reprocessability by melting, the materials and especially the resolution of these techniques are limited. In vat-based processes (**Figure 1.17**), however, covalently crosslinked polymer networks are formed by illumination from liquid monomers or pre-polymers to yield permanently cured specimens with exceptional mechanical strength and stiffness if needed. Typically a number of functional monomers, such as (meth)acrylates, epoxy resins, unsaturated polyesters, phenolic polymers and organosilicons, are used with cationic or radical photoinitiators, depending on the desired final material properties.^{162,163} The original 3D printing from liquid resin is **stereolithography (SLA)**, established in 1984 by Hull et al.¹⁶⁴ Using a point light source to cure one voxel at a time, the light source is scanning all across the layer before moving on to the next one. Illumination can either be done from above (bottom-up) or below (top-down) the build plate, with a small layer of liquid resin in-between. This layer is subject to spatially controlled curing. After the first layer is finished, the build platform is moved to allow new resin between the light source and layer 1. When adjusted to the correct distance, the next layer is illuminated

point-by-point as before. Due to the necessity of the light source/laser to scan across layers, the rate of production is limited in SLA processes to about 0.25mm/min. It is, however, a well developed technique with high resolution and accuracy (5-50 μ m) and used in many fields, such as dental, toys, molds, automotive, and many more.^{55,162,165,166}

Digital light processing (DLP) is up to 10-times faster than SLA, as it illuminates a whole layer at once. The principle of 3D part production is similar to SLA, however, the light source is now covering the whole build area instead of just one voxel at a time. The pattern for each layer is either produced via digital mirror device (DMD) or a liquid crystalline display (LCD) screen as filter in LCD-type printers. Due to the sophisticated DMD mirror array implemented, DLP printers are relatively expensive compared to LCD printers. While they show high resolution and are comparably cheaper, the intensity of the light source is dimmed significantly due to absorbance in the screen.^{165,167} In SLA and DLP printing, one rate limiting step is the switch to a new layer. Usually a printer has some kind of peeling step, carefully separating the built part from the film above the light source. During this step it is important for the connection between the layers to be stronger than the adhesion toward the film for the object not to break. This is usually done carefully and slowly at a preset tilting angle. Additionally, the build platform is moved further up than the thickness of the next layer, to let uncured resin flow in more easily and evenly distribute on the illumination site. This whole intermediate step, is often times more time consuming than the printing of the layer itself. Therefore a new technique was developed to decrease the adhesion of the newly printed layer towards the separating film, achieving uncomparable building speeds of 8-16 mm/min. This **Continuous liquid interface printing (CLIP)** was first introduced in 2015¹⁶⁸, utilizing an oxygen-permeable interface. As most radically induced polymerization reactions are inhibited by the formation of peroxides in the presence of oxygen, a thin layer of non-reactive resin is formed above the illumination source, creating a "dead-zone". This reduces adhesion and removes the need for the intermediate, time-consuming re-coating step for each layer, drastically increasing build speed by continuous processing. As the part production, resin renewal and build elevator movement occur simultaneously opposed to discrete steps in SLA and DLP, the layer thickness can be reduced to minimize the staircasing effect without affecting the overall build time.^{54,162,169,170}

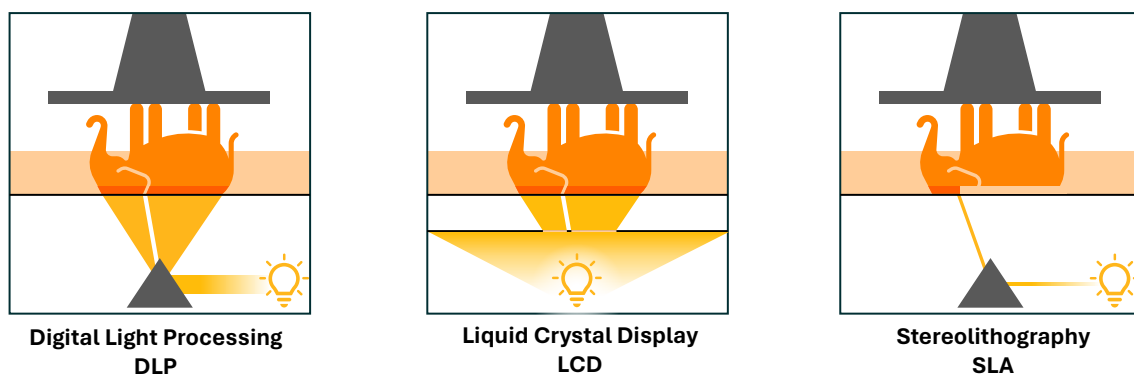


Figure 1.17 – Graphic representation of digital light processing (DLP), liquid crystal display printing (LCD) and stereolithography (SLA) as vat-based 3D printing processes.

A method derived from SLA is **Two-photon lithography (TPL)**, based on the principle of two-photon absorption (TPA). When a beam of an ultrafast laser is focused on a volume of photosensitive material, the polymerization process can be initiated, but only within the focal region.⁵² TPL is not a layer-by-layer technique, but the focal point of the laser can be moved freely within the resin, making it a true three-dimensional printing technique, capable

for building virtually any structure.^{54,55,171} The laser used in TPL is of a longer wavelength than the usual initiation wavelength in a one-photon process, allowing for less energy input. To activate the photoinitiator, more than one photon has to be absorbed by the same molecule to reach the excited state, which is possible via a virtual intermediate state. The intermediate excited stage is populated by the absorption of the first photon with the second photon being absorbed within the virtual state's lifetime of 10^{-4} to 10^{-9} s.^{12,172,173} As an extremely high power density is needed for TPA, ultrafast, high intensity lasers (femtosecond lasers; 10^{13} W/ μm^2) are used and tightly focused. Only in a very narrow region inside the focal plane can the necessary photon density be reached and the photoinitiator be activated. This leads to a very high resolution, even below the illumination wavelength, in the range of 100 nm.^{162,172,174,175} With its extremely high resolution, but low printing speed and small printing area, typical applications of TPL include refractive and diffractive optics, microfluidics, tissue scaffolds, mechanical metamaterials, photonics, and plasmonics.¹⁷⁶

Multi-Material Printing

With 3D printing emerging into every-day applications, the need for a variety of materials integrated in a single object is increasing. This makes multi-material stereolithography a method of growing interest.^{177,178} An intuitive way to implement multiple materials in SLA is to use **several resins**. The most straight forward way is to manually switch the resins or resin vats. To implement this into an automated process, several vats have been used on moving platforms or carousels for the change-over.^{179–183} A critical point when changing resin is cross-contamination. Therefore a lot of effort in process design went into the intermittent cleaning step as well as the reduction of resin contact area to reduce the amount of possible resin carry-over. The cleaning step involved approaches such as rinsing, brushing, wiping, blow-drying or ultrasonification.^{180,184}

Another option is the use of **two wavelengths** to trigger different chromophores and chemical reactions. In a mixed cationic and radical resin, containing acrylate as well as epoxy monomers, radical polymerization can be triggered independently from the cationic network formation at a higher wavelength. While this leads to a relatively soft network, the lower wavelength activation of both PIs or a dual-mode radical/cationic PI will form a more crosslinked, stiffer sample.^{36–38} Bowman et al. used the same principle for a combination of anionic thiol-Michael reaction and radical acrylate homopolymerization, achieving a difference in modulus of one order of magnitude and a ΔT_g of almost 70°C.⁴¹ Similarly, Rossegger et al. used a dimerization reaction for additional crosslinks. While a more flexible material was produced by radical thiol-ene polymerization at 405 nm, pendant coumarin groups were crosslinked upon partial irradiation with 365 nm, showing a distinct increase in glass transition temperature and modulus.^{39,185} Barner-Kowollik et al. used the cyclic dimerization of anthracene moieties to achieve a tunable material after direct laser writing of an acrylate-based structure. While anthracene dimers are originally present in the resin, they are partially cleaved during the polymerization step upon laser writing. A subsequent exposure to LED light of 415 nm resulted in a steady increase of re-formed anthracene crosslinks resulting in decreased fluorescence activity and increased material stiffness.¹⁸⁶ The same group also introduced one of the first truly orthogonal systems for dual-material additive manufacturing, using two chromophores to activate the dimerization of either o-methyl benzaldehyde at 330 nm or styrylpyrene at 435 nm.⁸⁴

In so-called **grey-scale** printing, the intensity of exposure is varied to achieve different degrees of conversion and therefore different material properties. While some used this approach to facilitate the removal of support structures during post processing¹⁸⁷, others were able to cover a wide range of final part properties from stretchy (at 55% conversion) to glassy (at 94% conversion) in an acrylate system.^{185,188,189} Within this thesis a dual-cure system capable of combining grey-scale printing with the dual-wavelength approach, selectively tuning material stiffness by irradiation dose of a second wavelength is achieved (Chapter 2.4).

Printing on Micro- and Nano-Scale

In the last decade 3D and 4D printing, especially on micro- and even nano-scale, has gained increasing interest.¹⁹⁰ The printing process has been improved upon resolution, reducing voxel size by combination of sophisticated optics and advanced photochemical processes. In 2014, Stefan Hell was awarded the Nobel Prize in Chemistry for the development of STED microscopy, which enables high resolution imaging below the diffraction limit, by the antagonistic interactions of two different colors of light. While a first wavelength excites the chromophore, a second wavelength, focused in a donut shape around, has a depleting function and deactivates the excited chromophore by stimulated emission, hence suppressing the crosslinking.^{190,191} This principle can be used for additive manufacturing, known as STED lithography. A synergistic approach was introduced in 2020 by Hecht et al. termed Xylography, using a photoswitchable photoinitiator in volumetric 3D printing to increase printing speed while maintaining a resolution of 10 μm (Figure 1.18).¹⁹² Barner-Kowollik et al. introduced a fully orthogonal system of photoswitches for this kind of 3D printing, where crosslinking of the two moieties is only possible when both, cis-isomer and ketene, are in their activated state. Using orthogonal chemistry like this in combination with an intricate optical setup, even higher resolution can be achieved.¹⁹³

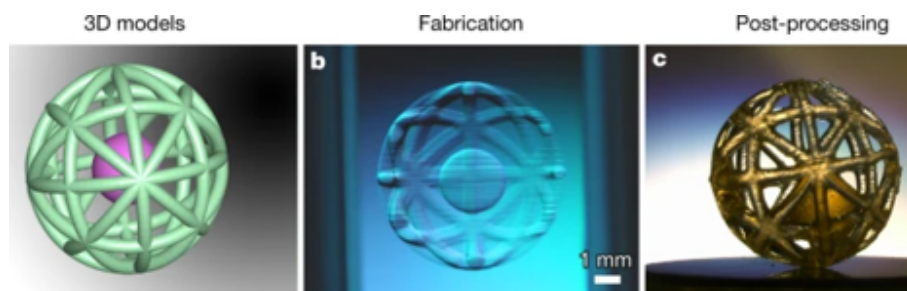


Figure 1.18 – Volumetric digital manufacturing by xylography show an extremely high resolution process. Reused with permission from¹⁹². Copyright 2020 Springer Nature Limited.

4D Printing: Smart Materials

The term 4D printing was introduced during a TED talk by Skylar Tibbits in 2013 and represents a significant advancement beyond traditional 3D printing, as it introduces the dimension of time into the fabrication process.^{194,195} Unlike static 3D-printed objects, 4D-printed structures are dynamic and responsive, capable of transforming their shape, structure, and functionality in response to external stimuli. This transformative ability is

enabled by the integration of smart materials and sophisticated design algorithms into the 3D printing process. By incorporating materials that can respond to various inputs such as heat, humidity, pH, magnetism, electricity, and light, 4D printing allows for the creation of structures that can self-assemble, deform, and self-repair over time.^{196–198}

Methods for advanced, phototriggered reactions applicable in 3D printing are just starting to emerge. The group of Barner-Kowollik and Gescheidt have done some pioneering work in this field, introducing the concept of action plots (see also **Chapter 1.1.3**), drastically changing the view on orthogonal reactions and opening up a tool-box for more approachable photochemistry.^{121,122}

4D printed, smart materials, including heat-sensitive hydrogels and shape memory materials, have found applications across diverse industries such as aerospace, soft robotics, biomedical, packaging, soft electronics, and textiles, as soft actuators or in smart valves.^{199,200} In fields like tissue engineering and regenerative medicine, 4D printing offers the potential to create constructs that adapt to the desired shape or function upon implantation, promoting better integration in biological systems.²⁰¹ Moreover, in healthcare, 4D printing holds promise for developing adaptive drug delivery systems, enhancing medical devices and prosthetics, and improving diagnostic sensors by enabling self-adjusting, self-assembling, or self-healing capabilities.²⁰² Recent advancements in new smart materials and printing techniques, such as multi-material and multi-axis printing, further expand the possibilities for creating complex and responsive 4D-printed structures.^{194,200,203,204} Some nature-inspired 4D-structures are presented in **Figure 1.19**.

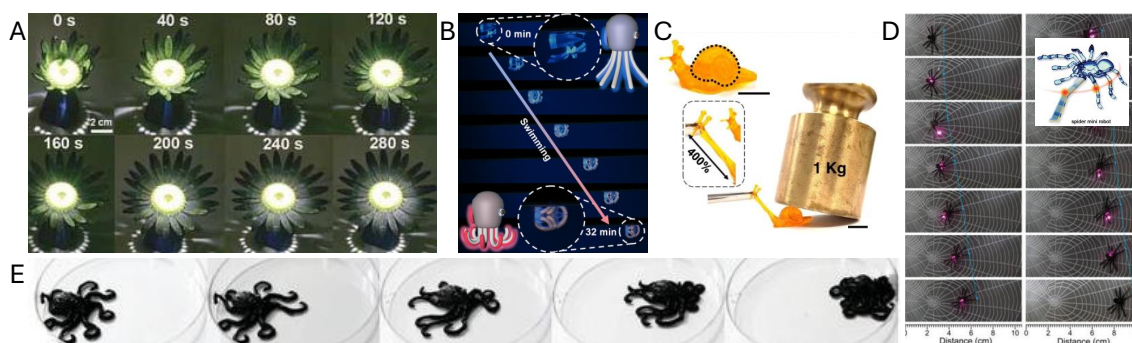


Figure 1.19 – Nature-inspired application of multi-material 3D and 4D printing. (A) A flower blooming upon illumination.²⁰⁵ (B) Octopus locomotion in water.²⁰⁶ (C) Grey-scale printing for massively different materials.¹⁸⁹ (D) Locomotion by light-triggered joint movement in a spider-robot.²⁰⁷ (E) Locomotion of a 3D printed octopus in a magnetic field.²⁰⁸ A - Copyright 2017 WILEY-VCH Verlag GmbH & Co. KGaA, Weinheim; B - Copyright 2021 Wiley-VCH GmbH; C - creative commons; D - Copyright 2018 WILEY-VCH Verlag GmbH & Co. KGaA, Weinheim; E - Copyright 2019 WILEY-VCH Verlag GmbH & Co. KGaA, Weinheim.

1.3.2 Applications

The concept of programmable smart structures created by 3D printing promises a wide range of applications in many industries. However, 4D printing is a relatively new technology with many mechanisms and concepts demonstrated on research scale, but still in the development phase. It is expected to find many practical uses in healthcare, electronics, automotive, aerospace, and consumer product sectors especially in otherwise inaccessible regions or on extremely small scales.²⁰⁴

Biomedical and Life Science

Initial application of 3D printing in medical devices involved mainly (mass) customization of hearing aids, dental prosthetics or orthoses.^{209,210} While filament-based additive manufacturing techniques have been used for the production of all kinds of larger medical aids, e.g. arm braces and lower limb prosthetics, vat based techniques have found their way into applications like **dental aligners** (**Figure 1.21**). Substituting fixed orthodontics, they aim for easy production and high consumer aesthetics. Starting with an intraoral scan of the patients teeth a digital model is created. A series of incremental changes to the model are transferred to the matching series of 3D printed clear aligners, skipping the steps of dental impression and cast modeling. The current material optimization focuses on low water absorption, creep, biocompatibility and sustained material properties.^{211–215}

3D printed smart materials are also being introduced to the medical field, up to now, mainly as stents. **Stents** are tiny tubular devices introduced in the body as scaffolds, typically used to keep weak or narrowed arteries and blood vessels, but also tracheal vessels, open. Oftentimes stents are the standard of care since they can be delivered via minimally invasive surgery with rapid recovery times and small surgical risk. Personalized stents can be adjusted to individual anatomical dimensions obtained from digital models and scans to eliminate the risk of stent migration and insertion-related complications.^{216,217} Prior to insertion, the stent is folded to reduce its circumference and make it passable in the artery. Upon exposure to body temperature or external stimuli (magnetic field) the shape memory process is activated and the stent expands to its working size (**Figure 1.20**). Recovery time and material stiffness can be controlled by resin composition²¹⁸ and additional functionalities have been implemented into some stents, such as biodegradability²¹⁹ or drug-release.^{204,220–222}

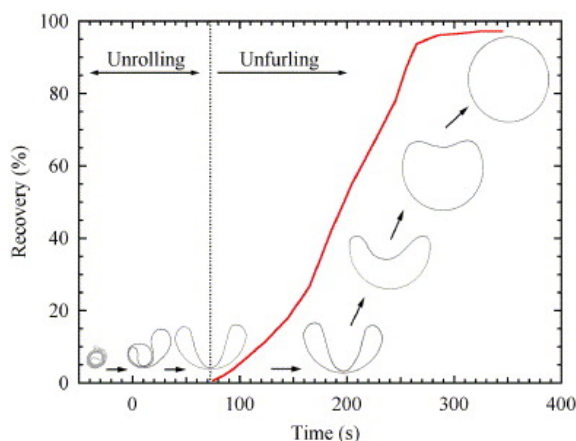


Figure 1.20 – Unfolding of a stent with the use of shape memory. Reused with permission from²¹⁸.



Figure 1.21 – A 3D-printed clear aligner.²²³

3D and 4D bioprinting, which facilitates **dynamic tissue** construction in vitro, offers promising solutions for the increasing need for pharmaceuticals and organs. Shape memory scaffolds enable minimally invasive tissue delivery, aided by wireless control and integration with bioelectronics and biodegradation equipment. Stem cells can be directly implanted

into these scaffolds using 3D bioprinting, advancing organ transplantation and tissue regeneration. Stereolithographic methods have been tested for the fabrication of bio-inspired structures.^{224,225} Grigoryan et al., for example, demonstrated a lung-mimetic design based on polyethyleneglycol diacrylate and gelatine methacrylate, populated with human lung fibroblasts. They showed, that human stem cells remain viable during the additive manufacturing process and functional vascular topologies for studies on fluid mixers, valves, intravascular transport, nutrient delivery, and host engraftment are feasible, simultaneously controlling tissue architecture and biomaterials.²²⁵ Huang et al. used DLP for construction of cell-laden hydrogel wound healing patches with high cell viability and precise cell spatial distribution control. Via a thiol-methacrylate click reaction to incorporate short peptide sequences, they were able to construct an accurate 3D printed all-peptide hydrogel platform for cell delivery and self-renewable growth factor therapy.²²⁶ Photo-triggered click reactions were also used by Anseth and co-workers for bioorthogonal coupling, realizing the controlled patterning of both peptides and proteins in PEG hydrogels, to introduce biological function into otherwise biologically inert structures. This spatial and temporal control by masked illumination adds complexity towards their use as cell micro-environments for biomedical applications and in the field of regenerative medicine.^{42,227,228}

While recent research demonstrates enormous progress towards clinical application, routine implementation of printed surrogates remains a distant goal, with current studies primarily limited to proof-of-concept endeavors and the urgent need for optimization before leaving the laboratory state.^{154,204,229}

At Micro- and Nano-Scale

Advancing into the micrometer scale, stimuli-induced movement becomes an even more crucial topic as other possibilities of actuation are limited. Several structures and mechanism have successfully been shrunk to sub-millimeter scales, making them available for biomedical devices, **drug delivery** or micro-manipulation. Hu et al. used functional micro-cages to trap SiO₂ particles upon pH responsive swelling and expansion of the pores from 8 to 12 μm on demand (A in **Figure 1.22**).²³⁰

Similarly Li et al. demonstrated a magnetic actuated pH-responsive hydrogel soft micro-robot for drug delivery, made from a bilayer structure of bio-compatible PHEMA and PEGDA with Fe₃O₄ nanoparticles upon masked illumination (B in **Figure 1.22**).²³¹ And Spiegel et al printed a smart box-like microstructure (20x20x15 μm) with a lid to trap microspheres and release them upon heating (C in **Figure 1.22**).²³²

Integration of similar opening and closing mechanisms can also be applied to **microfluidic devices** as different sorts of valves, pumps and stoppers. With advanced multimaterial, micro-printing techniques²³³, stimuli responsive valves can directly be implemented into microchannels.²³⁴ While it is already conveniently possible to 3D print high resolution fluid tunnels into transparent matrices, active components enable additional control and complex capabilities, further expanding the sophistication of 3D-printed lab-on-a-chip devices.²³⁵⁻²³⁸

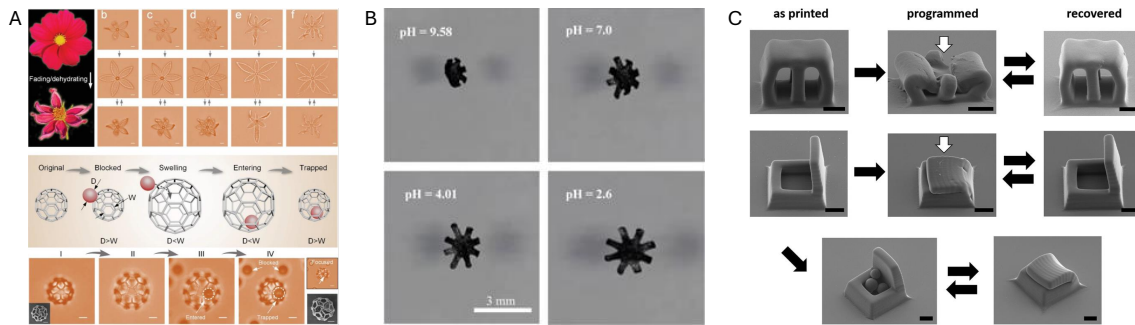


Figure 1.22 – Examples for 3D printed structures for drug release on micro-scale. (A) A cage-like ball, responsive to pH changes.²³⁰ (B) A magnetically activated gripper to catch and release small particles²³¹ (C) A Printed box-structure to store and release particles.²³² A - Copyright 2019 WILEY-VCH Verlag GmbH & Co. KGaA, Weinheim; B - Copyright 2016 IOP Publishing Ltd; C - creative commons.

Robotics

Compared to traditional robots, soft robotic devices are more flexible and adapted to biological and medical applications, safely interacting with humans and handling fragile objects. A number of gripping devices have been developed, taking advantage of shape memory or swelling behavior and being sensitive to variable stimuli such as temperature, pH, moisture or magnetic fields. Self-folding devices, micro-actuators, grippers and a variety of creative, moving shapes have been demonstrated, mostly being pure demonstrations of mechanisms possible for implementation into advanced devices yet to be developed.^{239,240}

As an example, Kim et al. introduced a ferromagnetic soft continuum robot for minimally invasive interventional procedures. The rod-like sub-millimeter device is composed of a printed elastomer core (polyurethane or polydimethylsiloxane) containing magnetizable NdFeB microparticles and a hydrogel skin for reduced friction. Upon activation of an external magnetic field, the robot can be actively stirred and is able to navigate complex three-dimensional networks, making it a promising tool for application in surgical procedures in hard-to-reach areas such as distal neurovasculature in a minimally invasive manner (Figure 1.23).^{239,240}

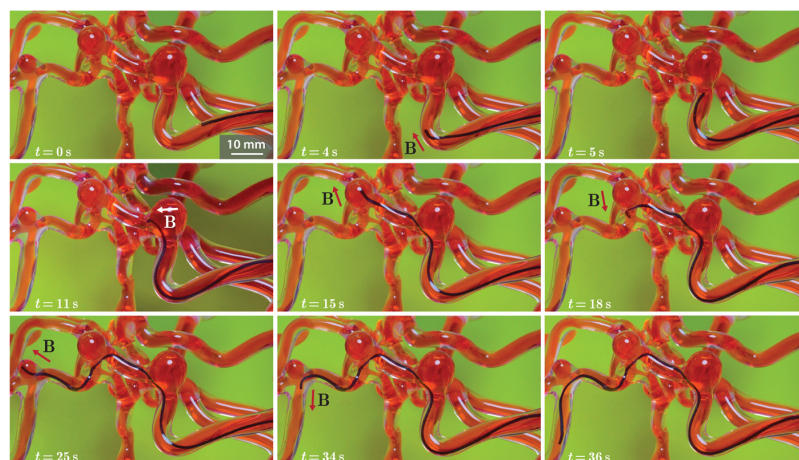


Figure 1.23 – A 3D fabricated soft continuum robot is stirred through a biomimetic maze by magnetic stimuli. From²³⁹. Reprinted with permission from AAAS.

Movement in such soft robotic devices is a combination of active materials and a clever design utilizing the strength of each material implemented. Hence, numerous bending and folding mechanisms have been investigated. Some are directly triggered by magnetism or by heat to activate pre-programmed shape memory states depending on glass transition temperatures to fold into distinct shapes,^{239,241–243} others use light sensitive ink to translate irradiation into heat to induce the same mechanism.²⁴⁴ Whereas systems of self-deploying structures such as antennas or solar panels are investigated for application in space²⁴⁵, an example of a self-folding robot was given by Felton et al. Using prestretched polystyrene as a shape memory polymer with integrated heating circuits, they were able to assemble and activate a crawling robot within 270s with no external human interaction (**Figure 1.24**).²⁴⁶

Not only in robotics, but also sensors and wearable devices, conductive materials and the possibility to implement electric circuits are of great interest. While it has been shown, that printed shape memory structures can hold conductive coatings and can be used to fabricate an electrical temperature switch²⁴⁷, most multimaterial printing techniques for electrically conductive materials are not light-based.^{154,248,249} Odent et al. however, showed a family of ionic composite hydrogels with excellent mechanical properties to be rapidly 3D-printed at high resolution. The SLA resin, composed of acrylamides and ionic, sulfonate-modified silica nanoparticles was polymerized with a riboflavin-based initiator system at 405 nm to yield a flexible, swellable hydrogel, able to act as an electronic connector for an LED lamp (**Figure 1.25**).²⁵⁰

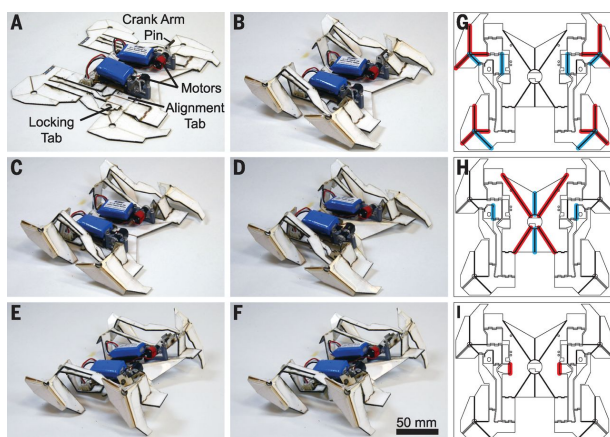


Figure 1.24 – A mostly flat robot, that is able to fold itself upon activation using thermally controlled shape memory. From²⁴⁶. Reprinted with permission from AAAS.



Figure 1.25 – A hydrogel-based bear structure was printed an electronic connector to demonstrate electric conductivity.²⁵⁰ Copyright 2017 WILEY-VCH Verlag GmbH & Co. KGaA, Weinheim

As mentioned before, 3D printing of active polymers is still in its infancy. While many new concepts are discovered and investigated continuously, they are not yet used in many real-life applications. However, the possibilities are seemingly endless, as there are practically no limitations in design and a vast number of materials to chose from. Special attention should be given to bio-inspired structures as novel designs try to mimic nature.

2

Dual-Cure Systems

Multi-material printing has been one of the major research interests since the development of sophisticated 3D printing. While there is the possibility of switching filaments or vats during the printing process to realize multiple-material implementation, this approach can suffer from increased print times, poor adhesion and material contamination.^{185,207,251} Changing a vat can be time-consuming if done by hand or needs additional space and coding if automated. It involves a cleaning and drying step to prevent material transfer between the vats and to provide a clean surface for further printing.^{185,252} Additionally, some structures might be difficult to print from the second resin due to laser shadowing, trapped volumes, and surface tension problems, which calls for meticulous planning.²⁵³

To overcome some of these challenges, approaches combining hardware modifications with special chemistry were introduced (**Chapter 1.3.1**). Instead of switching between resins, the variation in material properties is initiated by the light used. While the molecular structure of the molecules has to be decided before resin preparation and is not modifiable during the printing process, the grade of conversion, especially in light-triggered polymerization, is. Less illumination dose leads to a reduced number of reactive sites generated and, if stopped at the right time, an incomplete monomer conversion. This method has been used in so-called grey-scale printing, able to get continuously variable properties, reaching from soft and stretchy to glassy.^{185,188,189} In other approaches, two wavelengths were used to trigger the formation of two separate networks.³⁶⁻³⁸ Looking at these systems, a vast range of properties can be generated in the end product from only a single resin. There are no cleaning steps necessary and the printing process itself is relatively simple, however, there are some drawbacks as well. First and foremost, there are uncured monomers still in the product. The remaining, uncured monomers within the polymer network act as plasticizers, increasing the mobility of the network, increasing the homogeneity of the system and giving the possibility of leaching, as small molecules can diffuse through the network and escape into their surrounding. While this might not matter for some applications, leaching of potentially allergenic or non-biocompatible compounds is unthinkable for medical use.

As incomplete monomer conversion seems to have a number of disadvantages, herein methods were investigated to increase the crosslinking density by adding functional groups into the monomers. These active sites should not take part in the initial polymerization, but be implemented into the network as part of one of the monomers. They are covalently bound within the polymer, are homogeneously distributed and remain dormant until a reaction is initiated. Against the background of 3D printing, the most obvious and reasonable trigger for this is light. Ideally the crosslinker-groups are directly triggered by light to avoid a second photoinitiator or catalyst. Therefore, the focus was on finding light triggered reactions between two molecules of the same kind for a simple, straight forward material alteration without the formation of side products or the need for additional components.

Some long-known chemistry, namely photo-induced cycloaddition reactions, was recently re-discovered for the use in multi-wavelength 3D printing.³⁹ Dimerizable groups (coumarin) were implemented into a typical, radically cured network. Directly initiating the dimerization reaction with light leads to the formation of additional crosslinks and a change in bulk

material properties.

This chapter presents my recent work on photo-dimerizable groups and their implementation into a radically cured thiol-(meth)acrylate system. A number of potentially interesting functional groups were investigated upon their reaction behavior under irradiation in a small-molecule study. Consequently a chalconyl-based resin was demonstrated suitable for dual-wavelength printing on macro and micro-scale as well as several smart material applications. Additionally **Chapter 2.5** will give insight into another multimaterial printing approach based on orthogonally initiated polymerization mechanisms.

2.1 Network Homogeneity

Within a specific monomer mixture, crosslink density and homogeneity are two of the main factors influencing bulk properties. Usually, crosslink density depends on the functionality of the monomers, their molecular structure and the grade of conversion.

Network homogeneity is a crucial point if considering a polymer for shape memory applications. A homogeneous network exhibits a sharper change in material properties, as it does not exhibit regions, with slightly different behavior and reacts in a uniform way. This can be measured by the range of temperature (width of T_g) over which the glass transition occurs and the material switches from a glassy to a rubbery state. In shape memory, this transition is used to fixate a shape (programming) and trigger movement by releasing internal tension. The more precise this transition is, the easier it is to trigger motion at a specified temperature. Combining multiple materials with sharp T_g s, which are sufficiently spaced to be triggered separately, a multi-shape memory material can be designed.

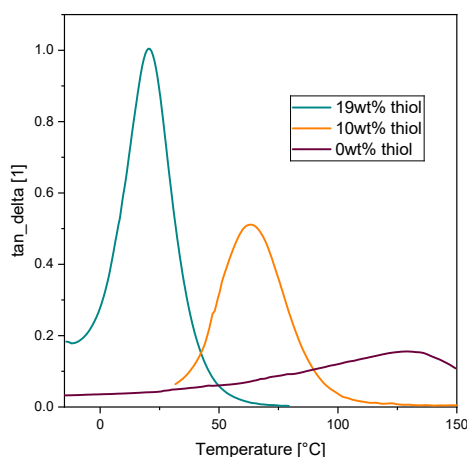


Figure 2.1 – Thiol influences the material properties of an acrylate-based resin in terms of network homogeneity and glass transition temperature. The DMA curves of a pure methacrylate system (0 wt%) as well as a thiol-acrylate resin with 10 and 19 wt%, respectively, are presented.

Pure polyacrylates or polymethacrylates are known to have a broad glass transition range due to the chain growth mechanism of their polymerization. Such resins show early gelation and develop high curing stress through limited diffusion and mobility upon higher conversions. Therefore thiol was added into the resin. Not only does thiol help overcoming

oxygen inhibition, but it also acts as chain transfer agent and reacts in a step-growth manner with (meth)acrylates. It thereby drastically increases network homogeneity, resulting in a sharper T_g for improved properties in shape memory. **Figure 2.1** shows how the very broad T_g of a pure methacrylate network can be optimized by adding up to 19 wt% thiol.

Shape memory polymers usually operate close to room temperature, which made 25 °C the target T_g for the thiol-(meth)acrylate network with the possibility to increase T_g by additional crosslinking. Choosing bifunctional monomers, as well as the addition of up to 19 wt% of thiol helped to achieve this goal.

2.2 Absorption Behavior and Reactivity

In order to work in a dual-cure system, the photo-active secondary crosslinkers need to react upon a separate light from the first polymerizing one. While illumination with the first wavelength forms a polymeric network from all (meth)acrylate and thiol monomers (blue), the crosslinkers (orange) remain untouched (**Figure 2.2**). This gives a material with a relatively low T_g due to lesser crosslink density. When illumination with a second, usually shorter wavelength is done, crosslinks are formed by dimerization and the T_g increases.

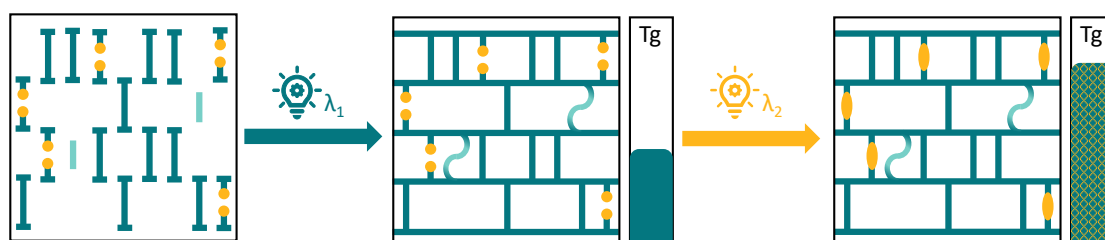


Figure 2.2 – A dual-cure process with two distinct wavelengths. Polymerization takes place between all (meth)acrylates (dark blue) and thiol monomers (light blue) upon illumination with λ_1 . Upon illumination with λ_2 , usually of a lower wavelength, additional crosslinkers (orange) are formed by dimerization. The T_g increases from step one to step two due to increased network density.

Three important conditions must be met in order for such systems to work.

1. Wavelength bandwidth: The emitted wavelength regions of the lamps used, must not overlap in a way that would spoil distinct matter interaction. Therefore light sources with a narrow emission spectrum, such as LEDs are favored. LEDs are typically available at output powers of several mW to about 3 W from 265 to 5200 nm (more commonly 300 - 900 nm), with bandwidths down to about 10 nm. Their affordable pricing, easy handling and moderate energy consumption make them a preferable light source.
2. Wavelength orthogonality: At least one reaction, in this case the dimerization of the additional crosslinkers, should be triggered by one of the two wavelengths only. As described in **Chapter 1.1.3**, full or sequential orthogonality must be assured in order to set up a dual-cure system.
3. Reaction orthogonality: There must not be any reactivity of the crosslinking-groups towards the polymerizing radical species or other sensitizing effects. The polymerization in the first step needs to be completely decoupled from the secondary crosslinking.

The following chapter will discuss a library of molecules or functional groups, which could be implemented into a dual-cure resin. They will be shortly presented upon their origin and known applications. Finally the measurements conducted in this work regarding their reactivity towards light, will be shown.

2.3 Library of Photo-Reactive Groups for Dual-cure 3D Printing

In this chapter, an overview of further potential groups in dual-cure 3D printing will be given in a small-molecule reactivity study. As absorptivity and reactivity upon a certain wavelength do not necessarily align, their reaction behavior under selective light sources was investigated.

From the perspective of DLP 3D printing, only a small number of activation wavelengths are feasible due to availability on the market, 405 nm being the standard wavelength in most commercially available DLP printers. The selection of these wavelengths is historically rooted in the spectrum of the frequently used mercury-vapor lamp, with some of the strongest peaks in the emission spectrum being at 253.7 nm, 365.4 nm (i-line) and 404.7 nm (h-line). Even as the LED technology made a great spectrum of emission wavelengths readily available, most manufacturers of more sophisticated light sources (high power, in 3D printers, etc.) stuck with ever the same wavelengths. Therefore 254 nm, 365 nm, 405 nm and 450 nm light sources were chosen for the following study.

A short summary of some functional groups (**Figure 2.3**), their respective structure, properties, known reactivity and applications will be given, followed by a brief investigation of their reactivity upon illumination.

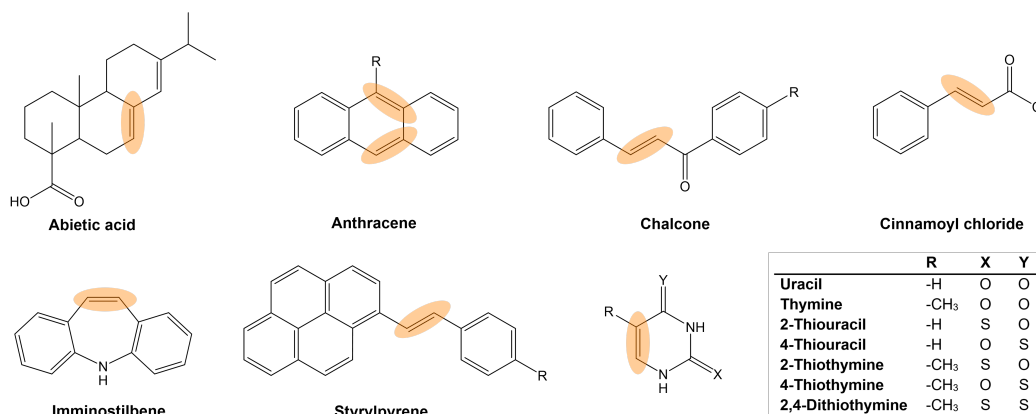


Figure 2.3 – A library of dimerizable groups with their reactive double-bond marked in yellow.

2.3.1 Abietate

Abietic acid belongs to the class of diterpenes and is an abieta-7,13-diene substituted with a carboxy group at position 18. It is a natural product found in certain pine trees as a main component of tree resin and has been used in paints, varnishes and soaps.^{254,255} Abietates produce dimers with an acidic catalyst, giving rise to a variety of up to 40 dimeric compounds,²⁵⁶ but are also known to undergo photoinduced dimerization.^{257,258}

In poly(vinylbenzyl abietate), the abietate moieties are responsible for increased crosslinking upon UV irradiation.^{259,260} In a first study by Kim et al. The insoluble fraction was about 78 % after only 10 min of UV irradiation, showing rapid formation of the crosslinked polymer by abietate dimerization. They also implemented the abietate into the sidegroup of a methacrylate by polymerizing methacryloyloxyethyl abietate and again crosslinking the abietate groups.²⁶¹

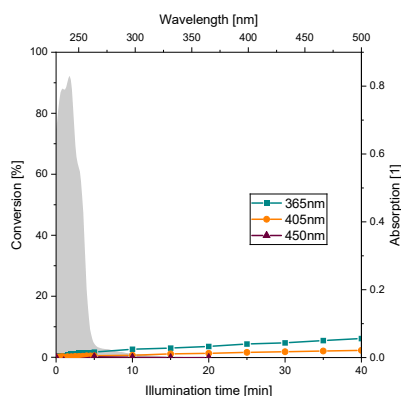


Figure 2.4 – Reaction kinetics of abietic acid upon illumination with different wavelengths and the respective UV-Vis spectrum (grey).

Eventhough photoinduced dimerization of abietate has been shown in literature, the number of studies are minuscule. The herein measured absorption spectrum suggests reactivity only in the deep UV region (<300 nm). In a kinetic study abietic acid was used as the model compound. In solution (0.05 mM; ACN) no reactivity at 450 nm and only less than 10 % final conversion to the dimer at 405 and 365 nm were found (**Figure 2.4**).

2.3.2 Anthracene

Anthracene consists of three linearly fused aromatic rings. It exhibits 14 delocalized π -electrons and can undergo [4+4] cycloaddition in the centered ring upon irradiation. Due to its unique properties as a good fluorophore and good charge mobility, it has found application as fluorescent tag, in sensors as well as in (photo)electrical applications.²⁶²

Anthracene (An) has been used for its phototriggered dimerization reaction in An-capped polymers for controlled co-polymerization or formation of macrocycles^{263,264} as well as a number of polymers with An-bearing sidegroups.^{262,265}

The reversible nature of the anthracene dimer through UVC light, elevated temperature or mechanically has been discussed extensively^{266–269}. Multiple crosslinking and cleavage cycles were shown in a variety of polymer networks either upon heating or illumination. Schlögl et al. applied this behavior in a photo resist for 2D microstructures²⁷⁰ and healing with light was demonstrated when re-introducing the cycloadduct after cleavage^{269,271}.

In network design the precise control over crosslink-formation via light was exploited for controlled formation and properties of hydrogels.²⁷² Introducing triazol-substituents as electron-rich groups in 9-position, bioorthogonal formation of a PEG hydrogel was demonstrated upon visible light (400-500 nm) irradiation.²⁷³ Anthracene dimers in the network

were able to be cleaved (thermally or with light) altering adhesion in rubbers²⁷⁴ or completely decomposing a thiol-ene network²⁷⁵. Additionally, anthracene-dimerization and cleavage was demonstrated to facilitate reversible switching in the wrinkling behavior for smart surfaces^{276,277} as well as the coiling of single-chain nanoparticles (SCNPs)^{278,279}.

Naturally, the substituent pattern of anthracene considerably influences its absorption behavior and reactivity. Long and flexible chains lead to faster dimerization while rigid main chains only show slow intermolecular reactions.²⁸⁰ The substitution pattern massively influences thermal cleavage, with up to 70 °C difference for tunable networks²⁸¹ and absorption can be red-shifted by 2,6-substitution²⁸² or the introduction of electron-rich groups at the 9-position.²⁷³

However, as investigated herein in UV-Vis spectroscopy, the maximum absorption wavelength of anthracene is still in the UV range. In solution (0.05 mM; ACN) anthracene methylacrylate showed almost complete and relatively fast conversion upon illumination at 365 and 405 nm, while no reaction was detected at 450 nm (**Figure 2.5**). Further examinations were conducted in a resin formulation (**Figure 2.5**). After the initial polymerization step at 450 nm with no anthracene dimerization happening, anthracene is crosslinked rapidly to full conversion at 405 nm. Acrylate or methacrylate derivatives of anthracene therefore pose a very promising group for further investigations and use in dual-wavelength 3D printing with 450/405 nm.

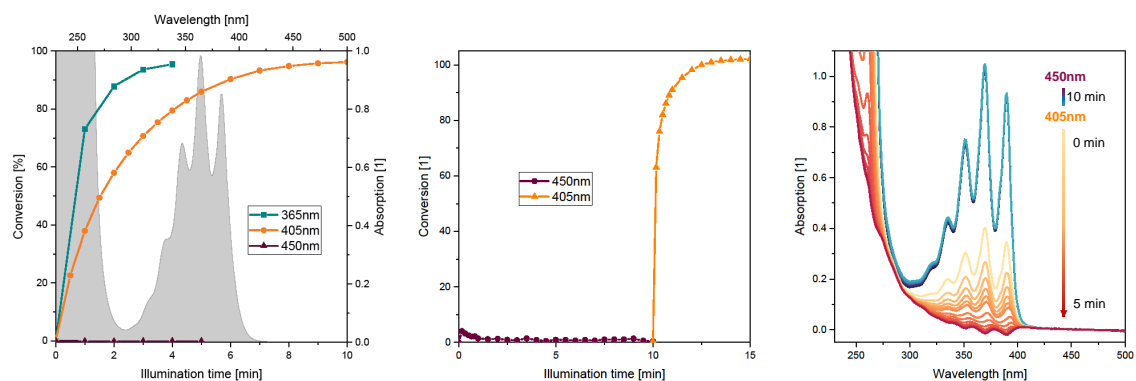


Figure 2.5 – Reaction kinetics of anthracene methyl acrylate upon illumination with different wavelengths in solution (left) and the respective UV-Vis spectrum (grey). Reaction kinetics of anthracene methyl acrylate in resin upon sequential illumination with 450 and 405 nm (middle). Evolution of the absorption spectra throughout sequential illumination (right).

2.3.3 Chalcone

Chalcone (or 1,3-diphenylprop-2-en-1-one) is a plant-derived compound with cytoprotective and modulatory functions. Its derivatives are known for their anti-inflammatory and anti-cancer potential.^{283,284} The photo-dimerizing behavior of chalcones has been known since the 1950s²⁸⁵, but has rarely been used in polymeric materials. The crosslinking behavior of the chalconyl group was used for the assembly of 2D layers²⁸⁶, liquid crystal alignment^{287,288} and in photoresists^{289–291}. However, the polymethacrylate containing side-chain chalconyl units was polymerized in solution with benzoyl peroxide, using different stimuli for polymerization and additional crosslinking.

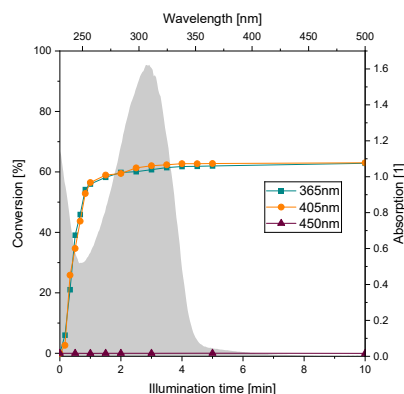


Figure 2.6 – Reaction kinetics of hydroxychalcone upon illumination with different wavelengths and the respective UV-Vis spectrum (grey).

Shown above (**Figure 2.6**), the absorption and reaction behavior of chalcone was evaluated for the implementation into an λ -orthogonal resin. While there was no dimerization recorded at 450 nm (0.05 mM; ACN), the reactivity at 365 and 405 nm was relatively fast, which depicts very high potential for λ -orthogonality in a resin. The low conversion could be attributed to the behavior in solution, as lower concentrations reduce the probability of dimerization taking place.

2.3.4 Cinnamoyl

Cinnamoyl (or 3-Phenylprop-2-enoyl) is the functional group derived from cinnamic acid. Its derivatives are widely found in nature in essential oils or spices such as in cinnamon, basil, strawberry and *Eucalyptus olida*.^{292,293} Some are used as anti-inflammatory agents, anti-oxidatives or antimicrobial agents.²⁹⁴ The knowledge of photoreactivity of compounds containing cinnamoyl groups can be dated back to the early 1950s²⁹⁵, Poly(vinyl cinnamate) was the first synthetic photopolymer^{296,297}. It used cinnamoyl groups in the side chain for crosslinking across polymer chains and subsequent solidification of the sample. Over time the reaction mechanism leading to the polymerization was found and more and more similar photoreactive polymers based on the cinnamoyl group were investigated.^{298–302} Currently, cinnamoyl groups have been implemented in various polymers as side groups or in the backbone. The photo-triggered dimerization within polymer chains (intramolecular) as well as among different chains (intermolecular) was shown,³⁰³ as well as different orientations of bonding (head-to-tail and tail-to-tail), forming truxillic acid or truxinic acid, respectively,³⁰⁴ and the competing photo-isomerization (cis-trans).³⁰²

Generally, the photoreaction is induced with UV light at wavelengths below 365nm, as the cinnamoyl unit shows maximum absorption in the region of 280 nm. However, depending on the chemical environment, the maximum absorption can be red-shifted. As an example, Kawatsuki et al. introduced a benzyl ring with various substituents, shifting the peak UV-Vis absorption to a maximum of 315 nm, improving reactivity upon 365 nm illumination.³⁰⁵ Dimerization as well as subsequent photo-cleavage of the cyclobutane ring is achieved by carefully selecting the excitation wavelengths, 365nm and 254 nm being a convenient pair due to the availability of light sources.³⁰⁶

Even though several publications claim to have modified cinnamoyl groups with illumination at 365 nm, these experiments were usually done at high light dosage and in thin films (nm - μm range).^{302,305-307}

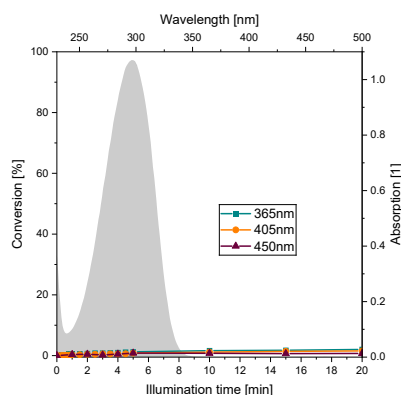


Figure 2.7 – Reaction kinetics of cinnamoyl-chloride upon illumination with different wavelengths and the respective UV-Vis spectrum (grey).

As the aim of the experiments presented in this work is to create a resin for 3D-printing, the light sources available have low intensity (ca. $20\text{-}200 \mu\text{W}/\text{cm}^2$) and the illumination times should be as short as possible. When cinnamoyl chloride was herein investigated in solution (0.05 mM; ACN), neither of the applied wavelengths (365, 405 and 450 nm) could achieve any significant reaction (**Figure 2.7**), therefore, the cinnamoyl moiety is not suitable for further investigations in an unmodified form.

2.3.5 Iminostilbene

Dibenzazepine (or Iminostilbene) is a chemical compound with two benzene rings connected to the seven-membered azepine ring, bearing a double-bond opposite the nitrogen. N-acryloyldibenz[b,f]azepine and its dimerizing behavior has been explored in thermally and photo cured co-polymers in the 1970s.³⁰⁸ Further investigations on the behavior of a variety of derivatives of iminostilbene has been done in the beginning of the 2000s, as Goerner et al. exemplified the enormous influence of substituents onto the absorption and reaction behavior.³⁰⁹ While some N-acyl derivatives showed high conversion towards dimerization, N-alkyl substituted molecules did not react at all. In 2020 Yagci et al. used an N-acyl derivative with ene-functionality to implement Dibenzazepine into a thiol-ene network via concurrent curing and dimerization at 365nm.³¹⁰ Subsequent illumination at 250 nm lead to well-defined cleavage of cyclobutane units and could liquify the sample.

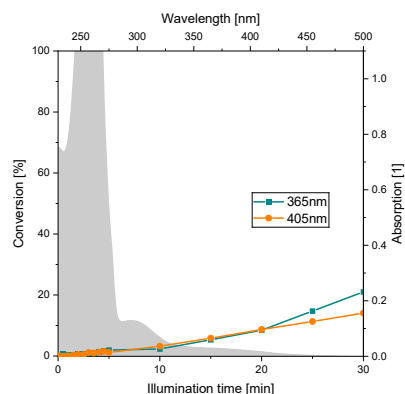


Figure 2.8 – Reaction kinetics of iminostilbene upon illumination with different wavelengths and the respective UV-Vis spectrum (grey).

Dibenzazepine derivatives, especially with spacers to provide for a lower melting point, pose promising functional groups for dual-cure 3D printing. The unsubstituted iminostilbene investigated in this study, however, did not show sufficient dimerization activity upon 365, nor 405 nm illumination (**Figure 2.8**).

2.3.6 Styrylpyrene

Styrylpyrene, also known as 1-[(E)-2-phenylethenyl]pyrene according to IUPAC, is similar to stilbene in its structure, but possesses a 4-membered fused benzene system (pyrene), which drastically red-shifts the absorption maximum from 294 nm^{107,108} to 375 nm³. In 1980, Kovalenko et al. first observed the dimerization and isomerization of styrylpyrene (SP) upon illumination, however, it was not until 2016 that its photoreactivity was used by Doi et al. in the reversible crosslinking of DNA strands. The mild conditions (455 nm, 280 mW LED, 20°C) necessary for dimerization made the application in such a fragile structure as DNA possible.³¹¹

In the following years the reactivity of hydroxy-styrylpyrene was studied in detail by the group of Barner-Kowollik. They evaluated the formation of different dimers⁴³, the maximum conversion wavelengths for dimerization and cleavage (at 435 and 330 nm, respectively)³, as well as the change in light-interaction when concentration or solvent are altered³¹². The application of SP-dimerization was shown in single-chain nanoparticles, as controlled folding was achieved through dimerization of side-chain SP-units³¹³ or an orthogonal system with SP and anthracene moieties.^{278,279} While irradiation at 470 nm led to selective [2+2] dimerization of styrylpyrene, illumination with 415 nm light could sequentially trigger full coiling of the polymer chain by [4+4] cycloaddition of anthracene.²⁷⁹ Alternatively, coiling (through anthracene) and single-chain ligation (through SP) can be orthogonally triggered using 330, 410 and 455 nm for folding, folding and ligation, or ligation only, respectively.²⁷⁸ Due to the low concentration of polymer chains in solution, the intramolecular dimerization exceeds the intermolecular reaction, which is anticipated for the selective coiling adverse to network formation.

Forsythe et al. investigated the behavior of poly(ethylene glycol) with styrylpyrene end-groups under mild irradiation conditions (visible light; 20mW/cm²).³¹⁴ The formation of

hydrogels from linear and 4-armed precursors and the photomodulation of their mechanical properties was demonstrated. SP-crosslinks could be repeatedly (6 cycles) cleaved upon 340 nm irradiation, which also led to light-induced self-healing properties of the presented material.

Employing SP for surface modification on metal-organic frameworks, Wang et al. created a light-triggered cage to trap cargo molecules and release them upon SP-cycloreversion at 356 nm.³¹⁵

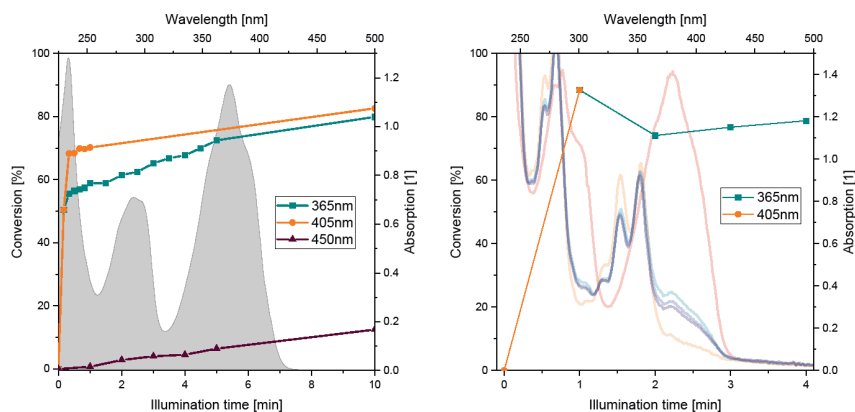


Figure 2.9 – Reaction kinetics of styrylpyrene upon illumination with different wavelengths in solution (left) and the respective UV-Vis spectrum (grey). Reaction kinetics of styrylpyrene acrylate in resin upon sequential illumination with 405 (orange) and 365 nm (blue). The conversion is shown, as well as the respective spectra in the background (right).

Styrylpyrene is a promising candidate for the use in dual-cure 3D printing and was evaluated in this work. While 365 and 405 nm both show rapid and sufficient conversion in solution (0.05 mM; ACN), illumination at 450 nm is significantly slower and reaches only up to 15% conversion (**Figure 2.9** - left). Additionally, the reversible nature of the styrylpyrene [2+2] cycloaddition at sufficiently long wavelengths, opens the possibility for creating a less crosslinked material upon secondary illumination. This was tested in a thiol-methacrylate resin with sequential illumination at 405, then 365 nm. While the dimerization proceeded rapidly, the cleavage of the crosslinks showed an efficiency of only 10% (**Figure 2.9** - right). To improve the styrylpyrene resin for dual-cure applications, the wavelength for dimer-cleavage as well as the resin composition should be altered and a spacer between the functional SP-group and the acrylate should be considered.

2.3.7 Uracil and Its Derivatives

Uracil, Pyrimidine-2,4(1H,3H)-dione, is one of the four nucleic acids, with thymine being its methylated derivative. Dimerization of the 5,6 carbon double bond in uracil (U) and thymine (T), respectively was found to be triggered by UV light. Contrary to thymine, uracil does not show reversibility, however, a higher sensitivity to photodimerization.^{316,317} The process was investigated in numerous studies with respect to compound concentration, wavelength, mechanistics, solvent and oxygen concentration in solution^{318–321}.

Nucleic acids have been subject to a number of photochemical studies with focus on biochemical processes, especially for DNA-related research and for drugs in chemotherapy.^{322–324} In simple crosslinking experiments, uracil and thymine showed the

formation of insoluble fractions when used in sidechains of poly(vinyl alcohol).^{316,325} Some studies already used thymine derivatives for applications like hydrogel formation³²⁶, for environmentally friendly water-soluble photoresists³²⁷ or light-triggered covalent bonding in self-assembled structures in bio-inspired thymine-based bolaamphiphilic molecules.³²⁸

Zhao et al. used thymine, immobilized on the surface of mesoporous silica nanoparticles, to create a gate-like structure and cage or release guest molecules upon irradiation (365 nm or 240 nm, respectively).³²⁹

Additionally, reactivity of uracil, thymine and their derivatives was investigated. While long alkyl chain substituents increased the reversibility of thymine compared to an ester derivative³¹⁷, 5-tert-butyl substituents blocked the formation of [2+2] cyclodimers due to steric hindrance³³⁰.

Several studies proposed to substitute one or both carbonyl-oxygens with sulfur atoms to generate red-shift. In uracil the absorption limit could be pushed to about 400 nm³³¹ and thymine shifted from absorption maximum of 267 nm (T), to 275 nm (2TT), 335 nm (4TT) and 363 nm for 2,4-dithiothymine (2,4TT).^{332,333} These molecules show higher triplet quantum yields and promise an increased effectiveness as UVA chemotherapeutic agents in deeper-tissue applications.^{324,332}

In this small molecule study, uracil and thymine showed no reactivity at 365 nm or higher (**Figure 2.10** and **Figure 2.10**). Therefore some of their thiolated derivatives were synthesized. The absorption spectra show a distinct red-shift upon implemented sulfur atoms. The double substituted 2,4-dithiothymine showed the highest shift with absorption up to 430 nm (**Figure 2.10**).

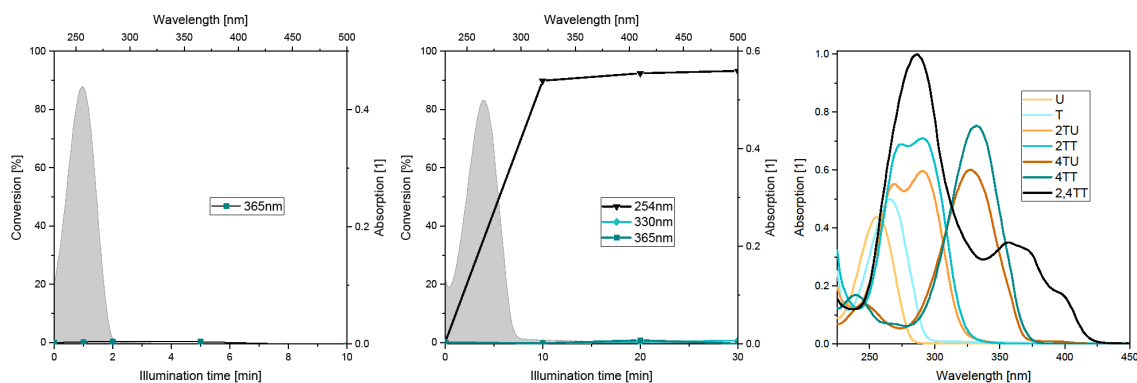


Figure 2.10 – Reaction kinetics of uracil (left) and thymine (middle) upon illumination with different wavelengths and the respective UV-Vis spectrum (grey). Thiolation of the carbonyl group results in a red-shift of the absorption spectra (right).

The two uracil derivatives, 2-thiouracil (2TU) and 4-thiouracil (4TU) were investigated in solution (0.05mM, ACN). 2TU showed no substantial dimerization at suitable wavelengths, only at 254 nm (**Figure 2.11**). 4TU showed reaction upon all illumination wavelengths with 365 nm having the fastest conversion, followed by 405 nm and 450 nm, which only reached 20% conversion in the investigated time-frame (**Figure 2.11**). Even though no full orthogonality could be achieved with 4TU, it could still be used if kinetics were taken into account and polymerization times were short.

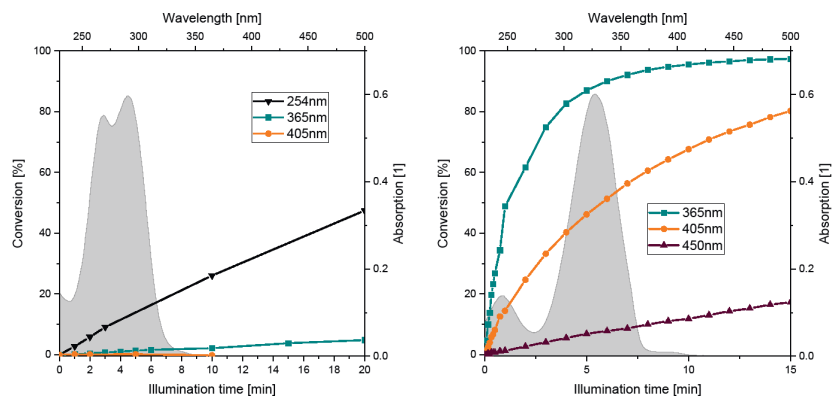


Figure 2.11 – Reaction kinetics of 2-thiouracil (left) and 4-thiouracil (right) upon illumination with different wavelengths and their respective UV-Vis spectra (grey).

The three thymine derivatives, 2-thiothymine, 4-thiothymine and 2,4-dithiothymine, were investigated in solution (0.05 mM, ACN). While 2TT showed only marginal reactivity (10%) at the desired wavelengths, 2,4TT showed high conversion at all wavelengths, even 450 nm (**Figure 2.12**). Therefore, they are both not suitable for dual-cure applications. 4TT, however, is a promising candidate as it shows relatively fast and almost full conversion at 365 nm, while dimerization at 450 nm is negligible (**Figure 2.12**).

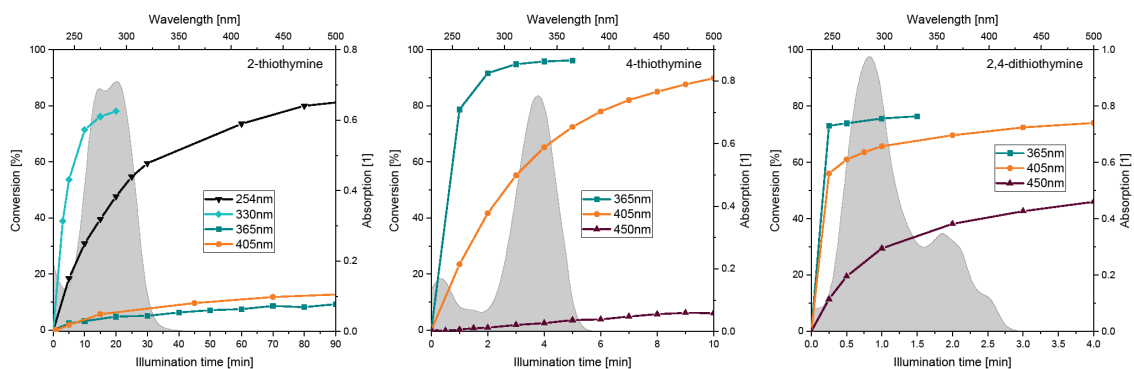


Figure 2.12 – Reaction kinetics of 2-thiothymine (left), 4-thiothymine (middle) and 2,4-dithiothymine (right) upon illumination with different wavelengths and their respective UV-Vis spectra (grey).

2.3.8 Conclusion

After investigation of the reaction behavior of several functional groups toward photo-induced dimerization in solution, only four show promising properties for further investigation. Chalcone, 4-thiothymine, anthracene and styrylpyrene display distinct conversion differences upon 450 nm and 365 nm or 405 nm irradiation. Their reactivity must be confirmed in resin formulations in the presence of a photoinitiator and possible sensitizing molecules. Additionally, styrylpyrene showed indications for cycloreversion, which should be further studied with respect to the choice of wavelength for bond cleavage and resin environment. Its potential use in dual-cure 3D printing would result from an initial fully crosslinked material, with light-triggered softening.

The chalconyl group was chosen as a first candidate for implementation into a

thiol-methacrylate dual-cure resin, which will be elaborated in the following chapter (Chapter 2.4).

2.3.9 Materials and Methods

Synthesis: Hydroxy-styrylpyrene (SP-OH) was synthesized adapting a previously published procedure.^{3,334} 1-Bromopyrene (3.0 g, 10.7 mmol) and Palladium(II)acetate (0.12 g, 0.53 mmol) were flushed with nitrogen in a round bottom flask for 10 min. Triethanolamine (2.9 ml, 21.4 mmol) and DMF (50 ml) were added with a syringe and the reaction is stirred until completely dissolved. 4-acetoxystyrene (2.0 ml, 12.8 mmol) was added slowly and the reaction mixture was heated to 100°C and stirred over night. After cooling to room temperature water (50 ml) was added and the solution was neutralized with 1N HCl. The product was extracted with ethyl acetate (3x50 ml), washed with brine (3x30 ml), dried over sodiumsulfate and the solvents removed under reduced pressure. Purification was done by column chromatography (cyclohexane:ethylacetate 4:1) and subsequent recrystallization from DCM. Yield: 23% NMR is displayed in **Figure 2.S1**

Styrylpyrene-acrylate (SP-A) was synthesized similar to a published procedure.³³⁵ 0.3 g of **SP-OH** (0.97 mmol) was flushed with nitrogen in a round bottom flask and dissolved in dry THF (10 ml). Trithylamine (0.2 ml, 1.45 mmol) was added and the mixture was cooled in an ice bath. Acrylcarbonylchlorid (131 mg, 1.45 mmol) was added dropwise. The reaction was stirred over night at RT, washed with HCl (3x20 ml), NaHCO₃ (50 ml) and brine, then dried, filtered and the solvent evaporated at reduced pressure. NMR is displayed in **Figure 2.S1**.

2-(2-(thymine-1-yl)acetoxyl) ethyl methacrylate (T-HEMA) was synthesized according to a two-step protocol.³³⁶ HEMA (13 g, 0.1 mol) and TEA (15 ml, 0.107 mol) were dissolved in CHCl₃ (300 mL) and bromoacetyl chloride (8.3 ml, 0.1 mol) was added drop-wise while cooling in an ice bath. After stirring for 2 days, any remaining bromoacetyl chloride was quenched with methanol (5 ml). The solution was stirred for an additional 30 minutes and then poured into saturated aqueous NaHCO₃ (100 ml). The organic phase was washed with water (2x100 ml), dried with anhydrous MgSO₄, filtered, and concentrated under vacuum, resulting in a brown oil. This product underwent further purification via column chromatography (ethyl acetate:hexane 1:4), yielding Br-HEMA as a colorless oil (10.5 g, 39% yield). Thymine (2 g, 14.2 mmol) and anhydrous K₂CO₃ (2.21 g, 14.2 mmol) were added to dry DMF (100 ml) and stirred for 30 min. Then tetrabutylammonium iodide (0.33 g, 0.9 mmol) was added and the mixture cooled in an ice bath. Br-HEMA (2 g, 8 mmol) was added dropwise and stirred for 2 days at RT. The mixture was filtered and the solvent was removed at reduced pressure. The remaining solid was extracted with DCM, filtered and concentrated. Column chromatography with MeOH:DCM (2:98) yielded a white solid after removal of solvents (1.2 g, 51% yield, **Figure 2.S2**).

4-thiouracil (4TU), 4-thiothymine (4TT) and 2,4-dithiothymine (2,4TT) were synthesized according to the protocol published by Lapucha et al.³³³ Tetrathosphorus decasulfide (4.4 g, 10 mmol) was dissolved in diglyme (100 ml) and the corresponding uracil derivative (uracil for 4TU, thymine for 4TT and 2-thiothymine for 2,4 dithiothymine; 10 mmol) was added slowly (evolution of carbon dioxide) while stirring. The mixture is stirred at 110°C until full turnover (TLC) and poured onto cold water. The solid product is isolated by filtration, washed with cold water, dried and recrystallized from water. The reaction was

confirmed by IR and UV spectroscopy (**Figure 2.S3**).

UV-Vis Spectroscopy: UV-Vis spectra were recorded on a Varian Cary 50 UV-Vis spectrophotometer (Agilent Technologies Inc, Santa Clara, USA; software: Cary WinUV Scan version 3.00(182)). Data processing was done with MestReNova version 14.2.0 and SpectraGryph version 1.2. All spectra were used without baseline correction. The signal change was recorded at the long-UV peak maximum. For basic absorption spectra and a first evaluation of dimerization reactivity the samples were diluted to a concentration of 0.05 mM in acetonitril. The spectra were recorded at 200-600 nm with a scan rate of 4800 nm min⁻¹ and a datapoint interval of 1.0 nm. Illumination was done directly in the quartz cuvette. To evaluate dimerization in a resin, the sample was dropcoated onto a calciumfluoride disc (thickness=1 mm; diameter=10 mm). The sample thickness was reduced until an absorption below 1 was achieved. The spectra were recorded as in solution. Illumination was done on external lamps in a stepwise manner. This allows for simultaneous investigation of FTIR and UV signals.

FTIR Spectroscopy: FTIR spectroscopy was done on a Bruker Vertex 70 FTIR spectrometer (Bruker Corporation, Billerica, USA) in a range of 4000-850 cm⁻¹ and a datapoint interval of 4 cm⁻¹ in transmission mode (software: OPUS version 6.0). Data processing was done with MestReNova version 14.2.0 and SpectraGryph version 1.2.

Irradiation: For each illumination step the sample was removed from the spectrometer, illuminated with the respective lamp and measured on the FTIR and/or UV-Vis spectrometer. The lamps used are listed in **Table 2.1**.

Table 2.1 – Lamps used in irradiation experiments for photo-reactive groups.

Wavelength nm	Label	Manufacturer	Intensity mWcm ²
254	Low pressure Hg lamp	unknown	2.2
330	OmniCure S1000 OmniCure with filter	EXFO Photonic Solutions	18
365	LED Control 5S-100W with a UV-LED Spot P	Opsytec Dr. Gröbel	470
405	LED Control 5S-100W with a UV-LED Spot P	Opsytec Dr. Gröbel	227
450	LY-A180 wireless LED dental curing lamp	Kongsin Dental	4.5

2.4 Chalcones as Sequentially Orthogonal Crosslinkers in Multi-material 3D printing of Macro- and Microscopic Soft Active Devices

Orthogonal photoreactions have recently gained increased attention in polymer chemistry and additive manufacturing processes, as they offer the possibility of a spatial and temporal control of material properties. Different UV-Vis absorption of at least two chromophores enables the individual activation of two separate reactions. However, only a few such systems with full λ -orthogonality have been published so far, as the overlap of absorption in the lower wavelength range often prevents selective activation.⁴⁰ They include, for example, λ -orthogonal deprotecting groups for surface modification developed by Bochet and co-workers,³³⁸ and a mixture of photoswitches containing azobenzene and a donor-acceptor Stenhouse adduct discovered by Feringa and co-workers.⁸⁵ Recently, Barner-Kowollik and co-workers published a λ -orthogonal two-color flow reaction, where a [2+2] cycloaddition reaction led to folding of a polymeric chain into macrocycles.³³⁹ Most of the applied systems, however, are not fully orthogonal, but show wavelength selectivity or sequential orthogonality, in which a certain order of illumination must be followed to separate the reactions.⁸³ While some restrictions are added by the order of reactions, these systems still retain the benefits of multi-step control over material properties.

While photoinitiators are commonly used for the curing of resins in light-controlled additive manufacturing technologies, the specific introduction of reactive chromophores into the formed 3D structure is still unexplored. However, these molecules offer the advantage of selective reactivity and the possibility to control the properties of materials spatially and temporally, which contributes to the increasing number of scientific publications in the field of polymer science over the last decade.^{340–344} In particular, photoinduced [2+2] cycloaddition reactions of conjugated π systems were found to be a versatile tool to alter crosslinking density in macromolecular systems.^{39,345–354} While cinnamic acid, coumarin, stilbene, chalcone, thymine, and their derivatives have been known for their reactivity under light for several decades^{285,355}, their application in photoresists, nanocarriers, self-healing and shape memory polymers has only been investigated within the last two decades.^{107,354,356} Recently, pendent cinnamate and coumarin groups have been exploited for the creation of temporary crosslinks in shape memory polymers (SMPs) enabling reversible shape fixation.^{345,346,348,349,351,357} Coumarin has also been used in star-shaped poly(ϵ -caprolactone) to realize SMPs with different shape transition behaviour³⁵⁰ and in a hydrogel to induce shape morphing as well as a different swelling behavior using light modulated cross-linking density.³⁵² Moreover, Rossegger et al. for the first time implemented coumarin as a crosslinkable functionality into a 3D-printable acrylate resin.³⁹ Although there are already some reports dealing with the control of cross-linking density in 3D structures using the photoreactivity of conjugated π systems,^{39,353,358} cycloaddition reactions are not yet sufficiently utilized in the field of additive manufacturing.

The development of photocurable resin systems containing polymerizable chromophores with orthogonal [2+2] reactivity paves the way towards spatial control of network density and thus the realization of multi-property 3D architectures. Herein, a dual-cure, single-vat resin was developed, based on the radical polymerization of a thiol-methacrylate monomer system containing covalently bound chalcone groups as dimerizable crosslinkers. Chalcones

This chapter was submitted for publication to *Advanced Materials* in 2024.³³⁷

are naturally occurring α,β -unsaturated carbonyl compounds, abundant in nature³⁵⁹ and have already been used in the side chain or backbone of polymers to alter the crosslinking density and material properties.^{360–373} By adding chalcone derivatives to both ends of a polymer chain, macrocycles could be created by simple illumination.³³⁹ In liquid crystals, chalcone units were used for controlled alignment³⁷⁴ and in ribbon-like crystals, a light-induced bending could be observed due to the solid-state [2+2] cycloaddition.³⁷⁵ In the current approach, thermo-mechanical properties of thiol-methacrylate networks are spatially and temporally controlled via the λ -orthogonal [2+2] cycloaddition reaction of pendent chalcone groups during printing or alternatively in a post-processing step. The change in crosslinking density enables a distinct control of the glass transition temperature (T_g), modulus, shape memory transition and swelling ability. Apart from conventional DLP printing, two-photon absorption lithography and micro molding have been used for the fabrication of stimulus-responsive microstructures, applicable for soft active devices.

2.4.1 Resin Design

The concept for the spatial control of the network density is based on the integration of chalcone groups into the photopolymer network exhibiting orthogonal photoreactivity to the photoinitiator used (**Figure 2.13-A**). Consequently, 4'-hydroxy chalcone was functionalized with methacrylate groups (**Figure 2.S4**) and was exploited as a co-monomer in a reactive thiol-methacrylate system consisting of triethylene glycol dimethacrylate, hexanedithiol, pyrogallol (stabilizer) and bis-(4-methoxybenzoyl)diethyl germane (BMBDG) as a photoinitiator (**Figure 2.13-B**). As shown in **Figure 2.13-C**, BMBDG provides significant absorption in the visible range (up to 470 nm), while the chalconyl chromophore of Ch-MA absorbs light primarily in the UV region.

The orthogonal reactivity of the PI and chalconyl moieties was demonstrated by FTIR and UV-Vis spectroscopy, respectively (**Figure 2.13-D**). The initial polymerization occurs under illumination with light of 450 nm (10.8 J/cm^2) by the mixed-mode radical reaction of methacrylate and thiol monomers. In this step, the chalconyl methacrylate is incorporated into the polymeric network via thiol-methacrylate and methacrylate homo-polymerization. While FTIR spectroscopy revealed a rapid decrease of thiol (2572 cm^{-1} ; 75% conversion) and methacrylate groups (1608 cm^{-1} ; 98% conversion), UV/Vis spectroscopy showed that the chalcone groups (absorption at 328 nm) are not reactive at 450 nm. The fact that (i) the subsequent irradiation at 405 nm (204 J/cm^2) leads to an almost quantitative conversion (95%) of the chalcone groups and (ii) the methacrylate groups show no further reaction at this wavelength proves the orthogonality of the two photoreactive systems.

The effect of the additional crosslinking formed by the dimerization of the pedant chalcone groups on the thermo-mechanical properties was investigated by dynamic mechanical analysis (DMA) as revealed in **Figure 2.13-E**. While the network without post-exposure (yellow line) shows a glass transition temperature of 18 °C, the T_g gradually increases up to 41 °C (817 J/cm^2) when irradiated with 405 nm. It is worth noting that the change in T_g correlates with the conversion of the chalcone groups (**Figure 2.S5-A**), highlighting the ability to selectively adjust the T_g by means of the illumination dose. The observed broadening of the loss factor can be explained by the introduction of inhomogeneities in the network. Since the light intensity decreases with the film thickness according to the Lambert-Beer law, the increase in network density is less prominent in bulk than on the surface. Importantly, increasing the concentration of chalconyl methacrylate in the

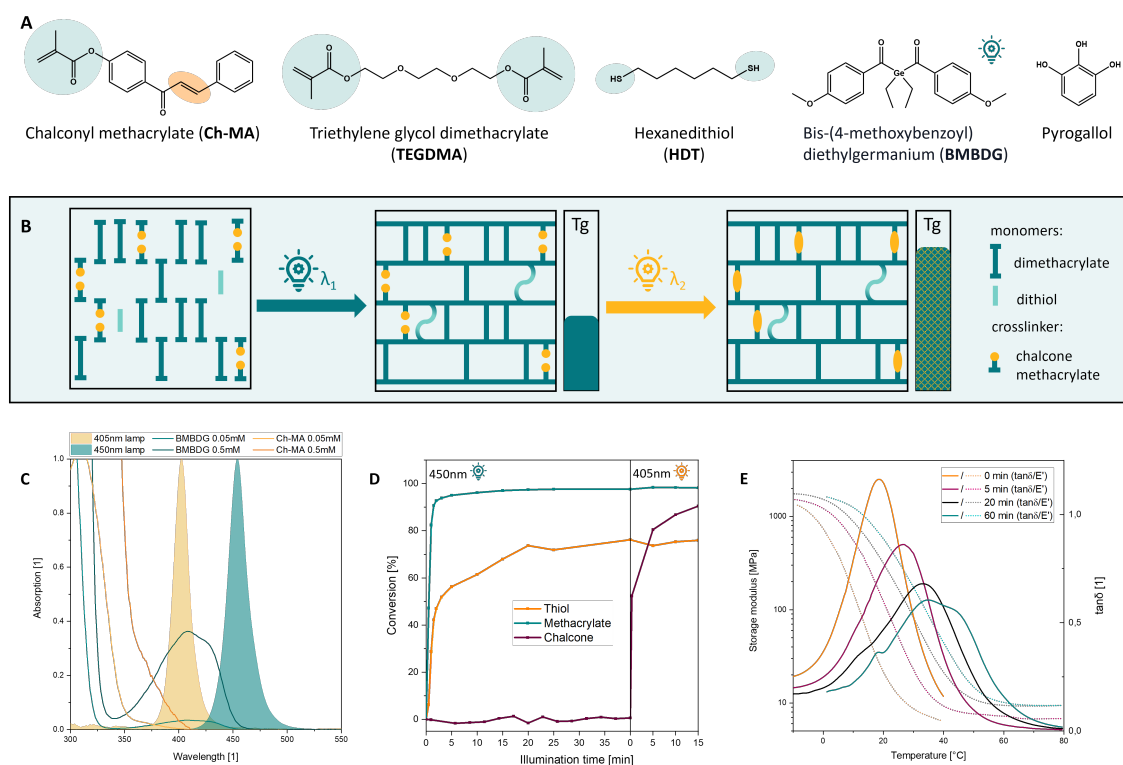


Figure 2.13 – (A) Molecular structure of the resin components. (B) Schematic representation of the spatial control of the network density using the orthogonal dimerization reaction of pendant chalcone groups. (C) Overlap of emission and absorption spectra of the photoreactive compounds and the light sources. (D) Reaction kinetics of functional groups (thiol: orange line; methacrylate green line; chalcone violet line) upon illumination with 450 nm (4.5 mW/cm^2) and 405 nm (227 mW/cm^2). The conversion was followed by FTIR (thiol, methacrylate) and UV (chalcone) spectroscopy. (E) Storage modulus (dashed line) and $\tan\delta$ (solid line) of thiol-methacrylate networks exposed (405 nm; 227 mW/cm^2) for different periods of time (orange line: 0 min; violet line 5 min; black line: 20 min; green line: 60 min).

resin from 20 to 40 mol% allowed for a more pronounced change in T_g (**Figure 2.S5-B**). While the addition of 40 mol% chalconyl groups had little effect on the glass transition temperature of the untreated network (18.4 ± 0.2 vs. 18.6 ± 0.3 °C), post-exposure with 405 nm resulted in an increase in T_g from 18.6 to a maximum of 47.7 °C (817 J/cm^2). In addition, the thiol-ene reactive system allows for tuning of the properties of the network by variation of the thiol concentration (**Figure 2.S5-C**). Increasing the hexanedithiol content reduces the degree of methacrylate homopolymerization, leading to higher conversion, homogeneity and lower T_g .¹³⁴ While the network without thiol exhibits a glass transition temperature of 128.2 °C, the addition of 10 wt% and 19 wt% hexanedithiol leads to a T_g of 71.9 and 18.4 °C, respectively. As shown in **Figure 2.S5-D**, the chalcone conversion is significantly influenced by the T_g and thus by the mobility of the pendent chalcone groups in the network. While the thiol-methacrylate network with 19 wt% hexanedithiol provides a conversion of 96%, only 27% of the chalcone groups have reacted in the methacrylate homopolymer.

2.4.2 Local Control of Network Density to Enable Stimuli-responsive 3D Macrostructures

The homogeneity of the thiol-methacrylate networks explains their narrow glass transition, which imparts a shape memory effect to such photopolymers. The spatial control of the glass transition temperature in 3D printed parts facilitates complex architectures with multiple shape memory transitions. To illustrate this concept, a butterfly structure was produced by molding under illumination of 450 nm, in which the lower wings were additionally exposed to light of 405 nm (408 J/cm^2) in a post-processing step, as shown in **Figure 2.14-A**. In a first step, the whole structure was heated above both T_{g_s} , i.e. $60 \text{ }^\circ\text{C}$, and deformed into a bent state (flapping wings). By cooling to $4 \text{ }^\circ\text{C}$ this deformation was fixed (programming step). Stepwise heating above T_{g_1} ($25 \text{ }^\circ\text{C}$) and subsequent heating above T_{g_2} ($60 \text{ }^\circ\text{C}$) induced a stepwise relaxation of the butterfly wings according to their illumination sequence. Most importantly, this concept also enables the permanent reshaping of the 3D printed object in the glassy state of the thiol-methacrylate network. To demonstrate this capability, a flat, U-shaped sample was 3D-printed at 450 nm, reshaped at RT and illuminated with 405 nm as illustrated in **Figure 2.14-B**. When the sample holder is removed after illumination, the sample retains the remolded shape due to new crosslinks formed during post irradiation.

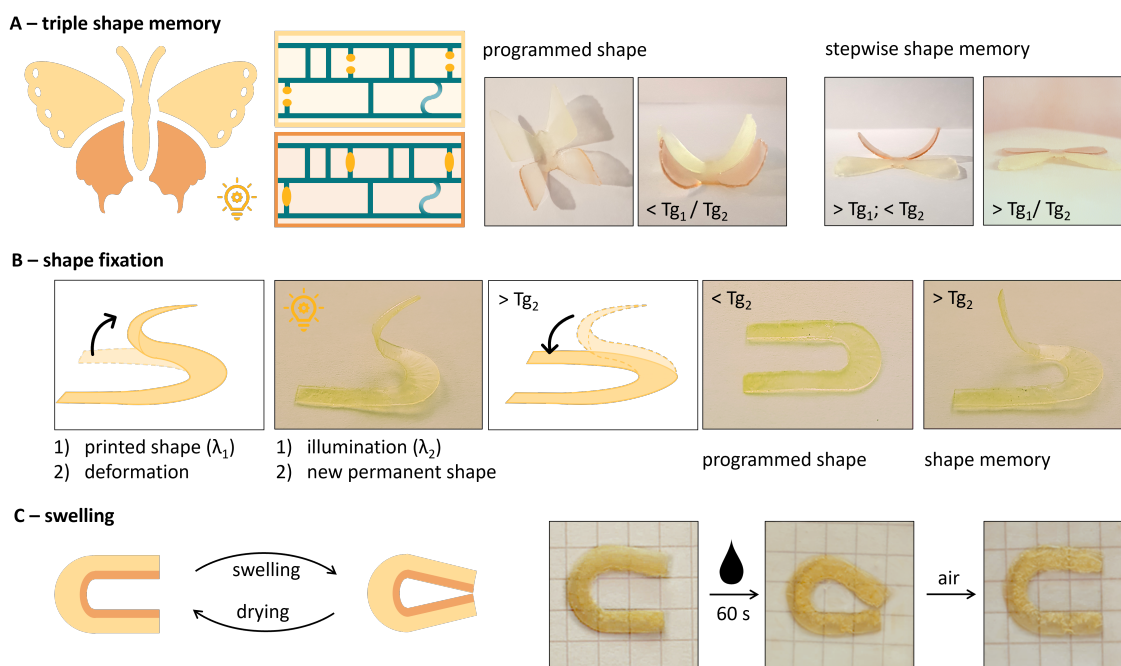


Figure 2.14 – (A) Schematic representation of the change in the polymeric network upon partial illumination with light of 405 nm (λ_2) and photographs monitoring the shape memory sequence. (B) Photographs and schemes showing the process of shape fixation. (C) Schematic representation of the gripper, which closes due to different cross-linking densities and thus swelling behavior of the orange (450 nm and 405 nm) and yellow areas (450 nm). Photographs of the reversible swelling process (right).

Besides the thermo-mechanical properties, the network density of photopolymers also determines their swelling behavior in organic solvents. In this context, the photoinduced crosslinking via pendant chalcone moieties was used to modulate the swelling behavior of the thiol-methacrylate networks in a spatially resolved manner. Consequently, a U-shaped gripper was printed at 450 nm, whereby the inner area - as shown in **Figure 2.14-C** - was additionally exposed to light of 405 nm. The immersion of the 3D structure in a solvent

mixture of dichloromethane (DCM) and ethanol (EtOH) (1:1) for 60 seconds leads to closure of the gripper. The observed motion is caused by the different swelling behavior of the inner and outer region. As shown in **Figure 2.S6**, the additional cross-linking leads to a significantly lower (approx. 25%) absorption of solvent.

2.4.3 Local Control of Network Density to Enable Stimuli-responsive 3D Microstructures

To illustrate the versatility of this approach for the fabrication of multifunctional micro architectures, pillar structures ($100 \times 40 \times 15 \mu\text{m}$) were fabricated by imprint lithography using 450 nm light. In a subsequent step, selected pillars were additionally exposed to 405 nm using a photomask (**Figure 2.15-A and B**). In a first step, the pillar assembly was heated above T_{g2} and bent by applying a compressive force using a metal plate. This shape was fixed by cooling to room temperature. When heated above T_{g1} , the columns that were not exposed to 405 nm returned to their original shape, while the others remained in the bent state until the temperature exceeded T_{g2} (**Figure 2.15-C and D**).

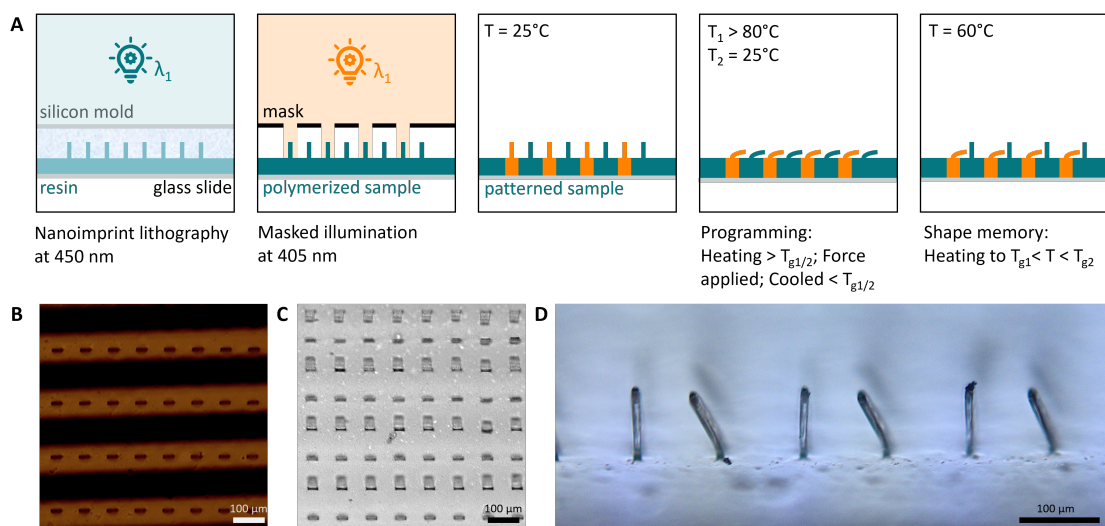


Figure 2.15 – (A) Schematic representation of the experimental setup for demonstrating the shape memory response of micro-imprinted pillars. (B) Photograph of the masking process, and (C) photograph showing different shape memory response of illuminated and non-illuminated pillars at 60°C top view and (D) side view.

For a more detailed investigation of the influence of the illumination dose on mechanical properties, squares with different doses (405 nm) were inscribed in a thin film using confocal laser lithography, which were subsequently tested by nanoindentation (**Figure 2.16**). A stepwise increase in modulus from 1.45 GPa (non-illuminated) to a maximum of 2.16 GPa (29.3 J/cm^2) was determined, resulting in an overall increase in modulus of 50% at the highest dose tested. The series of 16 scans shows good linearity with a plateau at the highest dose, which can be attributed to an intrinsic threshold of crosslinking activity due to the utilization of free chalcone groups. Apart from the exposure of printed and molded structures with light of 405 nm (see above) two-photon absorption lithography (TLP) enables an elegant way of addressing the pendant chalcone groups in the thiol-methacrylate network. This technique allows a focused and spatially resolved cross-linking reaction in 3D structures with resolutions in the sub- μm range. To investigate the two-photon induced dimerization reaction, $15 \mu\text{m}$ long line structures were inscribed into cured films using a

focused laser beam of 780 nm. As shown in **Figure 2.S7**, a clear difference in elastic modulus and adhesion was observed by atomic force microscopy. Exploiting this technique, selected pillars ($100 \times 40 \times 15 \mu\text{m}$, by imprint lithography) were subjected to exposure with 780 nm followed by the investigation of the programmed shape memory response (**Figure 2.S8**), where a less pronounced effect was observed. This may indicate a lower crosslinking efficiency at 780 nm due to a lower quantum yield of two-photon excitation.

In addition to selective crosslinking, TPL was applied to produce microstructures by exciting BMBDG with two-photon irradiation at 900 nm using a confocal microscopy laser setup. Firstly, the pattern fidelity of micron-scale features prepared of the dual-wavelength resin was determined as shown in Figure S6. Compared to mask dimensions (ideal size), positive features were $0.6 \pm 0.3 \mu\text{m}$ larger and negative features were $0.8 \pm 0.7 \mu\text{m}$ smaller than those of the digital mask, meaning that all patterned features were accurate to sub-micron resolution. Negative features are smaller on average than positive features in the patterned thiol-methacrylate networks due to diffusion of mobile species (e.g., radicals and low-molecular weight oligomers) out of the pattern boundaries.

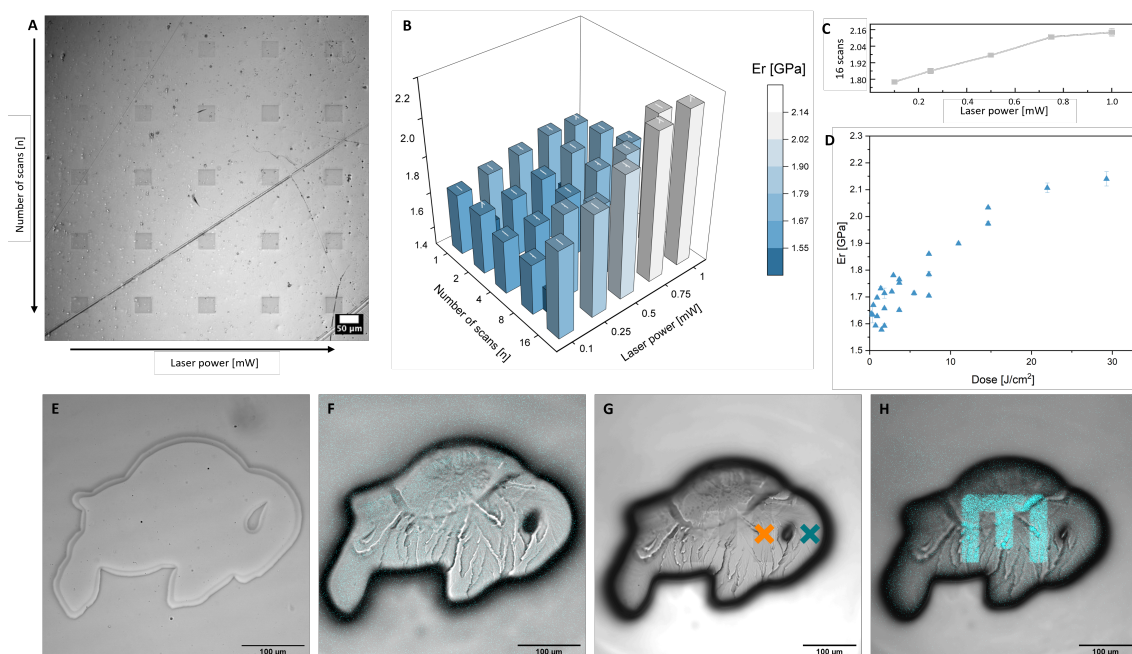


Figure 2.16 – (A) Dose test with alteration of illumination conditions in each square. Laser intensity was increased by row and the number of scans by line. The moduli measured by nano-indentation are plotted in (B), with an excerpt of the highest number of scans, also yielding the highest tested modulus (C). (D) displays the correlation between overall received dose and the observed moduli. (E) Microscope pictures of the polymerized 2.5D structures in the monomer matrix (F), after development and flood curing (G), after inscription of the additional pattern with light of 405 nm (H, J). The blue and orange circles in G indicate the nano-indentation sampling sites. (D) shows an overlay with the fluorescence channel, more clearly depicting the inscribed pattern.

Secondly, 2.5D microstructures were prepared by TPL (**Figure 2.16-E and F**) and subjected to additional crosslinking by structured exposure to 405 nm light. An increase in modulus of about 10% was observed in the exposed areas (**Figure 2.16-G**) by means of nanoindentation. Interestingly, fluorescence intensity ($I_{\text{ex}} = 405 \text{ nm}$) increased following chalcone dimerization, enabling enhanced visualization of the patterned region (**Figure 2.16-H**). One possible explanation for this unexpected photoinducible fluorescence is aggregation-induced emission (AIE)-type activity; some monomeric chalcones display this behavior^{376,377} and other [2+2] cycloadditions are known to yield AIEgens.^{378–380}

2.4.4 Conclusion

In this contribution, a dual-cure, single-vat resin was investigated, based on radical polymerization of a thiol-methacrylate monomer system containing covalently bound chalcone moieties as dimerizable crosslinkers. This approach enables spatial and temporal control of the thermo-mechanical properties of thiol-methacrylate networks via the λ -orthogonal [2+2] cycloaddition reaction of pendent chalcone groups during printing or alternatively in a post-processing step. Reaction kinetics were studied with infrared and ultraviolet-visible spectroscopy to demonstrate λ -orthogonality of the polymerization and crosslinking reaction. The additional cross-linking enabled selective control of the glass transition temperature and the modulus over a wide range by the illumination dose using light of 405 nm. Spatial control of the glass transition temperature in the thiol-methacrylate networks enabled complex architectures with multiple shape memory transitions, which was demonstrated on various 3D structures fabricated by DLP-based stereolithography and imprint lithography. Moreover, TPL provided an elegant way of dimerizing the pendant chalcone groups in thiol-methacrylate networks allowing a focused and spatially resolved cross-linking reaction in 3D structures with resolution in the sub- μm range. In addition to selective crosslinking, TPL was tested for the production of microstructures by activating the photoinitiator (i.e. BMBDG) employed with two-photon excitation at 900 nm using a confocal microscopy laser system. The analysis of printed test structures showed that resolution in the sub-micrometer range is achievable with this method. The ability to orthogonally excite both the photoinitiator and the chalcone groups with high spatial resolution allows the fabrication of multifunctional microstructures and represents a versatile concept for the fabrication of novel sensor systems or soft active devices along various length scales.

2.4.5 Materials and Methods

Material and Chemicals: 4'-Hydroxychalcone (TCI, > 95%), methacryloyl chloride (Fluka), bisphenol A glycerolate dimethacrylate (bisGMA, BOC-sciences), triethyleneglycol dimethacrylate (TEGDMA, Aldrich), pyrogallol (Merck, 99.5 %) and 1,6-hexanedithiol (HDT, TCI, >97.0 %) were purchased by the respective suppliers. Bis-(4-methoxybenzoyl) diethylgermanium (BMBDG) was kindly provided by Lithoz GmbH. All materials were used without further purification.

Monomer Synthesis: 4'-(methacryloyloxy) chalcone (Ch-MA) was synthesized from 4'-hydroxychalcone and methacryloyl chloride according to literature.³⁶⁰ 5 g (22.3 mmol; 1 eq.) of 4'hydroxychalcone was dissolved in 100ml toluene and 4.5 ml (32 mmol; 1.5 eq.) of triethylamine were added to the solution. After cooling to 0 °C in an ice bath 3.25 ml (33 mmol; 1.5 eq.) of methacryloyl chloride were added dropwise over the course of 10 minutes. The reaction was kept at 0 °C for 4 hours and was further stirred at RT overnight. The reaction was washed with NaOH (2 M), brine and deionized water. The organic phase was dried over sodium sulfate, filtered and the toluene removed at reduced pressure. The product was purified by column chromatography (silica gel 60, cyclohexane:diethyl ether = 5:1; R_f = 0.25) to yield a slightly yellow solid (71%). An ¹H NMR spectrum (CDCl₃, **Figure 2.S4**) showed peaks at 2.05 (3H, Me, s), 5.76 and 6.35 (2H, HC=CH, d) and 7.17-8.12 ppm (9H aromatic and 2H, C=CH₂, m).

Monomer Characterization: For the chemical characterization of the synthesized monomer

an ¹H NMR spectrum was recorded in chloroform-d with a Nanalysis-X552 nuclear magnetic resonance spectrometer. Infrared spectroscopy was performed on a Bruker Vertex 70 FTIR spectrometer (Bruker Corporation, Billerica, USA) in a range of 4000-400 cm⁻¹ and a datapoint interval of 4 cm⁻¹ in ATR-IR mode (software: OPUS version 6.0). UV-vis spectra were recorded with a Varian Cary 50 UV-Vis spectrophotometer (Agilent Technologies Inc, Santa Clara, USA; software: Cary WinUV Scan version 3.00(182)) at 0.05 mM in acetonitrile. Data processing was done with MestReNova version 14.2.0 and SpectraGryph version 1.2.

Resin Preparation: For the resin a variable composition of TEGDMA, bisGMA, Ivocerin (1 wt%), pyrogallol (0.1 wt%) and Ch-MA (20-40 mol% of MA-molecules) was mixed and dissolved on a stirring plate at 80 °C. When the mixture was clear it was cooled to room temperature and HDT (0-25 wt%) was added. The resin was processed within 30 minutes to preparation to prevent recrystallization of Ch-MA. For all kinetics and DMA studies the resin was used without bisGMA. For 3D-printed structures and further shape memory experiments bisGMA was added with a weight ration of bisGMA:TEGDMA = 2:1.

Table 2.2 – Composition of the different resin samples for investigation of the influence of thiol content (1-3) and chalcone content (3-5), as well as specialized for nano-scale 3D-printing (6).

	TEGDMA wt%	bisGMA ^b wt%	Ch-MA mol% ^a	wt%	HDT wt%	BMBDG wt%	Pyrogallol wt%
1	82	-	20	17	0	1	0.1
2	74	-	20	15	10	1	0.1
3	68	-	20	13	18	1	0.1
4	60	-	30	21	18	1	0.1
5	53	-	40	28	18	1	0.1
6	21	42	30	18	18	1	0.1

^a mol% of all methacrylate molecules; ^b bisGMA was added for increased viscosity for improved suitability for nano-scale 3D printing.

Investigation of Cure Kinetics: The resin was drop coated between two calcium fluoride discs. UV absorption (200-600 nm; scan rate: 4800 nm/min, datapoint interval: 1.0 nm) and IR spectra (4000-850 cm⁻¹ datapoint interval 4 cm⁻¹) were recorded from the same sample in transmission mode. For each illumination step the sample was removed from the spectrometer, illuminated with the respective lamp (450 nm: LY-A180 wireless LED dental curing lamp from Kongsin Dental (Zhengzhou, China), 4.5 mW/cm²; 405 nm: LED Control 5S-100W from Opsytec Dr. Gröbel (Ettlingen, Germany) with a UV-LED Spot P at 405 nm, 227 mW/cm²) and measured again. For graphical representation of functional group conversions, the integral of the respective peaks (acrylate at 1608 cm⁻¹; thiol at 2572 cm⁻¹ in IR and chalcone at 328 nm in UV) was evaluated and plotted versus illumination time.

Dynamic Mechanical Analysis: For the investigation of temperature dependent mechanical properties dynamic mechanical analysis was performed on a Mettler Toledo DMA/SDTA861e analyzer (Mettler Toledo, Columbus, USA). A maximum amplitude of 10 μm, maximum force of 5 N and a constant frequency of 1 Hz were applied at a temperature range between -30 and 150 °C (ramp 2 K/min), dependent on the expected glass transition (T_g) temperature. The T_g was calculated as the maximum of tan δ (ratio between storage and loss modulus = E'/E''). For the sample preparation the resin was poured into silica molds (20x4x1.5 mm), illuminated with 450 nm for 7 min under nitrogen atmosphere and further 23 min under ambient conditions. Then the mold was turned upside down and illuminated for another 10 minutes. After removal of the DMA samples from the mold they were illuminated for another 20 minutes per side at 70 °C. Polymerized samples were further illuminated with 405 nm at 70 °C for 5 to 60 minutes. Extended illumination times were used compared to

FTIR spectroscopy to ensure full conversion in the thicker samples.

Stimuli Responsive Experiments: For shape memory experiments a butterfly shape (ca. 4x5 cm) was created by molding, in the same way as the DMA samples. The upper wings were masked and only the lower wings illuminated with 405 nm for 30 min. For shape programming, the sample was heated to 60 °C in the oven, then fixed in bent shape inside a metal cylinder and cooled to 4 °C. To make the two T_g s visible, a first heating step to RT and a second heating step to 60 °C (heating plate) was performed. For the shape fixation experiment, grippers of the size of 1.5x2 cm were printed on a Lithoz (Austria) CeraFab 7500 printer at 450 nm. The thickness of the grippers was 0.4 mm, which was printed with a layer thickness of 50 μm , an energy of 102 mJ/cm^2 , an intensity of 102 mW/cm^2 and a tilt speed of 10 s^{-1} for all layers. The gripper was bent up and fixated with a clamp, while illuminated with 405 nm (227 mW/cm^2) for 30 min. The sample was heated above T_g in an oven (80 °C) for 10 min and flattened by hand while cooling to RT. Shape memory was followed while heating to 80 °C again. For swelling experiments, a gripper of the same dimensions was printed on a self-constructed dual-wavelength printer based on an Anycubic Photon Mono (Anycubic Technology Co., China) with an exchangeable LED setup operating at 450nm (added) and 405nm (original). The gripper was emerged into a solvent mixture of ethanol:dichloromethane = 1:1 for 60 seconds, then removed from the solvent showing closing of the gap in the original U-shape. Reversibility was shown after drying in ambient conditions. For patterning experiments, a thin film of polymer was produced by drop coating on a glass slide and illuminating with 450 nm (3.4 mW/cm^2), in the same way as the DMA samples. A chromium coated, simple line mask was directly placed on the sample and illuminated for 30 min with 405 nm (227 mW/cm^2). The samples were examined with an Olympus BX51 light microscope. For micro scale experiments pillars of 100x40x15 μm were formed by nanoimprint lithography with a silicone mask.

Two-Photon-Lithography (TPA) Experiments: TPA writing experiments from liquid resin were conducted in multi-photon lithography (MPL) with a custom lithography system (Workshop of Photonics (WOP), Lithuania) utilizing a ultra-short pulsed laser at 515nm (CARBIDE, 1MHz repetition rate, >290fs pulse duration, Light Conversion) and a 3-axis stage (AEROTECH Nanopositioner, USA) for sample movement, further described in³⁸¹. A 63x magnification objective lens (63x, NA 1.4, Zeiss, Germany) was used for MPL. For writing in polymerized films (1) an ultra-short pulsed laser at 780nm (C-Fiber 780, 80MHz repetition rate, <100fs pulse duration, Menlo Systems GmbH) was used with a 50x magnification objective lens (50x, 0.42 NA, Mitutoyo, Japan). General writing parameters were wet to: 1mm/s writing speed, 0.5mW Power in front of objective, 500nm hatch distance, 400nm slicing distance and 200nm overlap in z.

Atomic Force Microscopy: The topography (height), adhesion, and Young's modulus measurements were performed with an atomic force microscope (JPK Nano Wizard 4, Germany) mounted on top of the Zeiss AxioObserver inverted microscope. All measurements were done with a PPP-NCHR cantilever (Nanosensors, Germany; nominal spring constant = 42 N/m). Before each measurement, the exact cantilever spring constant and the sensitivity were determined on the substrate adjacent to the sample area using the contact-based calibration method (JPK, Germany). JPK QI@mode was used to record complete force–distance curves in each measured pixel. Height, adhesion, and Young's modulus (elasticity) were extracted from force–distance curves via JPK data processing software. Young's modulus was obtained by fitting Hertz-contact model (paraboloid tip shape; tip radius of 15 nm; Poisson's ratio of 0.40).

For imprint mask fabrication, the two-photon lithography (TPL) system PPGT 2 (Photonic Professional GT2, NanoScribe GmbH & Co. KG, Eggstein, Leopoldshafen, Germany) with the associated large features solution set was used, consisting of a 10x NA0.3 Objective, the negative-tone photoresist IP-Q (Nanoscribe GmbH & Co. KG, Eggstein-Leopoldshafen, Germany) and 1" x 1" silicon substrates. A silanization procedure was applied on the substrate to enhance the adhesion of the printed polymer to the substrate surface. herefore, the substrates were subjected to corona-plasma activation (custom built, Ahlbrandt System GmbH, Lauterbach, Germany), directly followed by submersion in a silane solution (27 ml ethanol (100%), 3 ml deionized water, 5 drops of glacial acetic acid and 300 μ l 3-(trimethoxysilyl)propyl acrylate (CAS:4369-14-6)) in a tape-sealed glass Petri dish for 24 h at 70 °C. Subsequently, the already hydrophobic plates were rinsed with ethanol, dried, and baked at 180 °C for another 8 h. The substrates were drily stored at room temperature within a desiccator until usage. For the preparation of the print files via the printer's associated software standard parameters were chosen (slicing distance: 5 μ m, hatching distance: 1 μ m, scan speed: 100 mm/s, laser power: 90% of the maximum laser power). Only a non-standard shifted in scanning direction of 90° between each printed layer was introduced. After writing, the development was performed through submersion in propylene-glycol-methyl-ether-acetate for 20 min and isopropyl alcohol for 5 min. The patterning of nano-pillars was performed with the above-mentioned device setup with a 20x NA0.5 air objective, slicing of 1 μ m, hatching of 0.5 μ m, 80% of maximum laser power and scan speed of 2 mm/s.

Micro-scale 3D-printing: Photopatterning and imaging were performed on a laser scanning confocal microscope (Zeiss LSM 710) equipped with a two-photon laser (Coherent Chameleon Ti:Sapphire) and a Plan-Apochromat 10X air objective (NA = 0.45). Samples were visualized using transmitted light from the 488 nm laser line to avoid unnecessary activation of the chalcone dimerization reaction. Image acquisition was performed with the 405 nm laser line at minimum power (0.2%). Laser powers, pixel and frame sizes, and pixel dwell and averaging settings are specified below for each experiment. The resolution test and printing of the university logo was done with 900 nm (2P) at 100% power, 0.42 μ m pixel (2X zoom), 1024x1024, 0.79 μ sec pixel dwell and 4 averaging steps (frame scan). The full volume of the CU Boulder buffalo logo was scanned in this manner two times. After washing away uncured resin and flood curing the freestanding structure with visible light (450 nm LED), the sample was aligned on the microscope stage and irradiated with 1P 405 nm light (100% power, 0.5 μ sec pixel dwell, 16 scans) to pattern the Montanuniversität Leoben "M" logo. The dose test was performed as follows: On a previously cured thin film (50 μ m, 450 nm LED) illumination was performed with 405 nm, 0.83 μ m pixel (1X zoom), 1024x1024, 6.30 μ sec pixel dwell.

Nanoindentation: A Hysitron TI 950 nanoindenter was used, utilizing a 5 μ m 60 deg conical probe (NS03221302) with a 10,000 μ N capacity, to determine the local modulus at each of the points of interest within each of the photo patterned samples. Using the Triboscan 9 software, a customized point array program was run, implementing a custom load function of 5 s load, 3 s hold, and 5 s release (3 s hold to account for any stress relaxation in the material). Additionally, the program was run with 60 s motor settle time, 45 s piezo settle time, and drift correction to mitigate any baseline noise. Replicate data was then averaged and spatially plotted to image the change in modulus across the sample.

2.5 Utilizing Disparate Polymerization Mechanisms for a Dual-Cure Resin

In addition to the above described dual-cure approach with free, dimerizable groups, the introduction of network disparity through the use of two disparate polymerization mechanisms was investigated.

The thiol-Michael and thiol-ene reactions were utilized in their distinctly different mechanisms and reactivities. The thiol-Michael addition is induced by basic compounds, it proceeds in a step-growth manner and consumes thiol and ene functionalities equimolarly. In a pure acrylate resin, this reaction cannot take place. In contrast, thiol-ene reaction is initiated by radicals and proceeds via a mixed mode thiol-ene and acrylate homopolymerization. In a pure acrylate network this reaction follows the chain-growth mechanism. In a resin comprised of bifunctional acrylates and thiols with access of acrylate, a radically initiated polymerization would lead to small domains of homopolymerized acrylates within the thiol-ene network (**Figure 2.17**). In comparison, a stepwise polymerization with a photo-base (thiol-Michael) and subsequent radical photoinitiator (thiol-ene/homopolymerization) would lead to larger domains of alternating thiol and acrylate molecules from the first step, as well as long chains of homopolymerized acrylates.

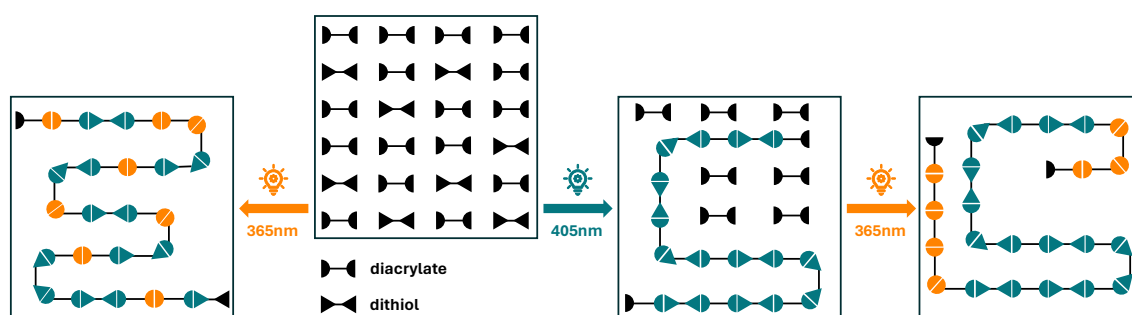


Figure 2.17 – A dual-cure approach utilizing thiol-Michael and thiol-ene chemistry is graphically depicted. Simultaneous curing of all monomers with 365 nm light (left) is shown compared to the stepwise crosslinking of thiol and acrylates (thiol-Michael addition) at 405 nm and subsequent acrylate homopolymerization (right).

The hypothesis was tested, that the difference in polymerization mechanism (step vs. chain growth) should alter the network characteristics in terms of crosslinks and chain lengths, and should therefore result in disparate mechanical properties of the fully cured resin. A resin was designed comprised of a multifunctional thiol, access of bifunctional acrylate and two photoinitiators, a long-wavelength photo base (2-(2-nitrophenyl)propyloxycarbonyl tetramethyl guanidine, NPPOC-TMG) and a shorter wavelength radical type I PI (2-Hydroxy-4'-(2-hydroxyethoxy)-2-methylpropiophenon, PI-2). The dual-cure sample would be exposed to 405 nm (thiol-Michael) before completing polymerization with 365 nm (acrylate homopolymerization), while the comparative second sample would only be exposed to 365 nm, radically inducing mixed-mode thiol-ene polymerization.

Looking at rheological measurements, the formation of a loose network through thiol-Michael polymerization is clearly visible as a step in the moduli (**Figure 2.18** - middle). IR kinetics show the change of the signals for thiol, which is depleted completely and acrylate, which is reduced to the corresponding 50 % mark as the ratio of thiol vs. ene is 1:2 (**Figure 2.18** - left). Access acrylate is subject to homopolymerization in the second

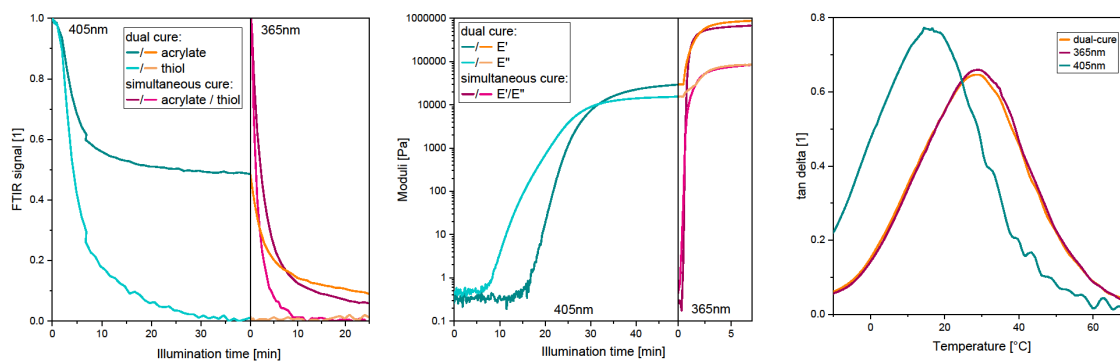


Figure 2.18 – Properties of a resin, cured in a stepwise manner, depending on the reaction regime. FTIR kinetics show the stepwise depletion of acrylate, while all thiol is consumed in the first step (left). Rheological measurements indicate the stepwise increase in mechanical integrity and network formation (middle). DMA confirms the difference between the first step and second step material in dual-cure, however shows no difference between dual-cure and 365 nm sample (right).

illumination step at 365 nm, where the signal drops below 10 % and further strengthening of the network can be monitored on the rheometer. As a second sample, the same resin was cured with 365 nm light exclusively. Rapid curing within the first minute takes place, completely crosslinking both, thiol and acrylate, at a similar speed. However, looking at the final values for the elastic and plastic moduli, the difference in material stiffness is only marginal. This can be confirmed in DMA samples (**Figure 2.18** - right) over a range of resin compositions (**Chapter 2.5.1**) with varied ratios of functionalities between thiol and acrylate as well as different branching (multifunctionality) of the thiol. The T_g for both, the dual-cure and the single-cure (365 nm) approach are comparable. However, for some resins it was possible to create an alternative material by stopping the illumination after the first step of the dual-cure approach, only crosslinking thiol and acrylate in a thiol-Michael fashion. The non-crosslinked acrylate leads to a significantly lower T_g as shown in **Figure 2.18** - right. Not all tested resins exhibited enough crosslinking within the anionic curing step to produce a solid material and therefore specimen for DMA testing.

Concluding, the hypothesis to achieve significant bulk material differences through tailored anionic-radical crosslinking could not be proved successfully. However, the stepwise crosslinking could be followed by FTIR, DMA and in rheological measurements and has potential for a different kind of dual-cure approach, exploiting the uncured acrylate for its softening influence on the material.

2.5.1 Materials and Methods

Synthesis: Synthesis of **2-(2-nitrophenyl)propyloxycarbonyl tetramethyl guanidine (NPPOC-TMG)** was done according to the protocol published by Zhang et al.⁴¹ 2-(2-Nitrophenyl)propyl chloroformate (NPPOC, 3.6 g, 15 mmol) were dissolved in 50 ml DCM. Tetramethylguanidine (2.88 g, 25 mmol) were also dissolved in DCM (100 ml) separately. The NPPOC solution was added dropwise and the reaction mixture was stirred over night at RT. The organic phase was washed with brine (3x30 ml), dried over sodiumsulfate, filtered and the solvent evaporated under reduced pressure. The product was obtained as white solvent (75% yield) and the NMR spectra are shown in **Figure 2.S11**.

Resins: Dual-cure resins were prepared according to **Table 2.3**. 1 g of resin contains 1 wt% PI-2, 1 wt% NPPOC-TMG and 0.2 wt% pyrogallol as stabilizer. The following diacrylates and thiols were used: Tricyclo[5.2.1.0^{2,6}]decandimethanoldiacrylat (TCDDA), Dipropylene glycol diacrylate (DPGDA), 1,4-Bis(acryloyloxy)butane (BDA), Tetraethylene glycol diacrylate (TEGDA), Trimethylolpropane tris(3-mercaptopropionate) (TMPMP), Pentaerythritol tetra(3-mercaptopropionate) (PETMP), 1,4-Butanediol bis(thioglycolate) (BDBTG). The measurements shown in **Figure 2.18** were sample c, a and d for FTIR kinetics, rheology and DMA, respectively.

Table 2.3 – Formulations for photoinitiator-based dual-cure resins.

Sample	Acrylate	Thiol	Thiol functionality	Acrylate excess [%]
a	TCDDA	TMPMP	3	50
b	TCDDA	TMPMP	3	200
c	TCDDA	PETMP	4	100
d	TCDDA	BDBTG	2	100
e	BDA	TMPMP	3	100
f	TEGDA	TMPMP	3	100
g	DPGDA	TMPMP	3	100

Rheology: Curing experiments were performed on an Anton Paar (Austria) Modular Compact Rheometer 102 with a measuring system in parallel-plate geometra (diameter = 25 mm). The measurement was conducted on a quartz glass plate and an external lamp was coupled to the system to allow bottom-up illumination during the measurement. A 405 nm light source (LED control, **Table 2.1**) and an OmniCure S1000 OmniCure (EXFO Photonic Solutions, Canada) with a spectrum of 320-500 nm were used. With a constant gap of 0.1 mm.

Dynamic Mechanical Analysis: For the investigation of temperature dependent mechanical properties dynamic mechanical analysis was performed on a Mettler Toledo DMA/SDTA861e analyzer (Mettler Toledo, Columbus, USA). A maximum amplitude of 10 μm , maximum force of 5 N and a constant frequency of 1 Hz were applied on a temperature range between -15 and 80 °C (ramp 2 K/min), dependent on the expected glass transition (T_g) temperature. The T_g was calculated as the maximum of $\tan\delta$ (ratio between storage and loss modulus = E'/E''). The samples were produced on the rheometer with a film thickness of 0.1 mm and cut to dimensions of 20x4 mm before testing.

2.6 Supporting Information Chapter 2

2.6.1 Supporting Information Chapter 2.3

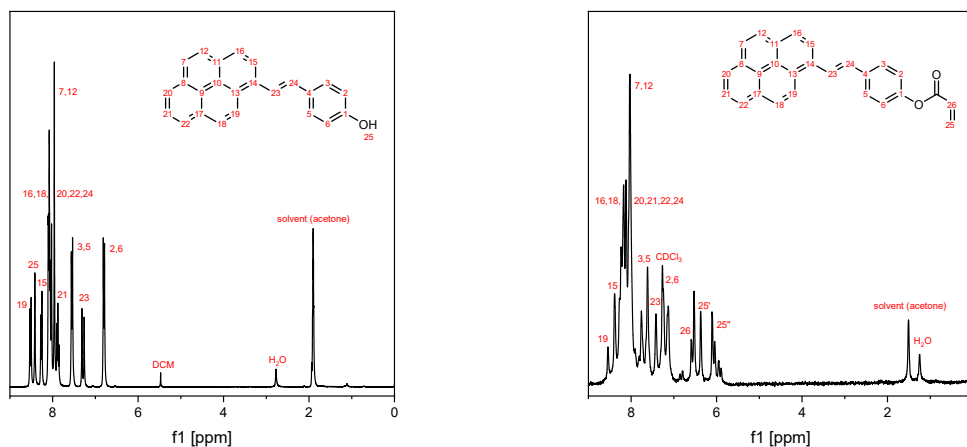


Figure 2.S1 – NMR spectra of hydroxy-styrylpyrene (SP-OH, left) and styrylpyrene acrylate (SPA, right).

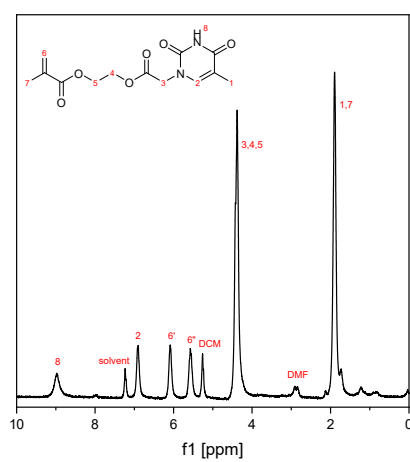


Figure 2.S2 – NMR spectrum of 2-(2-(thymine-1-yl)acetoxy) ethyl methacrylate (T-HEMA).

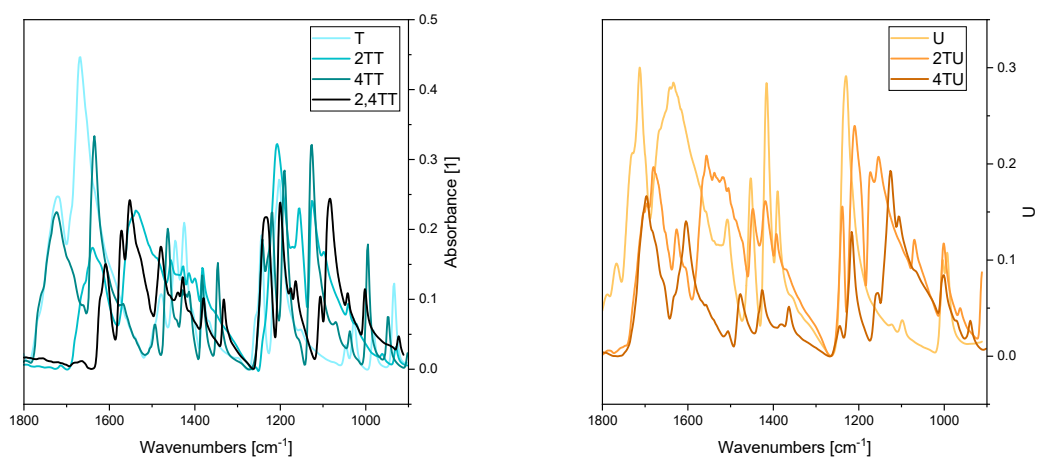


Figure 2.S3 – IR spectra of uracil and its derivatives. Structural conformation for 4TU, 4TT and 2,4TT.

2.6.2 Supporting Information Chapter 2.4

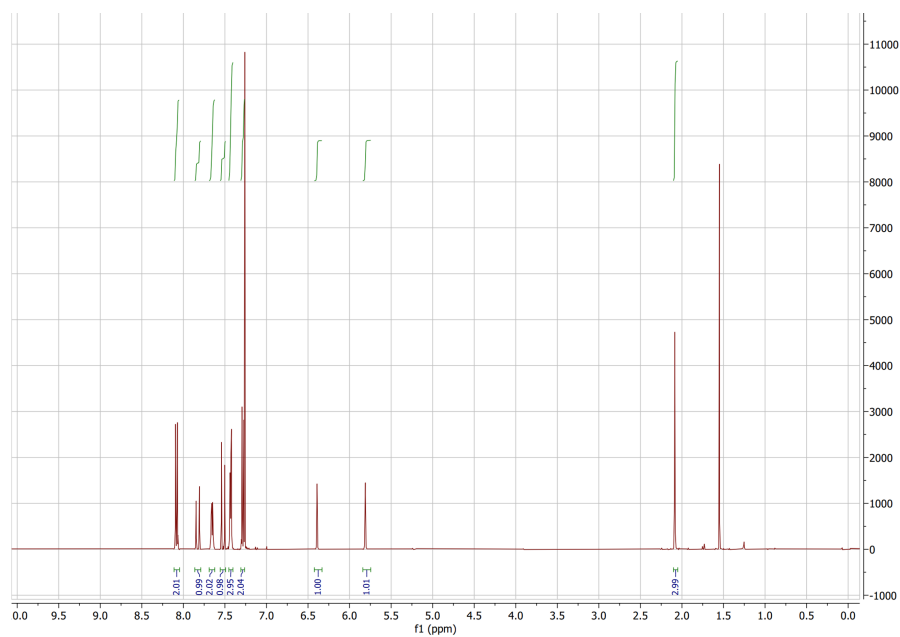


Figure 2.S4 – $^1\text{H-NMR}$ spectrum of 4'-(methacryloyloxy) chalcone (Ch-MA) after synthesis.

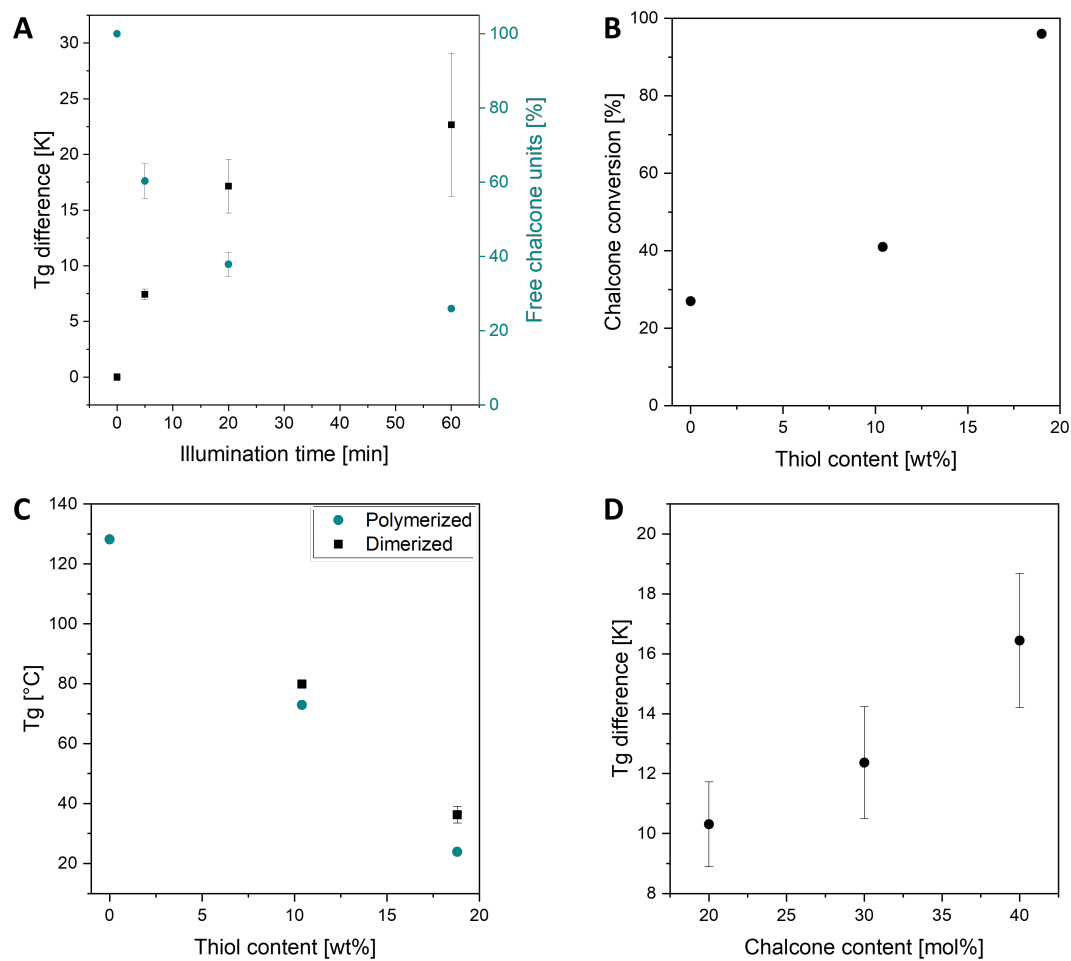


Figure 2.S5 – (A) Correlation between illumination time with 405 nm and the reduction in free chalcone units (right axis) and the achieved difference in T_g after the respective illumination times (left axis). (B) Correlation between the chalcone content and the maximum difference in T_g achievable by illumination. (C) Influence of the thiol content on the T_g with and without chalcone dimerization (black and blue, respectively). (D) Influence of the thiol content on the network mobility and the thereby achieved chalcone conversion.

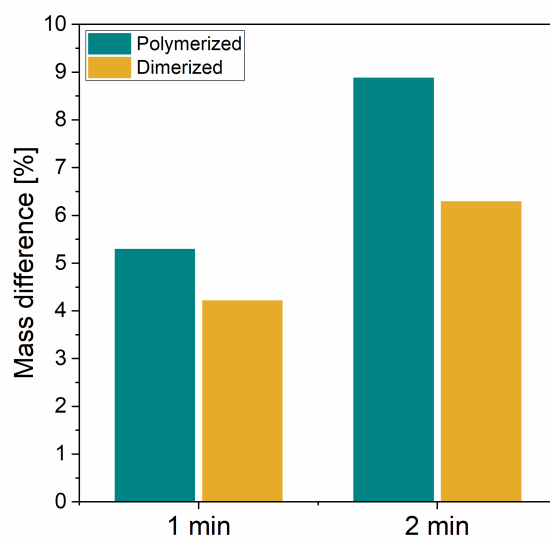


Figure 2.S6 – Mass difference in a swelling experiment between the original sample and the swollen sample. The difference in swelling behavior of the polymerized (green) and further crosslinked (yellow) sample is displayed.

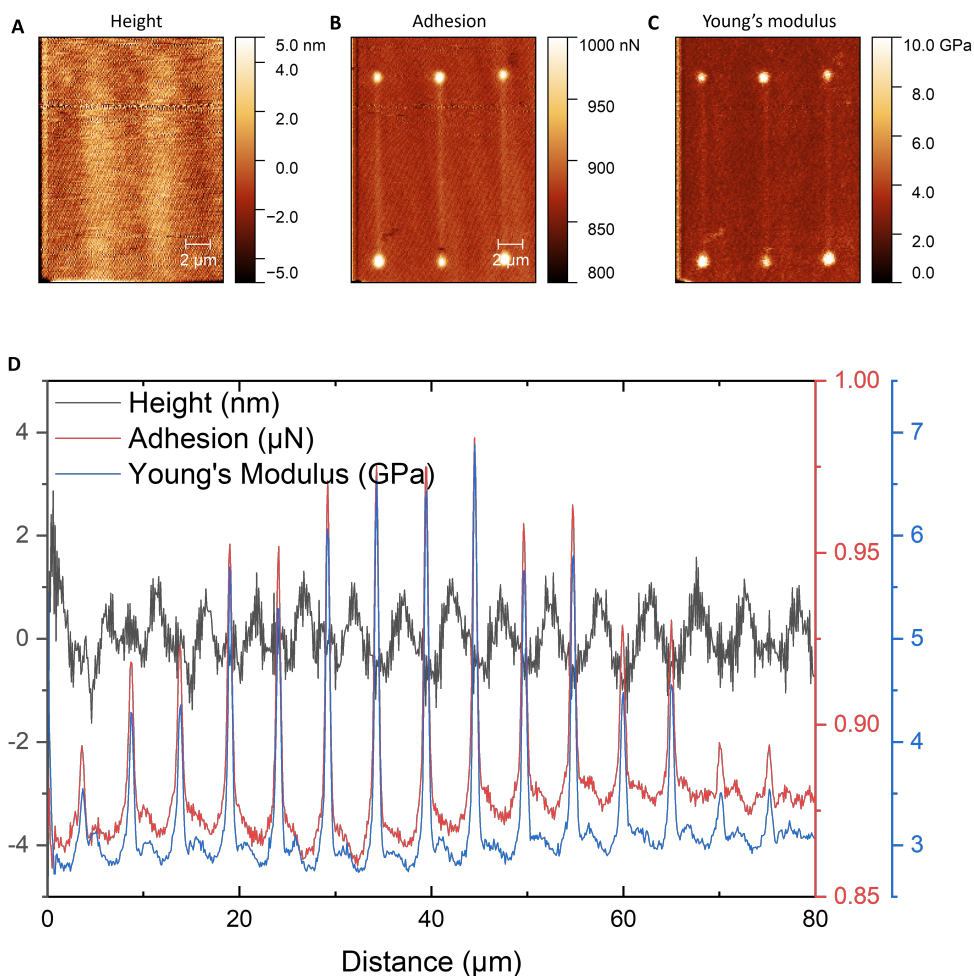


Figure 2.S7 – Lines were inscribed onto a thin film with a 780 nm laser. AFM measurements are depicted (top) with (A) the surface roughness, (B) adhesion and (C) young's modulus. (D) gives the graphical representation of the respective values.

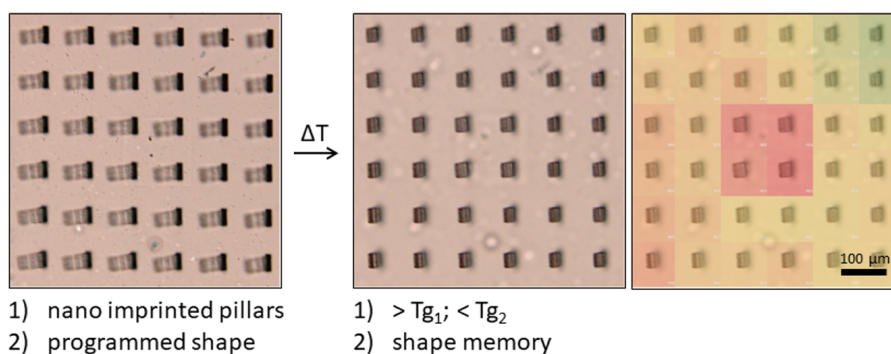


Figure 2.S8 – Shape memory experiment with nanoimprinted pillars.

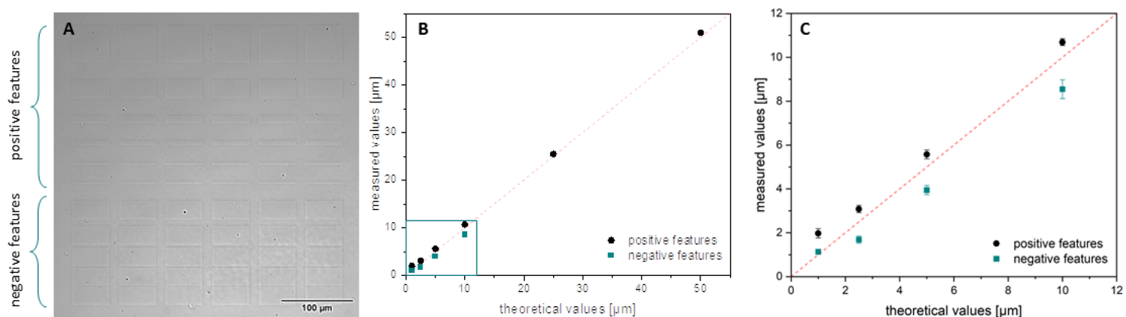


Figure 2.S9 – Resolution test of micro-scale 3D printing (900 nm; TPA) on thin film. (A) Picture of the printed structures. (B) Comparison of theoretical and measured values for the feature width with (C) magnification from B.

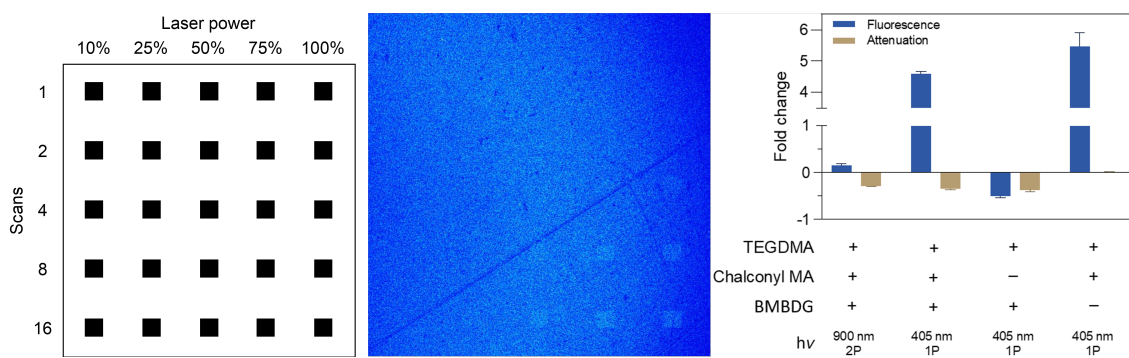


Figure 2.S10 – Matrix of varied laser power and number of scans, illustrating the optical effects of 405 nm photopatterning on a visible light-cured dual-wavelength photopolymer film (scheme left; fluorescence middle). (Right) Fluorescence (ex/em = 405/420-500 nm) and transmitted light intensity for varied formulations of dual-wavelength photopolymer. The sample containing no photoinitiator was a pre-cured film while all other samples were liquid monomer blends.

2.6.3 Supporting Information Chapter 2.5

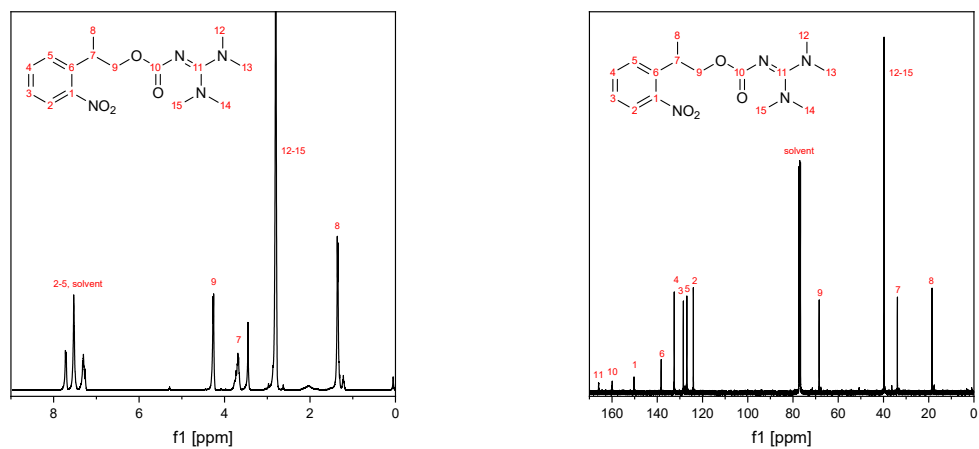


Figure 2.S11 – NMR spectra of 2-(2-nitrophenyl)propyloxycarbonyl tetramethyl guanidine (NPPOC-TMG). ^1H -NMR (left) and ^{13}C -NMR (right) measured in deuterated chloroform.

3

Photocuring Behavior of Novel Molecules and Resins

When novel monomers, photoinitiators or resins are introduced, their behavior upon illumination is crucial for comparison and possible future applications. A number of experiments are of use to characterize photo-reactive behavior, including photobleaching, UV or FTIR kinetics, rheological measurements and photo-DSC.

Novel type I radical photoinitiators, based on tin or germanium, were investigated upon their curing behavior. They can be used in future applications as an alternative to state-of-the-art phosphorous PIs with reduced toxicity¹ and pronounced reactivity in the energy-efficient, innocuous visible light region. Bio-based monomers with methacrylate, vinyl and alkyne functionalities were evaluated for their applicability in novel resins for 3D-printable biological scaffolds or coatings. Eugenyl- and vanillyl alcohol-based monomers show potential as sustainable alternatives for hydrophobic paper coatings with promising barrier and release performance. And amino acid-based monomers indicate the capability to be used in bone regeneration as they are 3D printable and their degradation products are bio-absorbable.

The following chapter will focus on FTIR kinetics and photo-DSC analysis as tools for monomer and photoinitiator characterization. After presenting some findings on biomass-derived methacrylate monomers for paper coatings (first author publication³⁸²), overall remarks on the methods of FTIR kinetics and photo-DSC analysis will be given on some examples from further publications (co-author³⁸³⁻³⁸⁷).

3.1 Low Molecular Weight Biomass-derived Methacrylate Monomers for Paper Coatings

When employing a novel photocurable resin in industry, finding the optimal reaction parameters for the photopolymerization process is a key point. While optimizing the material and reaction properties, feasibility and economic factors (e.g. time, energy, space) have to be taken into account. Up to now a variety of radically polymerized photocurable resins based on (meth)acrylates have been used in applications such as inkjet printing, photolithography and coatings^{388–390}. However, as the production and use of chemicals from renewable sources has been increasingly promoted, the investigation of biobased monomers is imperative.³⁹¹ Eugenol (2-methoxy-4-(2-propenyl) phenol), first isolated from *Eugenia caryophyllata* in 1929³⁹², and vanillyl alcohol (4-hydroxy-3-methoxybenzyl alcohol), derived from lignin, are notable for their chemical functionalization potential. Eugenol, found in plant oils such as clove, turmeric, and cinnamon oils, possesses antibacterial properties due to its aromatic ring and allyl group, effectively preventing microbial growth on coated surfaces³⁹³. Its structure, particularly the hydroxyl group, facilitates the formation of photocurable methacrylate esters. Vanillyl alcohol, in contrast, is produced by reducing the aldehyde group of vanillin, a lignin derivative.³⁹⁴ Lignin is a naturally occurring polymer distinguished by its complex chemical structure that makes up the wood tissue. Owing to the presence of methoxy, aldehyde, and hydroxyl functional group in the aromatic vanillin structure, it is possible to apply distinct functionalization approaches to this specific molecule.³⁹⁴ Vanillyl alcohol is preferred over vanillin for producing a liquid resin with methacrylic anhydride due to vanillin's tendency to form a less processable solid resin. Both compounds, eugenol and vanillyl alcohol, demonstrate significant versatility in chemical applications due to their unique functional groups.

The current study, explored two low molecular weight sustainable monomers – eugenyl methacrylate (EM) and vanillyl alcohol methacrylate (VAM) synthesized via methacrylic anhydride according to previously reported and adapted protocols.^{395,396} Using photo-DSC as a simple, but strong method for the analysis of reaction kinetics, EM and VAM were investigated upon their suitability for application in hydrophobic coatings on additive-containing paper (Glassine paper). Compared to previous works that used vegetable oil derivatives as prepolymers,^{397–401} herein we report for the first time on the paper coatings based on low molecular weight monomers. The study aimed to closely examine the polymerization kinetics across a wide temperature range in order to determine the most optimal curing conditions for the corresponding coatings. The resulting hydrophobic coatings demonstrated performance worthy of applications for packaging and release liners – paper carriers for adhesive labels.

3.1.1 Photocuring behavior

To determine the suitability of eugenol and vanillyl alcohol- based resins for biobased coatings, reaction kinetics of their respective resins were investigated. The conversion of double bonds was followed in real-time FTIR spectroscopy during a photoinitiator induced

This chapter was published as an article in *Journal of Polymer Research* on March 4th, 2024.³⁸² Reproduced with permission from Springer Nature.

radical polymerization (**Figure 3.S1**). The vanillyl alcohol-based resins (VAM and VPE) show close to full conversion (98 and 97%, respectively) while the conversion of the eugenyl based resins stops at 88 and 90% (EM and EPE, respectively) and progresses more slowly. This can be attributed to allylic proton abstraction as side reactions and the incomplete conversion of allyl double bonds.⁴⁰² When PDMS-ECEMS is added to the resin, the reaction of double bonds is slowed down intermittently, as PDMS-ECEMS acts as a diluent, to finally reach a slightly higher conversion for the eugenyl resin (EPE) compared to the pure monomer (EM) (Reaction kinetics EM VAM).

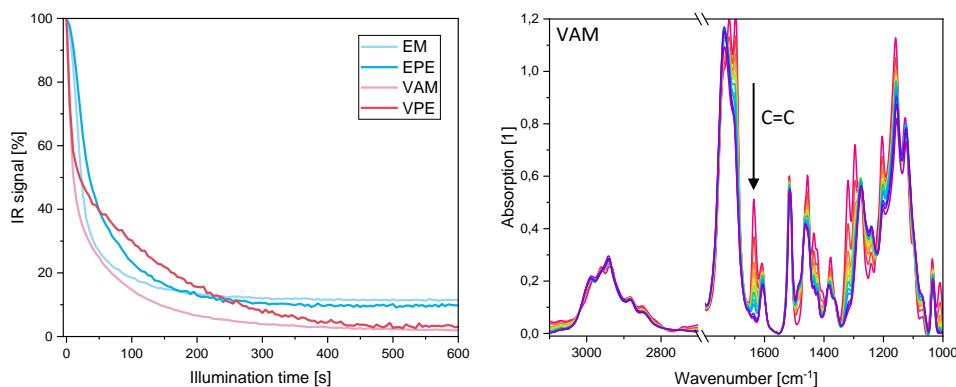


Figure 3.1 – Reaction kinetics of all resins measured on FTIR (left). Full IR spectrum of VAM over time (red to violet) during illumination (right). Double bond conversion was followed by integration of the IR signal at 1650 – 1620 cm^{-1} .

Photo-DSC measurements show a similar picture with relatively fast reaction of vanillyl-based resins within the first minute ($t_{95\%} = 27$ s and 34 s at 25 °C for VAM and VPE, respectively), while EPE and especially EM show very low heat flow and a prolonged time to 95% conversion of 3.5 min (EM) and 5 min (EPE). The difference in heat flow from eugenol-based and vanillyl alcohol-based resins can be attributed to structural differences. While VAM possesses two methacrylate groups taking part in the polymerization reaction, EM can crosslink through only one methacrylate group, with the allyl functionality being mostly inert in this process (**Figure 3.S2**). Additionally, in the PDMS-ECEMS resins, a higher heat flow can be observed, which can be attributed to epoxide rearrangement to carbonyl groups (**Figure 3.S2**) and subsequent radical addition to free double bonds.⁴⁰³ To investigate the influence of temperature on the propagation of the photoinduced curing, reaction conditions were altered in a range between -10 °C and 100 °C (**Figure 3.2** and **Figure 3.3**).

For all tested resins, the peak performance was found to be at 10–25 °C. While at lower temperatures the curing proceeded more slowly and to a lesser conversion, at higher temperatures a fast initial activity was observed. However, the increase in temperature also negatively influenced the amount of side reactions and degradation leading to a severely reduced overall conversion. Peak performance at ambient temperature is apparent in overall reaction heat (which can be linked to monomer conversion), as well as in peak heat flow (**Figure 3.S1**). This leads to the conclusion that, while a fast initial reactivity is preferred, the disadvantages of increased process costs at elevated temperatures and the reduction in final conversion outweigh the kinetic advantages.⁴⁰⁴

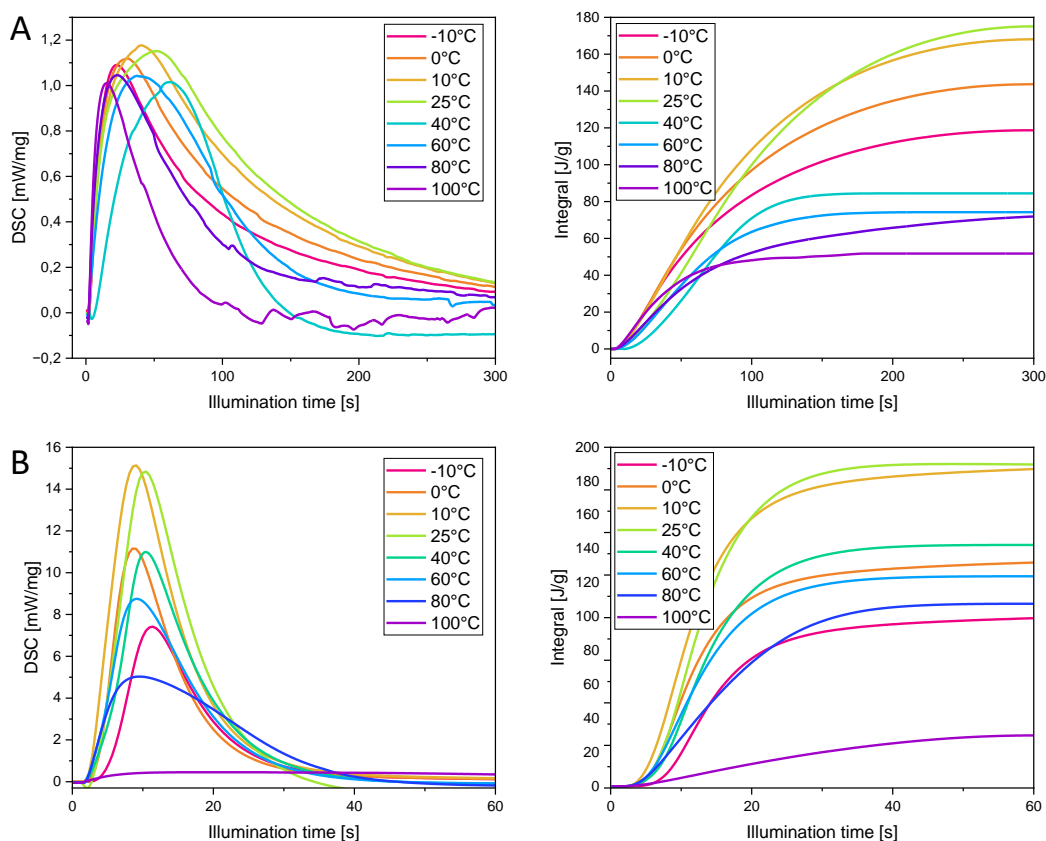


Figure 3.2 – Photo-DSC measurements of EM (A) and VAM (B) with the recorded heat flow [mW/mg], left, and the integral evolution over time, right. The overall integral can be compared to monomer or double bond conversion.

3.1.2 Photopolymerized EM and VAM coatings on paper

The hydrophobicity of eugenol and vanillyl alcohol-based coatings on paper was investigated through contact angle (CA) measurements. Pure EM and VAM exhibit a slightly hydrophilic surface finish with 83° and 70°, respectively (**Table 3.1**) and are comparable to previously published values for eugenol-derived coatings developed by Molina-Gutiérrez et al.⁴⁰⁵ varying from 82 to 92°. The slightly lower contact angle of VAM is being explained by the more oxygen-rich structure of the monomer and the tendency of these oxygen atoms to exhibit polar solvent interactions. To the best of our knowledge and literature findings, no data on the wettability of vanillin- based coatings have been available. Notably, Srikanthan et al. fabricated wood-mimicking macroporous vanillin methacrylate-based polymer matrices via porogen templating method yielding a hydrophilic porous surface and CA of 63°. ⁴⁰⁶ Upon addition of a hydrophobic additive, PDMS-ECEMS, EPE (EM with additive) and VPE (VAM with additive) coatings showed a substantial increase in hydrophobicity, with a contact angle of 106° for both. The pronounced increase in CA of 23° and 36°, respectively, shows a good compatibility between the additive and both monomers, while the low standard deviation indicates homogeneous distribution of PDMS-ECEMS withing the coating.

Comparing EPE and VPE to previously published biobased coatings on paper a good amount of hydrophobicity was achieved. While Parvathy and Sahoo developed hydrophobic paper coatings based on castor oil and epoxy methyl ricinoleate with the highest reached contact angle of 97°³⁹⁷, Loesch- Zhang et al. produced hydrophobic coatings using olive oil

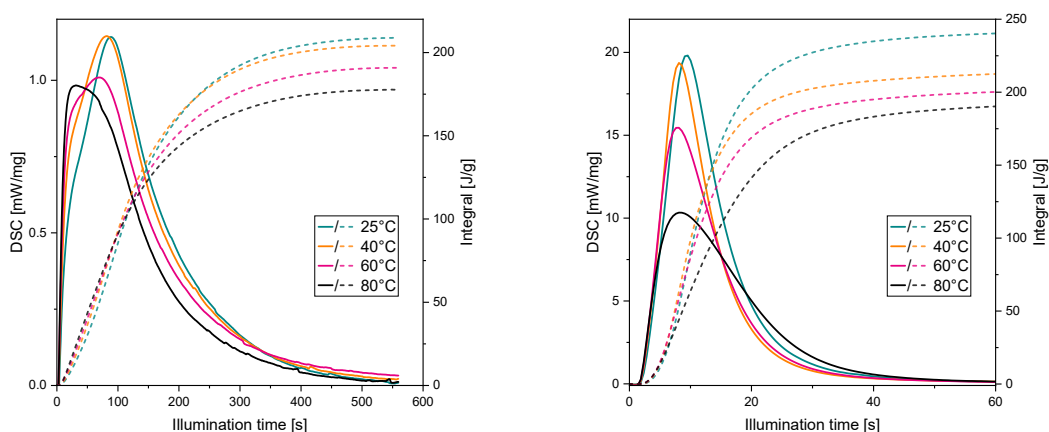


Figure 3.3 – Photo-DSC measurements of EPE (left) and VPE (right) with the recorded heat flow [mW/mg], solid line, and the normalized integral evolution over time, dashed line.

modified with 1,8-octanedithiol as a prepolymer with a contact angle of 120° ³⁹⁸. Employment of the modified vegetable oil coatings for paper packaging is on the rise. Freire's group reported on the tung oil-based photopolymerizable paper coatings with barrier function.³⁹⁹ Wettability of the coatings after being exposed to different irradiation times was significantly changed exhibiting a CA increase from 71 to 127° . The same group fabricated another type of photocurable paper coatings for packaging applications copolymerizing 2-ethylhexyl acrylate with a biobased prepolymer isobornyl acrylate.⁴⁰⁰

All the coating formulations displayed a remarkable improvement in hydrophobicity of the paper surface reaching the CA values higher than 120° . In a previous work the wettability of linseed oil-based thermoset paper coatings reinforced with distinct hydrophobic additives was studied.⁴⁰¹ The coated paper surface exhibited an average CA of 108° . In comparison to all above-referenced works, which employed vegetable oil-based molecules as prepolymers for paper coatings, this substantial study demonstrated the potential of low molecular weight monomers as an asset in the paper coatings arena and confirmed that current achievements on paper surface modification with biobased coatings likely pave the way for opening a new chapter in sustainable approach with positive prospects for paper industry.

Table 3.1 – Water contact angle of the UV-polymerized EM and VAM coatings on glassine paper.

Sample	Contact angle [°]
EM	83 ± 4
VAM	70 ± 1
EPE	106 ± 2
VPE	106 ± 3

3.1.3 Conclusion

In this study a comprehensive investigation of the photopolymerization behavior of eugenol and vanillyl alcohol-based resins was presented, emphasizing their application in the development of hydrophobic coatings for paper substrates. Through photo-DSC analysis and FTIR

spectroscopy, superior reactivity and conversion rates of vanillyl alcohol-based resins (VAM and VPE) compared to their eugenol-based counterparts (EM and EPE) were found and linked to the structural distinction between the resins, particularly the presence of multiple reactive sites in VAM. Moreover, the addition of PDMS-ECEMS as a hydrophobic additive significantly enhanced the surface hydrophobicity of the coatings, demonstrating the potential of both biobased resins in creating effective hydrophobic surfaces on paper. Temperature was found to play a crucial role in the polymerization process, with optimal reactivity observed at ambient temperatures (10-25 °C). Higher temperatures, while accelerating the initial reaction rate, adversely affected the overall conversion. This insight underscores the importance of carefully controlled reaction conditions to achieve efficient polymerization while minimizing costs and environmental impact. The findings of this research not only contribute to the growing body of knowledge on biobased photocurable resins but also highlight the practical implications of these materials in sustainable coating applications. By leveraging the unique properties of eugenol and vanillyl alcohol-derived resins, environmentally friendly alternatives for the paper coating industry can be further explored, aligning with the global shift towards renewable resources and sustainable manufacturing practices.

3.1.4 Materials and Methods

Materials: Eugenol 99%, vanillyl alcohol 98%, methacrylic anhydride 94%, 4-dimethylaminopyridine (DMAP) 99%, 1-hydroxycyclohexyl- phenylketone 99% (trade name Irgacure 184), dichloromethane 99.5%, ethyl acetate 99.5%, sodium bicarbonate 99.7%, molecular sieve 0.4 nm beads with moisture indicator and poly-dimethylsiloxane-co-(2-(3,4- epoxy cyclohexyl)-ethyl)-methylsiloxane (PDMS-ECEMS) were purchased from Sigma-Aldrich and used as received.

Synthesis and Resin Preparation: 20 g (121.8 mmol, 1 eq.) eugenol, 20.6 g (133.6 mmol, 1.1 eq.) methacrylic anhydride (MA) and 0.15 g (1.2 mmol, 0.01 eq.) DMAP was added to a round bottom flask equipped with a thermometer and a magnetic stirrer (200 rpm) and intensively gassed with nitrogen. The mixture was left to react for 24 h at 45 °C. Afterwards, the reaction mixture was diluted with ethyl acetate and dichloromethane and washed with 1 wt% solution of sodium bicarbonate. The mixture was left on a molecular sieve overnight and the solvents were evaporated to yield a yellow oil. **Figure 3.S3** 20 g (129.7 mmol, 1 eq.) vanillyl alcohol (VA), 40 g (259.5 mmol, 2 eq.) methacrylic anhydride and 0.2 g (1.6 mmol, 0.012 eq.) DMAP were reacted in the same way, however, the reaction took place for at least 48 h due to the low solubility of VA in MA yielding a colorless oil. Four formulations were prepared as follows (**Table 3.2**):

Table 3.2 – Photocurable formulations derived from EM and VAM resin.

Formulation	I184 [g]	EM [g]	VAM [g]	PDMS-ECEMS [g]
EM	0.02	1.0	-	-
VAM	0.02	-	1.0	-
EPE	0.02	1.0	-	0.1
VPE	0.02	-	1.0	0.1

Fourier transform infrared spectroscopy (FTIR): FTIR measurements from 4000 cm^{-1} to 850 cm^{-1} of the resin between two CaF_2 discs were performed on a Bruker (USA) VERTEX 70 FTIR spectrometer in transmission mode, using 2 scans and a resolution of 4 cm^{-1} . Spectra

were recorded every 5 s during illumination with UV light (OmniCure Series S1500, Lumen Dynamics 125 mWcm⁻²). For data analysis, SpectraGryph - optical spectroscopy software (version 1.2.15) was used. The spectra were baseline corrected and the development of the acrylate absorption bands (1650~1620 cm⁻¹) was analyzed by integration.

Photo-DSC Analysis: The photo-DSC measurements were conducted using a Netzsch DSC 204 F1 with an autosampler. The monomers (EM and VAM) were mixed with 2 wt% of Irgacure 184 in an ultra-sonic bath for 30 min at room temperature. 10 ± 1 mg of each formulation was weighed into an open aluminum pan and all formulations were analyzed in duplicate. The formulations were measured at different temperatures under inert atmosphere (N₂-flow = 20 mlmin⁻¹). After an equilibration phase of 4 min the samples were irradiated for at least 5 min with UV light from a Lumen Dynamics OmniCure Series S1500 (320-500 nm) with an intensity of 300 mWcm⁻². The heat flow of the polymerization reaction was recorded as a function of time.

UV polymerization on paper substrate: The prepared formulations were applied to Glassine paper surface with a coating blade (1 μm) and cured about 30 s with a mercury lamp (M-25-1-TR-SS IST from Metz GmbH; 180-450 nm) with an intensity of 660–810 mJcm⁻² (75% of maximum intensity). The UV energy was measured with a UV integrator (UV-Technik Meyer GmbH).

Contact Angle Measurement: The water contact angle was measured using the DataPhysics OCA 35 contact angle-measuring device. The drop volume was 1.5 μl, and the drop rate was 1 μls⁻¹. The contact angle was determined using the sessile drop method as the mean value of the right and left angle (ellipse fitting) and measured immediately after the droplet had stabilized on the surface, before swelling or evaporation effects appeared. The contact angle was measured at least five times for each sample at different positions, and the resulting values represent an average of all measured values.

3.2 Investigation of Reaction Kinetics by Photo-DSC and FTIR Spectroscopy

Reaction kinetics are a main point of interest when investigating the behavior of a resin under illumination. They can provide insight into the reactivity of the photoinitiator³⁸³ or monomers³⁸⁴, and give information about reacting species and pathways (see **Chapter 2.4**). Requiring a sample size of only 10 mg or less, photo-DSC and FTIR spectroscopy are excellent methods for the testing of novel systems and their potential use in photo-based coatings or additive manufacturing.

3.2.1 Differential Scanning Photo Calorimetry

Photo-DSC provides thermal information about the strength and speed of polymerization characterized by the values of reaction heat, peak height, time to peak maximum and time to 95% conversion.⁴⁰⁷

The basic principle of a photo-DSC lies in the comparison in temperature between two sensors. One sensor contains the "blank", an empty crucible, while the second sensor holds

a crucible filled with the sample of interest. The heat flow between the two is recorded and gives a curve of endo- and exothermic behavior, where endothermic is the the heat flow into and exothermic out of the sample. Compared to a regular DSC measurement the reaction is not triggered by temperature, but light. Two openings above the measurement sites allow for illumination of the sample inside the nitrogen-flooded chamber. To account for the light induced temperature change on the sensors depending on the sample's and crucible's absorption behavior, a second illumination step is necessary after the initial polymerization. The then inert sample is illuminated and these solely light induced changes in the signal can be subtracted from the original heat flow curve (**Figure 3.4**).

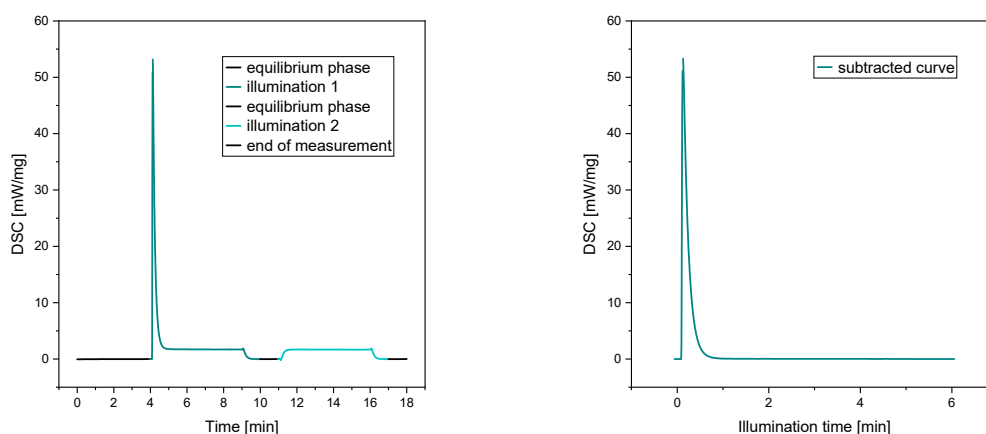


Figure 3.4 – Signal processing in photo-DSC: original photo-DSC curve (left) and subtracted curve (right).

In all experiments a photo-DSC 204 F1 Phoenix device from NETZSCH (Selb, Germany) was used with an autosampler, a NETZSCH Intracooler cooling system and an Omnicure S1500 (Lumen Dynamics, USA) high pressure mercury lamp. The irradiating light could be altered by intensity (up to 300 mWcm^{-2} at the sample surface) and emission spectrum with two available filters, 365 nm and 400-500 nm, or the full spectrum 320-500 nm. With the connected cooling system, measurements could be conducted in a temperature range from -30 to 100 °C. All measurements were done in nitrogen atmosphere (flow rate = 20 mlmin^{-1}) on samples of $10 \pm 1 \text{ mg}$.

In the conducted photo-DSC measurements, it can be differentiated between photoinitiator and monomer investigation.

When evaluating the reactivity and efficiency of a novel PI, the monomer system should be well characterized. If the theoretical heat of polymerization of the monomer $\Delta H_{0,\text{monomer}}$ is known, double bond conversion (DBC) can be calculated from the overall reaction enthalpy ΔH (area under curve) according to **Eq. (3.1)**.

$$\text{DBC [\%]} = 100 \cdot \frac{\Delta H}{\Delta H_{0,\text{monomer}}} \quad (3.1)$$

The DBC makes it possible to directly follow the polymerization process and determine the final monomer conversion. Additionally, the maximum rate of polymerization $R_{p,\text{max}}$ can be calculated using **Eq. (3.2)**, where h is the height of the exothermic DSC signal in

mWmg^{-1} and ρ is the density of the pure monomer at ambient temperature.

$$R_{p,\max} = \frac{h \cdot \rho}{\Delta H_{0,\text{monomer}}} \quad (3.2)$$

Typically, the DSC signal increases rapidly upon illumination, but an initial on-set phase is often present, which can in some systems be attributed to oxygen still remaining in the resin and its inhibiting effect on radical curing of (meth)acrylates. When the initial radicals are formed by the PI and the polymerization is in progress, the signal peaks before decreasing due to diffusion limitation and recombination events happening. The mark of 95% conversion is often times used as a further value for comparison, giving the time from the start of illumination as $t_{95\%}$.

In photoinitiators, a fast initial polymerization with little to no on-set is desirable, as well as a high peak value (fast polymerization rate), a high, ideally full, double bond conversion (DBC) and less pronounced fading out of reactivity, displayed through a low value of $t_{95\%}$.

A library of oligoacylgermanes as long-wavelength radical photoinitiators was presented by Frühwirth et al. in terms of synthesis and reactivity.³⁸⁵ In my contributing photo-DSC measurements the polymerization reactivity in 1,6-hexanediol diacrylate (HDDA) was compared to that of tetrakis(2,4,6-trimethylbenzoyl)germane (**1**) as a radical photoinitiator. At large the reactivity was found to be comparable to **1** at equifunctional (**Figure 3.5**) as well as equimolar (**Figure 3.6**) concentrations. The para-substituted digermane **4d**, however showed lower DBC, which proved consistent with its slower photobleaching under 385 nm light. All tested PIs showed a relatively long on-set of ca. 5.5 s, but a fast reaction ($t_{\max} = 1.9 - 2.5$ s) after that.

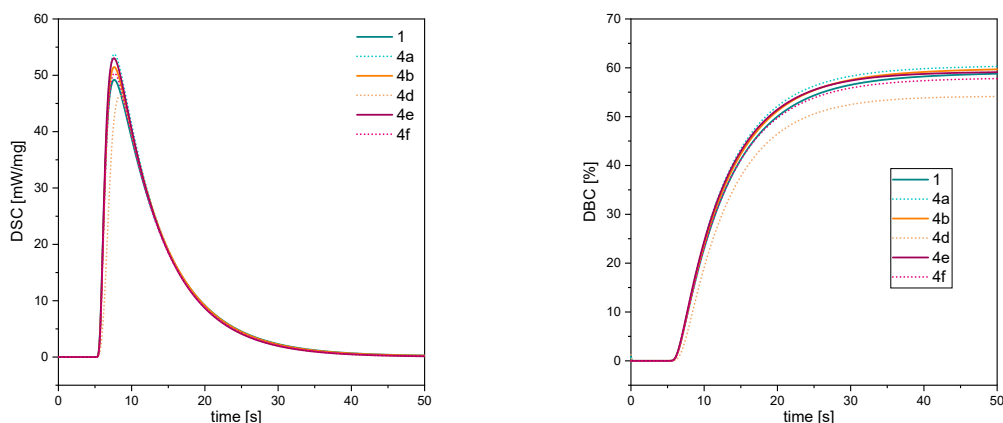


Figure 3.5 – Photo-DSC (left) and conversion plots (right) for the photopolymerization of HDDA with 0.3 mol% PI.

Several more novel photoinitiators were tested with the same method and published

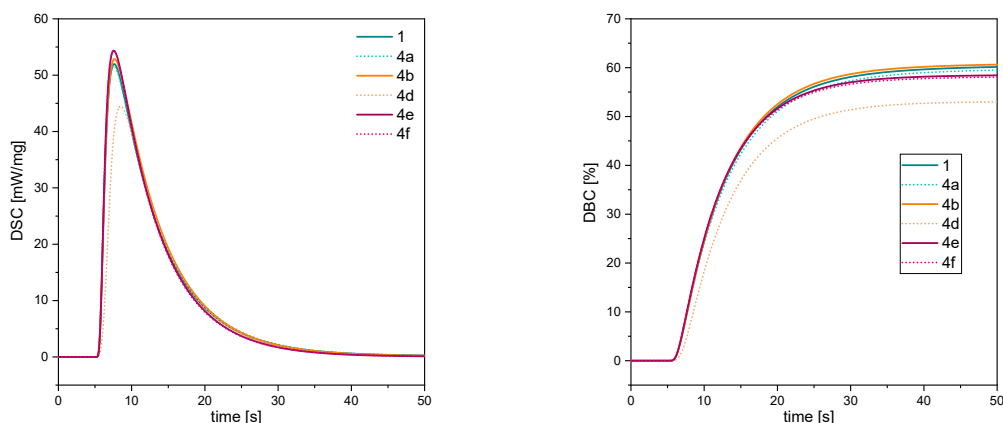


Figure 3.6 – Photo-DSC (left) and conversion plots (right) for the photopolymerization of HDDA with PI concentration with equimolar amounts of radically cleavable groups.

with Maier et al.³⁸³ and Püschmann et al.³⁸⁶. While the germanium-based photoinitiators showed little disparity in their initiating behavior in HDDA, the stanneolates showed a range of about 10 to 40 % of DBC in glycerol dimethacrylate, which was used due to better solubility. Again, the para-substituted derivative showed the least reactivity, despite its promising red-shifted absorption spectrum.

When investigating and comparing monomers instead of novel photoinitiators, the PI should be efficient and kept constant in all samples. The main comparison should be that of polymerization on-set and the time to reach maximum polymerization. In **Chapter 3.1** two novel, biobased methacrylate monomers were investigated upon their ideal curing conditions as pure monomers and with a hydrophobic additive. While the measurements cannot be used for comparison among the resins, their general reactivity and behavior at different temperatures can be evaluated. Due to the exothermic nature of the polymerization reaction, the overall conversion is reduced at elevated temperatures, even though the initial reaction rate is increased (**Figure 3.3**).

The above mentioned values provide information about the speed of polymerization, but detailed assertions about reaction kinetics would require knowledge of bonding energies. As different molecules show disparate polymerization enthalpies, their DSC signals cannot be compared directly and another method, such as FTIR spectroscopy, is needed to determine overall polymerization conversion.

3.2.2 Fourier-transform Infrared Spectroscopy

FTIR spectroscopy provides information about the chemical identity during conversion from monomer to polymer, following functional groups such as double bonds. Compared to photo-DSC it has a shorter response time if measured in real-time, a uniform sample thickness and provides additional information on reactants and possible intermediates.⁴⁰⁸

The principle of IR spectroscopy is based on light-matter interaction. The low energy wavelengths used (typically mid-IR of 2.5-25 μm or 4000-400 cm^{-1}) induce movement in

the molecule if the irradiation wavelength matches the vibrational frequency of a bond. The nature of the bond, the masses of the atoms and vibronic coupling influence the vibrational frequencies. Absorbed wavelengths appear as bands in an absorption spectrum and can be assigned to certain bond types. However, overlapping signals, especially in the lower energy range ("fingerprint area") pose a challenge in clean interpretation of kinetics.

FTIR kinetic experiments were conducted on a Bruker (USA) Vertex 70 spectrometer either in transmission mode or on a reflection module. In both setups, the sample was drop coated between two CaF_2 platelets of 1 cm diameter and 1 mm thickness. The sample thickness was reduced until the absorption of the main peaks was below 1 to remain in the linear region of the Lambert-Beer law. Due to the cut-off of CaF_2 the measured frequency range was $4000\text{-}850\text{ cm}^{-1}$. Illumination of the sample was done either directly in the device (real-time FTIR) or with an external illumination setup in a step-wise manner.

After the initial spectrum is recorded, the illumination process is started and the spectra changes according to the molecular rearrangements. To account for possible shrinkage of the sample, the spectra can be normalized. Thereby a signal needs to be chosen, which is not affected in size or position by the reaction, the corresponding bond remaining with the same bonding atoms and environment. Further, the signals of interest need to be determined. Typically absorption bands in the higher energy region are chosen as there is less overlap.

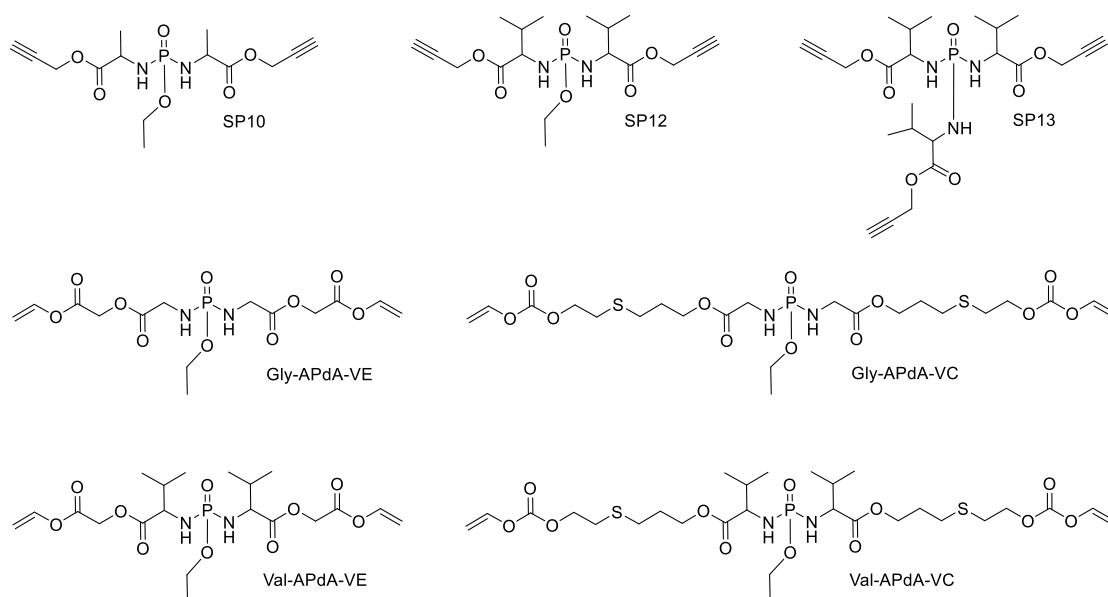


Figure 3.7 – Biodegradable monomers investigated in FTIR kinetics

In an investigation on novel, biodegradable monomers (**Figure 3.7**) in different resin systems, alkyne and thiol signals were followed with FTIR spectroscopy, monitoring their conversion and indicating the amount of homopolymerization. At equal concentrations of thiol and unsaturated bonds the resin with the bifunctional monomer (SP12) shows a slower conversion than the trifunctional SP13 (**Figure 3.9** - left). The rate of homopolymerization increases with illumination time and decreased monomer concentrations⁴⁰⁹, indicated by the divergence of the two conversion graphs. In similar glycine and valine-based monomers (**Figure 3.7**), the functionalization with vinyl esters (VE) and vinyl carbonates (VC) was tested. The ester derivatives showed a slightly higher monomer conversion in thin film

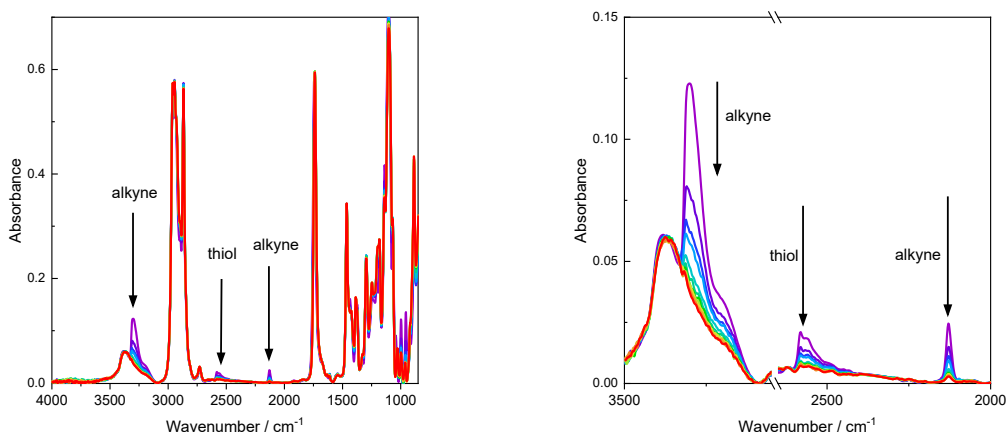


Figure 3.8 – FTIR spectrum of SP13 during illumination (left) with enlarged view of the signals of interest (right).

(FTIR measurement).³⁸⁷

In another resin system (**Chapter 2.5**), homo- and co-polymerization behavior was investigated in dependence of photoinitiators. While an anionic PI was activated in a first step to induce thiol-Michael step growth polymerization, a radical PI lead to acrylate homopolymerization in a secondary illumination step. The step-wise consumption of acrylate depending on the illumination regime is depicted in **Figure 3.9** - right.

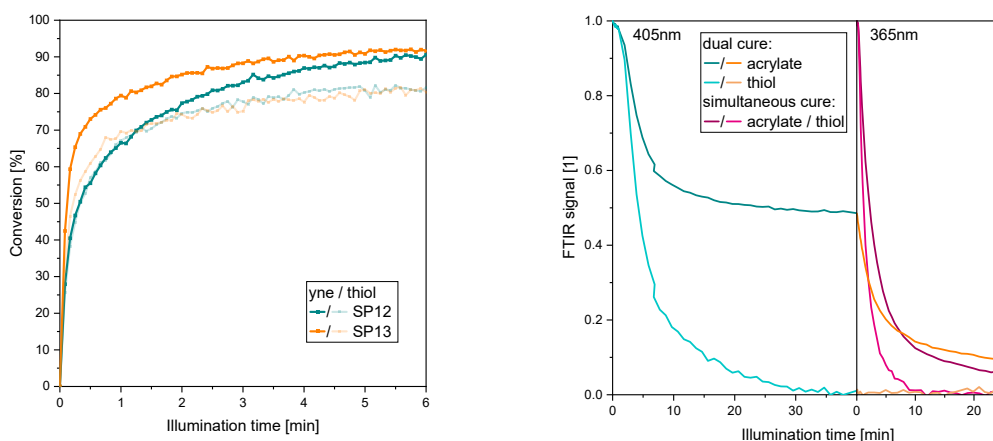


Figure 3.9 – FTIR kinetics of two biodegradable monomers in thiol-silylether resin (left) and of a dual-cure thiol-acrylate resin (right).

Concluding, FTIR spectroscopy is an important tool for fast information on molecule structure especially during light-induced polymer synthesis in a resin of mixed functional groups.

3.3 Supporting Information Chapter 3.1

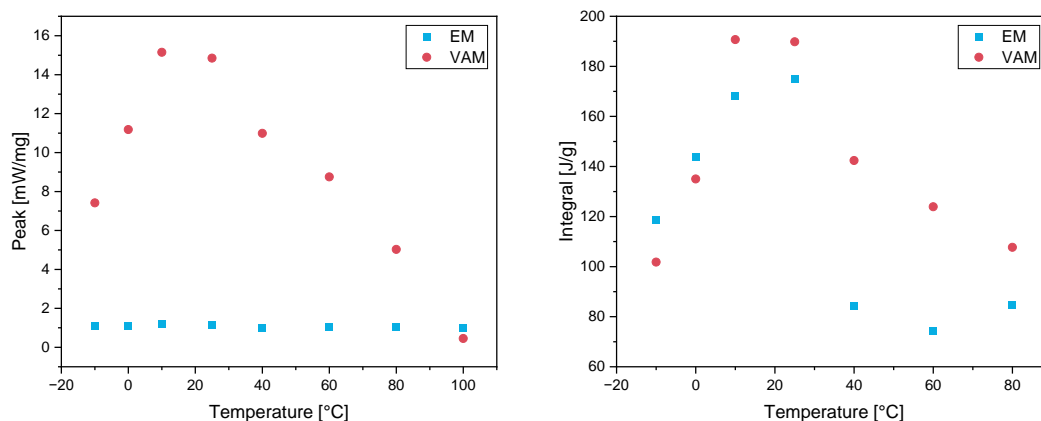


Figure 3.S1 – Peak heat of reaction (left) and Integral (right) of EM and VAM measured in photo-DSC.

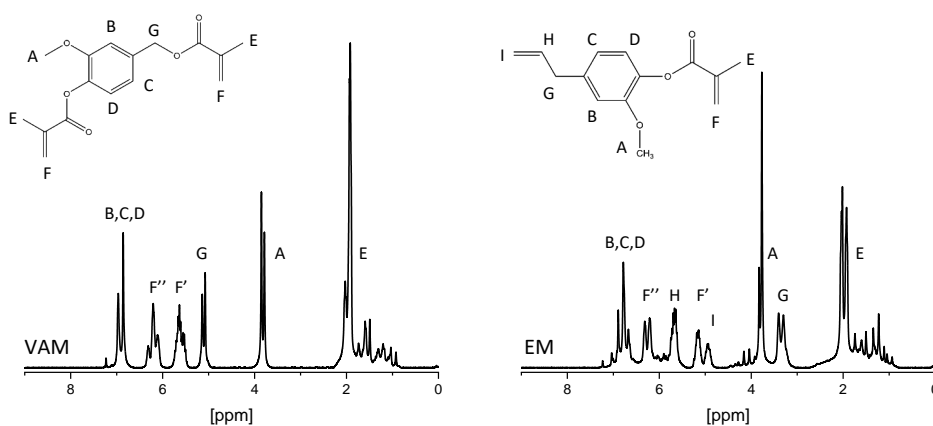


Figure 3.S3 – NMR spectra of the synthesis products VAM (left) and EM (right).

The ¹H NMR spectra were recorded on a Nanalysis (Canada) NMReady-60 spectrometer (60 MHz) with deuterated chloroform (CDCl₃) as solvent. Baseline correction and automatic phase correction was done in MestReNova (version 14.2.0).

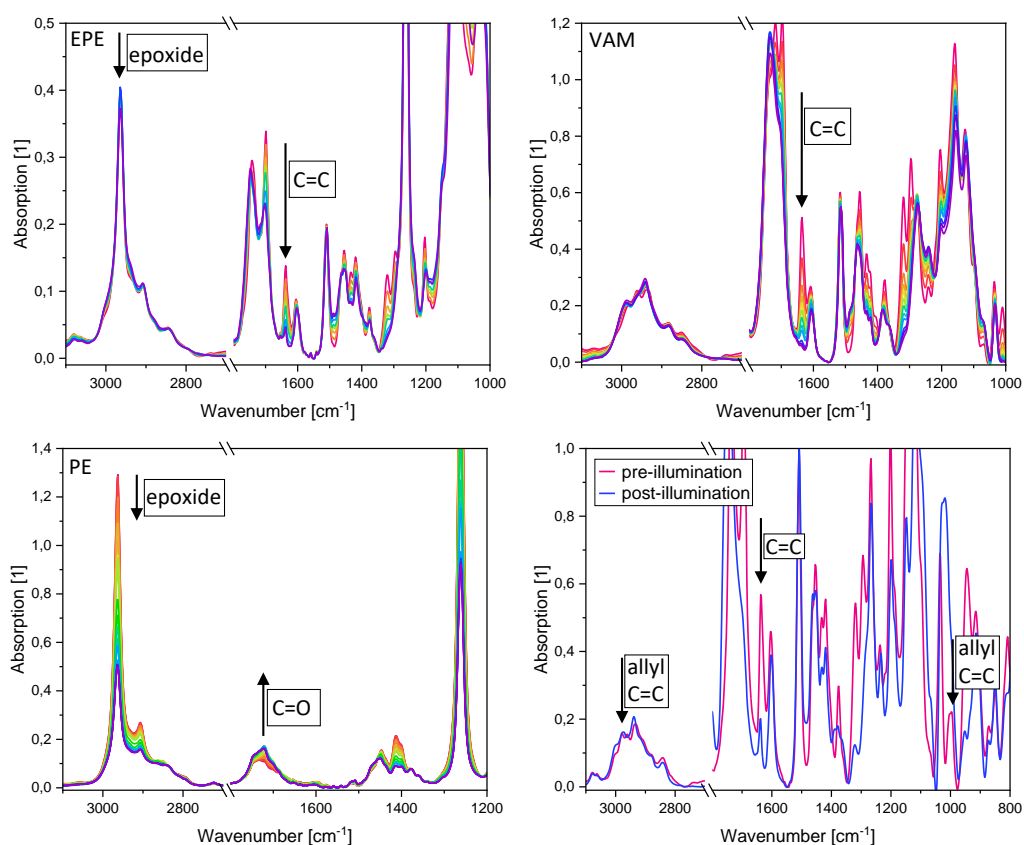
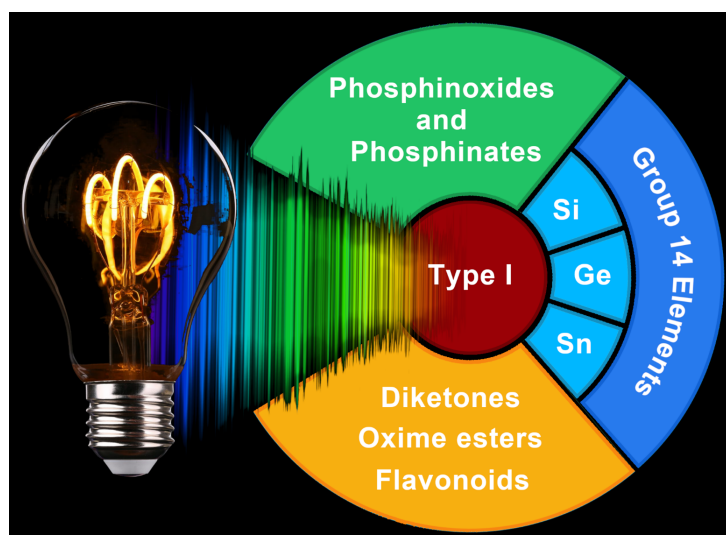


Figure 3.S2 – IR spectra during illumination. EPE showing reduction in double bonds at 1650 – 1620 cm⁻¹ and slight reduction in epoxide signal (2963 cm⁻¹) – top left. VAM showing reduction in double bonds – top right. PDMS-ECEMS (PE) showing partial rearrangement to carbonyl groups (1720 cm⁻¹) initiated by I184 – bottom left. ATR-IR spectrum of EM pre-illumination and after illumination, showing no significant reaction in allyl double bonds (2980 and 995 cm⁻¹) – bottom right.

4

Type I Photoinitiators for Visible Light Induced Photopolymerization

Photopolymerization is a light-induced crosslinking process of monomers and oligomers. Upon exposition to electromagnetic irradiation, electrons of the so-called photoinitiator (PI) are elevated to an excited state, which can thereafter form a reactive species that is able to start a polymerization reaction.⁴¹¹ The application of photopolymerizable formulations became very popular in the ink and coating industry because these resins provide several advantages such as low environmental pollution (no VOCs), fast curing rates, low energy consumption and reactivity at room temperature.⁴¹² Over the last few years, the applications of photopolymerizable resins extended from the field of coating, printing inks and adhesives to new, challenging applications such as stereolithography and 3D ink-jet printing.⁴¹¹ A crucial component in a photopolymerizable resin is an appropriate photoinitiator. It needs to produce suitable reactive species, i.e. radicals or ions, depending on the mechanism of polymerization, to a sufficient extent and in a short period of time. In addition, the PI has to provide an absorption spectrum with a good overlap with the emitting light source and a high extinction coefficient in that region. Depending on the application and the system used, solubility either in a liquid monomer, water or a suitable solvent is essential.^{411,413,414} Most PIs offer good absorption in the UV range, due to the high energy of the photons in this region and the facile excitation thereby.⁴¹⁵ However, UV light shows several disadvantages such as a low curing depth due to a high absorption, scattering in most materials and, moreover, it's harmfulness to DNA and cells.⁴¹⁶



Over the last decade there was an increasing interest in the investigation of PIs that initiate under visible light excitation. The introduction of LED based light sources paved the way towards an energy efficient curing. Besides low heat generation and energy

This chapter was published as a review article in *ChemPhotoChem* on June 27th, 2022.⁴¹⁰ This is an open-access article distributed under the terms and conditions of the *Creative Commons Attribution* (CC BY) license.

consumption, the narrow spectral width of those light sources bring a major advantage for photopolymerization. Light source and PI can be tuned for perfect spectral overlap and the best initiation performance at low energy input.¹³ Even λ -orthogonality can be realized in initiation systems.^{14,15} The focus of this review is set on type I PIs, which undergo a homolytic bond cleavage upon irradiation with visible light. In contrast to type II initiators, these PIs do not need an additional H-donor molecule to generate a reactive species. The mechanism of radical formation in type I PIs can be divided into two types of cleavage, namely alpha- (Norrish type I) and beta-scission. Upon excitation the molecule exhibits an excited singlet state and can undergo inter system crossing (ISC) to the triplet state. Relaxation of the triplet state can lead to bond cleavage in the alpha position of a carbonyl bond. Beta scission can occur, additionally or exclusively, when there is a weak bond between the carbonyl-alpha-carbon and a hetero atom,⁴¹⁷ as well as in beta-position to a conjugated system. Consequently, this can lead to molecules that are photoactive without the presence of carbonyl groups, such as trichloromethyl triazine derivatives, where the C-Cl bond is cleaved and Cl radicals are produced.⁴¹⁸ The first PIs for visible light photopolymerization were already introduced in the 1970s,^{11b, 419} namely camphorquinone (CQ)/amine, a two-component type II system. CQ is the colored sensitizer, with an absorption maximum at 468 nm, while the amine acts as an electron and proton donor, respectively^{420,421}. Although such CQ based PIs have already been applied in dental applications, two-component systems generally suffer from the disadvantage of a lower reaction rate and higher toxicity, which is caused by the amine synergist.⁴²²⁻⁴²⁵ Besides CQ, compounds based on naphthalimide⁴²⁶, benzoquinone^{427,428} and titanocenes⁴²⁹ were introduced and evaluated as type II PIs. However, limited by the rate of the hydrogen abstraction, the achieved reaction performance is comparatively low.^{425,430} During the last decade more research focused on one-component systems and type I PIs with high reactivity and an absorption behavior suitable for visible light excitation. Since phosphine oxides are the workhorse of modern photopolymerization, the main strategies for their synthesis are first presented. Subsequently, recent advances in group 14 photoinitiators and some selected examples of other initiator systems are reviewed.

4.1 Phosphinoxides and Phosphinates

Phosphine oxides (POs) have been known as photocleavable molecules since the 1980s.⁴³¹ Due to their high initiation performance, excellent bleaching behavior and absorption in the near UV-visible range, mono- and bisacylphosphine oxides (MAPO and BAPO, respectively) such as 2,4,6-trimethylbenzoyldiphenylphosphine oxide (R4) and phenylbis(2,4,6-trimethylbenzoyl)phosphine oxide (R2) are widely used in industrial coatings. Especially for the curing of thick and highly pigmented formulations, as well as white coatings (e.g. TiO₂ pigmented), where the disappearance of the PI's color during the polymerization process (i.e. photobleaching) is necessary,⁴¹⁷ these types of PIs are indispensable. Current research mainly focuses on the synthesis of PO derivatives with improved absorption behavior in the visible range or solubility in water.

Water-soluble photoinitiators are widely required for a range of applications in industry (inkjet inks⁴³², liquid crystal monomer production⁴³³, 3D printing technologies⁴³⁴) and life science, as their compatibility with physiological conditions makes them even suitable for biological applications (cell encapsulation⁴³⁵ and hydrogels⁴³⁶). In this context, Anseth et al. investigated the fabrication of hydrogels from a hydrophilic diacrylate using lithium

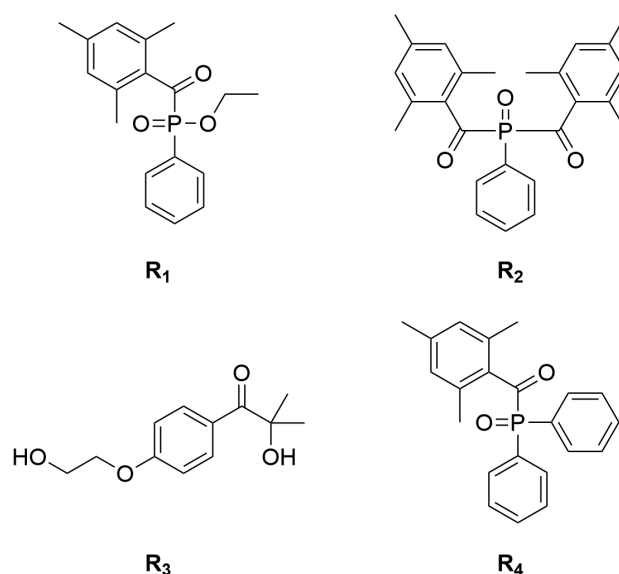


Figure 4.1 – Commercially available PIs, ethyl (2,4,6-trimethylbenzoyl) phenyl phosphinate (R1), phenylbis(2,4,6-trimethylbenzoyl)phosphine oxide (R2), 2-hydroxy-4'-(2-hydroxyethoxy)-2-methylpropiophenone (R3) and 2,4,6-trimethylbenzoyldiphenylphosphine oxide (R4), often used as references.

phenyl-2,4,6-trimethylbenzoylphosphinate (Li-TPO, **Figure 4.2**). This ionic PI showed not only a better water-solubility and faster conversion than the commonly used 2-hydroxy-4'-(2-hydroxyethoxy)-2-methylpropiophenone (R3), but it was also possible to achieve polymerization in the visible region.⁴³⁷ In another effort to make R3 water-soluble, Chemtob et al. introduced a tertiary amino group on the benzoyl moiety (MAPO-3, **Figure 4.2**). It can be converted to methyl triflate by quaternization, improving the water-solubility and the extinction coefficient.⁴³⁸ While Anseth and Chemtob used a mono acyl phosphine in their investigations, other research groups focused on bis-acylphosphine oxide salts for the polymerization of N - acryl morpholine.⁴²⁵ Compared to the work of Anseth a significant red-shift to approx. 440 nm is achieved with the lithium salt of bis(mesityl)phosphinic acid (BAPO-OLi, **Figure 4.2**). For the respective sodium salt (BAPO-ONa, **Figure 4.2**) an absorption can be observed even at 465 nm.^{437,439}

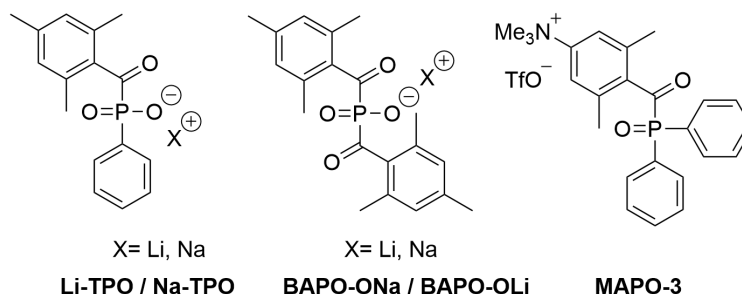


Figure 4.2 – Structures of water-soluble photoinitiators based on phosphine oxides.^{425,437,438}

Another possibility to enhance the water-solubility of POs, as well as their absorption wavelength offers the derivatization with hydrophilic and electron-donating groups,

respectively.⁴⁴⁰ Several research groups have worked on this approach over the last 20 years, introducing functional groups to the acyl, as well as the phosphorus site. One of the first derivatizations of BAPO was published by Liska and Moszner, using oligo(ethylene glycol) functionalized bis(2,4,6-trimethylbenzoyl)phenylphosphine oxide (**Figure 4.3**). The alkoxy-substitution on the benzoyl chromophore resulted in a strong redshift, while substitution on the P-aromatic moiety improved the extinction coefficient and storage stability.⁴⁴⁰

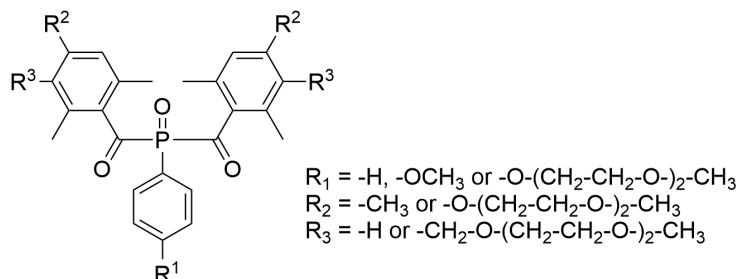


Figure 4.3 – A variation of bisacylphosphine oxide with alkoxy-substitution on the benzoyl moiety.[29]

Another BAPO derivative presented by Baudis and Grützmacher is poly(ethylene glycol) bisacylphosphine oxide (PEG-BAPO, **Figure 4.4**), combining water-compatibility and high absorption wavelengths. Compared to the previously mentioned BAPO salts (BAPO-OLi and BAPO-ONa), it shows a higher extinction coefficient at 430 nm and can induce polymerization even at 460 nm. With a dispersibility of 30 wt% (300 g/L) in water (by the formation of micells), it is highly suitable for the production of hydrogel structures.⁴⁴¹

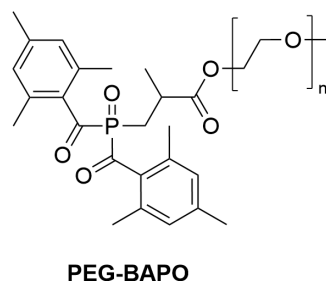


Figure 4.4 – Poly(ethylene glycol) bisacylphosphine oxide (PEG-BAPO).[30]

In a similar approach, the groups of Farsari and Gryko synthesized several acylphosphine oxide derivatives with varying functionalities in the acyl moiety (**Figure 4.5**).⁴⁴² It was shown that by adding a suitable donor group, a push-pull system is achieved and thus the absorption can be increased up to 440 nm. In this study, tertiary amino groups as donor caused the highest shift toward visible absorption, which is in good agreement with the results obtained by Wang, Yu et al.⁴⁴³ They showed that the absorption properties of a diethylamino functionalized mono PO are superior compared to the commercially available R4, especially at irradiation with light of 420 nm. The low tendency of leaching makes this PI potentially useful for inks and coatings for food packaging materials or biomedical applications.

Besides the realization of water-soluble PO derivatives, substantial research efforts have been made to improve the absorption behavior of POs in the visible range. In a recent publication, Lalevée and co-workers presented molecular modeling as a method to select potentially

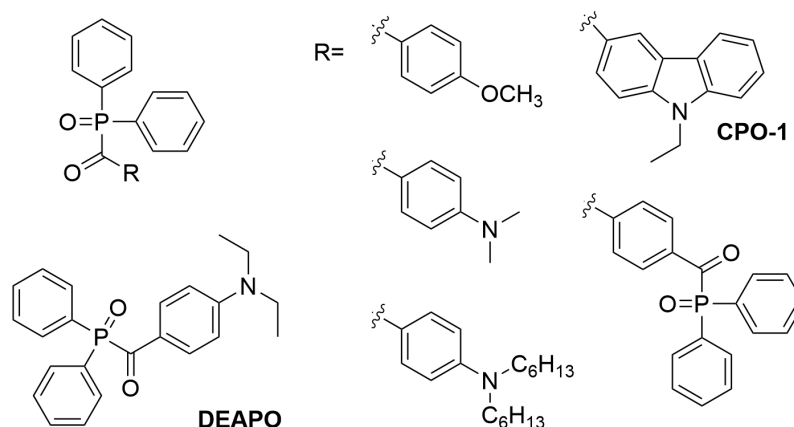


Figure 4.5 – A variation of acylphosphine oxides with different acyl group functionalities.^{442,443}

reactive compounds before their synthesis. They investigated a number of acyldiphenylphosphine oxides (ADPOs, **Figure 4.6**), which show comparable, or even better efficiencies than R1 or R2.⁴⁴⁴ Following this study, Lalevée et al. looked at further derivatization of acylphosphine oxides, using carbazole chromophores. The new carbazole based phosphine oxide (CPO-2, **Figure 4.6**), as well as the before mentioned CPO-1 (**Figure 4.5**)⁴⁴² show an enhanced absorption in the near UV-visible range compared to the standard PIs R1 and R2. Especially CPO-2, which exhibits a 50% increase of conversion at 395 nm compared to R1 and a far better solubility than R2, could provide potential for LED curing.⁴⁴⁵

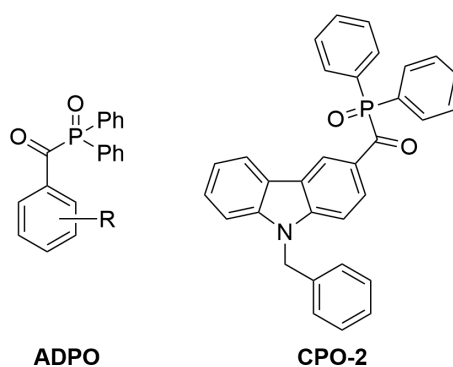


Figure 4.6 – Acyldiphenylphosphine oxides (ADPO[33] and CPO-2[34]) as photoinitiators with improved absorption behavior in the visible range.

Focusing on the effect of additional substituents, the groups of Grützmacher and Gescheidt synthesized derivatives of R2 with a different functionalization of the phosphorous site (**Figure 4.7**) and investigated their polymerization behavior in common monomers such as (meth)acrylates, 1-vinyl-2-pyrrolidone and styrene. The new, tested PIs showed absorptions up to 435 nm and the possibility to be used as anchors to specific environments (e.g., polyoxyethylene groups, Si-containing substituents, possibly intercalating π -systems), by the introduction of certain functional groups. Despite these modifications, the photoinitiating properties are similar to those of R2.⁴⁴⁶

In a recent publication, the group of Grützmacher explored new ways in the field of

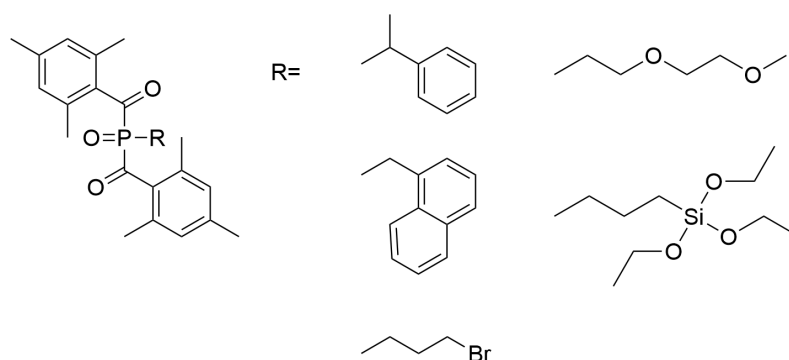


Figure 4.7 – A variation of bisacylphosphine oxides with different phosphorous functionalities.⁴⁴⁶

phosphine oxides [36]. By grafting BAPO molecules onto a cyclodextrine core, an efficient, multifunctional PI (BAPO- γ -CyD; 10 BAPO units per molecule, **Figure 4.8**) has been created, which can also be used as photocrosslinker for mono-functional acrylates. Using poly(ethylene glycol) methyl ether methacrylate, as a mono-functional monomer, an insoluble, but highly swellable (>660%) polymer was obtained without further additives.⁴⁴⁷

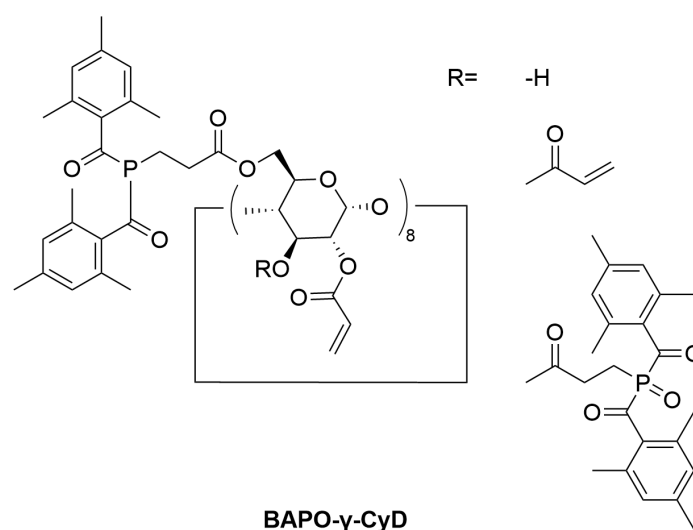
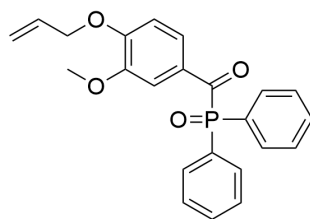


Figure 4.8 – BAPO- γ -CyD, a cyclodextrine based bisacylphosphine oxide.⁴⁴⁷

Besides the aims of improving water-solubility and absorption behavior, Versace et al. addressed the topic of green chemistry. They synthesized the first-known bio-sourced type I photoinitiator on the basis of vanillin (PM – (4-allyloxy-3-methoxybenzoyl)diphenylphosphine oxide, **Figure 4.9**). PM proved to be as effective as the commonly used R2 in initiating the radical polymerization of trimethylolpropane triacrylate (TMPTA) in laminate. While oxygen inhibition is still a challenge in the pure acrylate system, it can be partially overcome by the addition of a trifunctional thiol (1:1 thiol:PM ratio), resulting in conversions of 25% for TMPTA and 60% for soybean oil acrylate. Although no tests have yet been performed above 400 nm, this compound appears to be a promising candidate for visible light initiation.⁴⁴⁸

Even though, POs have been known as commercial photoinitiators for almost half a decade,



PM

Figure 4.9 – (4-allyloxy-3-methoxybenzoyl)diphenylphosphine oxide, a vanillin derived type I photoinitiator.⁴⁴⁸

there is still research needed to further improve not only the water-solubility and absorption properties, but also their efficiency in the surface cure of coatings. Quenching by oxygen inhibition is responsible for a poor polymerization at low depths limiting the applications of this class of PIs⁴¹⁷. Therefore, the field of research is increasingly expanding to other compounds and functional groups.

4.2 Heavier Group 14 Elements

4.2.1 Silicon

Although silanes and even acylsilanes have been known for decades,^{449–451} their use in photoinduced polymerization, especially in the visible light region, was only discovered recently. Historically speaking, silanes (R_3Si-H) were used as co-initiators in type II photoinitiating systems (PIS), where the silyl radical was generated by hydrogen abstraction. In these systems silanes can substitute toxic amines and overcome oxygen inhibition.⁴⁵² Silyl radicals react with O_2 with a nearly diffusion-controlled rate constant and form silylperoxy radicals, which help prevent oxygen inhibition in some polymerizations.⁴¹⁴ Recently more and more type I initiators have been developed, where the Si-Si, Si-C bonds cleave to generate silyl radicals. In the following, several examples of Si-containing PIs and PISs are discussed, whereby the majority is based on the formation of silyl radicals as radical source for photopolymerization.

Looking at silicon as a substituent, several systems have already been designed that involve modifications of known photocleavable structures, such as hydroxyalkylphenylketone, benzoin, etc. In most cases, however, the modified compounds do not generate new radicals and therefore behave like their parent molecules with absorption only in the UV range.^{453–455} In 2008 and 2009, Lalevée and co-workers reported on the formation of silyl radicals and showed their potential as promising PIs.^{456,457} A derivative of the type II chromophore thioxanthone (TX-O-Si, **Figure 4.10**) showed the formation of silyl radicals by Si-Si bond cleavage and an absorption tailing out into the visible light region up to 430 nm. In addition, they introduced the class of siloxyamines as silyl radical based PIs in 2011.⁴⁵⁸ Both compounds, shown in **Figure 4.10**, have low absorption maxima (SiN-1 at 267 and 303 nm and SiN-2 at 262 and 301 nm), but the absorption tails out into the visible light region. They offer a promising photoinitiating ability, also at irradiation above 400 nm. SiN-1 shows a 30% conversion of trimethylolpropane triacrylate (TMPTA) without additives.

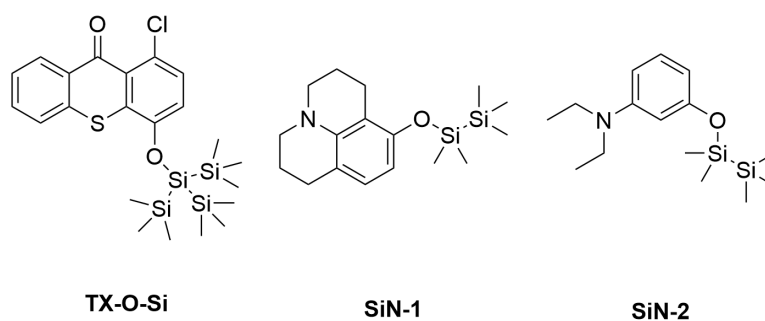


Figure 4.10 – Structures of radical photoinitiators with silicon groups.^{457,458}

Pertaining to acylsilanes, the first alpha-silyl ketones were already known in 1960 and the red shift in their absorption was noticed. However, it took several decades before they were tested for their ability to initiate photopolymerization.⁴⁴⁹ For the photochemical reactions of acylsilanes mainly two mechanisms are possible, either α -cleavage for the formation of radicals (Norrish type I) or Brook rearrangement, forming siloxycarbenes (Norrish type II).^{420,459} Which reaction type takes place depends on the acylsilane structure, the reaction medium as well as the reaction partner used.⁴⁶⁰ In 2008 Lalevée and co-workers presented some novel PIs, based on silyl radical chemistry, and investigated their cleavage behavior upon irradiation. Most molecules showed absorption in the UV range, but one molecule (PI-B, **Figure 4.11**) with an acylsilane structure was absorbing with a maximum at 365 nm (220 M⁻¹cm⁻¹) and was dissociated at the Si-carbonyl bond.⁴⁵⁶ This, as well as most other publications concentrate on monoacylsilanes.^{461,462} Liska and co-workers, however, synthesized a tetra-functional acylsilane (tetrakis(2,4,6-trimethylbenzoyl)silane; TTBS, **Figure 4.11**) and showed it's absorption being effective up to 460 nm ($\lambda_{\text{max}} = 382$ nm) with a good photobleaching behavior under air and argon. The polymerization ability was compared to the common bimolecular camphorquinone/amine PIS and similar reactivities of TTBS were found. For low initiator concentrations it even outperforms conventional PIS.⁴²⁰

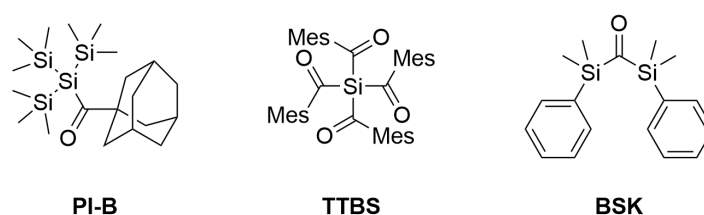


Figure 4.11 – Various acylsilanes for the generation of silyl radicals.^{420,456,463}

The groups of Lalevée and Klee investigated, again, a molecule which has already been described before, but has not been tested with respect to photoinitiating properties, namely a bisilylketone (BSK, **Figure 4.11**). With an exceptionally high absorption maximum at 530 nm (80 M⁻¹cm⁻¹) BSK was curable with a green laser diode (532 nm), but gave only a low double bond conversion in methacrylate systems and showed slow photobleaching.⁴⁶³

4.2.2 Germanium

The photoreactivity of certain germanium compounds have been known for more than half a century.^{451,464–467} Their synthesis and even their reactivity and mechanism of radical formation were described, however, their use as photoinitiators was not mentioned until 2008. When Liska et al. rediscovered the class of acylgermanes for photoinitiation purposes, they were looking at molecules similar to the well-known acylphosphine oxides.^{16,17} By substitution of the phosphine oxide by a germanium analogous they managed to tune the absorption wavelength of the PI and to increase the quantum yield. The presented dibenzoyldiethylgermane (Bis-Ge-a, **Figure 4.12**) provides an absorption tailing out to 490 nm ($\lambda_{\text{max}} = 418.5$ nm), while the benzoyl(trimethyl)germane offers a maximum absorption at 411 nm with a tail-out to 470 nm. Although both germanium compounds exceeded the curing efficiency of their phosphorous homologues (i.e. MAPO and BAPO) at higher wavelength (>430 nm), only the diacylgermane was able to outperform common photoinitiators like BAPO and CQ/amine in a dimethacrylate system.¹⁸ The field of acylgermanes became rapidly more popular and further research was done on a variation of substitution patterns. Bis(4-methoxybenzoyl)diethylgermane (Bis-Ge-d, **Figure 4.12**)⁴²¹ that can be obtained by an easy and efficient synthesis shows promising properties including a high extinction coefficient and a good curing performance.

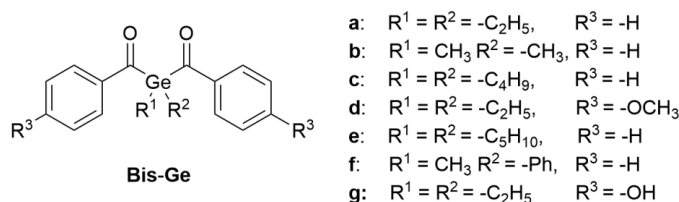


Figure 4.12 – Bisacylgermanes for the generation of germyl radicals.⁴²¹

Only shortly after the presentation of acylgermanes as photoinitiators, their versatility was shown by Yagci and co-workers, as they proved their capability to initiate a radically promoted cationic polymerization upon addition of Ph2I+PF6-. In a two-step reaction, a block copolymer of cyclohexane oxide and styrene was achieved by this bifunctional photoinitiator.^{19,468} Lalevée and co-workers looked at acetyltriphenylgermane (**Figure 4.13**) as an alternative to benzoyl derivatives and found that a highly reactive radical is formed, but only absorption up to 420 nm can be reached, which is in the lower range for acylgermanes.²⁰

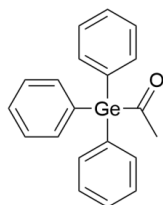


Figure 4.13 – Acetyltriphenylgermane for the generation of germyl radicals.²⁰

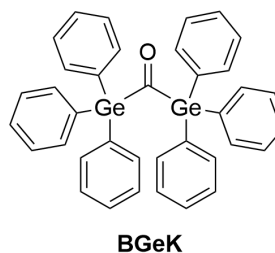


Figure 4.14 – Bis(triphenylgermyl)ketone as radical source.²¹

A molecule described long ago, namely bis(triphenylgermyl)ketone (BGeK, **Figure 4.14**) was presented as a new class of PIs in 2010. It was first described in 1968 and offers an excellent absorption spectrum with a maximum at 514 nm, good storage stability, a slightly lower polymerization rate but a higher final conversion than titanocene, the reference compound used.^{21,451}

Another wave of research was published from 2016 to 2019, when more substitution patterns were investigated[56] and the logical propagation led from mono- and bisacylgermanes to tris- and tetraacylgermanes.^{23,24} In the course of these studies a synthetic protocol allowing a straightforward access to these highly active compounds was developed. Even more complex Ge-compounds with an increasing number of chromophores were investigated (**Figure 4.15**), showing higher UV-Vis absorption and tailing up to 525 nm.²⁵

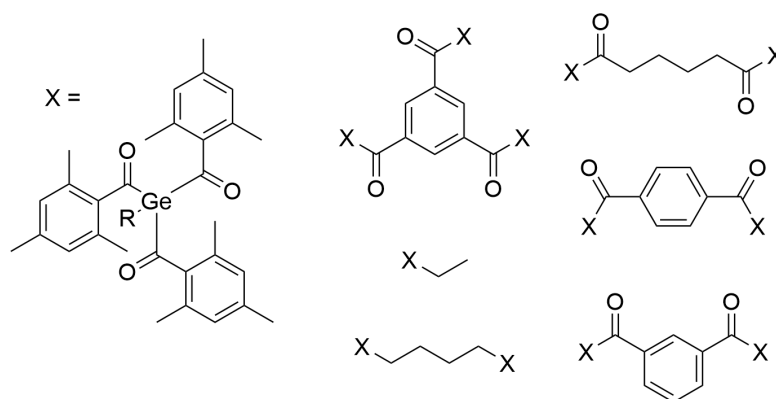


Figure 4.15 – More complex Ge-photoinitiators based on Ge-mesityl.²⁵

Furthermore, the Haas group investigated the group tolerance of their new synthetic pathway toward tetraacylgermanes and obtained a variety of compounds (**Figure 4.16**) that have a good absorption around 450 nm and high extinction coefficients.[58,60] The substitution pattern at the phenyl ring, can again be used for a more exact tuning of the absorption properties. While para-methoxy substituents and mesityl derivatives show a blue-shift, o-tolyl substituents induce a bathochromic shift. Ortho substitution in general gives more fine structures in the spectra and consequently broadens the absorption band to push the “edge” of the tailing.^{23,24,26}

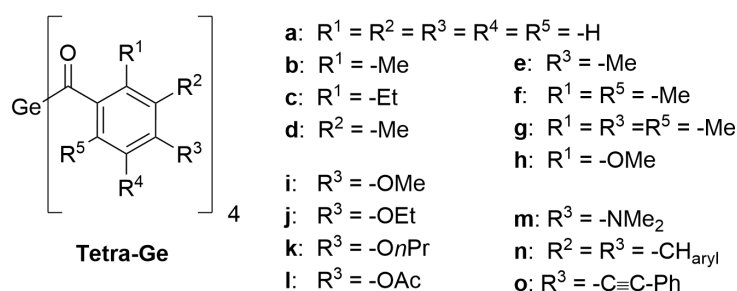


Figure 4.16 – Tetraacylgermanes as photoinitiators.^{23,24,26} If not noted otherwise all other substituents (R) are -H.

Two different research groups investigated the substitution patterns on benzoyl(trimethyl)germane (Figure 4.17) and agreed on the fact, that electron-withdrawing groups, such as cyano or nitro substituents in para position, stabilize the excited singlet state, decrease the amount of alpha-cleavage and reduce the conversion of monomers by radical polymerization.^{22,469}

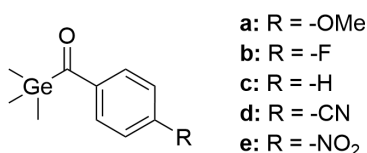


Figure 4.17 – Benzoyl(trimethyl)germane with various substitution patterns.²²

Wu and co-workers published an alternative synthetic protocol towards monoacylgermanes.⁴⁷⁰ The corresponding monoacylgermanes were synthesized starting from hexamethyldigermane, carbon monoxide and (hetero)aryl iodides in the presence of a Pd-catalyst and triorgano phosphite (Figure 4.18).

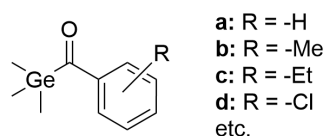


Figure 4.18 – Isolated monoacylgermanes via palladium-catalysed carbonylative reaction.⁴⁷⁰

Recently a synthetic strategy for the hitherto unknown geminal bisgermenolate was introduced. This compound represents a new synthon for the synthesis of a variety of different acylgermanes in good yields (Figure 4.19).²⁷

4.2.3 Tin

Silanes and germanes were shown to reduce the bandgap and red-shift the absorption maxima due to the interaction of their empty d-orbital with the π^* orbital of the carboxyl group. Tin as member of the same periodic group, was investigated for its use in PIs for the first time in 2018 by Liska and Haas.^{28,29}

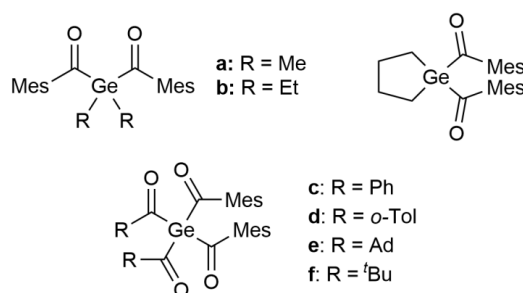


Figure 4.19 – Isolated acylgermanes using bisgermenolates as synthon.²⁷

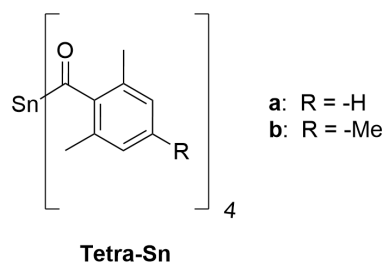


Figure 4.20 – Tetraacylstannanes as stannyl radical source.²⁹

Tetrakis(2,4,6-trimethylbenzoyl)stannane and tetrakis(2,6-dimethylbenzoyl)stannane were synthesized (Figure 4.20).²⁹ They both show absorption at very high wavelengths, tailing out until 550 and 520 nm, respectively. Especially tetrakis(2,4,6-trimethylbenzoyl)stannane outperformed Bis-Ge-d (Figure 4.12), a commonly used germane, and titanocene at 522 nm irradiation with respect to photobleaching, photocuring and final double bond conversion and showed low water-solubility as well as low cytotoxicity. In a follow-up publication, Haas et al. presented a reaction pathway and a variety of Sn-based PIs (Figure 4.21), similar to their germanium equivalents. These PIs show an even more pronounced red-shift with absorption up to 600 nm and reasonable photoinitiating capacity.³⁰

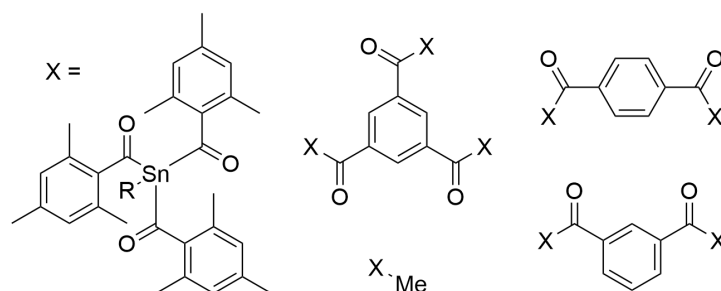


Figure 4.21 – A variety of acylstannanes for photoinitiation.³⁰

Further research on tin compounds would be interesting for the future. However, storage stability is a main topic for stannanes and might constitute their limit for commercial application.

4.3 Other Types of Photoinitiators

All the above described photoinitiators were based on the cleavage of a carbon-heteroatom bond in alpha position to a carbonyl group, which can be split with low energy irradiation (visible light). However, an increasing number of compounds have been discovered to exhibit similarly cleavable bonds, for example diketons or trichloromethyl triazine. As an example of β -cleavage, trichloromethyl triazine was explored for UV-initiated polymerization before.⁴⁷¹ Lalevée and co-workers managed to manipulate the triazine substituent in a way to achieve visible light absorption tailing out up to 460 nm (**Figure 4.22**).⁴¹⁸ Upon irradiation a chloride radical is formed, which can initiate a polymerization at 405 nm leading to an acrylate conversion of 58% (TMPTA in laminate). However, this PI is strongly inhibited by oxygen, which makes the addition of ethyl 4-(dimethylamino)benzoate or methyl diethanolamine necessary to compensate the decreased efficiency in surface cure. Li and co-workers have developed a new visible light PI ((*E*)-7-(diethylamino)-2-oxo-2H-chromene-3-carbaldehyde *o*-acryloyl oxime (DCCA), **Figure 4.22**) based on coumarin as a chromophore. This initiator bears an acrylate moiety and exhibits an absorption maximum at 436 nm. Even though it cannot compare with R2 in initiation performance, it outperforms R4 with an acrylate conversion of about 50% (TMPTA). In addition, low migration is achieved by copolymerization of the acrylate moiety of DCCA.⁴⁷²

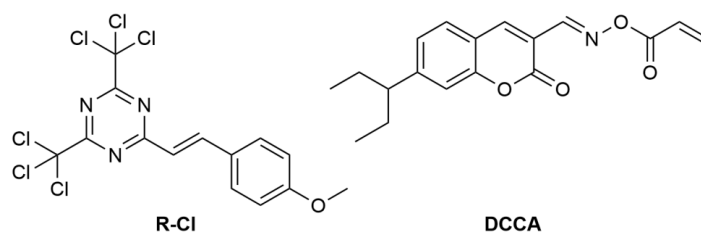


Figure 4.22 – Structure of 2-(4-methoxystyryl)-4,6-bis(trichloromethyl)-1,3,5-triazine (R-Cl)⁴¹⁸, a radical PI producing chloride radicals, and a coumarin based initiator (DCCA)⁴⁷².

In 2013 Lalevée and co-workers employed pyrene moieties to improve absorption of well-established PIs, such as 2,2-dimethoxy-2-phenylacetophenone (**Figure 4.23**). In this molecule they achieved a red-shift of 13 nm, increased the extinction coefficient by a factor of 100, and showed a generally higher monomer conversion with the modified PI upon illumination with visible light (405 nm).⁴⁷³

Another molecule type, namely silyl glyoxylate, was introduced into visible light photoinitiation by Lalevée and Klee in 2017.⁴⁷⁴ Alkylphenyl glyoxylates (APGs) were already described and investigated as UV-photoinitiators⁴⁷⁵ with methyl benzoylformate (MBF) being commercially available, however their absorption does not reach the visible light region. In their study Bouzrati-Zerelli and co-workers presented *t*-butyl(*t*-butyldimethyl)silyl glyoxylate (DKSi) and two derivatives with varied glyoxylate substituents (Et-DKSi and Bn-DKSi, **Figure 4.24**). The introduction of the silyl group strongly influences the delocalization of HOMO and LUMO and reduces the energy gap, resulting in a red shift in the absorption spectrum. The new PIs show a broad band in the visible wavelength range tailing up to 510 nm. A double bond conversion of 40-70% could be achieved upon illumination at 477 nm in a methacrylate system in laminate. The presented silyl glyoxylates exhibit a dual initiation behavior as type I and type II PIs. While undergoing homolytic cleavage

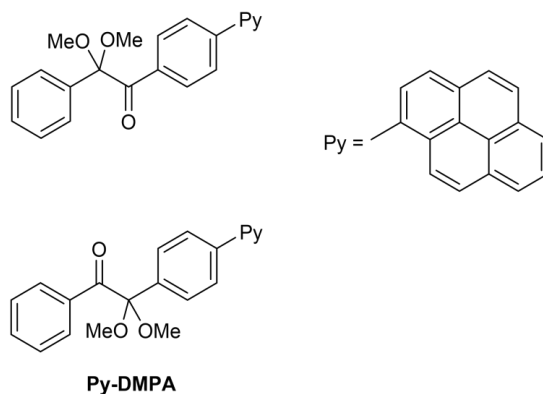


Figure 4.23 – Pyrene derivatives of 2,2-dimethoxy-2-phenylacetophenone.⁴⁷³

of the C-C carbonyl bond under separated conditions, DKSi, can undergo intra- or intermolecular hydrogen abstraction. Therefore, its polymerization efficiency can be improved in combination with additives, such as ethyldimethylaminobenzoate or diphenyliodonium hexafluorophosphate, to overcome oxygen inhibition.

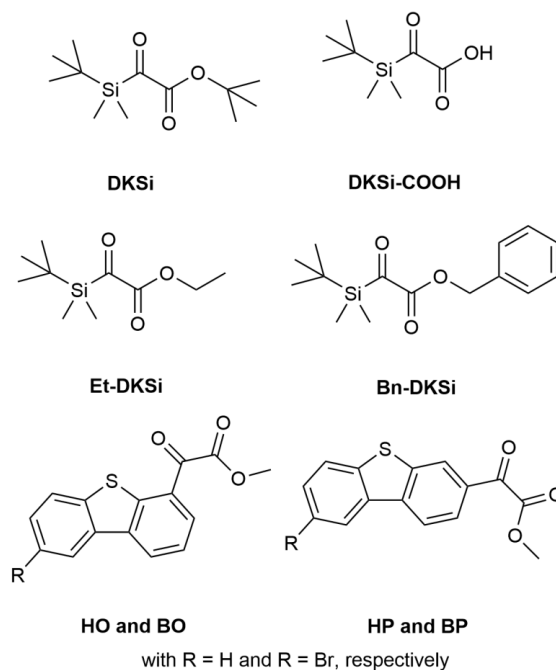


Figure 4.24 – Structures of some silyl- and phenylglyoxylates for the use as high-performance PIs.^{474,476,477}

Over the last two years, the groups of Malval, Lalevée and Wang published more studies on phenylglyoxylate-based PIs.^{476–479} Malval looked at the sulfur containing substituent dibenzothiophene with and without a bromide group (**Figure 4.24**). The reaction pathway is similar to the above described one but is followed by an elimination of carbon dioxide from the carboxyl radical to yield a methyl radical. At a curing wavelength of 425 nm an acrylate conversion of 80% was found in tripropylene glycol diacrylate (TPGDA) system.⁴⁷⁶ Wang et al. exchanged sulfur for nitrogen, looking at carbazole substituents in combination

with further aromatic groups (CO-P, CO-N, CO-C, **Figure 4.25**). They found absorption up to 460 nm and high efficiency in the polymerization of TPGDA with conversion between 73% and 89%, significantly higher than observed for a CQ/amine system.⁴⁷⁹ Lalevée had continued research on the silicon containing compounds changing up the silyl substituents as well as the second ketone substituent, by introducing a benzyl group. Two 1-aryl-2-(triisopropylsilyl)ethane-1,2-diones (SED1 and SED2, **Figure 4.25**) were synthesized, exhibiting absorption maxima at 486 and 468 nm, respectively. In the polymerization of methacrylates they showed a conversion of 40-50%, better than the previously reported DKSi at 520 nm.⁴⁷⁸

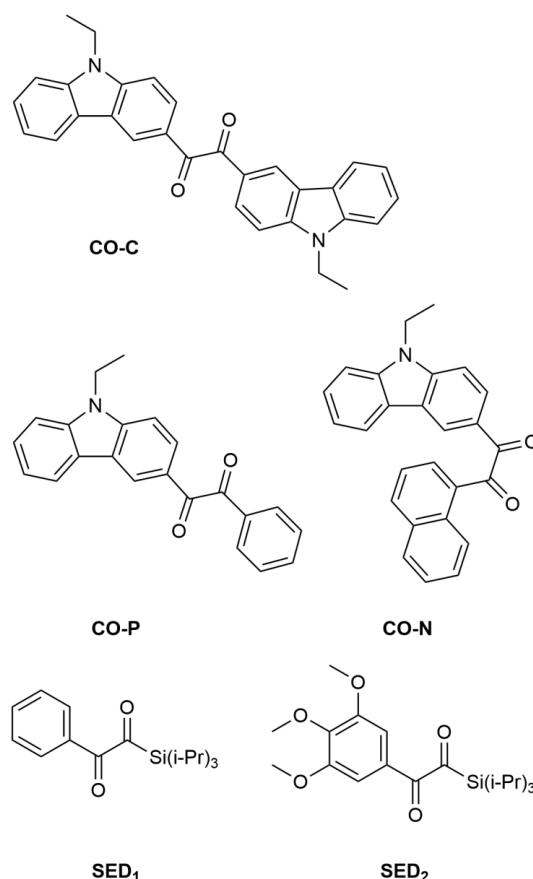


Figure 4.25 – Structure of various diketones for photoinitiation.^{478,479}

Recently, a water-soluble silyl diketone (DKSi-COOH, **Figure 4.24**) was described.⁴⁷⁷ With a prevalent type I initiation mechanism and an absorption maximum at 442 nm a very fast (20 s) double bond conversion of 70% can be achieved in methacrylate systems in thick films (1.4 mm) at 477 nm irradiation wavelength ($I_0 = 300 \text{ mW cm}^{-1}$). This photoinitiator might be a promising candidate for the use in dental applications. Combining nitrocarbazole, as a chromophore, with oxime esters, as a novel cleavable group, Lalevée and co-workers developed three new visible light PIs (OXE-M, OXE-V, OXE-P, **Figure 4.26**). While commercially available oxime esters (such as O-benzoyl- α -oxooxime and O-acetyloxime) have maximum absorption wavelengths of 326 and 338 nm, respectively, their absorption tails out until 450 nm, exhibiting higher molar extinction coefficients at 405 nm than R4. Upon illumination the N-O bond is cleaved, forming two radicals. While the iminyl radical is inactive for free radical polymerization, the second radical undergoes decarboxylation

and generates active free radicals, depending on the terminal group used. With methyl as an end-group, a final acrylate conversion of 69% (compared to 65% with R4) in TMPTA can be achieved.⁴⁸⁰

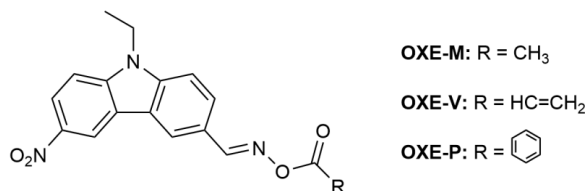


Figure 4.26 – A novel photoinitiator containing an oxime ester as cleavable group.⁴⁸⁰

In a similar approach, using conjugated carbazoles, Li et al. synthesized bifunctional oxime esters as PIs for one and two-photon absorption in the visible range (Figure 4.27). The 2,7-substituted carbazoles show higher molar extinction coefficients at 405 nm and vinyl-substituents yield higher double bond conversions in acrylate formulations. Therefore, the 2,7-substituted PI with vinyl initiation functionality has comparable photoinitiation efficiency to R4 and a lower threshold energy than that of commercial two-photon resists.⁴⁸¹

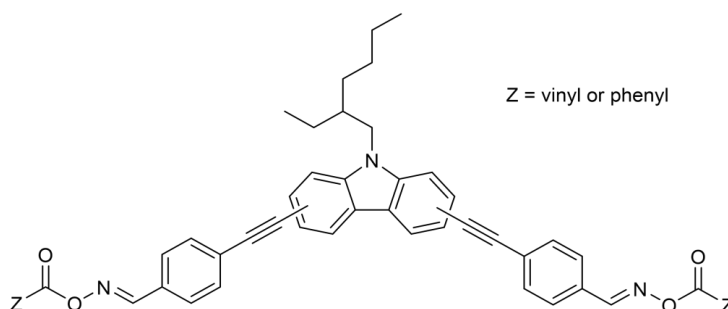


Figure 4.27 – Conjugated bifunctional carbazole-based oxime esters.⁴⁸¹

Besides Carbazoles, also other chromophores were tested in combination with oxime esters. Liu, Li and Dietliker used diethylaminocoumarin and investigated a variation of initiation functionalities (Figure 4.28). OEC poses one of these molecules, with a 4-substitution of the coumarin, in combination with a simple benzyl functionality for the initiating radical. With curing depths of up to 4.8 mm in a thiol-ene system under 450 nm illumination (200 mW/cm²) and fast (2 min) and deep (2.6 mm) photo-bleaching, OEC is a promising PI especially for dental applications.⁴⁸² Further, they showed that heterocyclic radicals efficiently initiate free radical polymerization of acrylates and thiol-ene systems as well as, being able to photo-cure materials with up to 10 mm thickness under 450 nm illumination (O-2).⁴⁸³

In an effort to explore even more molecules for their photoinitiating properties, Wang and co-workers investigated derivatives of flavonoids as type I radical initiators, but also for their acid generating abilities. Flavonol sulfonate (3HF-S, Figure 4.27), used at very low concentrations of 0.125%, showed a final acrylate conversion of 80% and 71% (TPGDA) upon illumination with 405 nm and 460 nm, respectively. Due to the high efficiency and mild polymerization conditions 3HF-S could play a role in the field of biocompatible polymers in future.⁴⁸⁴

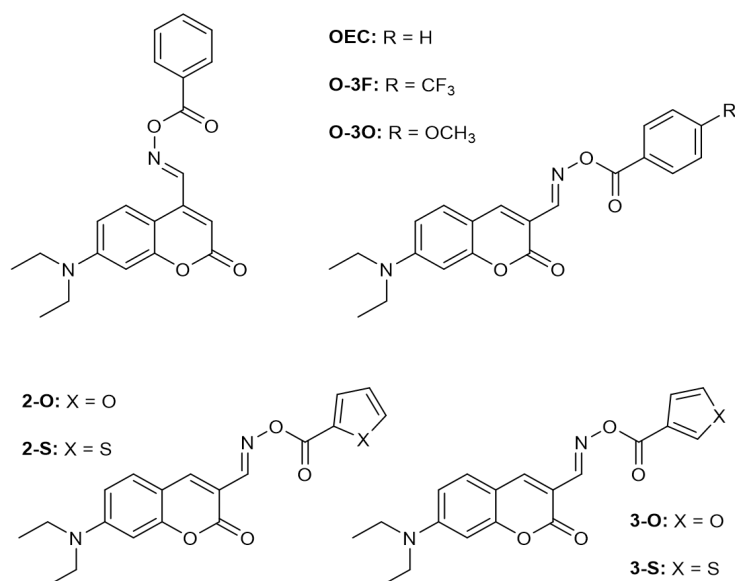


Figure 4.28 – Diethylaminocoumarin-based oxime esters for photo-initiation.^{482,483}

Recently, Yagci and Liu published another dual-use PI (P-PTh, **Figure 4.29**), which absorbs light through the UV, visible and near-IR region with an absorption maximum at 514 nm. Upon illumination it cleaves homolytically, forming phenacyl radicals, as well as Brønsted super acids. Thereby, two reactions can be initiated, free radical and cationic polymerization, respectively. These reactions can be utilized either in pure epoxy or acrylate systems or in a hybrid photopolymerization, using both reaction mechanisms at the same time.⁴⁸⁵

4.4 Summary and Outlook

Type I photoinitiators, which are reactive under visible light, have had a rapid development within the last ten to twenty years. Current research can be divided into three main areas: Phosphine oxides, Group 14 elements and other photocleavable structures. Phosphine oxides are the group of PIs, which are already well established and commercially available. New findings in this area address water-solubility and absorption behavior, which is tuned by variation of the phosphor-substituents. By introducing Group 14 elements into the compounds, a bathochromic shift can be achieved, and the illumination wavelength is pushed further into the visible light range. The different Group 14 elements pose various advantages and challenges. As silicon is an abundant resource, the PIs are relatively cheap and readily available, yet the maximum absorption wavelength seems to be still limited. This is overcome by germanium and especially tin compounds, with absorption up to 600 nm. However, the disadvantages of these compounds are their stability, their compatibility with high-throughput polymer synthesis and their occurrence in the earth's crust. To expand possibilities, research was recently advanced to other structures, such as oxime esters, diketones or flavonoids, with the goal of finding a water-soluble, high wavelength-absorption PI with high yield in synthesis and good photoinitiation performance. This review focused mainly on the comparison of absorption and bleaching behavior, as well as photoinitiation ability and water-solubility. However, there are some topics, such as toxicity and migration of the PI as well as the cleavage products, which will gain increasing interest

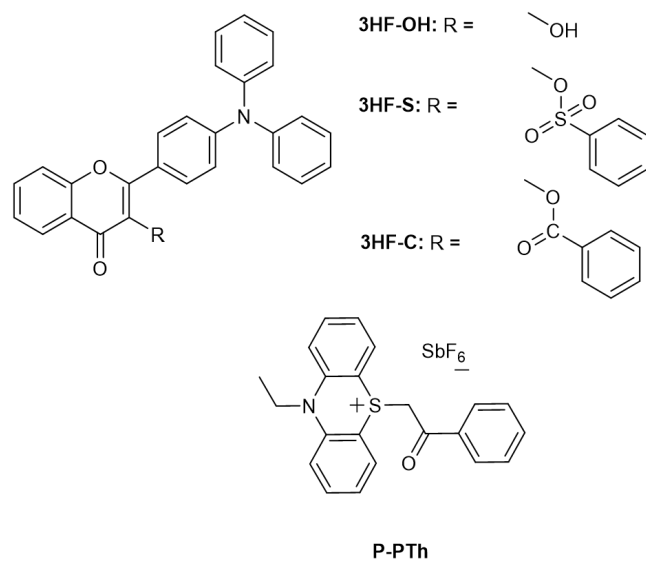


Figure 4.29 – Photoinitiators based on flavonol sulfonate⁴⁸⁴ and a phenothiazinium salt⁴⁸⁵.

and will need additional evaluation as visible light 3D printing is becoming a versatile tool in clinical and life-science applications.

Conclusion and Outlook

Additive manufacturing and the quest for novel, smart and renewable materials for 3D printing and light-based applications has become a major focus in polymer science. In material development this calls for a good and comprehensive understanding of all constituents used, their reaction mechanism, curing behavior and influence on the final material properties. Novel compounds should be thoroughly investigated to properly assess their role and behavior in the resin.

This thesis covered three topics: photoinitiators and their characterization, bio-based monomers for radical photo-polymerization and most prominent a library of molecules first implemented in dual-cure 3D printing of smart materials.

First, a novel group of crosslinkers for multi-material 3D printing was presented. Chalconyl moieties were implemented into a thiol-methacrylate resin to achieve a second lever for material property alterations during printing or in post-production (**Figure 5.1** - left).

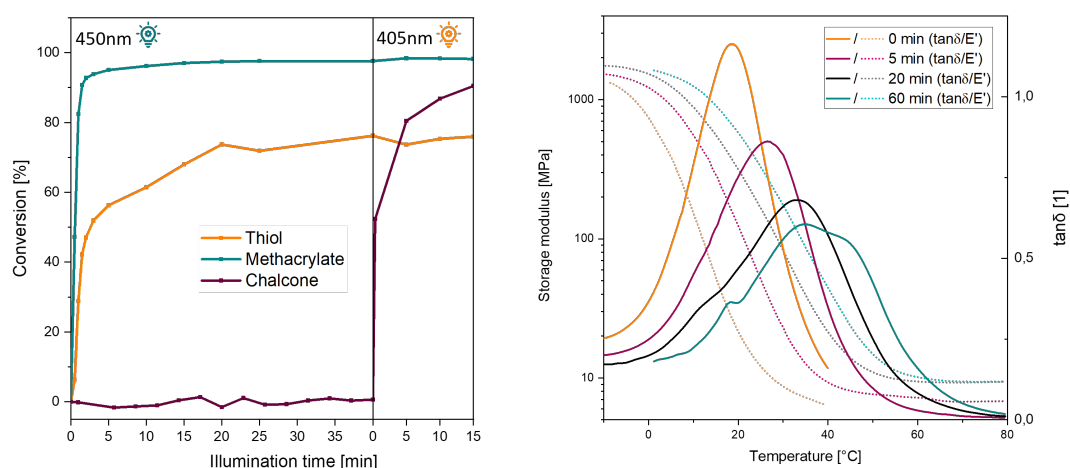


Figure 5.1 – Summary on chalcone as a photo-crosslinkable group with step-wise curing kinetics (left) and alteration of glass transition temperatures with increased illumination dose (right).

The primary material properties could be tuned by thiol content to achieve glass transition just below room temperature, attaining the most prominent gap in properties at ambient conditions (**Figure 5.1** - right). When looking at the introduction of crosslinks in the novel resin, secondary chalconyl crosslinks could be precisely triggered in terms of resolution and quantity. Chalconyl conversion can be controlled by light dose, which directly affects material properties (**Figure 5.2**). Therefore, continuous tuning of the final stiffness of the material was proven, yielding the possibility of implementing multiple material domains into a single specimen. Simple shape memory experiments as well as multi-wavelength 3D printing was shown on macro- and micro-scale to present the vast opportunities for this novel 3D-printable material.

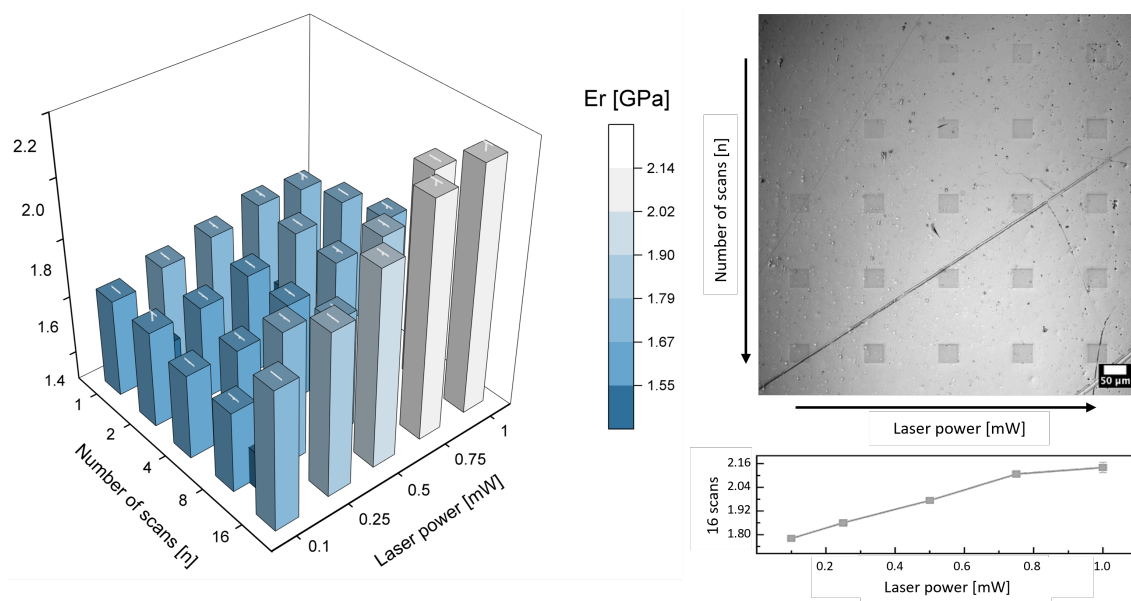


Figure 5.2 – Summary on chalcone as a photo-crosslinkable group showing the change in material properties with number of scans and light intensity on micro-scale.

Furthermore, a library of photo-crosslinkable molecules was established and their reactivity investigated under the most common light sources. The mismatch between absorption spectra and reactivity makes this kind of screening absolutely necessary to evaluate possible applicability of a certain functionality in an orthogonal system. 4-Thiothymine, anthracene and styrylpyrene displayed distinct conversion differences upon 450 nm and 365 nm or 405 nm irradiation, making them promising candidates for application in resins similar to the chalconyl group. Additionally, styrylpyrene showed indications for cycloreversion at said wavelengths. The advantage of the herein presented molecules is clearly in their direct and stepless control for crosslink density alterations and their bonding into the polymer, making dimerization optional while maintaining network integrity nonetheless.

Secondly, photo-DSC and IR kinetics were used as a tool to investigate and characterize a number of novel photoinitiators and bio-based molecules for advanced applications in future additive manufacturing. Two bio-based methacrylates, eugenyl methacrylate (EM) and vanillyl alcohol methacrylate (VAM) were investigated upon their curing behavior along a range of temperatures to optimize processing conditions in paper coating. Vanillyl alcohol-based resins exhibit faster polymerization and higher conversion rates compared to their eugenol-based homologues, attributed to their structural differences. Hydrophobic coatings with a water contact angle of 106° , comparable to those of conventional resins, could be achieved by incorporating PDMS-ECEMS. Eugenol and vanillyl alcohol-based resins were demonstrated as sustainable alternatives for hydrophobic paper coatings. Additionally the tracking of curing behavior was demonstrated by photo-DSC and FTIR spectroscopy on a wide range of molecules. Novel photoinitiators based on heavier group 14 elements were investigated as replacements of phosphorous-based PIs. And amino acid-based monomers were examined upon their suitability in 3D printing of biological scaffolds. Paving the way towards a more bio-compatible, renewable and sustainable future of 3D printing.

Finally, a literature review of advancing radical photoinitiators is given, as a comprehensive overview and library for fast and specialized polymerization reactions. The focus was put

on homolytically cleaved, type I PIs with excitation wavelengths in the visible region. The possibility to utilize electromagnetic irradiation above 400 nm for the initiation of polymerization reactions provides several advantages such as a lower energy demand and higher curing depths in pigmented reactive systems. Recent developments of PIs based on phosphorus and group 14 elements as well as other selected concepts for type I visible light initiators were outlined and discussed within this chapter.

Under the umbrella of radically induced thiol-ene and (meth)acrylate polymerization, some of the most important aspects towards 3D printing were addressed in this thesis. Investigations on photoinitiators and curing behavior as well as additionally crosslinkable moieties for smart materials and 4D printing.

Materials with advanced properties and modulation thereof will be of increasing interest as 3D printing is a clearly emerging technology with possible applications in all fields of everyday life. Focusing on benign conditions at room temperature and with excitation wavelengths in the visible region is not only advantageous for safety, but also from an ecological standpoint, reducing energy costs. Therefore some of the herein presented molecules will be subject to further investigations as photo-triggered crosslinkable groups in 3D and 4D printing. ■

*‘The only true wisdom
is in knowing
you know nothing.’*

~ Socrates

Bibliography

1. Wiesner, T.; Haas, M. *Dalton Transactions* **2021**, *50*, 12392–12398.
2. Saleh Alghamdi, S.; John, S.; Roy Choudhury, N.; Dutta, N. K. *Polymers* **2021**, *13*, 753.
3. Marschner, D. E.; Frisch, H.; Offenloch, J. T.; Tuten, B. T.; Becer, C. R.; Walther, A.; Goldmann, A. S.; Tzvetkova, P.; Barner-Kowollik, C. *Macromolecules* **2018**, *51*, 3802–3807.
4. Yagci, Y.; Jockusch, S.; Turro, N. J. *Macromolecules* **2010**, *43*, 6245–6260.
5. Kloosterboer, J. G. In *Electronic Applications*, Springer Berlin Heidelberg: Berlin, Heidelberg, **1988**, pp 1–61.
6. Bunning, T. J.; Natarajan, L. V.; Tondiglia, V. P.; Sutherland, R. L. *Annual Review of Materials Science* **2000**, *30*, 83–115.
7. Anseth, K. S.; Newman, S. M.; Bowman, C. N. In *Biopolymers II*, ed. by Peppas, N. A.; Langer, R. S., Springer Berlin Heidelberg: Berlin, Heidelberg, **1995**, pp 177–217.
8. Sun, H.-B.; Kawata, S. In *NMR 3D Analysis Photopolymerization*; Springer Berlin Heidelberg: Berlin, Heidelberg, **2004**, pp 169–273.
9. Fisher, J. P.; Dean, D.; Engel, P. S.; Mikos, A. G. *Annual Review of Materials Research* **2001**, *31*, 171–181.
10. Roffey, C. G., *Photogeneration of reactive species for UV curing*; Wiley: **1997**.
11. Davidson, R. S., *Exploring the science, technology and applications of UV and EB curing*; Sita Technology: **1999**.
12. Fouassier, J.-P. (*No Title*) **1995**.
13. Zhang, Y.; Xu, Y.; Simon-Masseron, A.; Lalevée, J. *Chemical Society Reviews* **2021**, *50*, 3824–3841.
14. Hurrle, S.; Lauer, A.; Gliemann, H.; Mutlu, H.; Wöll, C.; Goldmann, A. S.; Barner-Kowollik, C. *Macromolecular Rapid Communications* **2017**, *38*, 1600598.
15. Frisch, H.; Bloesser, F. R.; Barner-Kowollik, C. *Angewandte Chemie International Edition* **2019**, *58*, 3604–3609.
16. Ganster, B.; Fischer, U. K.; Moszner, N.; Liska, R. *Macromolecular rapid communications* **2008**, *29*, 57–62.
17. Ganster, B.; Fischer, U. K.; Moszner, N.; Liska, R. *Macromolecules* **2008**, *41*, 2394–2400.
18. Moszner, N.; Fischer, U. K.; Ganster, B.; Liska, R.; Rheinberger, V. *Dental Materials* **2008**, *24*, 901–907.
19. Durmaz, Y. Y.; Kukut, M.; Moszner, N.; Yagci, Y. *Journal of Polymer Science Part A: Polymer Chemistry* **2009**, *47*, 4793–4799.
20. Lalevee, J.; Allonas, X.; Fouassier, J.-P. *Chemical Physics Letters* **2009**, *469*, 298–303.
21. Tehfe, M.-A.; Blanchard, N.; Fries, C.; Lalevée, J.; Allonas, X.; Fouassier, J. P. *Macromolecular rapid communications* **2010**, *31*, 473–478.
22. Feuerstein, W.; Höfener, S.; Klopper, W.; Lamparth, I.; Moszner, N.; Barner-Kowollik, C.; Unterreiner, A.-N. *ChemPhysChem* **2016**, *17*, 3460–3469.
23. Radebner, J.; Eibel, A.; Leypold, M.; Gorsche, C.; Schuh, L.; Fischer, R.; Torvisco, A.; Neshchadin, D.; Geier, R.; Moszner, N., et al. *Angewandte Chemie International Edition* **2017**, *56*, 3103–3107.

24. Eibel, A.; Radebner, J.; Haas, M.; Fast, D. E.; Freißmuth, H.; Stadler, E.; Faschauner, P.; Torvisco, A.; Lamparth, I.; Moszner, N., et al. *Polymer Chemistry* **2018**, *9*, 38–47.
25. Fruühwirt, P.; Knoechl, A.; Pillinger, M.; Muüller, S. M.; Wasdin, P. T.; Fischer, R. C.; Radebner, J.; Torvisco, A.; Moszner, N.; Kelterer, A.-M., et al. *Inorganic chemistry* **2020**, *59*, 15204–15217.
26. Radebner, J.; Leybold, M.; Eibel, A.; Maier, J.; Schuh, L.; Torvisco, A.; Fischer, R.; Moszner, N.; Gescheidt, G.; Stueger, H., et al. *Organometallics* **2017**, *36*, 3624–3632.
27. Drusgala, M.; Frühwirt, P.; Glotz, G.; Hogrefe, K.; Torvisco, A.; Fischer, R. C.; Wilkening, H. M. R.; Kelterer, A.-M.; Gescheidt, G.; Haas, M. *Angewandte Chemie International Edition* **2021**, *60*, 23646–23650.
28. Mitterbauer, M.; Knaack, P.; Naumov, S.; Markovic, M.; Ovsianikov, A.; Moszner, N.; Liska, R. *Angewandte Chemie International Edition* **2018**, *57*, 12146–12150.
29. Radebner, J.; Eibel, A.; Leybold, M.; Jungwirth, N.; Pickl, T.; Torvisco, A.; Fischer, R.; Fischer, U. K.; Moszner, N.; Gescheidt, G., et al. *Chemistry—A European Journal* **2018**, *24*, 8281–8285.
30. Maier, J.; Müller, S. M.; Torvisco, A.; Glotz, G.; Fischer, R. C.; Griesser, T.; Kelterer, A.-M.; Haas, M. *ChemPhotoChem* **2022**, *6*, e202100213.
31. Herwig, G.; Pérez-Madrigal, M. M.; Dove, A. P. *Biomacromolecules* **2021**, *22*, 1472–1483.
32. Cader, H. K.; Rance, G. A.; Alexander, M. R.; Gonçalves, A. D.; Roberts, C. J.; Tuck, C. J.; Wildman, R. D. *International journal of pharmaceutics* **2019**, *564*, 359–368.
33. Uehlin, A. F.; Vines, J. B.; Feldman, D. S.; Dean, D. R.; Thomas, V. *JOM* **2022**, *74*, 3336–3348.
34. Hewes, S.; Wong, A. D.; Searson, P. C. *Bioprinting* **2017**, *7*, 14–18.
35. Barui, S.; Ghosh, D.; Laurencin, C. T. *Regenerative Biomaterials* **2023**, *10*, rbac109.
36. Schwartz, J.; Boydston, A. *Nature communications* **2019**, *10*, 791.
37. Dolinski, N. D.; Page, Z. A.; Callaway, E. B.; Eisenreich, F.; Garcia, R. V.; Chavez, R.; Bothman, D. P.; Hecht, S.; Zok, F. W.; Hawker, C. J. *Advanced Materials* **2018**, *30*, 1800364.
38. Cazin, I.; Gleirscher, M. O.; Fleisch, M.; Berer, M.; Sangermano, M.; Schlögl, S. *Additive Manufacturing* **2022**, *57*, 102977.
39. Rossegger, E.; Strasser, J.; Höller, R.; Fleisch, M.; Berer, M.; Schlögl, S. *Macromolecular rapid communications* **2023**, *44*, 2200586.
40. Lu, P.; Ahn, D.; Yunis, R.; Delafresnaye, L.; Corrigan, N.; Boyer, C.; Barner-Kowollik, C.; Page, Z. A. *Matter* **2021**, *4*, 2172–2229.
41. Zhang, X.; Xi, W.; Huang, S.; Long, K.; Bowman, C. N. *Macromolecules* **2017**, *50*, 5652–5660.
42. Gramlich, W. M.; Kim, I. L.; Burdick, J. A. *Biomaterials* **2013**, *34*, 9803–9811.
43. Marschner, D. Wavelength-Orthogonal Approaches Enabling Reprogrammable Gradient Materials, Ph.D. Thesis, Dissertation, Karlsruhe, Karlsruher Institut für Technologie (KIT), 2019, **2019**.
44. Marschner, D. E.; Frisch, H.; Offenloch, J. T.; Tuten, B. T.; Becer, C. R.; Walther, A.; Goldmann, A. S.; Tzvetkova, P.; Barner-Kowollik, C. *Macromolecules* **2018**, *51*, 3802–3807.
45. Rennie, R.; Law, J., *A Dictionary of Chemistry*.
46. Schalk, O.; Tapavicza, E., *Photochemistry*; ACS In Focus; American Chemical Society: 2021.
47. Smith, K. C. In *The Science of Photobiology*, Smith, K. C., Ed.; Springer US: Boston, MA, **1977**, pp 397–417.
48. Sheppard, S. E. *Journal of Chemical Education* **1927**, *4*, 298.
49. Lopez de Pariza, X.; Varela, O.; Catt, S. O.; Long, T. E.; Blasco, E.; Sardon, H. *Nature communications* **2023**, *14*, 5504.
50. Sanchez-Rexach, E.; Johnston, T. G.; Jehanno, C.; Sardon, H.; Nelson, A. *Chemistry of Materials* **2020**, *32*, 7105–7119.

51. Zhang, B.; Kowsari, K.; Serjouei, A.; Dunn, M.; Ge, Q. *Nature Communications* **2018**, *9*, DOI: 10.1038/s41467-018-04292-8.
52. Farsari, M.; Chichkov, B. N. *Nature photonics* **2009**, *3*, 450–452.
53. Chatani, S.; Kloxin, C.; Bowman, C. *Polym. Chem.* **2014**, *5*, DOI: 10.1039/C3PY01334K.
54. Ligon, S. C.; Liska, R.; Stampfl, J.; Gurr, M.; Mülhaupt, R. *Chemical reviews* **2017**, *117*, 10212–10290.
55. Stampfl, J.; Baudis, S.; Heller, C.; Liska, R.; Neumeister, A.; Kling, R.; Ostendorf, A.; Spitzbart, M. *Journal of Micromechanics and Microengineering* **2008**, *18*, 125014.
56. Schnabel, W., *Polymers and light: fundamentals and technical applications*; John Wiley & Sons: **2007**.
57. Ito, Y. *Photochemistry for Biomedical Applications*, **2018**.
58. Li, H.; Kamasah, A.; Matsika, S.; Suits, A. G. *Nature chemistry* **2019**, *11*, 123–128.
59. Mai, S.; Marquetand, P.; Gonzalez, L. *The Journal of Physical Chemistry Letters* **2016**, *7*, 1978–1983.
60. Cook, W. D. *Polymer* **1992**, *33*, 600–609.
61. Wang, Y.; Spencer, P.; Yao, X.; Ye, Q. *Journal of Biomedical Materials Research Part A: An Official Journal of The Society for Biomaterials, The Japanese Society for Biomaterials, and The Australian Society for Biomaterials and the Korean Society for Biomaterials* **2006**, *78*, 721–728.
62. Kowalska, A.; Sokolowski, J.; Bociong, K. *Polymers* **2021**, *13*, 470.
63. Pérez-Mondragón, A. A.; Cuevas-Suárez, C. E.; González-López, J. A.; Trejo-Carbajal, N.; Herrera-González, A. M. *Journal of Photochemistry and Photobiology A: Chemistry* **2020**, *403*, 112844.
64. Qin, X.-H.; Ovsianikov, A.; Stampfl, J.; Liska, R. *BioNanoMaterials* **2014**, *15*, 49–70.
65. Cosola, A.; Chiappone, A.; Martinengo, C.; Grützmacher, H.; Sangermano, M. *Polymers* **2019**, *11*, 1901.
66. Rudin, A.; Choi, P. In *The Elements of Polymer Science and Engineering (Third Edition)*, Rudin, A., Choi, P., Eds., Third Edition; Academic Press: Boston, **2013**, pp 341–389.
67. Moad, G.; Solomon, D. H. In *Comprehensive Polymer Science and Supplements*, Allen, G., Bevington, J. C., Eds.; Pergamon: Amsterdam, **1989**, pp 147–160.
68. Xia, W. Z.; Cook, W. D. *Polymer* **2003**, *44*, 79–88.
69. Gauthier, M.; Stangel, I.; Ellis, T.; Zhu, X. *Journal of dental research* **2005**, *84*, 725–9.
70. Husar, B.; Ligon, S. C.; Wutzel, H.; Hoffmann, H.; Liska, R. *Progress in Organic Coatings* **2014**, *77*, 1789–1798.
71. Shi, Y.; Yan, C.; Zhou, Y.; Wu, J.; Wang, Y.; Yu, S.; Chen, Y. In *Materials for Additive Manufacturing*, Shi, Y., Yan, C., Zhou, Y., Wu, J., Wang, Y., Yu, S., Chen, Y., Eds.; 3D Printing Technology Series; Academic Press: **2021**, pp 191–359.
72. Hale, A. In *Applications to Polymers and Plastics*, Cheng, S. Z., Ed.; Handbook of Thermal Analysis and Calorimetry, Vol. 3; Elsevier Science B.V.: **2002**, pp 295–354.
73. Smets, G; Aerts, A; Van Erum, J *Polymer Journal* **1980**, *12*, 539–547.
74. Crivello, J. V.; Lam, J. H. W. *Macromolecules* **1977**, *10*, 1307–1315.
75. Jarikov, V. V.; Neckers, D. C. *Macromolecules* **2000**, *33*, 7761–7764.
76. Ito, H. In *Applications of Anionic Polymerization Research*, **1998**; Chapter 17, pp 218–234.
77. Prabhakaran, P.; Lee, K.-S. In *Functional Polymers*, Jafar Mazumder, M. A., Sheardown, H., Al-Ahmed, A., Eds.; Springer International Publishing: Cham, **2019**, pp 1–52.
78. Sinha, J.; Podgórski, M.; Tomaschke, A.; Ferguson, V. L.; Bowman, C. N. *Macromolecules* **2020**, *53*, 6331–6340.

79. Al Mousawi, A.; Arar, A.; Ibrahim-Ouali, M.; Duval, S.; Dumur, F.; Garra, P.; Toufaily, J.; Hamieh, T.; Graff, B.; Gignes, D., et al. *Photochemical & Photobiological Sciences* **2018**, *17*, 578–585.
80. Salmi, H.; Allonas, X.; Ley, C.; Marechai, D.; Ak., A. *Journal of Photopolymer Science and Technology* **2012**, *25*, 147–151.
81. Kahveci, M. U.; Acik, G.; Yagci, Y. *Macromolecular Rapid Communications* **2012**, *33*, 309–313.
82. Chatani, S.; Gong, T.; Earle, B. A.; Podgorski, M.; Bowman, C. N. *ACS Macro Letters* **2014**, *3*, 315–318.
83. Corrigan, N.; Ciftci, M.; Jung, K.; Boyer, C. *Angewandte Chemie International Edition* **2021**, *60*, 1748–1781.
84. Bialas, S.; Michalek, L.; Marschner, D. E.; Krappitz, T.; Wegener, M.; Blinco, J.; Blasco, E.; Frisch, H.; Barner-Kowollik, C. *Advanced Materials* **2019**, *31*, 1807288.
85. Lerch, M. M.; Hansen, M. J.; Velema, W. A.; Szymanski, W.; Feringa, B. L. *Nature communications* **2016**, *7*, 12054.
86. Menzel, J. P.; Feist, F.; Tuten, B.; Weil, T.; Blinco, J. P.; Barner-Kowollik, C. *Angewandte Chemie International Edition* **2019**, *58*, 7470–7474.
87. Scott, T. F.; Kowalski, B. A.; Sullivan, A. C.; Bowman, C. N.; McLeod, R. R. *Science* **2009**, *324*, 913–917.
88. Bochet, C. G. *Tetrahedron Letters* **2000**, *41*, 6341–6346.
89. Hildebrandt, K.; Pauloehrl, T.; Blinco, J. P.; Linkert, K.; Boerner, H. G.; Barner-Kowollik, C. *Angewandte Chemie International Edition* **2015**, *54*, 2838–2843.
90. Barner-Kowollik, C.; Bastmeyer, M.; Blasco, E.; Delaittre, G.; Müller, P.; Richter, B.; Wegener, M. *Angewandte Chemie International Edition* **2017**, *56*, 15828–15845.
91. Xu, S.; Yeow, J.; Boyer, C. *ACS Macro Letters* **2018**, *7*, 1376–1382.
92. Ishida, S.; Fukaminato, T.; Kitagawa, D.; Kobatake, S.; Kim, S.; Ogata, T.; Kurihara, S. *Chemical Communications* **2017**, *53*, 8268–8271.
93. Bléger, D.; Hecht, S. *Angewandte Chemie International Edition* **2015**, *54*, 11338–11349.
94. Wu, M.; Lin, X.; Tan, X.; Li, J.; Wei, Z.; Zhang, D.; Zheng, Y.; Zheng, A.-x.; Zhao, B.; Zeng, Y., et al. *ACS applied materials & interfaces* **2018**, *10*, 19416–19427.
95. Fichte, M. A.; Weyel, X. M.; Junek, S.; Schäfer, F.; Herbivo, C.; Goeldner, M.; Specht, A.; Wachtveitl, J.; Heckel, A. *Angewandte Chemie* **2016**, *128*, 9094–9098.
96. Silami, F. D. J.; Mundim, F. M.; Garcia, L. F. R.; Sinhoreti, M.; de Souza, F. P. *Journal of dentistry* **2013**, *41 Suppl 3*, e62–6.
97. Rutsch, W.; Dietliker, K.; Leppard, D.; Kohler, M.; Misev, L.; Kolczak, U.; Rist, G. *Progress in Organic Coatings* **1978**, *27*, 227–239.
98. Majima, T.; Schnabel, W.; Weber, W. *Macromolecular Chemistry and Physics* **1991**, *192*, 2307–2315.
99. Henne, A. Process for the preparation of acylphosphine oxides, DE3139984, 1981.
100. Carey, F. A.; Sundberg, R. J., *Advanced organic chemistry: part b: reactions and synthesis*; Springer: **2007**; Vol. 3.
101. Diels, O.; Alder, K. *Justus Liebigs Annalen der Chemie* **1928**, *460*, 98–122.
102. Kamm, P. W. Understanding of lambda-orthogonal photo-induced reaction systems, Karlsruhe Institute of Technology, 2021.
103. Clayden, J.; Greeves, N.; Warren, S.; Glauner, F.; Mühle, K.; von der Saal, K., *Organische Chemie*; Springer Berlin Heidelberg: **2013**.
104. Huang, C.; Zheng, M.; Xu, J.; Zhang, Y. *Molecules* **2013**, *18*, 2942–2966.
105. Desvergne, J.-P.; Bouas-Laurent, H. *ChemInform* **2003**, *34*, no–no.

106. Skolia, E.; Kokotos, C. G. *ACS Organic & Inorganic Au* **2022**, *3*, 96–103.
107. Kaur, G.; Johnston, P.; Saito, K. *Polymer Chemistry* **2014**, *5*, 2171–2186.
108. Beale, R.; Roe, E. *Journal of the Chemical Society (Resumed)* **1953**, 2755–2763.
109. Svetlichnyi, V.; Meshalkin, Y. P. *Optics communications* **2007**, *280*, 379–386.
110. Schenck, G. O.; von Wilucki, I.; Krauch, C. H. *Chemische Berichte* **1962**, *95*, 1409–1412.
111. Schenck, G. O.; Hartmann, W.; Mannsfeld, S.-P.; Metzner, W.; Krauch, C. H. *Chemische Berichte* **1962**, *95*, 1642–1647.
112. Schenck, G. O.; Wolgast, R. *Naturwissenschaften* **1962**, *49*, 36–36.
113. Minsk, L.; Smith, J.; Van Deusen, W.; Wright, J. *Journal of Applied Polymer Science* **1959**, *2*, 302–307.
114. Robertson, E.; Van Deusen, W.; Minsk, L. *Journal of Applied Polymer Science* **1959**, *2*, 308–311.
115. Tanaka, H.; Otomegawa, E. *Journal of Polymer Science: Polymer Chemistry Edition* **1974**, *12*, 1125–1130.
116. Tsuda, M. *Journal of Polymer Science Part A-1: Polymer Chemistry* **1969**, *7*, 259–264.
117. Ichimura, K.; Watanabe, S. *Journal of Polymer Science: Polymer Letters Edition* **1980**, *18*, 613–617.
118. Bener, S.; Aydogan, C.; Yagci, Y. *Macromolecular Rapid Communications* **2020**, *41*, 2000369.
119. Hyde, P.; Kricka, L.; Ledwith, A. *Journal of Polymer Science: Polymer Letters Edition* **1973**, *11*, 415–419.
120. Kalayci, K.; Frisch, H.; Truong, V. X.; Barner-Kowollik, C. *Nature Communications* **2020**, *11*, 4193.
121. Fast, D. E.; Lauer, A.; Menzel, J. P.; Kelterer, A.-M.; Gescheidt, G.; Barner-Kowollik, C. *Macromolecules* **2017**, *50*, 1815–1823.
122. Walden, S. L.; Carroll, J. A.; Unterreiner, A.-N.; Barner-Kowollik, C. *Advanced Science* **2024**, 2306014.
123. Fermi, E.; Orear, J.; Rosenfeld, A.; Schluter, R., *Nuclear Physics: A Course Given by Enrico Fermi at the University of Chicago*; Committee on publications in the physical sciences / the University of Chicago; University of Chicago Press: **1950**.
124. Astholz, D.; Brouwer, L.; Troe, J. *Berichte der Bunsengesellschaft für physikalische Chemie* **1981**, *85*, 559–564.
125. Posner, T. *Berichte der deutschen chemischen Gesellschaft* **1905**, *38*, 646–657.
126. Michael, A. *Am Chem J* **1887**, *9*, 115.
127. Nair, D. P.; Podgorski, M.; Chatani, S.; Gong, T.; Xi, W.; Fenoli, C. R.; Bowman, C. N. *Chemistry of Materials* **2014**, *26*, 724–744.
128. Allen, C.; Fournier, J.; Humphlett, W. *Canadian Journal of Chemistry* **1964**, *42*, 2616–2620.
129. Rohit, K.; Ujwaldev, S.; Krishnan, K. K.; Anilkumar, G. *Asian Journal of Organic Chemistry* **2018**, *7*, 85–102.
130. Gao, S.; Tzeng, T.; Sastry, M.; Chu, C.-M.; Liu, J.-T.; Lin, C.; Yao, C.-F. *Tetrahedron Letters* **2006**, *47*, 1889–1893.
131. Lowe, A. B. *Polymer Chemistry* **2010**, *1*, 17–36.
132. Denes, F.; Pichowicz, M.; Povie, G.; Renaud, P. *Chemical reviews* **2014**, *114*, 2587–2693.
133. Rieger, P.; Pueschmann, S.; Haas, M.; Schmallegger, M.; Guedes de la Cruz, G.; Griesser, T. *Polymers* **2023**, *15*, DOI: 10.3390/polym15071647.
134. Hoyle, C. E.; Bowman, C. N. *Angewandte Chemie International Edition* **2010**, *49*, 1540–1573.
135. Hoyle, C. E.; Lee, T. Y.; Roper, T. *Journal of Polymer Science Part A: Polymer Chemistry* **2004**, *42*, 5301–5338.

136. Northrop, B. H.; Coffey, R. N. *Journal of the American Chemical Society* **2012**, *134*, 13804–13817.
137. Kolb, H. C.; Finn, M.; Sharpless, K. B. *Angewandte Chemie International Edition* **2001**, *40*, 2004–2021.
138. Kuroki, Y.; Lett, R. *Tetrahedron letters* **1984**, *25*, 197–200.
139. Vandenberg, J.; Ranieri, K.; Junkers, T. *Macromolecular Chemistry and Physics* **2012**, *213*, 2611–2617.
140. Lutolf, M.; Hubbell, J. *Biomacromolecules* **2003**, *4*, 713–722.
141. Salinas, C. N.; Cole, B. B.; Kasko, A. M.; Anseth, K. S. *Tissue engineering* **2007**, *13*, 1025–1034.
142. Crowe, J. A.; Genzer, J. *Journal of the American Chemical Society* **2005**, *127*, 17610–17611.
143. Jonkheijm, P.; Weinrich, D.; Köhn, M.; Engelkamp, H.; Christianen, P. C.; Kuhlmann, J.; Maan, J. C.; Nüsse, D.; Schroeder, H.; Wacker, R., et al. *Angewandte Chemie International Edition* **2008**, *47*, 4421–4424.
144. Tedja, R.; Soeriyadi, A. H.; Whittaker, M. R.; Lim, M.; Marquis, C.; Boyer, C.; Davis, T. P.; Amal, R. *Polymer Chemistry* **2012**, *3*, 2743–2751.
145. Nie, Z.; Kumacheva, E. *Nature materials* **2008**, *7*, 277–290.
146. Wagner, C.; Harned, N. *Nature Photonics* **2010**, *4*, 24–26.
147. Wang, Q.; Cui, H.; Wang, X.; Hu, Z.; Tao, P.; Li, M.; Wang, J.; Tang, Y.; Xu, H.; He, X. *Journal of the American Chemical Society* **2023**, *145*, 3064–3074.
148. Wang, X.; Tseng, L.-T.; Allenet, T.; Mochi, I.; Vockenhuber, M.; Yeh, C.-K.; van Lent-Protasova, L.; Santaclara, J. G.; Custers, R.; Ekinici, Y. In *Extreme Ultraviolet (EUV) Lithography XI*, **2020**; Vol. 11323, pp 56–66.
149. Smeets, C.; Benders, N.; Bornebroek, F.; Carbone, J.; van Es, R.; Minnaert, A.; Salmaso, G.; Young, S. In *Optical and EUV Nanolithography XXXVI*, **2023**; Vol. 12494, pp 34–42.
150. Buitrago, E.; Meeuwissen, M.; Yildirim, O.; Custers, R.; Hoefnagels, R.; Rispen, G.; Vockenhuber, M.; Mochi, I.; Fallica, R.; Tasdemir, Z., et al. In *Extreme Ultraviolet (EUV) Lithography VIII*, **2017**; Vol. 10143, pp 170–177.
151. Zheng, L.; Zywiets, U.; Birr, T.; Duderstadt, M.; Overmeyer, L.; Roth, B.; Reinhardt, C. *Microsystems & nanoengineering* **2021**, *7*, 64.
152. Voelkel, R.; Herzig, H. P.; Nussbaum, P.; Daendliker, R.; Hugel, W. B. *Optical Engineering* **1996**, *35*, 3323–3330.
153. Leggett, G. J. *Chemical Society Reviews* **2006**, *35*, 1150–1161.
154. Zhou, L.-Y.; Fu, J.; He, Y. *Advanced Functional Materials* **2020**, *30*, 2000187.
155. Oropallo, W.; Piegl, L. A. *Engineering with Computers* **2016**, *32*, 135–148.
156. Levy, G. N.; Schindel, R.; Kruth, J.-P. *CIRP annals* **2003**, *52*, 589–609.
157. Ngo, T. D.; Kashani, A.; Imbalzano, G.; Nguyen, K. T.; Hui, D. *Composites Part B: Engineering* **2018**, *143*, 172–196.
158. Jandyal, A.; Chaturvedi, I.; Wazir, I.; Raina, A.; Haq, M. I. U. *Sustainable Operations and Computers* **2022**, *3*, 33–42.
159. Adafruit Jake Evill's Cortex Reimagines the Cast for the 21st Century, [online; accessed 2024-03-12], **2013**.
160. Ningbo Yuefei Mould Co. 3D printing Tech. for coolingoptimaizeing Manufacturers, [online; accessed 2024-03-12].
161. Science Buddies Design and 3D Print Your Own Fabric, [online; accessed 2024-03-12].
162. Shaukat, U.; Rossegger, E.; Schlögl, S. *Polymers* **2022**, *14*, DOI: 10.3390/polym14122449.
163. Bîrcă, A.; Gherasim, O.; Grumezescu, V.; Grumezescu, A. M. In *Materials for biomedical engineering*; Elsevier: **2019**, pp 1–28.

164. Hull, C. W.; Spence, S. T.; Lewis, C. W.; Vinson, W. A.; Freed, R. S.; Smalley, D. R. Method of and apparatus for production of three-dimensional objects by stereolithography with reduced curl, US Patent 5,104,592, **1992**.
165. Quan, H.; Zhang, T.; Xu, H.; Luo, S.; Nie, J.; Zhu, X. *Bioactive Materials* **2020**, *5*, 110–115.
166. Liu, G.; Zhang, X.; Chen, X.; He, Y.; Cheng, L.; Huo, M.; Yin, J.; Hao, F.; Chen, S.; Wang, P., et al. *Materials Science and Engineering: R: Reports* **2021**, *145*, 100596.
167. Xometry All About Digital Light Process (DLP) 3D Printing, [online; accessed 2024-03-13], **2022**.
168. Tumbleston, J. R.; Shirvanyants, D.; Ermoshkin, N.; Januszewicz, R.; Johnson, A. R.; Kelly, D.; Chen, K.; Pinschmidt, R.; Rolland, J. P.; Ermoshkin, A., et al. *Science* **2015**, *347*, 1349–1352.
169. Davoudinejad, A. In *Additive Manufacturing*; Elsevier: **2021**, pp 159–181.
170. Januszewicz, R.; Tumbleston, J. R.; Quintanilla, A. L.; Mecham, S. J.; DeSimone, J. M. *Proceedings of the National Academy of Sciences* **2016**, *113*, 11703–11708.
171. Stampfl, J.; Liska, R.; Ovsianikov, A., *Multiphoton lithography: Techniques, materials, and applications*; John Wiley & Sons: 2016.
172. Park, S.-H.; Yang, D.-Y.; Lee, K.-S. *Laser & Photonics Reviews* **2009**, *3*, 1–11.
173. Varadan, V. K.; Jiang, X.; Varadan, V. V.
174. Appuhamillage, G. A.; Chartrain, N.; Meenakshisundaram, V.; Feller, K. D.; Williams, C. B.; Long, T. E. *Industrial & Engineering Chemistry Research* **2019**, *58*, 15109–15118.
175. Fatkullin, N.; Ikehara, T.; Jinnai, H.; Kawata, S.; Kimmich, R.; Nishi, T.; Nishikawa, Y.; Sun, H.-B.; Sun, H.-B.; Kawata, S. *NMR 3D Analysis Photopolymerization* **2004**, 169–273.
176. Gibson, I.; Rosen, D. W.; Stucker, B.; Khorasani, M.; Rosen, D.; Stucker, B.; Khorasani, M., *Additive manufacturing technologies*; Springer: **2021**; Vol. 17.
177. Rafiee, M.; Farahani, R. D.; Therriault, D. *Advanced Science* **2020**, *7*, 1902307.
178. Nazir, A.; Gokcekaya, O.; Billah, K. M. M.; Ertugrul, O.; Jiang, J.; Sun, J.; Hussain, S. *Materials & Design* **2023**, *226*, 111661.
179. Bártolo, P. J., *Stereolithography: materials, processes and applications*; Springer Science & Business Media: **2011**.
180. Zhou, C.; Chen, Y.; Yang, Z.; Khoshnevis, B. *Rapid Prototyping Journal* **2013**, *19*, 153–165.
181. Mapili, G.; Lu, Y.; Chen, S.; Roy, K. *Journal of Biomedical Materials Research Part B: Applied Biomaterials: An Official Journal of The Society for Biomaterials, The Japanese Society for Biomaterials, and The Australian Society for Biomaterials and the Korean Society for Biomaterials* **2005**, *75*, 414–424.
182. Lu, Y.; Mantha, S. N.; Crowder, D. C.; Chinchilla, S.; Shah, K. N.; Yun, Y. H.; Wicker, R. B.; Choi, J.-W. *Biofabrication* **2015**, *7*, 045001.
183. Kowsari, K.; Akbari, S.; Wang, D.; Fang, N. X.; Ge, Q. *3D Printing and Additive Manufacturing* **2018**, *5*, 185–193.
184. Grigoryan, B.; Sazer, D. W.; Avila, A.; Albritton, J. L.; Padhye, A.; Ta, A. H.; Greenfield, P. T.; Gibbons, D. L.; Miller, J. S. *Scientific reports* **2021**, *11*, 3171.
185. Sampson, K. L.; Deore, B.; Go, A.; Nayak, M. A.; Orth, A.; Gallerneault, M.; Malenfant, P. R. L.; Paquet, C. *ACS Applied Polymer Materials* **2021**, *3*, 4304–4324.
186. Gernhardt, M.; Frisch, H.; Welle, A.; Jones, R.; Wegener, M.; Blasco, E.; Barner-Kowollik, C. *Journal of Materials Chemistry C* **2020**, *8*, 10993–11000.
187. Xia, C.; Fang, N. *Journal of Micromechanics and Microengineering* **2009**, *19*, 115029.
188. Peterson, G. I.; Schwartz, J. J.; Zhang, D.; Weiss, B. M.; Ganter, M. A.; Storti, D. W.; Boydston, A. J. *ACS applied materials & interfaces* **2016**, *8*, 29037–29043.

189. Yue, L.; Macrae Montgomery, S.; Sun, X.; Yu, L.; Song, Y.; Nomura, T.; Tanaka, M.; Jerry Qi, H. *Nature Communications* **2023**, *14*, 1251.
190. Hobich, J.; Blasco, E.; Wegener, M.; Mutlu, H.; Barner-Kowollik, C. *Macromolecular Chemistry and Physics* **2023**, *224*, 2200318.
191. Möckl, L.; Lamb, D. C.; Bräuchle, C. *Angewandte Chemie International Edition* **2014**, *53*, 13972–13977.
192. Regehly, M.; Garmshausen, Y.; Reuter, M.; König, N. F.; Israel, E.; Kelly, D. P.; Chou, C.-Y.; Koch, K.; Asfari, B.; Hecht, S. *Nature* **2020**, *588*, 620–624.
193. Walden, S. L.; Rodrigues, L. L.; Alves, J.; Blinco, J. P.; Truong, V. X.; Barner-Kowollik, C. *Nature Communications* **2022**, *13*, 2943.
194. Ramezani, M.; Mohd Ripin, Z. *Journal of functional biomaterials* **2023**, *14*, 347.
195. https://www.ted.com/talks/skylar_tibbits_the_emergence_of_4d_printing..
196. Chu, H.; Yang, W.; Sun, L.; Cai, S.; Yang, R.; Liang, W.; Yu, H.; Liu, L. *Micromachines* **2020**, *11*, 796.
197. Ahmed, A.; Arya, S.; Gupta, V.; Furukawa, H.; Khosla, A. *Polymer* **2021**, *228*, 123926.
198. Rossegger, E.; Höller, R.; Hrbinič, K.; Sangermano, M.; Griesser, T.; Schlögl, S. *Advanced engineering materials* **2023**, *25*, 2200749.
199. Biswas, M. C.; Chakraborty, S.; Bhattacharjee, A.; Mohammed, Z. *Advanced Functional Materials* **2021**, *31*, 2100257.
200. Vatanparast, S.; Boschetto, A.; Bottini, L.; Gaudenzi, P. *Applied Sciences* **2023**, *13*, DOI: 10.3390/app13137744.
201. Zhang, C.; Cai, D.; Liao, P.; Su, J.-W.; Deng, H.; Vardhanabhuti, B.; Ulery, B. D.; Chen, S.-Y.; Lin, J. *Acta biomaterialia* **2021**, *122*, 101–110.
202. Zhang, Y.; Raza, A.; Xue, Y.-Q.; Yang, G.; Hayat, U.; Yu, J.; Liu, C.; Wang, H.-J.; Wang, J.-Y. *Bioactive Materials* **2023**, *23*, 343–352.
203. Fu, P.; Li, H.; Gong, J.; Fan, Z.; Smith, A. T.; Shen, K.; Khalfalla, T. O.; Huang, H.; Qian, X.; McCutcheon, J. R.; Sun, L. *Progress in Polymer Science* **2022**, *126*, 101506.
204. Mahmood, A.; Akram, T.; Shenggui, C.; Chen, H. *Composites Part B: Engineering* **2023**, *110952*.
205. Yang, H.; Leow, W. R.; Wang, T.; Wang, J.; Yu, J.; He, K.; Qi, D.; Wan, C.; Chen, X. *Advanced Materials* **2017**, *29*, 1701627.
206. Wu, S.; Shi, H.; Lu, W.; Wei, S.; Shang, H.; Liu, H.; Si, M.; Le, X.; Yin, G.; Theato, P., et al. *Angewandte Chemie International Edition* **2021**, *60*, 21890–21898.
207. Han, B.; Zhang, Y.-L.; Zhu, L.; Li, Y.; Ma, Z.-C.; Liu, Y.-Q.; Zhang, X.-L.; Cao, X.-W.; Chen, Q.-D.; Qiu, C.-W., et al. *Advanced Materials* **2019**, *31*, 1806386.
208. Chen, Z.; Zhao, D.; Liu, B.; Nian, G.; Li, X.; Yin, J.; Qu, S.; Yang, W. *Advanced Functional Materials* **2019**, *29*, 1900971.
209. Campbell, I.; Bourell, D.; Gibson, I. *Rapid prototyping journal* **2012**, *18*, 255–258.
210. Cazon, A.; Kelly, S.; Paterson, A. M.; Bibb, R. J.; Campbell, R. I. *Proceedings of the Institution of Mechanical Engineers, Part H: Journal of Engineering in Medicine* **2017**, *231*, 881–897.
211. Milovanović, A.; Sedmak, A.; Golubović, Z.; Zurkić, K. Z. M. A.; Trajković, I.; Milosević, M. *Journal of the Mechanical Behavior of Biomedical Materials* **2021**, *119*, 104494.
212. Buschang, P. H.; Ross, M.; Shaw, S. G.; Crosby, D.; Campbell, P. M. *The Angle Orthodontist* **2015**, *85*, 723–727.
213. Zhang, X.-J.; He, L.; Guo, H.-M.; Tian, J.; Bai, Y.-X.; Li, S. *The korean journal of orthodontics* **2015**, *45*, 275–281.

214. Tartaglia, G. M.; Mapelli, A.; Maspero, C.; Santaniello, T.; Serafin, M.; Farronato, M.; Caprioglio, A. *Materials* **2021**, *14*, 1799.
215. Bichu, Y. M.; Alwafi, A.; Liu, X.; Andrews, J.; Ludwig, B.; Bichu, A. Y.; Zou, B. *Bioactive Materials* **2023**, *22*, 384–403.
216. Zarek, M.; Mansour, N.; Shapira, S.; Cohn, D. *Macromolecular rapid communications* **2017**, *38*, 1600628.
217. Kirillova, A.; Maxson, R.; Stoychev, G.; Gomillion, C. T.; Ionov, L. *Advanced Materials* **2017**, *29*, 1703443.
218. Yakacki, C. M.; Shandas, R.; Lanning, C.; Rech, B.; Eckstein, A.; Gall, K. *Biomaterials* **2007**, *28*, 2255–2263.
219. Colombo, A.; Karvouni, E. *Biodegradable Stents: Fulfilling the Mission and Stepping Away*, 2000.
220. Palmaz, J. C. *Journal of endovascular therapy* **2004**, *11*, II–200.
221. Mirani, B.; Pagan, E.; Currie, B.; Siddiqui, M. A.; Hosseinzadeh, R.; Mostafalu, P.; Zhang, Y. S.; Ghahary, A.; Akbari, M. *Advanced healthcare materials* **2017**, *6*, 1700718.
222. Tao, Y.; Chan, H. F.; Shi, B.; Li, M.; Leong, K. W. *Advanced Functional Materials* **2020**, *30*, 2005029.
223. LusCreo 3D Direct Print Clear Aligner Manufacturing, [online; accessed 2024-03-16].
224. Kainz, M.; Perak, S.; Stubauer, G.; Kopp, S.; Kauscheder, S.; Hemetzberger, J.; Cendrero, A.; Diaz Lantada, A.; Tupe, D.; Major, Z.; Hanetseder, D.; Hruschka, V.; Wolbank, S.; Presen, D.; Mühlberger, M.; Guillén, E. *Polymers* **2024**, *16*, 655.
225. Grigoryan, B.; Paulsen, S. J.; Corbett, D. C.; Sazer, D. W.; Fortin, C. L.; Zaita, A. J.; Greenfield, P. T.; Calafat, N. J.; Gounley, J. P.; Ta, A. H., et al. *Science* **2019**, *364*, 458–464.
226. Huang, J.; Yang, R.; Jiao, J.; Li, Z.; Wang, P.; Liu, Y.; Li, S.; Chen, C.; Li, Z.; Qu, G., et al. *Nature Communications* **2023**, *14*, 7856.
227. Grim, J. C.; Marozas, I. A.; Anseth, K. S. *Journal of Controlled Release* **2015**, *219*, Drug Delivery Research in North America - Part I, 95–106.
228. Polizzotti, B. D.; Fairbanks, B. D.; Anseth, K. S. *Biomacromolecules* **2008**, *9*, 1084–1087.
229. Levato, R.; Dudaryeva, O.; Garciamendez-Mijares, C. E.; Kirkpatrick, B. E.; Rizzo, R.; Schimelman, J.; Anseth, K. S.; Chen, S.; Zenobi-Wong, M.; Zhang, Y. S. *Nature Reviews Methods Primers* **2023**, *3*, 47.
230. Hu, Y.; Wang, Z.; Jin, D.; Zhang, C.; Sun, R.; Li, Z.; Hu, K.; Ni, J.; Cai, Z.; Pan, D., et al. *Advanced Functional Materials* **2020**, *30*, 1907377.
231. Li, H.; Go, G.; Ko, S. Y.; Park, J.-O.; Park, S. *Smart Materials and Structures* **2016**, *25*, 027001.
232. Spiegel, C. A.; Hackner, M.; Bothe, V. P.; Spatz, J. P.; Blasco, E. *Advanced Functional Materials* **2022**, *32*, 2110580.
233. Mayer, F.; Richter, S.; Westhauser, J.; Blasco, E.; Barner-Kowollik, C.; Wegener, M. *Science advances* **2019**, *5*, eaau9160.
234. Hippler, M.; Blasco, E.; Qu, J.; Tanaka, M.; Barner-Kowollik, C.; Wegener, M.; Bastmeyer, M. *Nature communications* **2019**, *10*, 232.
235. Amin, R.; Knowlton, S.; Hart, A.; Yenilmez, B.; Ghaderinezhad, F.; Katebifar, S.; Messina, M.; Khademhosseini, A.; Tasoglu, S. *Biofabrication* **2016**, *8*, 022001.
236. Comina, G.; Suska, A.; Filippini, D. *Lab on a Chip* **2014**, *14*, 424–430.
237. Shallan, A. I.; Smejkal, P.; Corban, M.; Guijt, R. M.; Breadmore, M. C. *Analytical chemistry* **2014**, *86*, 3124–3130.
238. Spiegel, C. A.; Hippler, M.; Münchinger, A.; Bastmeyer, M.; Barner-Kowollik, C.; Wegener, M.; Blasco, E. *Advanced Functional Materials* **2020**, *30*, 1907615.

239. Kim, Y.; Parada, G. A.; Liu, S.; Zhao, X. *Science Robotics* **2019**, *4*, eaax7329.
240. Kim, Y.; Yuk, H.; Zhao, R.; Chester, S. A.; Zhao, X. *Nature* **2018**, *558*, 274–279.
241. Wei, H.; Zhang, Q.; Yao, Y.; Liu, L.; Liu, Y.; Leng, J. *ACS applied materials & interfaces* **2017**, *9*, 876–883.
242. Mao, Y.; Yu, K.; Isakov, M. S.; Wu, J.; Dunn, M. L.; Jerry Qi, H. *Scientific reports* **2015**, *5*, 13616.
243. Ge, Q.; Dunn, C. K.; Qi, H. J.; Dunn, M. L. *Smart materials and structures* **2014**, *23*, 094007.
244. Liu, Y.; Boyles, J. K.; Genzer, J.; Dickey, M. D. *Soft matter* **2012**, *8*, 1764–1769.
245. Sokolowski, W.; Tan, S. *Journal of Spacecraft and Rockets - J SPACECRAFT ROCKET* **2007**, *44*, 750–754.
246. Felton, S.; Tolley, M.; Demaine, E.; Rus, D.; Wood, R. *Science* **2014**, *345*, 644–646.
247. Zarek, M.; Layani, M.; Cooperstein, I.; Sachyani, E.; Cohn, D.; Magdassi, S. *Advanced Materials (Deerfield Beach, Fla.)* **2015**, *28*, 4449–4454.
248. Yao, S.; Zhu, Y. *Advanced Materials* **2015**, *27*, 1480–1511.
249. Valentine, A. D.; Busbee, T. A.; Boley, J. W.; Raney, J. R.; Chortos, A.; Kotikian, A.; Berrigan, J. D.; Durstock, M. F.; Lewis, J. A. *Advanced Materials* **2017**, *29*, 1703817.
250. Odent, J.; Wallin, T. J.; Pan, W.; Kruemplestaedter, K.; Shepherd, R. F.; Giannelis, E. P. *Advanced Functional Materials* **2017**, *27*, 1701807.
251. Khudiakova, A.; Arbeiter, F.; Spoerk, M.; Wolfahrt, M.; Godec, D.; Pinter, G. *Additive Manufacturing* **2019**, *28*, 184–193.
252. Zhang, F.; Zhu, L.; Li, Z.; Wang, S.; Shi, J.; Tang, W.; Li, N.; Yang, J. *Additive Manufacturing* **2021**, *48*, 102423.
253. Choi, J.-W.; Kim, H.-C.; Wicker, R. *Journal of Materials Processing Technology* **2011**, *211*, 318–328.
254. National Library of Medicine Compound summary: Abietic acid, [online; accessed 2024-03-26].
255. Wikipedia.org Abietic acid, [online; accessed 2024-03-26].
256. Fujii, R.; Arimoto, K.; Zinkel, D. F. *Journal of the American Oil Chemists Society* **1987**, *64*, 1144–1149.
257. Enoki, A.; KITAO, K. *Wood research: bulletin of the Wood Research Institute Kyoto University* **1974**, *57*, 1–9.
258. Von G, M.; Rottländer, R. C. *Tetrahedron letters* **1971**, *12*, 1295–1298.
259. Kim, W.-S.; Jang, H.-S.; Hong, K.-H.; Seo, K.-H. *Macromolecular rapid communications* **2001**, *22*, 825–828.
260. Kim, W.-S.; Byun, K.-R.; Lee, D.-H.; Min, K.-E.; Park, L.-S.; Seo, K.-H.; Kang, I.-K.; Park, S.-Y. *Polymer journal* **2003**, *35*, 450–454.
261. Kwak, G.; Choi, J.-U.; Seo, K.-H.; Park, L.-S.; Hyun, S.-H.; Kim, W.-S. *Chemistry of materials* **2007**, *19*, 2898–2902.
262. Van Damme, J.; Du Prez, F. *Progress in polymer science* **2018**, *82*, 92–119.
263. Goldbach, J. T.; Russell, T. P.; Penelle, J. *Macromolecules* **2002**, *35*, 4271–4276.
264. Yamamoto, T.; Yagyu, S.; Tezuka, Y. *Journal of the American Chemical Society* **2016**, *138*, 3904–3911.
265. Radl, S. V.; Roth, M.; Gassner, M.; Wolfberger, A.; Lang, A.; Hirschmann, B.; Trimmel, G.; Kern, W.; Griesser, T. *European polymer journal* **2014**, *52*, 98–104.
266. Claus, T. K.; Telitel, S.; Welle, A.; Bastmeyer, M.; Vogt, A. P.; Delaittre, G.; Barner-Kowollik, C. *Chemical communications* **2017**, *53*, 1599–1602.

267. Li, Y.; Goswami, M.; Zhang, Y.; Liu, T.; Zhang, J.; Kessler, M. R.; Wang, L.; Rios, O. *Scientific Reports* **2020**, *10*, 20214.
268. Koo, B.; Nofen, E.; Chattopadhyay, A.; Dai, L. *Computational Materials Science* **2017**, *133*, 167–174.
269. Radl, S.; Kreimer, M.; Griesser, T.; Oesterreicher, A.; Moser, A.; Kern, W.; Schloegl, S. *Polymer* **2015**, *80*, 76–87.
270. Manhart, J.; Ayalur-Karunakaran, S.; Radl, S.; Oesterreicher, A.; Moser, A.; Ganser, C.; Teichert, C.; Pinter, G.; Kern, W.; Griesser, T.; Schlögl, S. *Polymer* **2016**, *102*, 10–20.
271. Hughes, T.; Simon, G. P.; Saito, K. *ACS applied materials & interfaces* **2019**, *11*, 19429–19443.
272. Batool, S. R.; Nazeer, M. A.; Ekinici, D.; Sahin, A.; Kizilel, S. *International journal of biological macromolecules* **2020**, *150*, 315–325.
273. Truong, V. X.; Li, F.; Forsythe, J. S. *ACS Macro Letters* **2017**, *6*, 657–662.
274. Kaiser, S.; Radl, S. V.; Manhart, J.; Ayalur-Karunakaran, S.; Griesser, T.; Moser, A.; Ganser, C.; Teichert, C.; Kern, W.; Schlögl, S. *Soft Matter* **2018**, *14*, 2547–2559.
275. Van Damme, J.; van den Berg, O.; Brancart, J.; Vlaminck, L.; Huyck, C.; Van Assche, G.; Van Mele, B.; Du Prez, F. *Macromolecules* **2017**, *50*, 1930–1938.
276. Li, F.; Hou, H.; Yin, J.; Jiang, X. *Acs Macro Letters* **2017**, *6*, 848–853.
277. Wang, D.; Xu, L.; Zhang, L.; Zhang, L.; Zhang, A. *Chemical Engineering Journal* **2021**, *420*, 127679.
278. Frisch, H.; Bloesser, F. R.; Barner-Kowollik, C. *Angewandte Chemie International Edition* **2019**, *58*, 3604–3609.
279. Frisch, H.; Kodura, D.; Bloesser, F. R.; Michalek, L.; Barner-Kowollik, C. *Macromolecular Rapid Communications* **2020**, *41*, 1900414.
280. Tazuke, S.; Banba, F. *Journal of Polymer Science: Polymer Chemistry Edition* **1976**, *14*, 2463–2478.
281. Van Damme, J.; Vlaminck, L.; Van Assche, G.; Van Mele, B.; van den Berg, O.; Du Prez, F. *Tetrahedron* **2016**, *72*, 4303–4311.
282. Van Damme, J.; van den Berg, O.; Brancart, J.; Van Assche, G.; Du Prez, F. *Tetrahedron* **2019**, *75*, 912–920.
283. Mahapatra, D. K.; Bharti, S. K.; Asati, V. *Current topics in medicinal chemistry* **2017**, *17*, 3146–3169.
284. Valavanidis, A.; Vlachogianni, T. In *Studies in Natural Products Chemistry*, ur Rahman, A., Ed.; Studies in Natural Products Chemistry, Vol. 39; Elsevier: **2013**, pp 269–295.
285. Mustafa, A. *Chemical Reviews* **1952**, *51*, 1–23.
286. Van Heijst, J.; Corda, M.; Lukin, O. *Polymer* **2015**, *70*, 1–7.
287. Choi, K.-S.; Kim, H.-W.; Kim, Y.-B.; Kim, J.-D. *Liquid crystals* **2004**, *31*, 639–647.
288. Tunell, H.; Selo, M.; Skarp, K.; Hilborn, J. *Polymer journal* **2006**, *38*, 716–723.
289. Subramanian, K.; Krishnasamy, V.; Nanjundan, S.; Reddy, A. R. *European polymer journal* **2000**, *36*, 2343–2350.
290. Reddy, A. R.; Subramanian, K.; Krishnasamy, V.; Ravichandran, J. *European polymer journal* **1996**, *32*, 919–926.
291. Choi, D.-H.; Ban, S.-Y.; Kim, J.-H. *Bulletin of the Korean Chemical Society* **2003**, *24*, 441–445.
292. Viña, A.; Murillo, E. *Journal of the Brazilian chemical society* **2003**, *14*, 744–749.
293. Boland, D. J.; Brophy, J.; House, A., *Eucalyptus leaf oils: use, chemistry, distillation and marketing*. **1991**.
294. Ragavendran, V.; Muthunatesan, S.; Santhanam, V.; Arsic, B. *Journal of Molecular Structure* **2019**, *1184*, 593–603.

295. Galun, A. B., *Polymerization and Copolymerization of Ethylenic Ketones*; University of Illinois at Urbana-Champaign: **1954**.
296. Minsk, L. pat., 2 725 377, **1955**.
297. Egerton, P.; Pitts, E; Reiser, A *Macromolecules* **1981**, *14*, 95–100.
298. Kosar, J Inc, *New York, USA* **1965**, 820.
299. Williams, J.; Farid, S.; Doty, J.; Daly, R.; Specht, D.; Searle, R; Borden, D.; Chang, H.; Martic, P. In *Photochemical Processes in Polymer Chemistry–2*; Elsevier: **1977**, pp 523–538.
300. Tanaka, H.; Tsuda, M.; Nakanishi, H. *Journal of Polymer Science Part A-1: Polymer Chemistry* **1972**, *10*, 1729–1743.
301. Tanaka, H.; Otomegawa, E. *Journal of Polymer Science: Polymer Chemistry Edition* **1974**, *12*, 1125–1130.
302. Coqueret, X. *Macromolecular Chemistry and Physics* **1999**, *200*, 1567–1579.
303. Shindo, Y.; Sugimura, T.; Horie, K.; Mita, I. *European polymer journal* **1986**, *22*, 859–863.
304. Tangirala, R.; Baer, E.; Hiltner, A.; Weder, C. *Advanced Functional Materials* **2004**, *14*, 595–604.
305. Ikoma, H.; Kondo, M.; Kawatsuki, N. *Journal of Photopolymer Science and Technology* **2017**, *30*, 451–456.
306. Li, X.; Cui, J.; Zhang, W.; Huang, J.; Li, W.; Lin, C.; Jiang, Y.; Zhang, Y.; Li, G. *Journal of Materials Chemistry* **2011**, *21*, 17953–17959.
307. Zhang, H.; Li, X.; Lin, Y.; Gao, F.; Tang, Z.; Su, P.; Zhang, W.; Xu, Y.; Weng, W.; Boulatov, R. *Nature communications* **2017**, *8*, 1147.
308. Hyde, P; Kricka, L.; Ledwith, A *Journal of Polymer Science: Polymer Letters Edition* **1973**, *11*, 415–419.
309. Querner, J.; Wolff, T.; Görner, H. *Chemistry–A European Journal* **2004**, *10*, 283–293.
310. Bener, S.; Aydogan, C.; Yagci, Y. *Macromolecular Rapid Communications* **2020**, *41*, 2000369.
311. Doi, T.; Kawai, H.; Murayama, K.; Kashida, H.; Asanuma, H. *Chemistry–A European Journal* **2016**, *22*, 10533–10538.
312. Marschner, D. E.; Kamm, P. W.; Frisch, H.; Unterreiner, A.-N.; Barner-Kowollik, C. *Chemical Communications* **2020**, *56*, 14043–14046.
313. Frisch, H.; Menzel, J. P.; Bloesser, F. R.; Marschner, D. E.; Mundsinger, K.; Barner-Kowollik, C. *Journal of the American Chemical Society* **2018**, *140*, 9551–9557.
314. Truong, V. X.; Li, F.; Ercole, F.; Forsythe, J. S. *ACS Macro Letters* **2018**, *7*, 464–469.
315. Ou, R.; Zhang, H.; Zhao, C.; Hegab, H. M.; Jiang, L.; Truong, V. X.; Wang, H. *Chemistry of Materials* **2020**, *32*, 10621–10627.
316. Ohtani, Y.; Inaki, Y.; Miyata, M. *Journal of Photopolymer Science and Technology* **2001**, *14*, 295–296.
317. INAKI, Y.; WANG, Y.; Kubo, M.; Takemoto, K. *Journal of Photopolymer Science and Technology* **1991**, *4*, 259–266.
318. Brown, I.; Johns, H. *Photochemistry and Photobiology* **1968**, *8*, 273–286.
319. Wacker, A; Lodemann, E *Angewandte Chemie International Edition in English* **1965**, *4*, 150–150.
320. Fisher, G.; Johns, H. *Photochemistry and Photobiology* **1970**, *11*, 429–444.
321. Fisher, G.; Johns, H. by SY Wang, *Academic Press, New York* **1976**, *1*, 225–294.
322. Lamola, A. *Pure and Applied Chemistry* **1973**, *34*, 281–304.
323. Pollum, M.; Martinez-Fernandez, L.; Crespo-Hernandez, C. E. *Photoinduced Phenomena in Nucleic Acids I: Nucleobases in the Gas Phase and in Solvents* **2015**, 245–327.

324. Manae, M. A.; Hazra, A. *The Journal of Physical Chemistry A* **2019**, *123*, 10862–10867.
325. Inaki, Y.; Hiratsuka, H. *Journal of Photopolymer Science and Technology* **2000**, *13*, 739–744.
326. Yang, K.; Zeng, M. *New Journal of Chemistry* **2013**, *37*, 920–926.
327. Trakhtenberg, S.; Warner, J. C.; Nagarajan, R.; Bruno, F. F.; Samuelson, L. A.; Kumar, J. *Chemistry of materials* **2006**, *18*, 2873–2878.
328. Inada, M.; Udagawa, A.; Sato, S.; Asahi, T.; Saito, K. *Photochemical & Photobiological Sciences* **2022**, *21*, 2169–2177.
329. He, D.; He, X.; Wang, K.; Cao, J.; Zhao, Y. *Langmuir* **2012**, *28*, 4003–4008.
330. Vendrell-Criado, V.; Lhiaubet-Vallet, V.; Yamaji, M.; Cuquerella, M. C.; Miranda, M. A. *Organic & biomolecular chemistry* **2016**, *14*, 4110–4115.
331. Pollum, M.; Jockusch, S.; Crespo-Hernández, C. E. *Physical Chemistry Chemical Physics* **2015**, *17*, 27851–27861.
332. Pollum, M.; Jockusch, S.; Crespo-Hernandez, C. E. *Journal of the American Chemical Society* **2014**, *136*, 17930–17933.
333. Lapucha, A. R. *Synthesis* **1987**, *1987*, 256–258.
334. Piane, J. J.; Chamberlain, L. E.; Huss, S.; Alameda, L. T.; Hoover, A. C.; Elacqua, E. *ACS Catalysis* **2020**, *10*, 13251–13256.
335. Kötteritzsch, J.; Geitner, R.; Ahner, J.; Abend, M.; Zechel, S.; Vitz, J.; Hoepfener, S.; Dietzek, B.; Schmitt, M.; Popp, J., et al. *Journal of Applied Polymer Science* **2018**, *135*, 45916.
336. Kang, Y.; Lu, A.; Ellington, A.; Jewett, M. C.; O'Reilly, R. K. *ACS Macro Letters* **2013**, *2*, 581–586.
337. Müller, S. M.; Nelson, B. R.; Jelinek, A.; Kirkpatrick, B. E.; Keyser, S.; Naderer, C.; Sivun, D.; Jacak, J.; Anseth, K. S.; Bowman, C. N.; Schlögl, S.; Griesser, T. *Advanced Materials* **submitted**.
338. Del Campo, A.; Boos, D.; Spiess, H. W.; Jonas, U. *Angewandte Chemie International Edition* **2005**, *44*, 4707–4712.
339. Van De Walle, M.; De Bruycker, K.; Blinco, J. P.; Barner-Kowollik, C. *Angewandte Chemie International Edition* **2020**, *59*, 14143–14147.
340. Batchelor, R.; Messer, T.; Hippler, M.; Wegener, M.; Barner-Kowollik, C.; Blasco, E. *Advanced Materials* **2019**, *31*, 1904085.
341. Müller, P.; Müller, R.; Hammer, L.; Barner-Kowollik, C.; Wegener, M.; Blasco, E. *Chemistry of Materials* **2019**, *31*, 1966–1972.
342. Zhou, H.; Xue, C.; Weis, P.; Suzuki, Y.; Huang, S.; Koynov, K.; Auernhammer, G. K.; Berger, R.; Butt, H.-J.; Wu, S. *Nature chemistry* **2017**, *9*, 145–151.
343. Zha, R. H.; Vantomme, G.; Berrocal, J. A.; Gosens, R.; de Waal, B.; Meskers, S.; Meijer, E. *Advanced Functional Materials* **2018**, *28*, 1703952.
344. Kuenstler, A. S.; Clark, K. D.; Read de Alaniz, J.; Hayward, R. C. *ACS Macro Letters* **2020**, *9*, 902–909.
345. Rochette, J. M.; Ashby, V. S. *Macromolecules* **2013**, *46*, 2134–2140.
346. Wu, L.; Jin, C.; Sun, X. *Biomacromolecules* **2011**, *12*, 235–241.
347. Pilate, F.; Stoclet, G.; Mincheva, R.; Dubois, P.; Raquez, J.-M. *Macromolecular Chemistry and Physics* **2018**, *219*, 1700345.
348. Leng, J.; Li, S.; Yang, M.; Hu, J. *Journal of Materials Research* **2019**, *34*, 1795–1804.
349. Zhao, X.; Dang, Y.; Deng, J.; Zhang, J. *Colloid and Polymer Science* **2014**, *292*, 85–95.
350. Defize, T.; Thomassin, J.-M.; Ottevaere, H.; Malherbe, C.; Eppe, G.; Jellali, R.; Alexandre, M.; Jerome, C.; Riva, R. *Macromolecules* **2018**, *52*, 444–456.
351. Lendlein, A.; Jiang, H.; Jünger, O.; Langer, R. *Nature* **2005**, *434*, 879–882.

352. Zhu, C. N.; Li, C. Y.; Wang, H.; Hong, W.; Huang, F.; Zheng, Q.; Wu, Z. L. *Advanced Materials* **2021**, *33*, 2008057.
353. Benkhaled, B. T.; Belkhir, K.; Brossier, T.; Chatard, C.; Graillot, A.; Lonetti, B.; Mingotaud, A.-F.; Catrouillet, S.; Blanquer, S.; Lapinte, V. *European Polymer Journal* **2022**, *179*, 111570.
354. Liu, X.; Wu, J.; Tang, Z.; Wu, J.; Huang, Z.; Yin, X.; Du, J.; Lin, X.; Lin, W.; Yi, G. *ACS Applied Materials & Interfaces* **2022**, *14*, 33829–33841.
355. Wagner, P. J.; Bucheck, D. J. *Journal of the American Chemical Society* **1970**, *92*, 181–185.
356. Gadek, M.; Strachota, B.; Matějka, L. *Polymer International* **2021**, *70*, 1225–1233.
357. Snyder, E. A.; Tong, T. H. *MRS Online Proceedings Library (OPL)* **2005**, *872*, J18–6.
358. Gernhardt, M.; Frisch, H.; Welle, A.; Jones, R.; Wegener, M.; Blasco, E.; Barner-Kowollik, C. *Journal of Materials Chemistry C* **2020**, *8*, 10993–11000.
359. Tang, F.; Tang, L.; Guan, Z.; He, Y.-H. *Tetrahedron* **2018**, *74*, 6694–6703.
360. Akelah, A.; Selim, A.; Salah Ei-Deen, N.; Kandil, S. *Polymer international* **1992**, *28*, 307–312.
361. Akelah, A.; Selim, A.; El-Deen, N. S. *Polymer international* **1993**, *32*, 423–434.
362. Tamilvanan, M.; Pandurangan, A.; Reddy, B. S.; Subramanian, K. *Polymer international* **2007**, *56*, 104–111.
363. Luo, Q.; Liu, H.; Li, D.; Dai, J.; Xia, L.; Jiang, J.; Xu, Y.; Zeng, B.; Luo, W.; Dai, L. *Carbohydrate Polymers* **2024**, *326*, 121610.
364. Rehab, A. *European polymer journal* **1998**, *34*, 1845–1855.
365. Rehab, A.; Salahuddin, N. *Polymer* **1999**, *40*, 2197–2207.
366. Choi, D. H.; Oh, S. J. *European polymer journal* **2002**, *38*, 1559–1564.
367. Wang, W.; Wu, Q.; Ding, L.; Yang, Z.; Zhang, A. *Journal of applied polymer science* **2008**, *107*, 593–598.
368. Guo, M.; Wang, X. *European polymer journal* **2009**, *45*, 888–898.
369. Goretzki, C.; Ritter, H. *Macromolecular Chemistry and Physics* **1997**, *198*, 59–69.
370. Lee, I.-H.; Gong, M.-S.; Kim, J.-G. *Macromolecular Research* **2010**, *18*, 1218–1225.
371. Shiraishi, K.; Yusa, S.-i.; Ito, M.; Nakai, K.; Yokoyama, M. *Polymers* **2017**, *9*, 710.
372. Li, X.-D.; Zhong, Z.-X.; Kim, J. J.; Lee, M.-H. In *Passive Components and Fiber-based Devices*, 2005; Vol. 5623, pp 1029–1036.
373. Güler, B.; Önen, H.; Karahasanoğlu, M.; Serhatlı, E.; Çanak, T. Ç. *Progress in Organic Coatings* **2017**, *109*, 152–159.
374. Li, X.-D.; Zhong, Z.-X.; Lee, S. H.; Ghang, G.; Lee, M.-H. *Japanese journal of applied physics* **2006**, *45*, 906.
375. Shu, Y.; Ye, K.; Sun, J.; Yue, Y.; Liu, C.; Wang, H.; Lu, R. *Chemistry—A European Journal* **2021**, *27*, 17960–17969.
376. Kagatkar, S.; Sunil, D. *Chemical Papers* **2021**, *75*, 6147–6156.
377. Budziak-Wieczorek, I.; Kamiński, D.; Skrzypek, A.; Ciołek, A.; Skrzypek, T.; Janik-Zabrotowicz, E.; Arczewska, M. *Molecules* **2023**, *28*, 3412.
378. Li, J.; Zhuang, Z.; Lou, X.; Zhao, Z.; Tang, B. Z. *Chemical & Biomedical Imaging* **2023**, *1*, 785–795.
379. Ping, X.; Zhan, J.; Zhu, Y.; Wu, Y.; Hu, C.; Pan, J.; Yao, C.; Zuo, J.; Feng, H.; Qian, Z. *Chemistry—A European Journal* **2023**, *29*, e202301520.
380. Wei, H.; Zhu, H.; Li, Q.; Zheng, X. *Journal of Materials Chemistry C* **2024**.
381. Buchroithner, B.; Hartmann, D.; Mayr, S.; Oh, Y. J.; Sivun, D.; Karner, A.; Buchegger, B.; Griesser, T.; Hinterdorfer, P.; Klar, T. A., et al. *Nanoscale advances* **2020**, *2*, 2422–2428.

382. Husić, I.; Müller, S. M.; Mahendran, A. R.; Sinic, J.; Jocham, C.; Lammer, H.; Griesser, T. *Journal of Polymer Research* **2024**, *31*, 85.
383. Maier, J.; Müller, S. M.; Torvisco, A.; Glotz, G.; Fischer, R. C.; Griesser, T.; Kelterer, A.-M.; Haas, M. *ChemPhotoChem* **2022**, *6*, e202100213.
384. Haudum, S.; Lenhart, S.; Müller, S. M.; Tupe, D.; Naderer, C.; Dehne, T.; Sittinger, M.; Major, Z.; Griesser, T.; Brüggemann, O., et al. *ACS Macro Letters* **2023**, *12*, 673–678.
385. Frühwirt, P.; Knoechl, A.; Pillinger, M.; Müller, S. M.; Wasdin, P. T.; Fischer, R. C.; Radebner, J.; Torvisco, A.; Moszner, N.; Kelterer, A.-M., et al. *Inorganic chemistry* **2020**, *59*, 15204–15217.
386. Püschmann, S. D.; Frühwirt, P.; Müller, S. M.; Wagner, S. H.; Torvisco, A.; Fischer, R. C.; Kelterer, A.-M.; Griesser, T.; Gescheidt, G.; Haas, M. *Dalton Transactions* **2021**, *50*, 11965–11974.
387. Haudum, S.; Demirdögen, B.; Müller-Müchler, L.; Döttl, S. C.; Müller, S. M.; Naderer, C.; Brüggemann, O.; Griesser, T.; Jacak, J.; Priglinger, E.; Teasdale, I. *European Polymer Journal* **2024**, *211*, 113037.
388. Bachmann, J.; Gleis, E.; Schmolzer, S.; Fruhmann, G.; Hinrichsen, O. *Analytica Chimica Acta* **2021**, *1153*, 338268.
389. Zheng, X.; Ji, C.; Liu, J.; Liu, R.; Mu, Q.; Liu, X. *Industrial & Engineering Chemistry Research* **2018**, *57*, 6790–6796.
390. Pezzana, L.; Mousa, M.; Malmström, E.; Johansson, M.; Sangermano, M. *Progress in Organic Coatings* **2021**, *150*, 105986.
391. De Espinosa, L. M.; Meier, M. A. *European Polymer Journal* **2011**, *47*, 837–852.
392. Ulanowska, M.; Olas, B. *International journal of molecular sciences* **2021**, *22*, 3671.
393. Kerosenewala, J.; Vaidya, P.; Ozarkar, V.; Shirapure, Y.; More, A. P. *Polymer Bulletin* **2023**, *80*, 7047–7099.
394. Gendron, D. *Frontiers in Chemistry* **2022**, *10*, 949355.
395. Wu, Y.; Fei, M.; Qiu, R.; Liu, W.; Qiu, J. *Polymers* **2019**, *11*, 1815.
396. Stanzione III, J. F.; Sadler, J. M.; La Scala, J. J.; Reno, K. H.; Wool, R. P. *Green Chemistry* **2012**, *14*, 2346–2352.
397. Parvathy, P.; Sahoo, S. K. *Progress in Organic Coatings* **2021**, *158*, 106347.
398. Loesch-Zhang, A.; Cordt, C.; Geissler, A.; Biesalski, M. *Polymers* **2022**, *14*, 1773.
399. Silva, F. M.; Pinto, R. J.; Barros-Timmons, A. M.; Freire, C. S. *Progress in Organic Coatings* **2023**, *178*, 107476.
400. Silva, F. M.; Pinto, R. J.; Barros-Timmons, A.; Freire, C. S. *Polymers* **2023**, *15*, 1069.
401. Husić, I.; Mahendran, A. R.; Sinic, J.; Jocham, C.; Lammer, H. *Journal of Plastic Film & Sheeting* **2023**, *39*, 427–446.
402. Molina-Gutiérrez, S.; Manseri, A.; Ladmiral, V.; Bongiovanni, R.; Caillol, S.; Lacroix-Desmazes, P. *Macromolecular Chemistry and Physics* **2019**, *220*, 1900179.
403. Wallace, T.; Gritter, R. *Tetrahedron* **1963**, *19*, 657–665.
404. Andrzejewska, E.; Andrzejewski, M. *Journal of Polymer Science Part A: Polymer Chemistry* **1998**, *36*, 665–673.
405. Molina-Gutiérrez, S.; Dalle Vacche, S.; Vitale, A.; Ladmiral, V.; Caillol, S.; Bongiovanni, R.; Lacroix-Desmazes, P. *Molecules* **2020**, *25*, 3444.
406. Srikanthan, V.; Pitois, O.; Coussot, P.; Le Droumaguet, B.; Grande, D. *Polymers* **2021**, *13*, 2692.
407. Bachmann, J.; Schmolzer, S.; Ruderer, M. A.; Fruhmann, G.; Hinrichsen, O. *SPE Polymers* **2022**, *3*, 41–53.
408. Scherzer, T.; Decker, U. *Vibrational Spectroscopy* **1999**, *19*, 385–398.

409. Fairbanks, B. D.; Scott, T. F.; Kloxin, C. J.; Anseth, K. S.; Bowman, C. N. *Macromolecules* **2009**, *42*, 211–217.
410. Müller, S. M.; Schlögl, S.; Wiesner, T.; Haas, M.; Griesser, T. *ChemPhotoChem* **2022**, *6*, e202200091.
411. Fouassier, J.-P.; Lalevée, J., *Photoinitiators: Structures, Reactivity and Applications in Polymerization*; John Wiley & Sons: **2021**.
412. Jagtap, A.; More, A. *Polymer Bulletin* **2022**, *79*, 8057–8091.
413. Qiu, J.; Wei, J. *Journal of Applied Polymer Science* **2014**, *131*.
414. Fouassier, J.-P.; Lalevée, J., *Photoinitiators for polymer synthesis: scope, reactivity, and efficiency*; John Wiley & Sons: **2012**.
415. Bagheri, A.; Jin, J. *ACS Applied Polymer Materials* **2019**, *1*, 593–611.
416. Bahney, C.; Lujan, T.; Hsu, C.; Bottlang, M.; West, J.; Johnstone, B. *European cells & materials* **2011**, *22*, 43.
417. Green, W. A., *Industrial photoinitiators: a technical guide*; CRC Press: **2010**.
418. Zhang, J.; Xiao, P.; Morlet-Savary, F.; Graff, B.; Fouassier, J. P.; Lalevée, J. *Polymer Chemistry* **2014**, *5*, 6019–6026.
419. Klee, J.; Maier, M; Fik, C. **2015**.
420. Mitterbauer, M.; Haas, M.; Stüger, H.; Moszner, N.; Liska, R. *Macromolecular Materials and Engineering* **2017**, *302*, 1600536.
421. Moszner, N.; Zeuner, F.; Lamparth, I.; Fischer, U. K. *Macromolecular Materials and Engineering* **2009**, *294*, 877–886.
422. Jauk, S.; Liska, R. *Macromolecular rapid communications* **2005**, *26*, 1687–1692.
423. Sprick, E.; Becht, J.-M.; Tigges, T.; Neuhaus, K.; Weber, C.; Lalevée, J. *Macromolecular Chemistry and Physics* **2020**, *221*, 2000211.
424. Sprick, E.; Becht, J.-M.; Graff, B.; Salomon, J.-P.; Tigges, T.; Weber, C.; Lalevée, J. *Dental Materials* **2021**, *37*, 382–390.
425. Benedikt, S.; Wang, J.; Markovic, M.; Moszner, N.; Dietliker, K.; Ovsianikov, A.; Grützmacher, H.; Liska, R. *Journal of Polymer Science Part A: Polymer Chemistry* **2016**, *54*, 473–479.
426. Zhang, J.; Dumur, F.; Xiao, P.; Graff, B.; Bardelang, D.; Gigmès, D.; Fouassier, J. P.; Lalevée, J. *Macromolecules* **2015**, *48*, 2054–2063.
427. Lougnot, D.; Fouassier, J. *Journal of Polymer Science Part A: Polymer Chemistry* **1988**, *26*, 1021–1033.
428. Chesnokov, S.; Cherkasov, V.; Abakumov, G.; Mamysheva, O.; Zakharina, M. Y.; Shushunova, N. Y.; Chechet, Y. V.; Kuropatov, V. *Polymer Science Series B* **2014**, *56*, 11–20.
429. Kitano, H.; Ramachandran, K.; Bowden, N. B.; Scranton, A. B. *Journal of applied polymer science* **2013**, *128*, 611–618.
430. Zhang, J.; Zivic, N.; Dumur, F.; Xiao, P.; Graff, B.; Fouassier, J. P.; Gigmès, D.; Lalevée, J. *ChemPhotoChem* **2018**, *2*, 481–489.
431. Baxter, J. E.; Davidson, R. S.; Hageman, H. J.; McLauchlan, K. A.; Stevens, D. G. *Journal of the Chemical Society, Chemical Communications* **1987**, 73–75.
432. El-Molla, M. *Dyes and Pigments* **2007**, *74*, 371–379.
433. Smith, R. C.; Fischer, W. M.; Gin, D. L. *Journal of the American Chemical Society* **1997**, *119*, 4092–4093.
434. Zhang, X.; Jiang, X.; Sun, C. *Sensors and Actuators A: Physical* **1999**, *77*, 149–156.
435. Du, J.-Z.; Sun, T.-M.; Weng, S.-Q.; Chen, X.-S.; Wang, J. *Biomacromolecules* **2007**, *8*, 3375–3381.

436. DeLong, S. A.; Moon, J. J.; West, J. L. *Biomaterials* **2005**, *26*, 3227–3234.
437. Fairbanks, B. D.; Schwartz, M. P.; Bowman, C. N.; Anseth, K. S. *Biomaterials* **2009**, *30*, 6702–6707.
438. Le, C. M. Q.; Petitoy, T.; Wu, X.; Spangenberg, A.; Ortyl, J.; Galek, M.; Infante, L.; Thérien-Aubin, H.; Chemtob, A. *Macromolecular Chemistry and Physics* **2021**, *222*, 2100217.
439. Müller, G.; Zalibera, M.; Gescheidt, G.; Rosenthal, A.; Santiso-Quinones, G.; Dietliker, K.; Grützmacher, H. *Macromolecular rapid communications* **2015**, *36*, 553–557.
440. Ullrich, G.; Ganster, B.; Salz, U.; Moszner, N.; Liska, R. *Journal of Polymer Science Part A: Polymer Chemistry* **2006**, *44*, 1686–1700.
441. Wang, J.; Stanic, S.; Altun, A. A.; Schwentenwein, M.; Dietliker, K.; Jin, L.; Stampfl, J.; Baudis, S.; Liska, R.; Grützmacher, H. *Chemical communications* **2018**, *54*, 920–923.
442. Nazir, R.; Danilevicius, P.; Gray, D.; Farsari, M.; Gryko, D. T. *Macromolecules* **2013**, *46*, 7239–7244.
443. Xie, C.; Wang, Z.; Liu, Y.; Song, L.; Liu, L.; Wang, Z.; Yu, Q. *Progress in Organic Coatings* **2019**, *135*, 34–40.
444. Dietlin, C.; Trinh, T. T.; Schweizer, S.; Graff, B.; Morlet-Savary, F.; Noirot, P.-A.; Lalevée, J. *Macromolecules* **2019**, *52*, 7886–7893.
445. Dietlin, C.; Trinh, T. T.; Schweizer, S.; Graff, B.; Morlet-Savary, F.; Noirot, P.-A.; Lalevée, J. *Molecules* **2020**, *25*, 1671.
446. Eibel, A.; Schmallegger, M.; Zalibera, M.; Huber, A.; Bürkl, Y.; Grützmacher, H.; Gescheidt, G. *European Journal of Inorganic Chemistry* **2017**, *2017*, 2469–2478.
447. Cosola, A.; Conti, R.; Rana, V. K.; Sangermano, M.; Chiappone, A.; Levalois-Grützmacher, J.; Grützmacher, H. *Chemical communications* **2020**, *56*, 4828–4831.
448. Breloy, L.; Negrell, C.; Mora, A.-S.; Li, W. J.; Brezová, V.; Caillol, S.; Versace, D.-L. *European Polymer Journal* **2020**, *132*, 109727.
449. Brook, A.; Quigley, M.; Peddle, G.; Schwartz, N.; Warner, C. *Journal of the American Chemical Society* **1960**, *82*, 5102–5106.
450. Gilman, H.; Atwell, W. H.; Sen, P. K.; Smith, C. L. *Journal of Organometallic Chemistry* **1965**, *4*, 163–167.
451. Brook, A.; Jones, P. F.; Peddle, G. *Canadian Journal of Chemistry* **1968**, *46*, 2119–2127.
452. Lalevee, J.; Dirani, A.; El-Roz, M.; Allonas, X.; Fouassier, J.-P. *Macromolecules* **2008**, *41*, 2003–2010.
453. Liska, R.; Knaus, S.; Gruber, H.; Wendrinsky, J. *Surface Coatings International* **2000**, *83*, 297–303.
454. Balta, D. K.; Arsu, N.; Yagci, Y.; Jockusch, S.; Turro, N. J. *Macromolecules* **2007**, *40*, 4138–4141.
455. Aydin, M.; Arsu, N.; Yagci, Y.; Jockusch, S.; Turro, N. J. *Macromolecules* **2005**, *38*, 4133–4138.
456. Lalevee, J.; Blanchard, N.; El-Roz, M.; Graff, B.; Allonas, X.; Fouassier, J.-P. *Macromolecules* **2008**, *41*, 4180–4186.
457. Lalevee, J.; Blanchard, N.; Chany, A.-C.; El-Roz, M.; Souane, R.; Graff, B.; Allonas, X.; Fouassier, J. *Macromolecules* **2009**, *42*, 6031–6037.
458. Versace, D. L.; Tehfe, M. A.; Lalevée, J.; Casarotto, V.; Blanchard, N.; Morlet-Savary, F.; Fouassier, J.-P. *Journal of Physical Organic Chemistry* **2011**, *24*, 342–350.
459. Trommer, M.; Sander, W. *Organometallics* **1996**, *15*, 189–193.
460. Zhang, H.-J.; Priebsenow, D. L.; Bolm, C. *Chemical Society Reviews* **2013**, *42*, 8540–8571.
461. Yamamoto, K.; Hayashi, A.; Suzuki, S.; Tsuji, J. *Organometallics* **1987**, *6*, 974–979.
462. Yamamoto, K.; Hayashi, A.; Suzuki, S.; Tsuji, J. *Organometallics* **1987**, *6*, 979–982.

463. Graff, B.; Klee, J. E.; Fik, C.; Maier, M.; Fouassier, J. P.; Lalevée, J. *Macromolecular Rapid Communications* **2017**, *38*, 1600470.
464. Mochida, K.; Okui, S.; Ichikawa, K.; Kanakubo, O.; Tsuchiya, T.; Yamamoto, K. *Chemistry Letters* **1986**, *15*, 805–808.
465. Hayashi, H.; Mochida, K. *Chemical physics letters* **1983**, *101*, 307–311.
466. Taraban, M.; Maryasova, V.; Leshina, T.; Rybin, L.; Gendin, D.; Vyazankin, N. *Journal of organometallic chemistry* **1987**, *326*, 347–355.
467. Wakasa, M.; Mochida, K.; Sakaguchi, Y.; Nakamura, J.; Hayashi, H. *The Journal of Physical Chemistry* **1991**, *95*, 2241–2246.
468. Durmaz, Y. Y.; Moszner, N.; Yagci, Y. *Macromolecules* **2008**, *41*, 6714–6718.
469. Joöckle, P.; Schweigert, C.; Lamparth, I.; Moszner, N.; Unterreiner, A.-N.; Barner-Kowollik, C. *Macromolecules* **2017**, *50*, 8894–8906.
470. Yuan, Y.; Zhang, Y.; Chen, B.; Wu, X.-F. *Iscience* **2020**, *23*.
471. Kabatc, J.; Czech, Z.; Kowalczyk, A. *Journal of Photochemistry and Photobiology A: Chemistry* **2011**, *219*, 16–25.
472. Qiu, W.; Zhu, J.; Dietliker, K.; Li, Z. *ChemPhotoChem* **2020**, *4*, 5296–5303.
473. Tehfe, M.-A.; Dumur, F.; Graff, B.; Morlet-Savary, F.; Gigmès, D.; Fouassier, J.-P.; Lalevée, J. *Polymer Chemistry* **2013**, *4*, 2313–2324.
474. Bouzrati-Zerelli, M.; Kirschner, J.; Fik, C. P.; Maier, M.; Dietlin, C.; Morlet-Savary, F.; Fouassier, J. P.; Becht, J.-M.; Klee, J. E.; Lalevée, J. *Macromolecules* **2017**, *50*, 6911–6923.
475. Dietliker, K. In 2002.
476. Pan, H.; Chen, S.; Jin, M.; Malval, J.-P.; Wan, D.; Morlet-Savary, F. *Polymer Chemistry* **2019**, *10*, 1599–1609.
477. Kirschner, J.; Paillard, J.; Graff, B.; Becht, J.-M.; Klee, J. E.; Lalevée, J. *Macromolecular Chemistry and Physics* **2020**, *221*, 1900495.
478. Kirschner, J.; Baralle, A.; Graff, B.; Becht, J.-M.; Klee, J. E.; Lalevée, J. *Macromolecular Rapid Communications* **2019**, *40*, 1900319.
479. Ma, X.; Cao, D.; Hu, X.; Nie, J.; Wang, T. *Progress in Organic Coatings* **2020**, *144*, 105651.
480. Liu, S.; Graff, B.; Xiao, P.; Dumur, F.; Lalevée, J. *Macromolecular Rapid Communications* **2021**, *42*, 2100207.
481. Hu, P.; Qiu, W.; Naumov, S.; Scherzer, T.; Hu, Z.; Chen, Q.; Knolle, W.; Li, Z. *ChemPhotoChem* **2020**, *4*, 224–232.
482. Li, Z.; Zou, X.; Zhu, G.; Liu, X.; Liu, R. *ACS applied materials & interfaces* **2018**, *10*, 16113–16123.
483. Qiu, W.; Li, M.; Yang, Y.; Li, Z.; Dietliker, K. *Polymer Chemistry* **2020**, *11*, 1356–1363.
484. You, J.; Cao, D.; Hu, T.; Ye, Y.; Jia, X.; Li, H.; Hu, X.; Dong, Y.; Ma, Y.; Wang, T. *Dyes and Pigments* **2021**, *184*, 108865.
485. Zhu, Y.; Xu, D.; Zhang, Y.; Zhou, Y.; Yagci, Y.; Liu, R. *Angewandte Chemie International Edition* **2021**, *60*, 16917–16921.

List of relevant abbreviations

λ	Wavelength
2,4TT	2,4-Dithiothymine
2TT	2-Thiothymine
2TU	2-Thiouracil
3D	3-Dimensional
4D	4-dimensional
4TT	4-Thiothymine
4TU	4-Thiouracil
ACN	Acetonitrile
AIBN	Azo(bisisobutyronitrile)
AM	Additive manufacturing
ATR	Attenuated total reflectance
BAPO	Phenylbis(2,4,6-trimethylbenzoyl)phosphine oxide
BDA	1,4-Bis(acryloyloxy)butane
BDBTG	1,4-Butanediol bis(thioglycolate)
BisGMA	Bisphenol A-glycidyl methacrylate
CA	Contact angle
CAD	Computer aided design
CH	Cyclohexane
CLIP	Continuous liquid interface printing
CPO	Carbazole based phosphine oxide
CQ	Camphorquinone
DBC	Double bond conversion
DCCA	(<i>E</i>)-7-(diethylamino)-2-oxo-2H-chromene-3-carbaldehyde <i>o</i> -acryloyl oxime
DCM	Dichloromethane
DLP	Digital light processing
DMA	Dynamic mechanical analysis
DMD	Digital mirror device
DMF	Dimethylformamide
DMSO	Dimethyl sulfoxide
DNA	Desoxyribonucleic acid
E	Energy
EM	Eugenyl methacrylate
FMO	Frontal molecular orbital

List of Abbreviations

FTIR	Fourier-transform infrared spectroscopy
H-	Hydrogen
$h\nu$	Light
HDDA	1,6-Hexanediol diacrylate
HOMO	Highest occupied molecular orbital
I	Initiator
IC	Internal conversion
IR	Infrared
ISC	Intersystem crossing
ISC	Intersystem crossing
IUPAC	International union of pure and applied chemistry
LCD	Liquid crystal display
LED	Light emitting diode
Li-TPO	Lithium phenyl-2,4,6-trimethylbenzoylphosphinate
LUMO	lowest unoccupied molecular orbital
M	Molar weight
MAPO	Monoacylphosphine oxide
NIR	Near infrared
NMR	Nuclear magnetic resonance
NPPOC	2-(2-Nitrophenyl)propyloxycarbonyl
P	Product
PAG	Photo acid generator
PB	Photo base
PBG	Photo base generator
PDMS-ECEMS	Poly-dimethylsiloxane-co-(2-(3,4-epoxycyclohexyl)-ethyl)-methylsiloxane
PEG	Polyethylene glycol
PEGDA	Polyethyleneglycol diacrylate
PHEMA	Poly(2-hydroxyethyl methacrylate)
photo-DSC	Differential scanning photo calorimetry
PI	Photoinitiator
PI-2	2-Hydroxy-4'-(2-hydroxyethoxy)-2-methylpropiophenon (I2959)
PI-I	Bis(4-methoxybenzoyl)diethylgermanium (Ivocerin™)
PIS	Photoinitiating system
pK_a	Acid dissociation constant
POs	Phosphineoxides
PVA	Polyvinyl alcohole
RT	Room temperature (25°C)
S_n	Singlet state

SCNPs	Single-chain nanoparticles
-SH	Thiol
SLA	Stereolithography
SNOM	Scanning near field optical microscopy
SOS	Singlet oxygen scavenger
SOS	Singlet oxygen scavenger
SP	Styrylpyrene
SP-A	Styrylpyrene-acrylate
SP-OH	Hydroxy-styrylpyrene
STED	Stimulation emission depletion
T	Thymine
T	Temperature [K]
T _g	Glass transition temperature
T _n	Triplet state
TCDDA	Tricyclo[5.2.1.0 ^{2,6}]decandimethanoldiacrylat
TED	Thiuram disulfide
TED	Thiuram disulfide
TEGDA	Tetraethylene glycol diacrylate
TGA	Thermogravimetical analysis
T-HEMA	2-(2-(Thymin-1-yl)acetoxy) ethyl methacrylate
THF	Tetrahydrofurane
TLC	Thin-layer chromatography
TMG	Tetramethylguanidine
TMPMP	Trimethylolpropane tris(3-mercaptopropionate)
TMPTA	Trimethylolpropane triacrylate
TPA	Two photon absorption
TPA	Two-photon absorption
TPGDA	Tripropylene glycol diacrylate
TPL	Two photon lithography
TTBS	Tetrakis(2,4,6-trimethylbenzoyl)silane
U	Uracil
UV	Ultraviolet
UVA	Ultraviolet radiation 315-400nm
UVB	Ultraviolet radiation 280-315nm
UVC	Ultraviolet radiation 200-280nm
UV-Vis	Ultraviolet-Visible light spectroscopy
VAM	Vanillyl alcohol methacrylate
VC	Vinylcarbonates

List of Abbreviations

VE	Vinylesters
Vis	Visible
VOC	Volatile organic compounds
VR	Vibrational relaxation

List of Figures

1.1 Jablonski diagram	6
1.2 Radical formation upon irradiation	7
1.3 Radical polymerization	8
1.4 Oxygen inhibition	9
1.5 Cationic polymerization	10
1.6 Photo base generation	11
1.7 Scheme of possible orbital transitions upon photon absorption.	12
1.8 Orthogonality	13
1.9 Types of cycloaddition reactions	14
1.10 Woodward-Hoffmann rules	14
1.11 Some cycloaddition reactions	16
1.12 Action plot example	17
1.13 Mechanism of the thiol-Michael addition reaction	19
1.14 Radical thiol-ene polymerization	20
1.15 Double bond reactivity toward thiol-ene reaction by functional group	20
1.16 Applied 3D printing	23
1.17 Vat-based 3D printing techniques: DLP, LCD and SLA	24
1.18 High resolution 3D printing by xylography	26
1.19 Nature-inspired application of multi-material 3D and 4D printing	27
1.20 3D printed stent	28
1.21 3D printed clear aligners	28
1.22 Micro-actuators for drug release	30

1.23 Soft robotics: soft continuum robot in biomimetic maze	30
1.24 Self folding robot	31
1.25 Conductive 3D printed hydrogel	31



2.1 The influence on thiol on material properties in DMA	33
2.2 Dual-cure polymerization	34
2.3 A library of dimerizable groups	35
2.4 Abietic acid kinetics	36
2.5 Anthracene methyl acrylate kinetics	37
2.6 Chalcone kinetics	38
2.7 Cinnamoyl-chloride kinetics	39
2.8 Iminostilbene kinetics	40
2.9 Styrylpyrene kinetics in solution and in resin	41
2.10 Uracil and thymine kinetics and their derivatives	42
2.11 Uracil derivatives and their kinetics	43
2.12 Thymine derivatives and their kinetics	43
2.13 Chalcone resin system, its orthogonal and thermo-chemical behavior	48
2.14 3D-printed and molded shapes for smart applications with temperature and solvent stimuli	49
2.15 Demonstration of shape-memory behavior on micro-scale	50
2.16 Demonstration of 2.5D printing and thermo-mechanical properties on micro-scale	51
2.17 A dual-cure approach with thiol-Michael/thiol-ene chemistry	56
2.18 Utilizing disparate polymerization mechanisms for a dual-cure resin	57

2.S1 NMR spectra of hydroxy-styrylpyrene and styrylpyrene acrylate	59
2.S2 NMR spectra of a thymine methacrylate	59
2.S3 IR spectra of a uracil and its derivatives	60
2.S4 ¹ H-NMR spectrum of 4'-(methacryloyloxy) chalcone (Ch-MA) after synthesis.	60
2.S5 Correlations between chemistry and thermo-mechanical properties in a chalconyl dual-cure resin	61
2.S6 Swelling behavior	62
2.S7 Surface properties after crosslinking with TPA at 780 nm	63
2.S8 Shape memory experiment with nanoimprinted pillars.	63
2.S9 Resolution test for micro-3D printing with 900 nm	64
2.S10 Fluorescence experiments	64
2.S11 NMR spectra of 2-(2-nitrophenyl)propyloxycarbonyl tetramethyl guanidine (NPPOC-TMG)	65



3.1 Reaction kinetics of EM and VAM resins	68
3.2 Photo-DSC measurements of EM and VAM	69
3.3 Photo-DSC measurements of EPE and VPE	70
3.4 Signal processing in photo-DSC	73
3.5 Photo-DSC and conversion plots for the photopolymerization of HDDA with 0.3 mol% PIs	74
3.6 Photo-DSC and conversion plots for the photopolymerization of HDDA with equimolar PI concentration	75
3.7 Biodegradable monomers investigated in FTIR kinetics	76
3.8 IR spectrum of a biodegradable thiol-silylether resin during illumination	77

3.9 FTIR kinetics of two biodegradable thiol-silylether resins and a dual cure system	77
3.S1 Temperature dependent behavior of EM and VAM	78
3.S3 NMR spectra of EM and VAM	78
3.S2 IR spectra during illumination	79



4.1 Commercially available PIs	82
4.2 Water-soluble PIs	82
4.3 Variation of bisacylphosphine oxide	83
4.4 Poly(ethylene glycol) bisacylphosphine oxide (PEG-BAPO)	83
4.5 Variation of acylphosphine oxides	84
4.6 Acyldiphenylphosphine oxides	84
4.7 Variation of bisacylphosphine oxides with phosphorous functionalities	85
4.8 Cyclodextrine based bisacylphosphine oxide	85
4.9 A vanillin derived Type I photoinitiator	86
4.10 Radical photoinitiators with silicon groups	87
4.11 Acylsilanes for the generation of silyl radicals	87
4.12 Bisacylgermanes for the generation of germyl radicals	88
4.13 Acetyltriphenylgermane for the generation of germyl radicals	89
4.14 Bis(triphenylgermyl)ketone as radical source	89
4.15 Photoinitiators based on Ge-mesitoyl	89
4.16 Tetraacylgermanes	90
4.17 Benzoyl(trimethyl)germane	90

4.18 Isolated monoacylgermanes	90
4.19 Isolated acylgermanes	91
4.20 Tetraacylstannanes	91
4.21 Acylstannanes for photoinitiation	91
4.22 Other types of photoinitiators	92
4.23 Pyrene derivatives	93
4.24 Silyl- and phenylglyoxylates as PIs	93
4.25 Diketones for photoinitiation	94
4.26 Oxime ester groups in PIs	95
4.27 Conjugated bifunctional carbazole-based oxime esters	95
4.28 Diethylaminocoumarin-based oxime esters	96
4.29 Flavonol sulfonate and phenothiazinium salt based PIs	97
5.1 Summary of photo-crosslinkable groups	98
5.2 Summary of photo-crosslinkable groups	99

List of Tables

1.1	Correlation between orbital electron transition and absorption region. . .	12
1.2	Bathochromic shift of conjugated systems	15



2.1	Lamps used in irradiation experiments for photo-reactive groups	45
2.2	Composition of chalconyl dual-cure resins	53
2.3	Formulations for photoinitiator-based dual-cure resins	58



3.1	Contact angles of EM and VAM coatings on glassine paper	70
3.2	Photocurable formulations derived from EM and VAM resin	71



Complete List of Publications

Peer-reviewed Papers as First Author

1. **Müller, Stefanie Monika**; Nelson, Benjamin R.; Jelinek, Alexander; Kirkpatrick, Bruce E.; Keyser, Sean; Naderer, Christoph; Sivun, Dmitry; Jacak, Jaroslav; Anseth, Kristi S.; Bowman, Christopher N.; Schlögl, Sandra and Griesser, Thomas. “*Chalcones as wavelength selective crosslinkers: Additive manufacturing of macro- and microscopic structures for soft active devices*”. *Advanced Materials*, **submitted**
2. Husić, Indira; **Müller, Stefanie Monika**; Mahendran, Arunjunai Raj; Sinic, Judith; Jocham, Christoph; Lammer, Herfried and Griesser, Thomas. “*Photocuring behavior of low molecular weight biomass-derived methacrylate monomers for paper coatings*”. *Journal of Polymer Research*, 31(3), **2024**. DOI: 10.1007/s10965-024-03937-1
3. **Müller, Stefanie Monika**; Schlögl, Sandra; Wiesner, Tanja; Haas, Michael and Griesser, Thomas. “*Recent advances in type I photoinitiators for visible light induced photopolymerization*”. *ChemPhotoChem*, 6(11), **2022**. DOI: 10.1002/cptc.202200091

Peer-reviewed Papers as a Co-author

1. Haudum, Stephan; Kainz, Michael; Stubauer, Gerald; Wanko, Stefan; Guilen, Elena; Brüggemann, Oliver; **Müller, Stefanie Monika**; Dehne, Tilo; Schulz, Daria Patrycja; Engels, Andreas; Rinner, Uwe; Griesser, Thomas; Teasdale, Ian. “*Solvent-free, biodegradable resins for 3D Inkjet Printing based on Silyl-Ether and Amino Acid Phosphoramidate Photomonomers*”. *Macromolecular rapid communications*, **submitted**
2. Haudum, Stephan; Demirdögen, Berfin; Müller-Müchler, Laura; Döttl, Sophie Carolin; **Müller, Stefanie Monika**; Naderer, Christoph; Brüggemann, Oliver; Griesser, Thomas; Jacak, Jaroslav; Priglinger, Elin; Teasdale, Ian. “*Biodegradable resins for photochemical 3D printing via vinyl ester and vinyl carbonate functionalized amino acid-phosphoramidates*”. *European Polymer Journal*, 211, **2024**. DOI: 10.1016/j.eurpolymj.2024.113037
3. Sommer, Katharina; Rieger, Paul; **Müller, Stefanie Monika**; Schwarz, Romana; Trimmel, Gregor; Feuchter, Michael; Griesser, Thomas. “*3D Printing of Dual-Cure Networks Based on (Meth) acrylate/Bispropargyl Ether Building Blocks*”. *Advanced engineering materials*, 25(7), **2023**. DOI: 10.1002/adem.202200901
4. Haudum, Stephan; Lenhart, Stefan; **Müller, Stefanie Monika**; Tupe, Disha; Naderer, Christoph; Dehne, Tilo; Sittinger, Michael; Major, Zoltan; Griesser, Thomas; Brüggemann, Oliver; Jacak, Jaroslav; Teasdale, Ian. “*Amino acid-based polyphosphorodiamidates with hydrolytically labile bonds for degradation-tuned photopolymers*”. *ACS Macro Letters*, 12(6), **2023**. DOI: 10.1021/acsmacrolett.3c00173
5. Maier, Janine; **Müller, Stefanie Monika**; Torvisco, Ana; Glotz, Gabriel; Fischer, Roland

C.; Griesser, Thomas; Kelterer, Anne-Marie; Haas, Michael. "Isolable Stannenolates Enable the Synthesis of Visible-Light Photoinitiators". *ChemPhotoChem*, 6(3), **2022**. DOI: 10.1002/cptc.202100213

6. Püschmann, Sabrina; Frühwirt, Phillip; **Müller, Stefanie Monika**; Wagner, Stefan H.; Torvisco, Ana; Fischer, Roland C.; Kelterer, Anne-Marie; Griesser, Thomas; Gescheidt Georg; Haas, Michael. "Synthesis and characterization of diacylgermanes: persistent derivatives with superior photoreactivity". *Dalton Transactions*, 50(34), **2021**. DOI: 10.1039/D1DT02091A
7. Frühwirt, Phillip; Knoechl, Andreas; Pillinger, Michael; **Müller, Stefanie Monika**; Wasdin, Perry T.; Fischer, Roland C.; Radebner, Judith; Torvisco, Ana; Moszner, Norbert; Kelterer, Anne-Marie; Griesser, Thomas; Gescheidt, Georg; Haas, Michael. "The Chemistry of Acylgermanes: Triacylgermenolates Represent Valuable Building Blocks for the Synthesis of a Variety of Germanium-Based Photoinitiators". *Inorganic Chemistry*, 59(20), **2020**. DOI: 10.1002/jcc.21600
8. Ferstl, Esther; Gabriel, Martin; Gomernik, Florian; **Müller, Stefanie Monika**; Selinger, Julian; Thaler, Ferula; Bauer, Wolfgang; Spirk, Stefan; Chemelli, Angela. "Investigation of the adsorption behavior of jet-cooked cationic starches on pulp fibers". *Polymers*, 12(10), **2020**. DOI: 10.3390/polym12102249

Posters and Oral Talks at Conferences

1. **Müller, Stefanie Monika**; Nelson, Benjamin R.; Naderer, Christoph; Sivun, Dmitry; Jacak, Jaroslav; Schlögl, Sandra and Griesser, Thomas. "Sequential orthogonal by [2+2] cycloadditions in dual-cure photopolymers". Poster, Polymerization Fundamentals, September, 19-22, **2023**, Boulder, Colorado
2. **Müller, Stefanie Monika**; Nelson, Benjamin R.; Schlögl, Sandra and Griesser, Thomas. "Sequential λ -orthogonality by [2+2] cycloadditions in dual-cure photopolymers". Oral talk, International Symposium on Smart Materials, June, 14-15, **2023**, Leoben, Austria.
3. **Müller, Stefanie Monika**; Nelson, Benjamin R.; Schlögl, Sandra and Griesser, Thomas. "Chalcones as sequential λ -orthogonal crosslinkers in dual-cure photopolymers". Oral talk, 7th European Symposium of Photopolymer Science (ESPS), September, 19-22, **2022**, Istanbul, Turkey.
4. **Müller, Stefanie Monika**; Nelson, Benjamin R.; Schlögl, Sandra and Griesser, Thomas. "Chalcone [2+2] cycloaddition for λ -orthogonal dual-cure photopolymers". Poster, European Polymer Congress (EPF), June, 27-01, **2022**, Prag, Czech Republic.
5. Niegelhell, Katrin; **Müller, Stefanie Monika**; Chemelly, Angela; Hobisch, Josefine; Griesser, Thomas; Reiter, Heidemarie; Hirn, Ulrich; Spirk, Stefan. "Industrially relevant cationic starches and cellulose". Oral talk, 23rd Austrian Carbohydrate Workshop, February, 14-15, **2019**, Graz, Austria.

6. **Müller, Stefanie Monika**; Schlemmer, Werner; Zajki-Zechmeister, Krisztina; Plank, Harald; Spirk, Stefan. “*Thin Films from Acetylated Lignin*”. Poster, 3rd EPNOE Junior Scientist Meeting, May, 14-15, **2018**, Maribor, Slovenia.

Invention Disclosures

1. Haas, Michael; Wiesner, Tanja; Gfader, Zeno; Griesser, Thomas; **Müller, Stefanie Monika**; *Oligoacylphosphinoxides as Photoinitiators with Low Migration* . **2024**

Curriculum Vitae

Stefanie Monika Müller, MSc



Personal Information

Address Ziegeleistr. 3d
5110 Oberndorf bei Salzburg
Date of birth 29th of March 1994
Nationality Austrian
Mobile +0043 677/61690663
E-mail stefanie.mueller@sbg.at

Work Experience

- Since 01/2020 **Research assistant and Ph.D. candidate at the *Chair of Chemistry of Polymeric Materials* at the *Montanuniversitaet Leoben***
- Research for a doctoral dissertation on “*Orthogonal Photoreactions for the Preparation of Multifunctional Photopolymers*”.
 - Cooperation with project partners in plastics industry.
 - Supervisor: Thomas Grießer
- 09/2023
- 11/2023 **Research stay at the *University of Colorado, Boulder* in Colorado, United States**
- Research on dual-cure resins for holography under the supervision of Christopher N. Bowman.
- 09/2018
- 02/2019 **Project assistant at the *Institute of Paper, Pulp and Fibre Technology* at the *Graz University of Technology***
- Coordination and lab work for a project in cooperation with companies from the Austrian paper-making industry.
 - Supervision of student lab courses.
- 07/2017
- 09/2017 **Internship at *Durst Phototechnik Digital Technology GmbH***
- Lab work at the department of research and development of water-based inks for ink-jet printing.
 - Preparation of a series of inks at lab scale; design and evaluation of analytical methods for ink tests.
- 07/2016
- 09/2016 **Internship at *Sandoz GmbH Kundl***
- Analytical lab work for testing screening and inoculation samples for different active ingredients, analysis with HPLC and independent evaluation of the measurements.
- Summer 2011
- 2013 **Internship at *Landesapotheke Salzburg***
- Preparation of drug deliveries for hospitals and hospital wards.

Education

- 10/2016
- 02/2019 **Master's program in Technical Chemistry (Dipl.Ing.)**
at the *Graz University of Technology* and the *Karl-Franzens University Graz*
(joint degree) with main focus on renewable resources.
- 10/2016
- 11/2018 **Master's degree in chemistry (MSc)**
at the *Graz University of Technology* and the *Karl-Franzens University Graz*
(joint degree).
Graduation on the 14th of November 2018 (pass with distinction).
Thesis topic: ***Characterization and Patterning of Lignin Based Thin Films.***
Supervisor: Stefan Spirk
Merit-based scholarship in 2016/17.
- 08/2015
- 06/2016 **Student exchange** in Trondheim, Norway
and studies at the *Norwegian University of Science and Technology*
as part of *Erasmus+*.
- 10/2012
- 11/2015 **Bachelor's degree in chemistry (BSc)**
at the *Graz University of Technology* and the *Karl-Franzens University Graz*
(joint degree).
Graduation in November 2015 with grade average of 1.6.
Thesis Topic: ***Tetrylenes – Synthesis of a Bisphosphanylgermylene.***
Supervisor: Michaela Flock
Merit-based scholarship in 2012/13.
- 09/2004
- 05/2012 **Middle and High School at *Musisches Gymnasium Salzburg***
with focus on fine arts.
Graduation in May 2012 (pass with distinction).

Voluntary Commitment and Accomplishments

- Since 04/2022 **Team leader of the youth group at *Akademische Sektion Graz - Austrian Alpine Association (ÖAV)***
 - Coordination of all tour guides and activities.
 - Active participation in board meetings.
- 08/2021 **Participation in the *European Forum Alpbach* as a Scholarship holder**
 - Seminars on '*Collaboration through the Power of Music*' and '*The Who and How of Europe's Future of Energy*'.
- 04/2019
- 10/2019 **Thru-hike of the *Pacific Crest National Scenic Trail (PCT)***
 - A backpacking trip over 2650 miles from Mexico to Canada.

Since 2014	Voluntary work at the <i>Austrian Alpine Association (ÖAV)</i> “Umweltbaustelle“ <ul style="list-style-type: none"> · Renovation of hiking trails and reforestation. · Removal of shrubs and trees from mountain pastures. Member of the youth group at <i>Akademische Sektion Graz</i> <ul style="list-style-type: none"> · Training as a youth leader and ski touring guide. · Guiding of outdoor adventures for small groups.
2016 - 2019	Voluntary work for the <i>Foodsharing Association</i> <ul style="list-style-type: none"> · Saving and distributing surplus food from retailers and producers.
2013 - 2014	“Erstsemestrigen Tutorium“ <ul style="list-style-type: none"> · Tutoring and social activities for first semester students.

Languages

German (native language)
 English (C1)
 Norwegian (B1)
 French (A1)

Additional Skills

IT knowledge	MS Office (Excel, Word, PowerPoint) – advanced level Origin – good working knowledge MATLAB – basic knowledge for data processing LaTeX – basic working knowledge
Special Software	OPUS (IR); Advance (CA); Vision 64 (profilometry); STARE (DMA, TGA); NanoScope Analysis (AFM); MestRe Nove (NMR); RheoCompass (rheology); SpectraGryph; Citavi; Photoshop; Chemdraw;
driver’s licence	class B

Hobbies

Drawing, mountaineering, climbing, skiing, photography, long distance hiking, handicrafts

